SEASONAL CYCLING IN ELECTRICAL RESISTIVITIES AT TEN THIN PERMAFROST SITES, SOUTHERN YUKON AND NORTHERN BRITISH COLUMBIA

Christina Miceli

Thesis submitted to the
Faculty of Graduate and Postdoctural Studies
In partial fulfillment of the requirements
For the Master of Science degree in Geography

Department of Geography
Faculty of Arts
University of Ottawa

ABSTRACT

Permanent electrode arrays were set up at ten monitoring sites from Whitehorse, Yukon, to Fort St. John, British Columbia, in order to gain a clearer perspective of the effectiveness of electrical resistivity tomography (ERT) monitoring over an annual cycle of freezing and thawing. This research forms part of a longer-term project that is attempting to use ERT to examine changes in permafrost resulting from climate change.

Inter-site and intra-site variability were examined by installing and maintaining data-loggers to monitor active layer and shallow permafrost temperatures, air temperatures, and snow depths at each site from August 2010 – August 2011. Additional site information was collected on each ERT survey date, including frost table depths, snow depths, and vegetation heights.

Based on nearby community records, the climate in the region has been warming by a rate of 0.3 to 0.5 °C per decade since 1970. The permafrost at all ten sites was characteristic of sporadic discontinuous and isolated patches permafrost zones, and is classified as Ecosystem-protected. Nine of the ten permafrost sites had permafrost that was thinner than the 14 or 7 m penetration depth of the ERT survey (three-layer system consisting of an active layer, permafrost, and sub-permafrost perennially unfrozen zone). The most predictable results were achieved at the two-layer system site (active layer overlying permafrost to the base of the profile) in each of its virtual resistivity boreholes, relative resistivity change comparisons, and mean near-surface apparent resistivity progressions.

ERT is an effective method of delineating permafrost boundaries in thin permafrost environments and does show strength when monitoring areas of seasonally frozen ground. Repeat surveys at a site indicate seasonal changes in three-layer conditions, but not as predictably as those in a two-layer system. In order to receive the most accurate information regarding permafrost extent and thickness, it appears ideal to conduct ERT surveys annually, within the same month as the previous year's survey.

ACKNOWLEDGEMENTS

This project would not have been possible without the financial support from the Royal Canadian Geographical Society's Expedition of the Year Award (which was financed by the Royal Bank of Canada's Blue Water Project), the Natural Sciences and Engineering Research Council of Canada, Aboriginal Affairs and Northern Development Canada's Northern Scientific Training Program, the Geological Survey of Canada, and the Faculty of Arts, University of Ottawa.

In addition to financial support, this project would not have been possible without emotional and intellectual guidance from many individuals. I must thank my supervisor, Antoni Lewkowicz, for sharing his knowledge, time and energy with me during this processes. Max Duguay, Alex Bevington and Graham Pope all provided excellent field assistance in the sun, snow, and rain.

There were numerous faculty, staff, and students within the University of Ottawa who I gained guidance and insight from. Although this list is far from comprehensive, I must thank Philip Bonnaventure, Sam Darling, Lothar Schrott, and Megan James.

I would also like to thank my amazing family, especially my partner, Graham. Without their love and support this process would have been much harder. Graham provided some much needed help during the editing process.

Lastly, I would be remiss if I did not mention the people I met during the over 100 days I spent in southern Yukon and northern British Columbia. Their friendliness, curiosity, and the occasional free battery charge were always appreciated.

TABLE OF CONTENTS

LIST OF FIGURES

LIST OF TABLES

1.0 INTRODUCTION

1.1 General

Permafrost, ground that remains below 0 °C for a minimum of two years consecutively, is the largest element of the cryosphere in areal extent (Intergovernmental Panel on Climate Change [IPCC] 2007). Approximately 22% of the world falls into a permafrost zone, and approximately 50% of Canada is within a permafrost zone (Brown et al. 1997; NRCan 2007). Permafrost thickness and distribution is widely controlled by climate (Lewkowicz et al. 2012; Throop et al. 2012). Global climate is changing, with land north of 60° latitude expected to experience the greatest effects (Arctic Climate Impact Assessment [ACIA] 2005). This change will have a profound effect on permafrost. Global temperatures in most locations around the world are becoming warmer. Although some of these changes can be attributed to short-term variability like the El Niño-Southern Oscillation and inter-decadal Arctic Oscillation, the major contributor is the increasing concentration of greenhouse gases within the atmosphere due to anthropogenic activities (ACIA 2005). From 1906-2005, an increase of 0.74 °C ± 0.18 °C occurred in global mean surface temperatures, and the rate of warming over the last 50 years was almost double that of the last 100 years (IPCC 2007). Land north of 60° latitude has experienced warming of approximately twice the global mean, mostly due to changes in feedback processes (ACIA 2005). This warming occurred predominately within the winter months, having a large effect on all elements of the cryosphere (ACIA 2005). This trend is predicted to continue, with the A2 climate scenario estimating an increase of 3 °C worldwide and of 7 °C for land poleward of 60°N by the end of this century (IPCC 2007).

Permafrost can vary greatly in both temperature (from close to 0 °C, to much lower than -10 °C) and thickness (from a few centimeters to hundreds of meters) (United Nations Environment Programme [UNEP] 2007). Since the effects of shifting climate on permafrost occur meters below the ground surface it is difficult to determine the changes that are taking place. Traditional monitoring methods, such as active layer probing or borehole temperature monitoring, are limited in

their ability to detect small changes in permafrost bodies or provide only one-dimensional perspectives. Frost probing only allows for the identification of the presence or absence of permafrost and active layer thickness, while boreholes are often very costly to drill and the equipment is difficult to mobilize in challenging terrain. New technology is needed in order to understand and monitor the changes occurring with permafrost areas.

Electrical Resistivity Tomography (ERT) (also known as Direct Current (DC) Resistivity Profiling) uses an electrical current passed into the ground to map out an area's resistivity (Loke 1999). This geophysical technique can be employed for detecting permafrost boundaries, and has been used frequently for permafrost investigations in Europe (Kneisel et al. 2000; Hilbich et al. 2009). This technique has potential for investigating changes in thin permafrost as well as the processes of freeze-thaw which are relevant to infrastructure planning.

1.2 Research Objectives and Expected Results

The central objective of this thesis is to determine what changes in thin permafrost and seasonally frozen ground can be detected by ERT over an annual cycle of freezing and thawing. This research forms part of a longer-term project that is attempting to use ERT to examine changes in permafrost resulting from climate change. Little is known about the most effective execution of multiple ERT surveys to monitor long-term changes in thin permafrost, such as the importance of the date of monitoring. This research will provide a clearer understanding of the most effective way to use ERT for this purpose.

To gain better understanding of the effectiveness of ERT monitoring, permanent electrode arrays were set up at ten monitoring sites in August 2010. Inter-site and intra-site variability over the following year were examined by repeated ERT surveys combined with installing and maintaining data-loggers to monitor active layer and shallow permafrost temperatures, air temperatures, and snow depths at each site. Lastly, additional site information was collected at each ERT survey date, including frost table depths, snow depths, and vegetation heights.

Based on the results from a similar project by Hilbich et al. (2011) which took place in mountain permafrost in the Swiss Alps (explained in detail in Section 2.7.2) there are three expected results for this project:

1. The spatial mean apparent resistivity should be at its minimum in the August 2010 surveys for all sites due to the complete thaw of the active layer.
2. There should be visible differences in apparent resistivity values within the active layer between surveys, which represent the effects of when the active layer is deeply thawed (August), when it is frozen (March), and when there are transitions between these two states (May, June, July).
3. The inverted resistivity relative percent change based on the first survey (August 2010) should show maximum change in the near-surface in the March survey due to the changes in active layer thickness.

Overall, the results received from all the surveys should be valuable for permafrost and climate research.

1.3 Structure of the Thesis

The thesis is divided into the following seven sections.

Section One	-	Introduction	Provides a general overview.
Section Two	-	Background	Outlines the background information of permafrost dynamics and ERT monitoring.
Section Three	-	Study Area	Describes the study area and the specific climate and environmental characteristics.
Section Four	-	Methods	Describes the methodology necessary to conduct the research project.
Section Five	-	Results	Presents the results of the research.
Section Six	-	Discussion	Discusses and analyzes the data collected
Section Seven	-	Conclusion	Presents concluding thoughts on the project

2.0 BACKGROUND

2.1 Permafrost Classification

Permafrost is classified into specific zones based on the percentage of land which it underlies. Permafrost that underlies more than 90% of the landscape, with typically only deep rivers and water bodies not underlain, is classified as continuous (ACIA 2005; French 2007; UNEP 2007). Areas with less than 90% but more than 10% are classified as discontinuous, although there are definitional differences within the literature relating to the percent boundary between extensive discontinuous and sporadic discontinuous permafrost. Heginbottom et al. (1995) and Brown et al. (1997) define the sporadic discontinuous zone as 10% to 50%, while the ACIA (2005) defines it as 10% to 30%. Areas with permafrost occupying less than 10% of the landscape are classified as isolated patches (ACIA 2005; French 2007; UNEP 2007). In areas where permafrost is only present in small islands of peaty or silty soil, Zoltai (1971) has used the term localized (French and Egorov 1998). Without specific area testing, however, the identification of these localized islands is difficult (French and Egorov 1998).

Climate in an area can be favourable, neutral, or unfavourable to permafrost (Shur and Jorgenson 2007). However, as indicated above, present and past climate conditions are rarely identical, and an area that was once favourable can now be neutral or unfavourable. In these cases, permafrost can either disappear, or remain in the landscape due to other environmental factors (Shur and Jorgenson 2007). Determining the southern limit of permafrost can be difficult because permafrost is present in some locations and not in others, due to balance between an area's climate and ecosystem conditions (Shur and Jorgenson 2007).

Shur and Jorgenson (2007) distinguish permafrost based on factors that allow for its development and sustainability. Climate-driven permafrost is controlled entirely by climate, and newly exposed land can develop permafrost rapidly. Climate-driven, ecosystem-modified permafrost is formed by climatic conditions, but becomes less reliant on climate for its continued existence due to vegetation succession in the area. Climate-driven, ecosystem-protected permafrost is formed by

past climate conditions, but can withstand climate warming due to its ecosystem properties. These areas are usually covered by mosses and peat, and are generally permafrost neutral. Ecosystem-driven permafrost forms under heavy ecosystem influence and only in certain parts of the landscape, such as north-facing slopes and peatlands. These areas are less favourable for permafrost and human activity or forest fire would permanently thaw them. Lastly, Ecosystem-protected permafrost has similar characteristics to Ecosystem-driven permafrost, but occurs where mean annual air temperatures (MAATs) are 2 °C to -2 °C. Climate warming that results in increases above this range will eventually cause these areas to thaw.

2.2 Thermal Dynamics of Permafrost

The strongest control on permafrost existence at the macro-scale is climate (Lewkowicz et al. 2012; Throop et al. 2012). However, the climate-permafrost relationship is complex and hard to quantify (Smith and Riseborough 2002).

In equilibrium conditions, the climate-permafrost relationship is frequently described by using the mean annual temperatures at three different levels (Smith and Riseborough 1996). These are the mean annual air temperature (MAAT), mean annual ground surface temperature (MAGST) and the temperature at the top of permafrost (TTOP) (Smith and Riseborough 1996; Smith and Riseborough 2002). When no permafrost is present, the mean temperature at the depth of zero annual amplitude is used in substitution for the TTOP value.

The MAAT represents the effect that regional climate has on a location (Smith and Riseborough 1996). The MAAT is also a representation of the heat exchange that is occurring within an area (Smith and Riseborough 1996).

In contrast, the MAGST and the TTOP reflect not just the regional climate, but the local area characteristics (Smith and Riseborough 1996; Smith and Riseborough 2002). These local characteristics are described in further detail in Section 2.4. The TTOP is measured at the base of the active layer, but is independent of active layer thickness (Smith and Riseborough 1996). The active

layer is defined as that layer which freezes in winter and thaws in summer (French 2007). This TTOP value remains fairly constant since the ground below the active layer does not undergo significant phase change (Smith and Riseborough 1996). This characteristic keeps the soil thermal properties constant, therefore keeping the temperature fairly consistent. Monitoring the active layer thickness is not an indicator of TTOP change; an increase in active layer thickness does not necessarily mean an increase in permafrost temperatures (Smith and Riseborough 1996).

Another common annual measurement is the mean annual ground temperature (MAGT). This value is measured at the depth of zero annual amplitude (Smith and Riseborough 2002). At this depth, seasonal variations no longer affect the ground temperature, which therefore remains constant over the short term (Williams and Smith 1989). The depth of zero annual amplitude occurs at 10 to 15 m in soil, but can be much greater in bedrock sites (Williams and Smith 1989). The MAGT is usually 0.2 to 0.4 °C higher than the TTOP value due to the geothermal gradient (Smith and Riseborough 2002). The geothermal gradient is the result of the earth's internal heat moving towards the surface (Williams and Smith 1989).

2.2.1 Surface and Thermal Offsets

Under equilibrium conditions the annual air temperature and the relationship between annual air temperature and ground temperature dictate the presence and thickness of permafrost. The surface offset is the difference between the MAGST and the MAAT:

$$\text{Surface Offset} = \text{MAGST} - \text{MAAT}$$

The surface offset is mainly affected by the amount and duration of snow cover (Smith and Riseborough 1996; Smith and Riseborough 2002). The effects of snow cover are discussed in Section 2.4. In addition, the surface offset is also affected by vegetation, moisture availability and the presence or absence of permafrost (Smith and Riseborough 2002; Karunaratne and Burn 2004). The thermal offset is the relationship between TTOP and MAGST:

$$\text{Thermal Offset} = \text{TTOP-MAGST}$$

The thermal offset is dependent on the ratio of thermal conductivities of the active layer (defined in Section 2.3) when frozen and unfrozen, and on the thawing degree days (Section 2.2.2) (Smith and Riseborough 1996; Smith and Riseborough 2002; French 2007). In areas of solid bedrock the thermal offset is close to zero, but typical values are usually between -0.6 ºC to -0.9 ºC for mineral soils (Smith and Riseborough 2002). Areas in peaty soils can have values between -0.3 ºC to -1.0 ºC, depending on the saturation level (French 2007). It should be noted that the thermal offset is normally considered only in relation to permafrost that is in equilibrium. Permafrost that is in the process of warming or thawing could exhibit a thermal offset larger than predicted by the ratio of thermal conductivities (Smith and Riseborough 2002).

2.2.2 Degree Days

Degree day sums are useful indices to describe the temperature range of a particular site. The freezing degree days total (DDF) is the sum of the daily mean temperatures below 0ºC during the freezing season. The thawing degree days total (DDT) is the sum of the daily mean temperatures that are above 0 ºC during the thawing season (Klene et al. 2001). Degree days are calculated for the surface (DDT_s) and the air (DDT_A) (Klene et al. 2001). These degree day values are used to calculate n-factors.

2.2.3 N-Factors

Lunardini (1978) quantified the effect of local factors on permafrost with the use of n-factors. N-factors are ratios of thawing and freezing degree day sums, for both thawing and freezing seasons. The thawing n-factor (n_t) and freezing n-factor (n_t) are defined as:

$$n_t = \frac{DDT_S}{DDT_A}$$

$$n_f = \frac{DDF_S}{DDF_A}$$

N-factors range from zero to greater than unity. The ratio of air to ground temperatures for both the thawing and freezing seasons reveals the effects of both vegetation and snow cover (Smith and Riseborough 1996). The thawing n-factor is predominantly affected by vegetation, which can reduce heat flux into the ground through interception of solar radiation and shading (Smith and Riseborough 1996; Shur and Jorgenson 2007). Heat penetration is directly related to a soil's thermal diffusivity, therefore soil with a high thermal diffusivity will have a higher n_t (French 2007). Vegetation can also trap blowing snow, allowing a thicker snow cover to accumulate (Smith and Riseborough 2002). The freezing n-factor characterizes the effect of snow cover, substrate, and moisture content conditions in an area (Smith and Riseborough 2002; Throop et al. 2012). For any given snow depth, the n_f value increases as the MAAT decreases (Smith and Riseborough 2002). In addition to revealing the factors affecting a specific site, n-factor values can also be used to estimate ground surface temperatures in areas where data cannot be collected.

2.3 Thermal Dynamics of the Active Layer

The active layer is defined as the ground above permafrost that freezes and thaws each year. This layer can extend to depths greater than 3 m into the ground (Williams and Smith 1989). Due to the complexities of freezing and thawing in the active layer, different phase regimes occur during an annual cycle. During the winter freezing regime the ground in the active layer is completely frozen (Outcalt and Hinkel 1996). When higher air temperatures occur in the early spring the snowmelt

regime begins (Outcalt and Hinkel 1996). After the snow cover has disappeared the active layer thaw regime occurs during the spring and summer (Outcalt and Hinkel 1996). During the fall, when air temperatures begin to decrease, the ground within the active layer begins to freeze and the start of the zero curtain (defined in Section 2.3.3) regime begins (Outcalt and Hinkel 1996).

In any given area, the active layer's seasonal cycling at a site is mostly dependent on the soil's moisture content and thermal conductivity (French 2007).

2.3.1 Moisture Content

Water in soil pores can be frozen or unfrozen. Soils with smaller soil particles, such as clays and silts, have the highest porosity. These soils have bulk water, which exists in the middle of the soil pores, and water is attracted to the soil particles due to adsorption and capillarity (Williams and Smith 1989; French 2007). The bulk water has a freezing point that is close to 0 °C (Williams and Smith 1989; French 2007). When soil is cooled, the purest water within the centre of the pore space freezes first (Williams and Smith 1989; French 2007). This freezing confines the unfrozen water to progressively less space, which is referred to as cryosuction (Williams and Smith 1989). Lower temperatures are required for the remaining unfrozen moisture to change phase (Williams and Smith 1989; French 2007). Therefore, there is unfrozen moisture content in soils at temperatures of less than 0 °C (Williams and Smith 1989; French 2007). Soils with smaller pore spaces will have a higher unfrozen moisture content than those with larger pore spaces at the same temperature. This relationship is illustrated in Figure 1, which shows the unfrozen moisture content of different soils over a range of sub-zero temperatures.

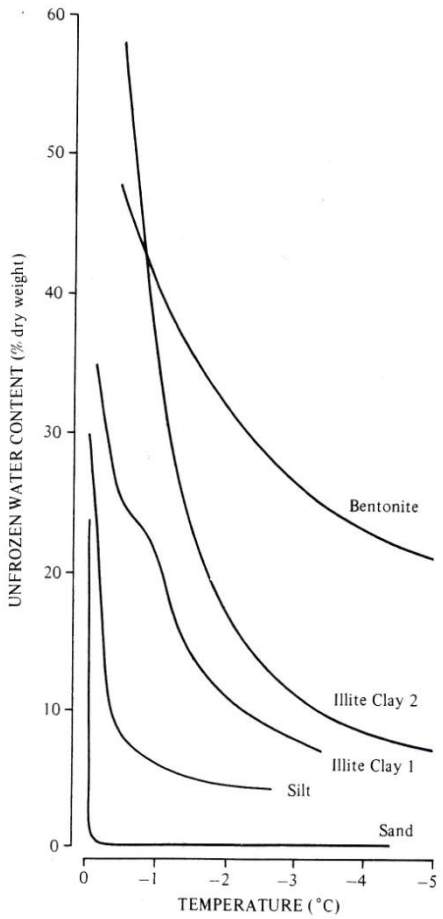

Figure 1 - Soil freezing characteristic curve for various soil types (Williams and Smith 1989)

2.3.2 Thermal Conductivity

In addition to moisture content, the thermal conductivity of a soil affects the freeze-thaw cycle of the active layer. Thermal conductivity is the ability of a soil to transfer heat through conduction. Materials with high thermal conductivities (e.g., granite) will be more responsive to thermal gradients than materials with low conductivity values (e.g., dry peat) (French 2007).

2.3.3 Latent Heat and the Zero Curtain Effect

The zero curtain regime occurs when the active layer is undergoing the zero curtain effect. The zero curtain effect is a condition that maintains soil temperatures at just below 0 ºC (Outcalt and Hinkel 1996) and can occur in both the spring and fall seasons. In the fall season when ground begins to freeze, the process releases latent heat into the unfrozen soil, which offsets the colder air temperatures and temporarily prevents the soil from reaching temperatures less than approximately -

2 °C (French 2007). The temperature value at which the ground temperature pauses is dependent on the initial freezing point and the freezing curve of the soil water (Williams and Smith 1989). Eventually a large portion of the water within the active layer freezes, which then allows the ground temperatures to decrease more rapidly (Williams and Smith 1989). In the spring a zero curtain can occur due to the melting snow water seeping into the ground and freezing due to the cold ground temperatures.

The zero curtain effect is affected by air temperature, soil moisture, and snow cover. Very low air temperatures cause the zero curtain effect period to end quickly. At sites with no moisture content (such as massive igneous bedrock) there is no zero curtain effect (Williams and Smith 1989). A late snowfall that occurs after a prolonged period of low air temperatures allows the active layer to freeze more quickly in the fall, resulting in a short or absent zero curtain effect (Outcalt and Hinkel 1996).

2.4 Local Factors Affecting Thermal Dynamics

Factors at the local scale may have a larger effect on the thermal conditions of permafrost and the active layer than the overall climate (Smith and Riseborough 1996; French and Egorov 1998). These factors include snow cover, vegetation, relief, rock type, forest fires, and water bodies (French 2007).

Snow cover can have a large effect on the thermal dynamics of permafrost and seasonally frozen ground due to its low thermal conductivity and presence only during the colder part of the year. For density values of 100 to 400 kg m^{-3} snow has a thermal diffusivity of approximately 0.01 $m^2\,day^{-1}$ (Williams and Smith 1989). Thermal diffusivity is the thermal conductivity of a substance divided by the product of its density and its specific heat capacity (Williams and Smith 1989). In comparison, the thermal diffusivity of frozen ground is approximately 0.1 $m^2\,day^{-1}$, or ten times greater than snow (Williams and Smith 1989). It is this quality that prevents low air temperatures from penetrating through to the ground surface when snow cover is present (Williams and Smith

1989). Thick snow cover also restricts heat from escaping from the ground, limiting the frost penetration during the winter (Smith and Riseborough 1996). This effect raises the MAGT, and can be the principal reason for the surface offset (Williams and Smith 1989). If an area has a MAAT that is close to 0 °C a seasonal snow cover may be the most important factor for permafrost presence (Zhang 2005).

In addition to a low thermal diffusivity, snow has a high albedo, which is the characteristic of reflecting a large proportion of solar energy (Smith and Riseborough 1996; Zhang 2005; Gądek and Leszkiewicz 2010). Values typically range from approximately 60% to 85%, but can be even greater than 90% under certain weather conditions (Zhang 2005). These high values prevent the snow cover from absorbing much solar energy, thereby slowing snowmelt (Zhang 2005).

When snow cover is present on permafrost with an organic layer over fine-grained soil, the ground surface temperature has a slower decrease of temperature into the winter (Goodrich 1982). This pattern is mirrored in the spring when there is a slower increase in temperatures (Goodrich 1982). Additionally, the minimum ground temperature is much higher than in an area with no snow cover and identical soil conditions (Goodrich 1982). The increased ground temperature allows the ground to experience a deeper thaw depth in the summer and autumn months (Goodrich 1982).

There are certain factors that change the effect that snow cover has on permafrost. The early onset of snow cover can drastically delay or even eliminate the freezing of the ground surface (Goodrich 1982). An early onset of snow can cause the degradation of permafrost (Williams and Smith 1989). However, a thin snow cover in autumn allows heat to flow out of the ground (Ishikawa 2003). For example, an area of permafrost with a maximum snow depth of 50 cm will have a deeper thaw depth and higher mean annual ground surface temperature than an area with half of this snow depth (Goodrich 1982).

The dynamics of snow cover on seasonally frozen ground have not been as thoroughly investigated as the effects of snow cover on permafrost areas (Zhang 2005). A characteristic that is unique to seasonally frozen ground is the potential for snow cover to increase the moisture content in

a soil. During the spring snow melt the snow cover prevents the ground from freezing if temperatures decrease rapidly, allowing water to percolate through the ground from the melting snow (Zhang 2005). Similarly, some ground may begin to freeze before the first snowfall, or before the first substantial snowfall, allowing the frost to penetrate into the ground (Zhang 2005). The frozen ground may decrease in thickness or disappear entirely if a substantial snow cover eventually arrives: heat from the unfrozen ground is prevented from entering the atmosphere and is used instead to thaw the previously frozen layer near the surface (Zhang 2005). In general, the effects of timing and depth of snow cover appear to have very similar impacts on seasonally frozen ground and permafrost (Goodrich 1982).

2.5 Permafrost and Global Warming

In Western North America, permafrost temperatures have almost all increased at almost all monitoring borehole sites over the last 20-30 years (Smith et al. 2010). This warming trend has been more rapid at colder permafrost sites than at warmer ones (Smith et al. 2010). In the sporadic discontinuous zone, permafrost is limited to organic terrain, and has temperatures close to 0 °C (Smith et al. 2010). This warm permafrost, although generally remaining below 0 °C, is already undergoing internal thaw (Smith et al. 2010).

Permafrost thaw can have profound effects in an area (UNEP 2007). Increased thaw depth can cause active layer detachments, destroying local vegetation and effecting the topography (UNEP 2007). The thawing of ice-rich permafrost can cause pitted relief and lake development, thereby altering the surface drainage of an area (UNEP 2007). This drainage alteration can lead to other changes in the ecosystem, including changes in wildlife presence. Permafrost thaw can also affect human development. Because frozen saturated ground is substantially stronger than unfrozen soil, ground subsidence can impact infrastructure, including buildings, buried utilities and transportation routes.

A decrease in permafrost area can also further contribute to global climate change. It is estimated that there is approximately 1672 Pg of organic carbon stored within permafrost in the northern hemisphere (Tarnocai et al. 2009). When permafrost thaws, methane and carbon dioxide can be released into the atmosphere, increasing greenhouse gas concentrations. The Intergovernmental Panel on Climate Change (IPCC) has not considered the release of soil organic carbon in its climate change scenarios (Kuhry et al. 2010).

2.6 Previous Research

In 1964 R.J.E. Brown executed a permafrost investigation from British Columbia, north of 56° N, to the Yukon, south of 65° N. This investigation took place in late summer, when seasonal thaw is at its deepest. Approximately 90% of the sites were between Whitehorse, Yukon and Fort St. John, B.C. (Brown 1967). The sites were all close to the Alaska Highway in order to facilitate access in the mountainous terrain (Brown 1967). Permafrost was found at 55% of the sites visited, and was generally within poorly drained, north-facing slopes (Brown 1967). Vegetation in these permafrost areas usually included a thick ground cover of Sphagnum, lichen, Labrador tea (*Rhododendron groenlandicum*), and scattered black spruce (P*icea mariana*) and tamarack (*Larix laricina*) (Brown 1967; Wahl et al. 1987).

In 2007 and 2008, James (2010) located 55 of the 86 sites Brown identified as having permafrost between Whitehorse, Yukon and Fort St. John, B.C. These sites were re-examined in late summer to determine if near-surface frozen ground was present in order to quantify the change in permafrost distribution (James 2010). From 1965-2008, climate in the area had warmed at a rate of 0.4 to 0.5 °C per decade (James 2010). As a result of this warming, half of the sites no longer had permafrost present within 2 m of the ground surface (James 2010). Most sites (81%) that no longer had permafrost present were in the southern section of the study area between Fort Nelson and Fort St. John. These observations indicate that the southern limit of permafrost in the study region had shifted approximately 75 km north.

In September 2008 ERT surveys (described in Section 2.7) were conducted at three sites used by both Brown and James (Mile Post [MP] 788.5, MP 825.2, and MP 844.1) (Lewkowicz et al. 2011). These surveys, in combination with temperature data, were used to infer permafrost thickness at these sites (Lewkowicz et al. 2011). Permafrost did not exceed 15 m in depth and at most places along the resistivity profiles it was much thinner (Lewkowicz et al. 2011). Additionally, the permafrost bodies within the surveys coincided with frost table presence examined by probing conducted at the sites and with site topography. Mean TTOP for both MP 825.2 and MP 844.1 was 0 °C (Lewkowicz et al. 2011). These sites also had large thermal offsets. If the MAAT at these sites were to rise by approximately 3 °C, the permafrost would actively degrade (Lewkowicz et al. 2011). Another possibility is that the presence of permafrost at these sites is what is creating these large thermal offsets (Lewkowicz et al. 2011). Regardless of the scenario, the permafrost at these three sites can be classified as Ecosystem-protected.

2.7 Electrical Resistivity Tomography

Electrical Resistivity Tomography (ERT) is a geophysical technique that is particularly effective for investigating permafrost (Hauck and Kneisel 2008). An electrical current is passed into the ground through two electrodes, and the resulting voltage is measured at two other electrodes (Loke 1999). From this measurement, the apparent resistivity (p_a) can be calculated as follows:

$$p_a = \frac{kV}{I}$$

where k is the geometric factor, V is voltage and I is current(Loke 1999). When a series of electrodes are used to measure resistivity along a linear transect, a two-dimensional subsurface survey can be acquired (Hilbich et al. 2008). Two-dimensional electrical imaging can take into account both horizontal and vertical changes in the subsurface (Loke 2011). Therefore, a two-dimensional survey allows for, among other things, the determination of information on advancing and retreating freezing fronts (Hauck 2002).

Electrodes can be placed in different arrays in order to be effective at detecting different subsurface structures. When constructing a 2-D electrical profile it is assumed that resistivity does not change perpendicular to the survey line (Loke 2011). For areas of permafrost bodies this assumption is usually reasonable (Loke 2011). Although 3-D resistivity surveys allow for a more complete picture of the subsurface, they require more time and money in order to be undertaken (Loke 2011).

The Wenner array has become widely accepted as the most effective in surveying permafrost bodies (Hauck et al. 2003). As seen in Figure 2, the sensitivity plot of a Wenner array shows contours that are almost horizontal in the centre of the plot. Therefore, a Wenner array is most sensitive to vertical resistivity changes within the centre of a survey (Loke 1999; Loke 2011). Hence, horizontal subsurface structures, such as permafrost, are more likely to be identified (Loke 1999).

The sensitivity plot also shows areas of low sensitivity values near the surface of the plot. This results in an underestimation of resistivity values if a high resistivity body is present within this area (Loke 2011). The converse occurs in areas of high sensitivity (Loke 2011).

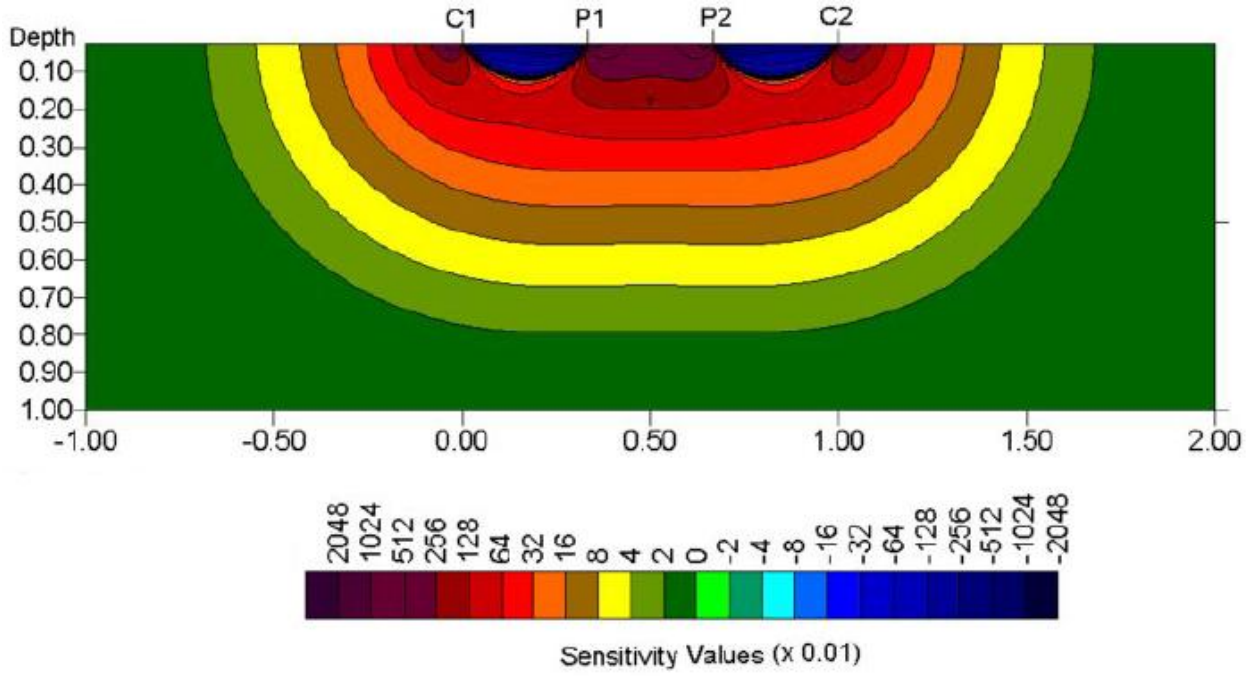

Figure 2 – Wenner array sensitivity plot (Loke 2011).

The Wenner array has the smallest geometric factor of any array (Hauck et al. 2003). The geometric factor is inversely proportional to signal strength, so Wenner arrays are able to penetrate to greater depths (Loke 1999). However, when electrode spacing is increased, this array obtains very low horizontal coverage, meaning no data will be collected in the lower areas under the edges of the array (Loke 1999).

The successful use of ERT investigations relies on the range of known resistivity values for different earth materials (Hauck and Kneisel 2008). If the material can be identified based on its resistivity value, subsurface conditions in an area can be determined. However, different materials can have overlapping resistivity values, allowing for a range of interpretations (Table 1).

Table 1 - Resistivity values for different earth materials (Hauck and Kneisel 2008)

Material	Range of Resistivity (Ωm)
Clay (unfrozen)	1-100
Sand (unfrozen)	100 - 5×10^3
Gravel (unfrozen)	100 - 4×10^3
Granite (unfrozen)	5×10^3 - 10^6
Gneiss (unfrozen)	100 - 10^3
Schist (unfrozen)	100 - 10^4
Groundwater	10-300
Frozen sediments (ground ice, mountain permafrost)	$1 \times 10^3 – 10^6$
Glacier ice (temperate)	$10^6 – 10^8$
Air	Infinity

There are many factors that affect the resistivity of a material, including lithology and texture. However, there are also factors that are not dependent on the host material, including the chemical properties of the pore water, water saturation, and pore volume temperature (Hauck and Kneisel 2008). These ‘outside factors’ are all related to water content, making it a very important control on resistivity values (Hauck and Kneisel 2008). When water becomes frozen its resistivity increases dramatically (Hauck et al. 2003). This increase in resistivity is due to the decrease in electrical conduction that occurs when the ions in water are frozen. In most materials, as the quantity of unfrozen moisture decreases, the resistivity increases almost exponentially (Kneisel et al. 2008).

Due to the strong relationship between unfrozen moisture content and resistivity, permafrost bodies can be identified without excavation. Assuming lithology, pore space, and electrode coupling remain constant, changes in resistivity can be attributed to changes in unfrozen moisture content (Hilbich et al. 2008).

2.7.1 Resistivity Post-Processing

Post-processing, using computer software to invert the data, is necessary in order to convert the apparent resistivity values measured in the field to "true" resistivity values. One of these inversion programs is RES2DINV. When the apparent resistivity plot is loaded into RES2DINV it is called the pseudosection. The pseudosection is only used for a preliminary view of the data and to look for points that may need to be eliminated because they are unrealistic (Loke 2011). Once unrealistic data points have been eliminated, the inversion can take place.

The relationship between apparent and true resistivity is quite complex (Loke 1999). The majority of resistivity surveys are undertaken by people that are not knowledgeable in geophysical inversion theory (Loke 1999). Programs such as RES2DINV attempt to simplify this process by allowing only minimal input by the user (Loke 1999). In RES2DINV a cell-based method is used to invert resistivity data, therefore there are model parameters and model data. The former are the resistivity values of the model blocks, and the data are the measured apparent resistivity (Loke 1999). For one apparent resistivity profile there can be several calculated resistivity results (Loke 1999). These possible multiple results are due to the additional constraints that can be modified during the inversion process (Loke 1999). Several iterations of the inversion model are necessary in order for the difference between the observed data and model response to be reduced (Loke 2011). For subsurface areas with homogenous bodies surrounded by sharp boundaries, such as permafrost, a robust inversion method is used (Loke 2011). Lastly, topography is another parameter which can be added to a profile in order to gain a better perspective on the subsurface characteristics (Hilbich et al. 2008).

2.7.2 ERT Monitoring

Executing multiple ERT surveys along the same profile allows permafrost changes to be monitored. In addition, conducting these multiple surveys using different survey intervals can reveal different subsurface properties. For example, annual surveys can allow for the identification of long-term resistivity changes due to changes in climate (Noetzli et al. 2008). Additionally, seasonal or monthly surveys can identify the active layer and other ice-free zones, as well as the time of year with maximum resistivity change (Hauck 2002; Noetzli et al. 2008).

The introduction of automated ERT (A-ERT) measurements has proven to be extremely useful in areas of alpine permafrost where frequent visits are difficult to achieve (Hilbich et al. 2011). In Hilbich et al. (2011), more than one resistivity survey was conducted daily for a complete year at the Schilthorn monitoring station in the Swiss Alps. The maximum active layer thickness at this site was 5 m, with permafrost at least 100 m thick based on borehole investigations (Hilbich et al. 2011).

For each survey conducted, the apparent and inverted resistivities were analyzed. The spatial mean apparent resistivities were at their minimum from August to October, when active layer thickness was at its maximum. The maximum apparent resistivities occurred from March to May when the active layer was frozen. The inverted resistivity percent change was calculated for monthly intervals based on the first survey conducted on April 4. In the near-surface, the greatest percent change occurred between April and May due to infiltrating meltwater. At greater depths (approximately 10 m) the greatest percent change occurred between May and August/September during maximum active layer thickness and January, the beginning of winter. The high frequency of surveys allowed for certain stages of the freeze-thaw cycle to be recorded, such as the start of the thaw season and the beginning of the zero curtain effect (Hilbich et al. 2011). This method of conducting high frequency surveys showed great potential for increasing the understanding of freeze-thaw processes, and was proven to be both consistent and useful in terms of the two-dimensional profiles (Hilbich et al. 2011).

2.7.3 Electrical Resistivity Tomography Weaknesses

ERT has two notable areas of weakness associated with field work. Firstly, the resolution of a resistivity profile can be either large or small, depending on the distance between the electrodes. Surveys with large distances between electrodes are less effective at identifying small subsurface features or a thin active layer but penetrate more deeply, while lesser spacing provides more detail but shallower penetration depth. Secondly, in order to receive accurate resistivity measurements, good coupling must occur between the electrode and the ground. This relationship becomes an issue in coarse, rocky terrain, such as rock glaciers (Vonder Mühll et al. 2002). In these areas additional steps need to be taken to ensure good contact, including attaching sponges soaked with salt water to the bottom of the electrodes (Vonder Mühll et al. 2002). Without good electrical contact, noise can be introduced to the resistivity profile (Hilbich et al. 2009).

Post-processing of resistivity data can also lead to potential problems. Inversion of the field data may cause artefacts, which are areas of the resistivity profile with low accuracy (Hilbich et al. 2009). This problem can be amplified when taking multiple surveys within the same location because different artefacts can occur in different surveys. These artefacts may be incorrectly identified as resistivity change (Hauck and Kneisel 2008).

It is these weaknesses, along with the weakness associated with field work, which demonstrate that ERT is not meant to replace conventional thermal monitoring, but to complement it. Resistivity profiles can be more easily interpreted if ancillary data are present. Ancillary data include temperature data, ground penetrating radar, surveys or frost probing.

3.0 STUDY AREA

3.1 Physical Location

The study area is located along approximately 1,200 km of the Alaska Highway between Whitehorse, Yukon and Fort St. John, British Columbia. This area is within the sporadic discontinuous and isolated patches permafrost zones (Heginbottom et al. 1995). Permafrost within this area was most likely formed within the Little Ice Age, roughly 300 to 500 years ago (Vitt et al. 1994; Zhang et al. 2006). During the Little Ice Age, temperatures within the areas are estimated to have been 1 °C colder than at present (Vitt et al. 1994). Figure 3 shows the ten sites and the major communities within the study area. All sites are numbered by the nearest historic Mile Post. The sites are all located less than 500 m off the Alaska Highway, with the exception of MP 178.0, which is located on a year-round accessible side road.

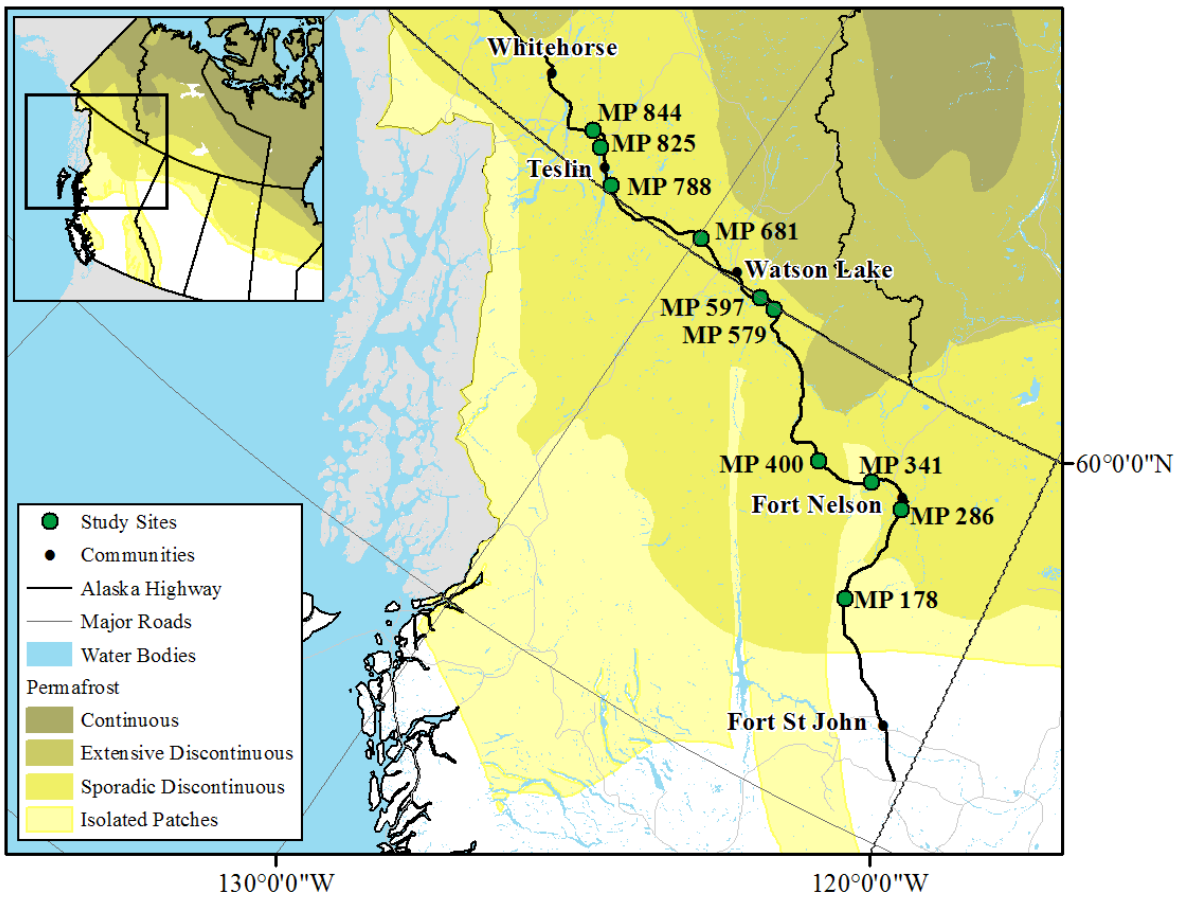

Figure 3 – Study sites along the Alaska Highway in relation to permafrost zones (Heginbottom et al. 1995).

3.2 Climate

The study region is located within the Boreal Cordillera ecozone (Parks Canada 2003; Smith 2004). This area is characterized by long, cold winters and short warm summers (Parks Canada 2003). Daily mean January temperatures range from -15 °C to -27 °C, and daily mean July temperatures range from 12 °C to 15 °C (Parks Canada 2003). Precipitation ranges from 400 mm to more than 1500 mm, with lower precipitation values in the intermontane plains and higher precipitation on the mountains in the east (Parks Canada 2003).

The climate of northern British Columbia and the Yukon is greatly influenced by the proximity to the Pacific and Arctic Oceans, as well as variation in both elevation and latitude (Taylor 1997). In general it is these factors, along with the Westerlies, prevailing winds that blow from the west to the east, that produce the known climate patterns in the region (Taylor 1997). During the winter, the jet stream brings warm, Pacific air into southern British Columbia, producing high cloud cover and high levels of precipitation (Taylor 1997).

3.1.1 Climatic Regions

Regional climates in the study area have been examined Taylor (1997) and by Wahl et al. (1987) (Figure 4).

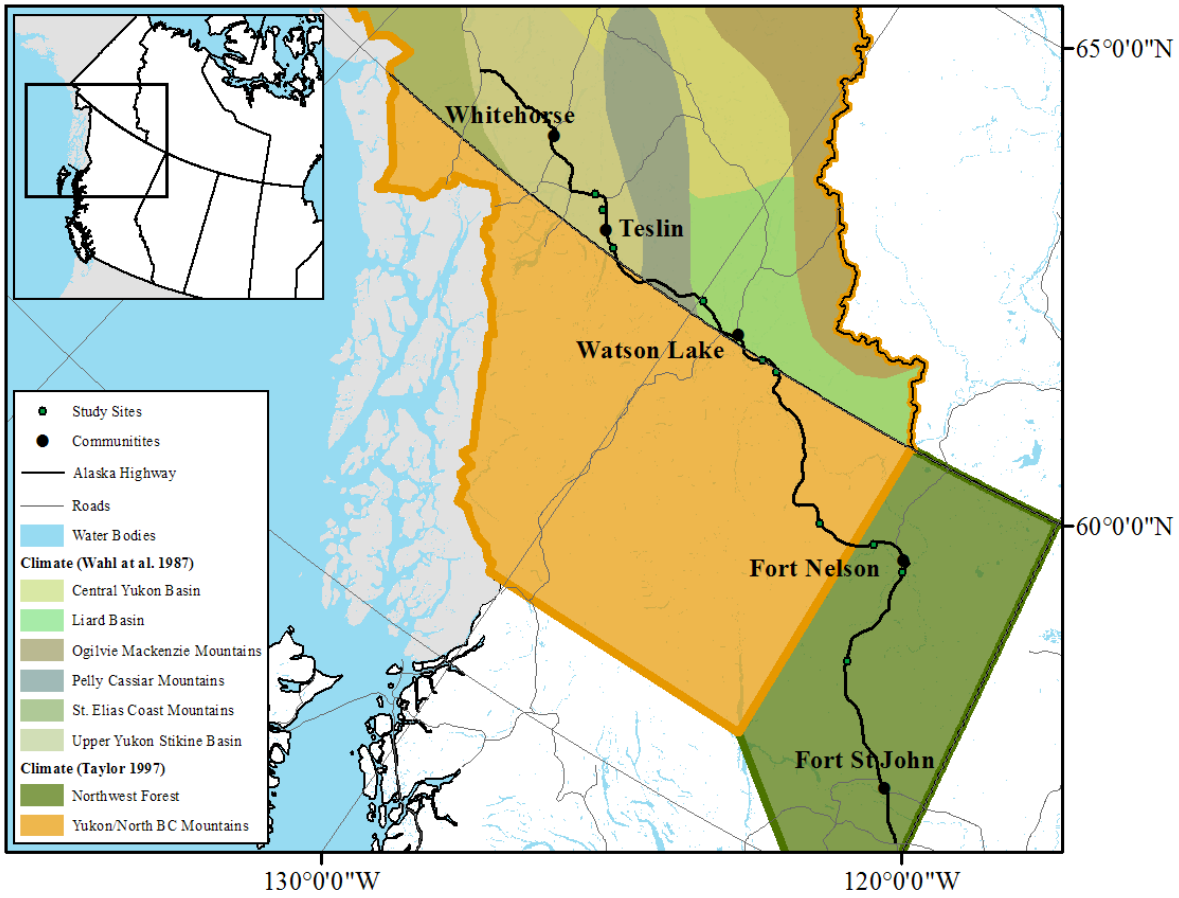

Figure 4 – Climatic regions within the study area (Wahl et al. 1987; Taylor 1997).

According to Taylor (1997), there are two climatic regions within the study area; the Yukon/North BC Mountains, and the Northwestern Forest. The Northwestern Forest encompasses the northeastern portion of British Columbia, including Fort Nelson and Fort St. John. Elevation in this area ranges from 900 to 1200 metres above sea level (m asl). This area has long, cold winters and short summers with high seasonal variation. There is a 40 °C difference between the January daily minimum and the July daily maximum, and annual precipitation is less than 500 mm (Taylor 1997). The Yukon/North BC Mountains region encompasses the entire Yukon and has both mountain and lowland terrain (Taylor 1997). Precipitation is approximately 500 mm annually (Taylor 1997).

Taylor's Yukon/North BC Mountains region is further subdivided by Wahl et al. (1987) into six climate zones, three of which are located in the study area. These are: the Upper Yukon-Stikine Basin, the Pelly-Cassiar Mountains and the Liard Basin.

The Upper Yukon-Stikine Basin climatic region extends from beyond the western edge of the study area to approximately MP 850. This area has relatively high elevations ranging from 600 to 2000 m asl (Wahl et al. 1987). The continental temperature regime provides a temperature range that is less than other climate zones in the area, such as the Liard Basin (Wahl et al. 1987). The St. Elias-Coast Mountains prevent high precipitation values; some areas receive less than 200 mm annually (Wahl et al. 1987). The Upper Yukon-Stikine Basin has the highest wind velocity within the study area with Whitehorse as the most consistently windy location (Wahl et al. 1987).

The Pelly-Cassiar Mountains climatic region encompasses the south-central Yukon and northern British Columbia, from approximately MP 850 to 700 (Wahl et al. 1987). This zone has the highest elevations within the study area with some mountains reaching 2500 m asl. (Wahl et al. 1987). Precipitation values range from 500 to 700 mm with the highest precipitation received during fall and early winter (Wahl et al. 1987). Winter temperatures are less severe due to common mild spells and temperatures remain cool during the summer months (Wahl et al. 1987). This climate zone has relatively light winds (Wahl et al. 1987).

The Liard Basin climatic region encompasses the northeastern portion of the Alaska Highway, including Watson Lake, from approximately MP 700 to 600 (Wahl et al. 1987). The topography is relatively flat, ranging from 700 to 1000 m asl. (Wahl et al. 1987). Precipitation ranges from 400 to 600 mm annually with the majority of it falling as snow (Wahl et al. 1987). The Liard Basin has the highest number of precipitation days within the study area (Wahl et al. 1987). Summers are warm and wind within the area is moderate (Wahl et al. 1987).

3.1.2 Recent Climate Trends

There are four communities within the study area with long-term climate monitoring since the 1940s: Whitehorse, Watson Lake, Fort Nelson, and Fort St. John (Figure 3). The MAAT and five year running mean for each year from 1970 to the present are shown in Figure 5.

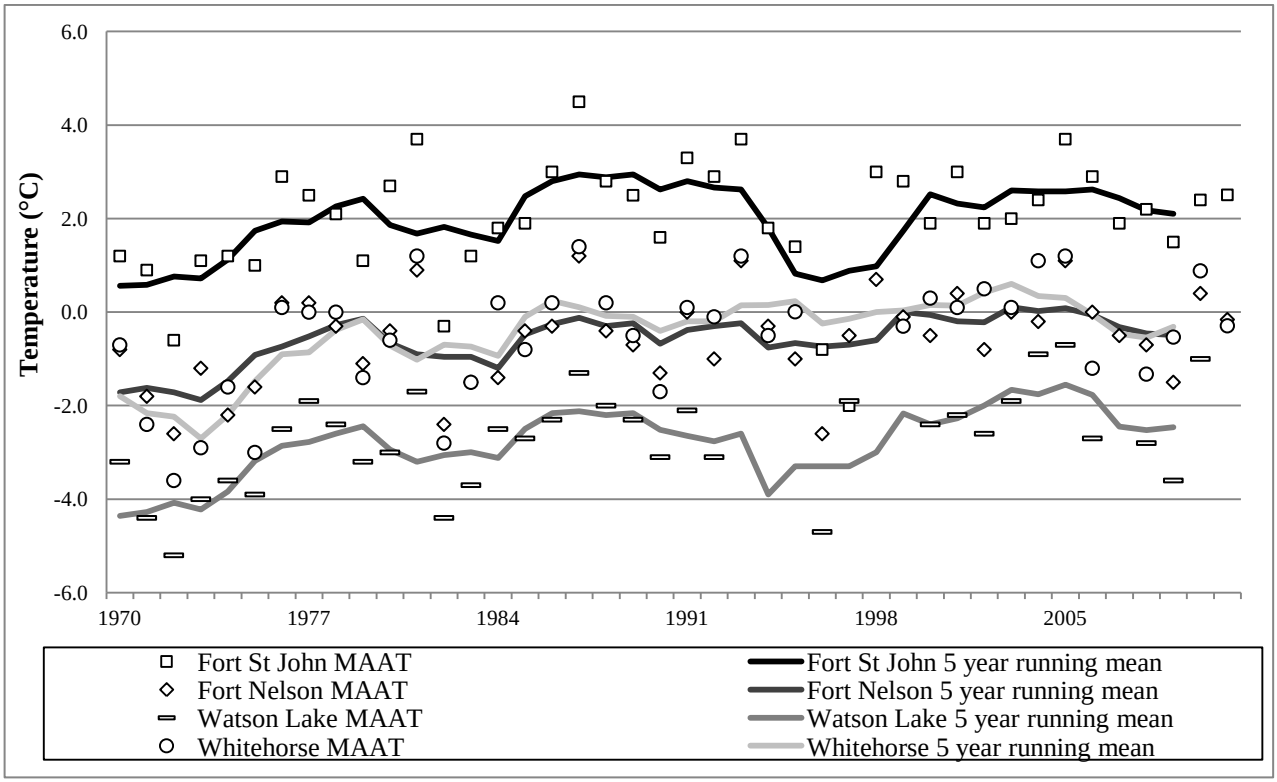

Figure 5 – MAATs (1970-2011) and five year running means (1970-2009) for the major communities within the study area (Environment Canada 2012a).

The five year running means show an increase in temperatures in each community since the 1970s. This trend is reflected in the climate normals, which show an increase of 0.2 to 0.4 °C for each community from the 1961-1990 normals compared to the 1971-2000 normals (James 2010; Environment Canada 2012b; Environment Canada 2012c).

Table 2 displays the Climate Normals for 1971 – 2000 as well as the means for the year of field measurements (September 2010 to August 2011) for the four main communities within the study area (Environment Canada 2012a).

Table 2 – 1971-2000 Climate normals and September 2010 – August 2011 means (Environment Canada 2012a; Environment Canada 2012b).

				1971-2000 Climate Normals			September 2010 – August 2011 Means		
Community	Latitude	Longitude	Elevation (m asl)	MAAT(°C)	Rainfall (mm)	Snowfall (cm)	MAAT (°C)	Rainfall (mm)	Snowfall (cm)
Fort St. John, BC	56°14' N	120°44' W	695	2.0	313	186	1.1	403	275
Fort Nelson, BC	58°50' N	122°36' W	382	-0.7	320	178	-0.8	349	194
Watson Lake, YT	60°72' N	128°49' W	687	-2.9	255	197	-2.2	164	160
Whitehorse, YT	60°42' N	135°04' W	706	-0.7	163	145	-0.8	225	184

The MAAT values for both the climate normals and the 2010-2011 data show that Watson Lake is the coldest community and Fort St. John is the warmest. The 2010-2011 MAAT values were 0.7 ºC warmer than normal in Watson Lake, almost normal in Whitehorse and Fort Nelson and 0.9 ºC colder than normal in Fort St. John. There was higher than normal total precipitation (rainfall and snowfall) in Fort St. John and Fort Nelson and lower than normal precipitation in Watson Lake and Whitehorse.

The differences between the climate normals and 2010-2011 did not occur uniformly over the annual cycle (Figure 6). The study site's seasonality is most accurately described as follows: from September to October is the autumn season, from December to March is the winter season, from April to May is the spring season, and June to August is the summer season.

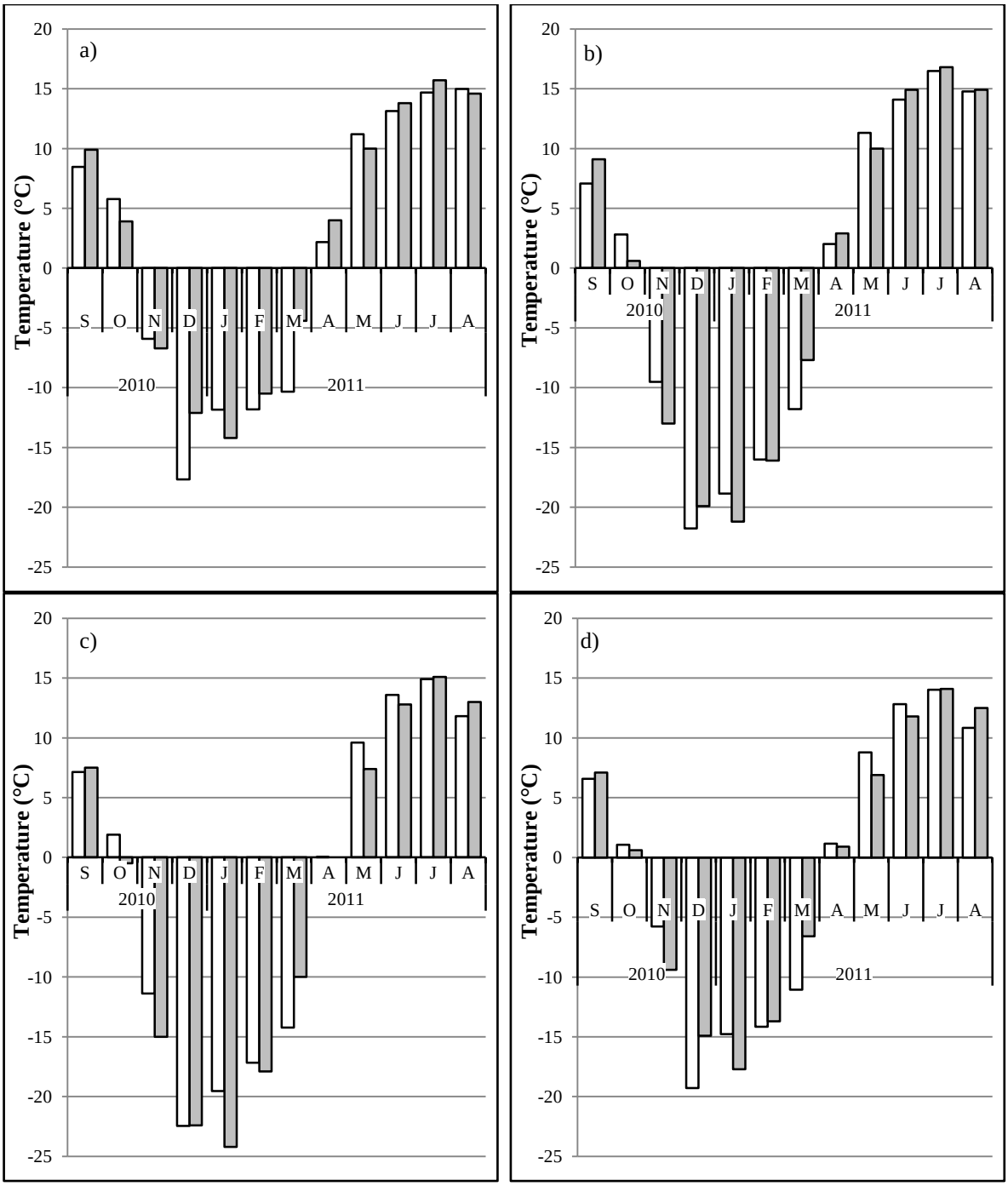

Figure 6 - August 2010-2011 air temperatures (white) and 1971-2000 climate normals (grey) for a) Fort St. John; b) Fort Nelson; c) Watson Lake; d)Whitehorse (Environment Canada 2012a).

Fort St. John (Figure 6a) experienced a mean of 2 °C in absolute temperature differences throughout 2010-2011 when compared to the climate normals. The largest difference occurred in March, when the mean monthly air temperature (MMAT) was 5.9 °C cooler than the month's

normal. This community, on average, had a larger temperature difference in months that were cooler than the normals (2.5 °C) than months that were warmer (1.3 °C). There were seven months that were below normal MMATs and five months that were above. The winter months had the largest mean difference, followed by the fall, spring, and summer seasons.

Fort Nelson (Figure 6b) experienced a mean of 1.6 °C in absolute temperature differences throughout 2010-2011 when compared to the climate normals. The maximum difference occurred in March when 2010-2011 was 4.1 °C cooler than normal. Fort Nelson experienced a mean of 1.4 °C in months that were both warmer than normal and in months that were cooler than normal. There were seven months that were below climate normals and five months that were above. The largest amount of difference occurred during the winter months, followed by the autumn, spring, and then summer.

Watson Lake (Figure 6c) experienced a mean of 1.7 °C in absolute temperature differences when comparing the 2010-2011 annual cycle to the climate normals. The maximum difference occurred in January when Watson Lake was 4.7 °C warmer in 2010-2011 than the normal. Watson Lake experienced a greater mean difference in the months that were warmer (2.4 °C) than normal compared to the mean difference in months that were cooler than normal (1.2 °C). Five months were cooler than normal, six months were warmer than normal, and April was the same as the normal. The winter months experienced the greatest differences in temperature, followed by the autumn, spring, and then summer.

Whitehorse (Figure 6d) experienced a mean of 1.8 °C in absolute temperature difference between 2010 -2011 and the climate normals. The largest change occurred in March when the MMAT was 4.5 °C cooler in 2010-2011 than the normal. In Whitehorse half of the months were above climate normals and half of the months were below. There was only 0.3 °C difference between the mean difference in months that were cooling (2.0 °C) and months that were warming (1.7 °C). The largest change occurred in the winter months, followed by the autumn, spring, and then summer months.

For all of the communities there was a larger difference in temperature in the fall and winter months than in the spring and summer. They all had their greatest seasonal difference in the winter months, and the greatest monthly negative difference in March. The greatest positive difference occurred in January for Fort St. John and Watson Lake, and in November for Fort Nelson and Whitehorse. Fort St. John experienced the greatest mean difference from normal and the largest monthly difference in temperature (i.e., March, 5.9 °C). Fort Nelson experienced the smallest mean change and the smallest maximum monthly difference (i.e., March, 4.1 °C). Watson Lake was the only community to have a larger mean for monthly temperature increases in comparison to mean monthly temperature decreases. Consequently, it was the only community to have 2010-2011 MAAT higher than its climate normal.

In addition to the difference in air temperature there were variations in precipitation. Figure 7 shows the total monthly snowfall and the depth of snow at the end of the month for both the climate normals and the October 2010- April 2011 data. Due to trace amounts of snow during other portions of the annual cycle the sum of the values in Figure 7 will be close to, but not equal to, the total snowfall values in Table 2.

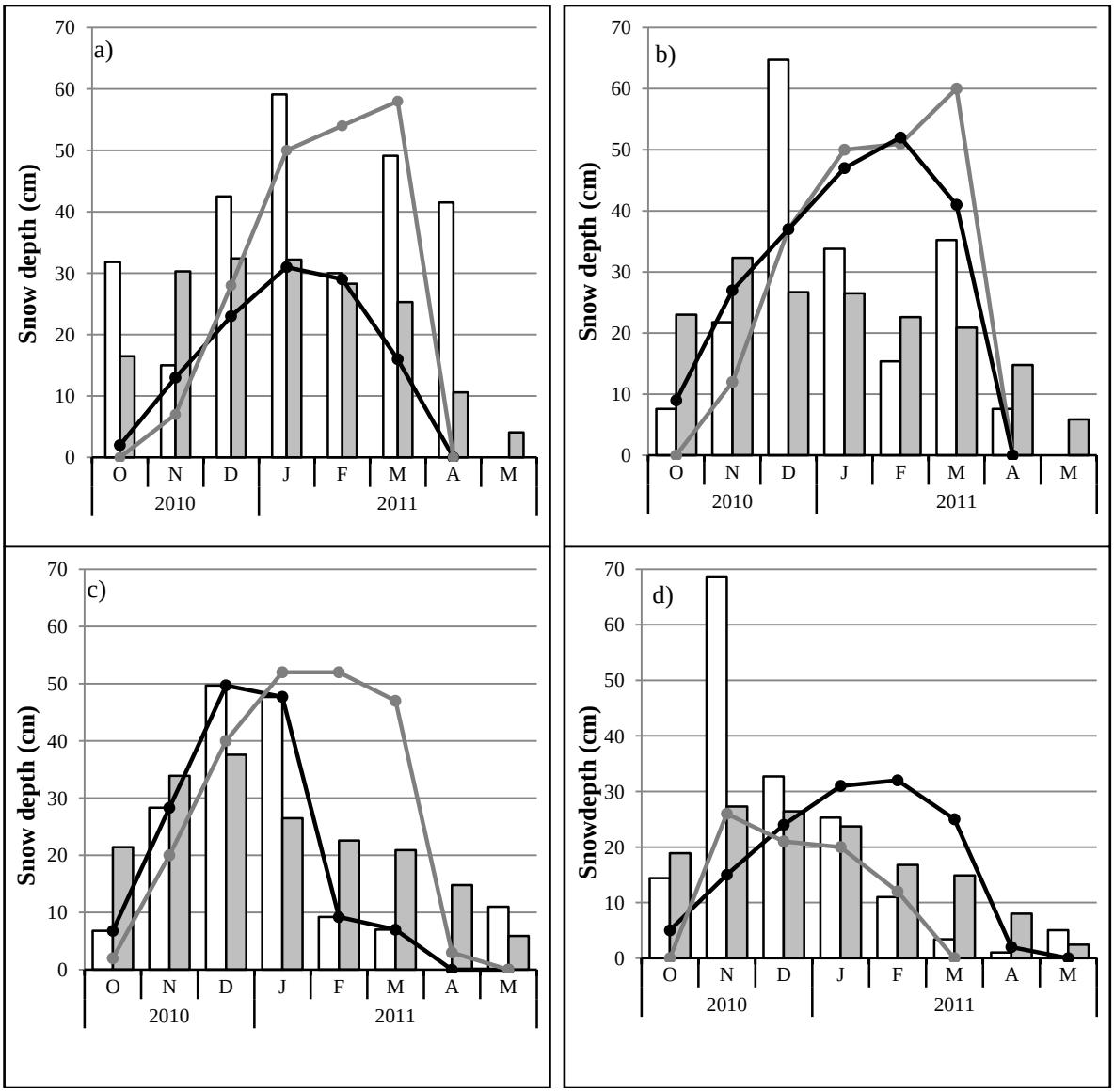

Figure 7 – Snowfall (bar graph) and snow depth at the end of the month (line graph) from October 2010 – May 2011 (white bars, black line) and for the 1971 - 2000 climate normals (grey bars and grey line) for a) Fort St. John; b) Fort Nelson; c) Watson Lake; d) Whitehorse (Environment Canada 2012a).

Fort St. John (Figure 7a) experienced greater snowfall but lesser snow depths in 2010-2011 in comparison to the climate normals. The maximum difference in snowfall occurred in April, when there was 31 cm more than normal. The maximum difference in snow depths occurred in February, when there was 25 cm less snow on the ground than normal. From December 2010 - April 2011 each month received more snowfall than normal but had less accumulation.

Fort Nelson (Figure 7b) experienced greater snowfall and slightly greater snow depths in 2010-2011 than the climate normals. Snowfall was less than normal at the beginning of the season, but more snow accumulated. Although there was greater snowfall during the middle of the season, less snow accumulation occurred. December had the largest difference in snowfall (i.e., 38 cm) and equal snow depths when compared to the normals.

Watson Lake (Figure 7c) had a decrease in snowfall and lower snow depths in 2010-2011 when compared with the climate normals. The snowfall was less than normal during the first two months of the season until December, when there were two months of higher than average snowfalls. In contrast, the first portion of the snow season had greater snow depths than normal, while the second portion had lesser depths. January had 21 cm more snowfall than normal, which was the largest difference in snowfall at Watson Lake. The largest difference in snow depth occurred in February, when there was a 43 cm decrease in month-end depth.

Whitehorse (Figure 7d) had an increase in snowfall and snow depth in 2010-2011 when compared with the climate normals. The largest difference in snowfall occurred in November, when there was 41 cm more than normal.

All of the communities experienced slightly greater than normal snow depths at the beginning of the snow season, but different communities experienced different snow cover depending on their MMATs and their snowfall. Fort Nelson and Whitehorse both experienced greater snowfall and greater snow depths in 2010-2011 when compared to the climate normals. Fort Nelson and Whitehorse also experienced less extreme differences in MMATs when compared to the climate normals. Watson Lake experienced less snowfall and less snow depth, and was the only community to have higher than normal MAAT in 2010-2011. Fort St. John experienced the largest increase in snowfall but the largest decrease in snow depth.

It should be noted that the communities that experienced greater snowfall also received greater rainfall and vice versa.

In general, the air temperatures and snow conditions in 2010-2011 were similar to climate normals. The largest deviations in air temperature occurred in winter, when all communities except for Watson Lake experienced slightly cooler temperature. However, these communities also experienced greater snowfall, which would likely counteract any effect the lower temperatures would have on permafrost. Watson Lake experienced a slightly warmer winter, but also received less snowfall, which would also have the same effect. Therefore, the results received from this study can be taken to be 'typical' in relation to the current climate of the region.

3.2 Topography

The Western Cordillera changes orientation in the Yukon, from southeast-northwest in British Columbia, to southwest in Alaska (Wahl et al. 1987). Topography in the study area reflects this shift with numerous mountains, valleys, and plateaus (Figure 8) (Brown 1967). The Alaska Highway itself remains less variable in elevation compared to the surrounding area with a maximum elevation difference of approximately 900 m (Brown 1967). Summit Lake, west of Fort Nelson, is the highest point along the highway within the study area with an elevation of approximately 1325 m asl (Brown 1967). The elevation of the study sites varies from 417 m to 1098 m asl. Within each study site local relief does not exceed several meters, with the maximum relief at MP 400.5 of approximately 6 m.

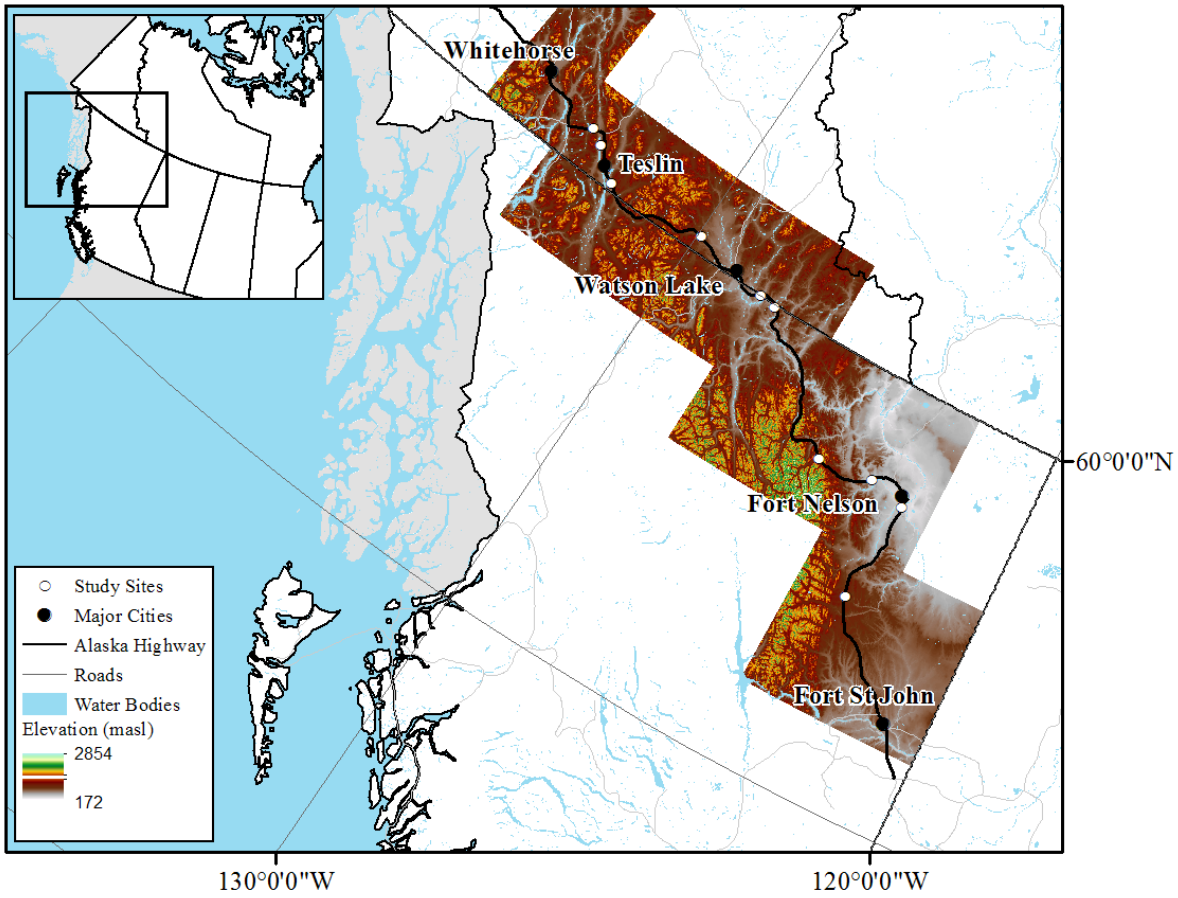

Figure 8 - Topography of the study area (Canadian Digital Elevation Data 1998).

3.3 Vegetation

The study area includes the Boreal Cordillera, Taiga Plain and Boreal Plains ecozones. Rowe (1972) classified the forest within the study area into five separate sections: the Central Yukon, the Eastern Yukon, the Upper Liard, the Northern Foothills, and the Lower Foothills.

Each of these regions has similar tree species which commonly include Lodgepole Pine (*Pinus contorta*), black spruce, white spruce (*Picea glauca*), aspen (*Populus tremuloides*) and balsam poplar (*Populus balsamifera*) (Rowe 1972). Some of these areas include other species such as subalpine fir (*Abies lasiocarpa*), paper birch (*Betula papyrifera*), tamarack and jack pine (*Pinus banksiana*) (Rowe 1972). Understorey vegetation is fairly consistent throughout the study area with feather and club mosses, lichen, and Labrador tea (Rowe 1972).

3.4 Glaciations

After the last interglacial period (130 – 107 ky BP) a dramatic decrease in temperature occurred worldwide (ACIA 2005). In the Yukon the climate and proximity to the Pacific Ocean promoted the rapid growth of the Laurentide and Cordilleran Ice Sheets (Jackson et al. 1991). The southern Yukon and British Columbia were most affected by ice sheets that began in the western Cordilleran Coast Mountains and Cassiar Mountains. These ice sheets formed ice lobes and advanced into lower elevations (Bond 2003).

Since there were numerous glacial advances during the Pleistocene the older advances are harder to distinguish from one another. Glaciations that occurred before the Reid glaciation (300 – 230 ka BP) are classified as Pre-Reid, and occurred from 2.9 Ma to 400.5 ka BP. These glaciations are believed to be the most extensive (Duk-Rodkin 2004). The evidence of these glaciations was mostly destroyed in the study area due to the subsequent ice sheet advances (Bond 2003; Duk-Rodkin 2004). The Reid glaciation was less extensive than the Pre-Reid glaciations, and the McConnell glaciation (23.9 – 10.7 ka BP) is believed to be the youngest and least extensive of all three glaciations (Duk-Rodkin 2004).

The glaciations and subsequent deglaciations altered over 95% of the drainage systems in northwest Canada (Duk-Rodkin 2004). Pro-glacial lakes such as Champagne and Laberge, which were formed during the McConnell Glaciation, created glacial outwash channels and deep incisions into previously deposited glaciolacustrine deposits (Bond 2003).

Following the Last Glacial Maximum a rapid global warming occurred, and by approximately 10 ky BP temperatures resembled those of present day (ACIA 2005). Holocene thermal maximums in northwest Canada occurred between approximately 11.3 to 9.1 ka BP, with temperatures 1.6 ± 0.8 °C higher than 20th century means (Kaufman et al. 2004).

The surficial geology of the study area is mostly glacial veneers and tills (Bond et al. 2004). The soils within the southern Yukon were formed in a semi-arid climate, but vary based on the parent material and glacial history (Smith 2004). From Whitehorse to Teslin the parent material is

generally calcareous, so the majority of soils are within the Brunisol order (Smith 2004). These soils form under grasslands and forests with aspen, pine, and spruce (Soil Classification Working Group 1998; Smith 2004). In the Pelly Mountains (between Teslin and Watson Lake), strong leaching is common due to the high precipitation in the area (Smith 2004). These conditions form Dystric Brunisols, which develop under coniferous forests (Smith 2004). In the valleys and basins near Watson Lake, an increase in precipitation and different parent material can produce Eutric Brunisols (coarser-textured parent material) or Grey Luvisols (finer-textured parent material) (Smith 2004). Grey Luvisols are formed in glacial deposits that are clay-rich, such as alluvial deposits (Soil Classification Working Group 1998). Areas that are underlain by permafrost are Cryosols (Smith 2004). Within the study area these soils are predominantly within north-facing wetlands and peat plateaus, and can be affected by frost churning in the upper soil horizons (Soil Classification Working Group 1998; Smith 2004).

4.0 METHODS

This research was accomplished through the initial installation of field equipment, the execution of field work, and the processing of collected data. The sections below outline each of these steps in detail.

1. Selecting ten of Roger Brown's permafrost sites for study
2. Installing a permanent ERT array in areas of confirmed permafrost at each site
3. Installing climate monitoring systems along each ERT array
4. Water-jet drilling where possible to determine permafrost presence/absence, and depth
5. Undertaking resistivity surveys during different stages of the freeze-thaw cycle
6. Recording relevant vegetation, relief and active layer thickness information along the resistivity profile at each site
7. Analyzing collected ERT surveys using RES2DINV and Surfer
8. Calculating climate statistics for collected temperature data

4.1 Selecting Permafrost Sites

Ten study sites for this research were chosen based on the presence of permafrost in Brown's 1964 survey (Brown 1967) and its persistence to 2007-2008 (James 2010). Other factors that were considered included the presence of previously installed weather stations and boreholes, ease of access in both summer and winter, and an even distribution of sites along the study transect. The sites were located using Geographic Positioning Systems (GPS) coordinates (UTM, WGS 84) provided by James (2010). Appendix A contains the GPS coordinates for each of the ten sites, as well as the monitoring equipment installed at each location.

4.2 Installation of ERT Profiles

ERT electrode arrays (i.e., profiles) were installed at each site with the length of the profile running roughly perpendicular to the Alaska Highway. Profile locations were determined by frost probing; permafrost absence was assumed for areas with late-summer unfrozen ground greater than

112 cm in depth. In areas of exceptionally thin permafrost, profiles were installed from areas where a frost table was absent to areas where permafrost was identified. At sites with previously installed climate stations, the resistivity arrays were set up in-line with, or no more than 2 m from, these stations, preferably locating the stations in the centre of the ERT profile.

Profiles were 80 m in length at eight of the sites and 40 m at MP 286.0 and MP 178.0. A Wenner configuration was used in all cases. The length of the array was shortened if a site had very localized and thin permafrost bodies. Stainless steel rods, 130 cm long and approximately 8 mm in diameter were inserted into the ground to a depth of 40 cm. These electrodes were permanent and their exposed height of 90 cm allowed them to be accessible when snow was present. Figure 9 displays the distribution of steel electrodes for both the 80 m and 40 m profiles. The centre of the profile, with a higher distribution of electrodes, yields a higher resolution in the resistivity results. The ERT penetration depth for the 80 m surveys was approximately 12 m, and 6 m for the 40 m surveys.

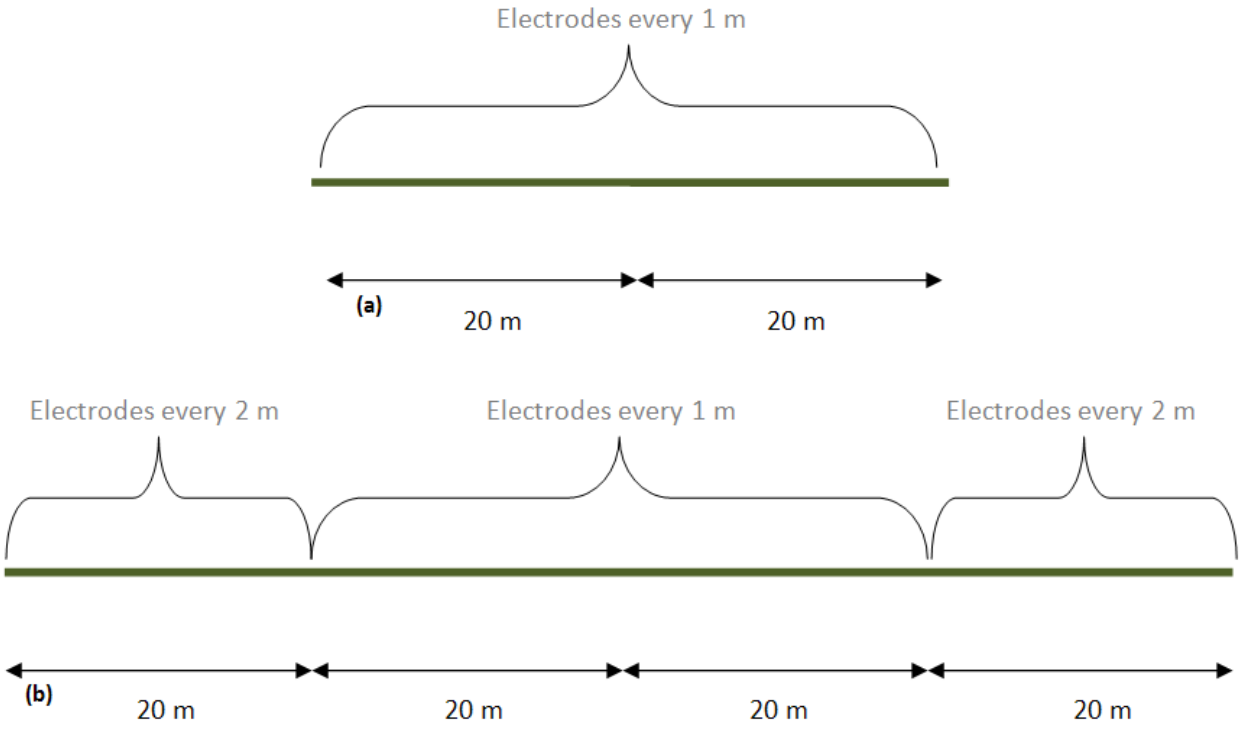

Figure 9 – The distribution of electrodes for a) 40 m surveys; b) 80 m surveys.

4.3 Installation of Climate Stations

Central climate stations were installed in the middle of each resistivity profile. These stations were equipped with automatic loggers recording temperatures at scheduled time intervals. Of the ten sites, six of these had previously installed central stations. Each central station included monitoring of air temperature, ground temperature and snow depth. In addition, each site had two subsidiary stations with ground temperature and snow depth monitoring. Figure 10 displays the general location of the temperature monitoring stations at the 80 m and 40 m resistivity plot sites. The exact location of each station at each site is given in Appendix A.

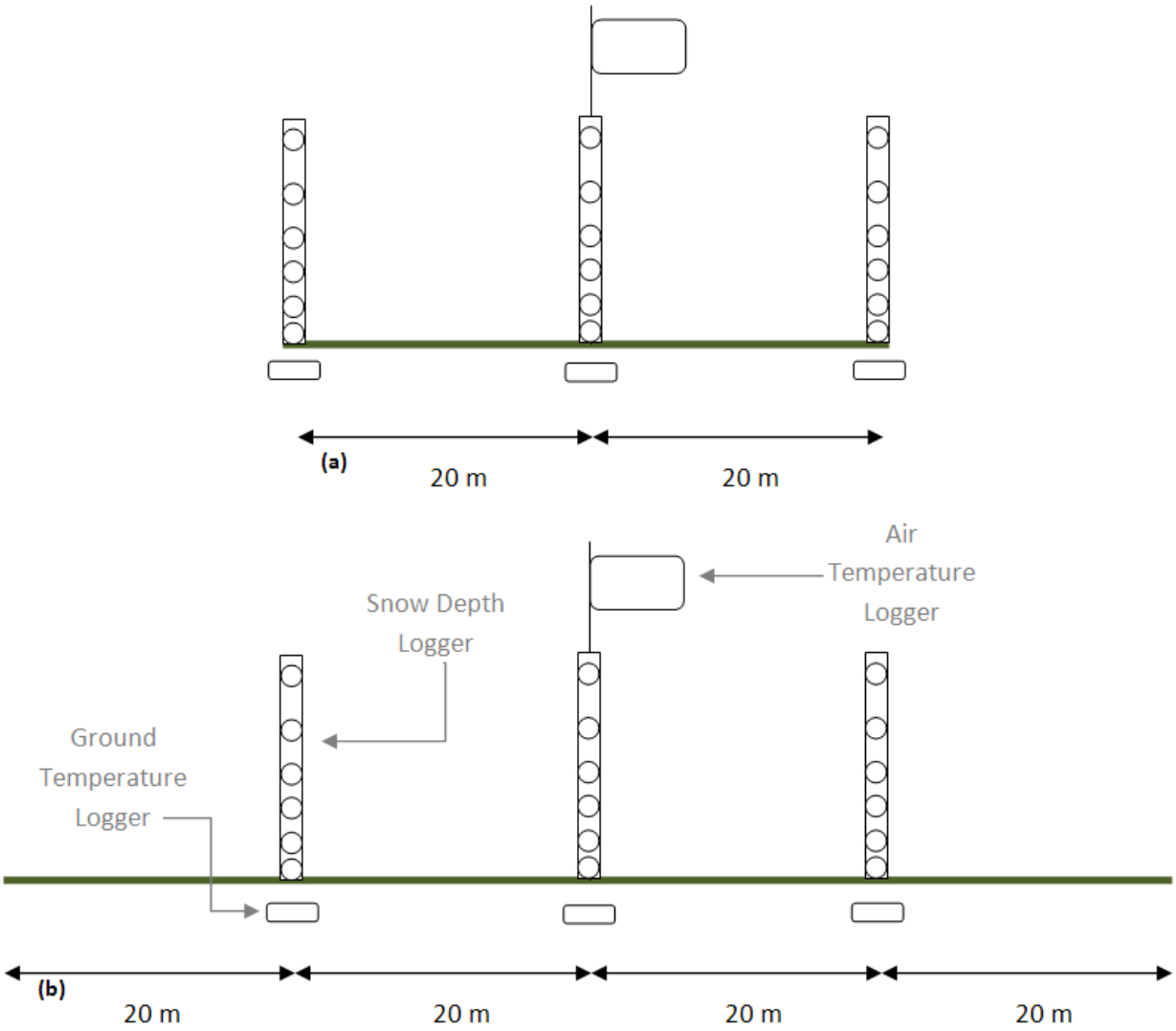

Figure 10 – Idealized location of climate stations for a) 40 m surveys; b) 80 m surveys. Exceptions are detailed in Appendix A.

Air temperature was measured every hour with an external temperature probe installed 1.6 m above the ground within a solar radiation shield. Ground temperature was measured every four hours at each station. Temperatures were recorded by HOBO Pro Data Loggers with an accuracy of ±0.2 °C (Onset HOBO Data Loggers 2012). For ground temperature loggers, a frost probe was hammered into the ground to a maximum depth of 1 m. A bamboo stake was then measured in order to fit into the hole made by the probe. Three external probes were taped to the maximum depth, mid-point and ground surface of the bamboo stake.

Snow depth was measured by Thermochron ibutton temperature loggers which have an accuracy of ±1 °C (Maxim Integrated Products 2012). Wooden stakes were fitted with nine ibuttons located at 5, 10, 20, 30, 40, 50, 60, 80 and 100 cm above ground surface. The depth of snow was determined by analyzing the temperature patterns at each height based on the fact temperatures above and below snow are quite different (Lewkowicz 2008).

Sites with previously installed central climate stations had temperature loggers downloaded during the August 2010 site visit. Batteries, desiccants, and broken loggers were replaced. Temperature data were subsequently downloaded in June and August 2011.

4.4 Borehole Temperature Monitoring

Two study sites had borehole temperature loggers previously installed. MP 286.0 had a borehole that was installed on August 12, 2008 (James 2010). When visiting the borehole in August 2010 it appeared to be completely thawed but monitoring continued. Temperatures were measured using two HOBO Pro data loggers.

MP 825.2 has had a borehole with ongoing temperature monitoring since September 2008. Temperature is measured by an eight-channel data logger manufactured by RBR Ltd. which has a calibrated accuracy of ± 0.002 °C (RBR 2012).

In August 2010, a borehole was water-jet drilled to a depth of 3.75 m at MP 788.5. Temperatures were measured using three HOBO Pro data loggers with external thermisters.

4.5 Resistivity Surveys

ERT surveys were executed with an ABEM Terrameter LS. Four electrode cables, two for the 40 m arrays, each 40 m in length were attached to the permanent electrodes with jumper cables. Two electrode selectors were used to connect the two peripheral cables with the two central cables allowing the expansion of the profile to 80 m. For ease of post-processing, the start of the profile was always located at the end closest to the road.

The first round of ERT surveys was performed from August 9 – August 15, 2010. These surveys were undertaken to represent maximum seasonal thaw depths but it is recognized that some further thawing continued for several weeks after the survey dates, as shown by TTOP temperatures that warmed through to the first half of September. Additional surveys were undertaken from March 9 – 14, May 13 – 17, June 8 – 14, July 3 – 7, and August 19 – 23, 2011. Appendix B displays the field work conducted during each field day.

4.6 Additional Fieldwork

In order to properly interpret the resistivity results collected at each site the surface relief, frost table depths, and snow depths were recorded.

Relief was measured with an abney level using the break-of-slope method. Measurements were taken along the profile with the assistance of a field assistant who moved to each break-point in topography.

The thawed layer thickness at each site was measured at each electrode using a 1.1 m long, 1 cm diameter titanium frost probe. In areas where the frost table could not be identified by probing, the thawed layer thickness was recorded as ">112 cm". In addition, information such as probe location (e.g., peat mound, low area, etc) and sub-surface characteristics (e.g., gravel, roots etc.) were recorded. Frost table depth was measured at each site visit with the exception of the visits in March and May when the ground was still frozen.

In the winter, snow depth was recorded at each electrode in order to obtain additional detailed information on the distribution of snow.

Lastly, photographs of the central climate station and other relevant items were taken at each site during each visit.

4.7 Resistivity Post-Processing

In order to have consistent and accurate ERT data, each site underwent the same post-processing procedure adapted from Hilbich et al. (2011). First, any negative resistivity values within

the data were deleted, since these values were erroneous. These negative values were rare, and at most accounted for 1% of the total data points within one survey. The edited data were used to calculate the spatial mean apparent resistivity for each survey for each site.

After editing the data, the apparent resistivity data needed to be converted to true resistivities. This conversion was accomplished by inverting the apparent resistivity data in RES2DINV software. The data were inverted using the same parameters for each data set to ensure comparability. Due to the presence of permafrost bodies with defined boundaries within each of these surveys, a robust inversion model was used. The Extended-Model was used in order to minimize any artefacts within the central region of the plot, and to reduce the importance of the edges with the inversion process. The model blocks at the sides and bottom of the array are much larger than in other areas of the profile, and therefore not as accurate (Loke 2011). The Damping Factor with Depth changes the size of the model blocks at lower depths (Loke 2011). An increase in model block size decreases incorrect oscillations in the lower section of the profile (Loke 2011). The Damping Factor with Depth was changed from 1.05 to 1.15, which increased the size of the model blocks in the deeper areas of the plot. The model blocks were made to be half the size of the electrode spacing in order to properly display the resistivity changes in the near-surface.

Lastly, the maximum number of inversion iterations was set to 5 and the convergence limit was set to 5.00. Therefore, the inversion process stopped after 5 iterations or if the percent relative change in root mean squared error (RMSE) was less than 5%. ERT data is typically most accurate between 3 – 5 iterations, even though the RMSE can continue to decrease after the 5th iteration (Hilbich et al. 2008). Iterations greater than five can overfit the data, and can lead to an increase in the maximum resistivity value within a profile (Hauck and Mühll 2003). For this research 48 of the 50 surveys used in this thesis are from the 4th iteration while the remaining 2 of 50 are from the 3rd iteration. The complete inversion parameter information is given in Appendix C.

The inversion of the resistivity data using these parameters produced a RMSE less than 5% in 86% of the surveys. An RMSE of 5- 10% was obtained in 10% of the surveys, and the remaining

4% of the surveys had an RMSE between 10- 20%. Resistivity plots with an RMSE greater than 10% occurred during the March field visit, where the cold temperatures produced very high resistivity values in the near-surface and therefore a very high range of resistivity values over the whole plot.

Topography was added to each resistivity survey by calculating XYZ coordinates from the break-of-slope data recorded during fieldwork and remained consistent for each site.

Permafrost bodies were delineated by studying the resistivity gradients in each profile, as well as using particular resistivity values as the boundary between frozen and unfrozen ground. At sites where boreholes were present, the data acquired from temperature logging helped in determining the permafrost boundaries. Due to the complexities of the subsurface, resistivity values were classified as unfrozen, indeterminate or frozen. In order to classify each model block into these categories, Golden Software's Surfer was used. From RES2DINV, the data were exported into a Surfer format, which is essentially in XYZ format where X represents the location of the climate station, Y represents the various depths and Z is the resistivity measurement. From Surfer, the model blocks could be re-classified in order to access the accuracy of the permafrost boundaries.

In addition to determining the resistivity patterns of an entire profile, virtual boreholes at the locations of the three climate stations were constructed for each study site. The virtual boreholes were constructed by using the Surfer export files by extracting every resistivity measurement (Z) for a given climate station location (X) at every depth (Y). The virtual boreholes were compared to the climate data and frost probing data from each climate station to ensure the permafrost boundaries chosen for the site were appropriate. This method was an iterative process and each boundary was the best estimate based on the three pieces of data available (i.e., ERT data, climate data, frost probing data).

Lastly, the relative percent change based on each site's August 2010 survey was calculated for every survey at every site. This calculation was done in order to determine if the results of this study are consistent with those in Hilbich et al. (2011). The Surfer export files were used for the

inverted resistivity values, and the equation below shows an example of how the percent change was calculated for the March survey based on the August survey.

$$\text{Percent Change} = \left(\frac{(\text{March } \Omega\text{m block x}) - (\text{August } \Omega\text{m for model block x})}{\text{August } \Omega\text{m for model block x}}\right) \times 100$$

The calculated values were converted to a .dat file, which were then imported into Surfer and converted into a .grd file for visualization. Visualization was based off on Figure 5b in Hilbich et al. (2011). For some model blocks, values increased by greater than 100%, and were shown as ≥100%.

4.8 Climate Data Post-processing

The climate data were analyzed in order to determine mean annual temperatures. Preliminary processing required that data be examined for any impossible and improbable measurements; these points were eliminated.

All subsidiary stations and central climate stations that were installed in August 2010 had mean annual temperatures calculated for August 2010-2011.

The air temperature sensor at MP 844.1 malfunctioned almost immediately after the August installation. Due to MP 844.1's several years of T_{air} data and its close proximity to MP 825.2, the T_{air} from the two sites were cross-correlated in order to determine the strength of the relationship between them. The R^2 value for the hourly data was 0.96 (n = 7,535), therefore the missing T_{air} data for MP 844.1 was estimated using the MP 825.2 data. MP 681.1's air temperature sensor began to malfunction in June 2011 and the same procedure was completed using Watson Lake Environment Canada data (R^2 = 0.93, n = 18,191).

Snow depth was determined by using the methods in Lewkowicz (2008). The ibutton data from each stake at each interval, in combination with the ground and air temperatures, were organized together within one Excel document. When an ibutton made a significant departure from the temperature of the air and the temperature of the ibutton above, it was classified as below snow. Once the pattern of snowfall was outlined, the snow depth days (SDD) for each stake were

calculated. SDD were obtained by multiplying the number of days the snow remained at a set depth by the depth it remained at, then summing these values. Snow levels were assumed to be mid-way between the highest ibutton that was covered and the one above it that was uncovered.

Degree days and n-factors were calculated for each site using the equations found in Section 2.2.3. Since each site had only one air temperature value but several ground surface temperature values, some sites have a range of n-factor values.

4.9 Frost Table Depth Post-Processing

In order to accurately identify permafrost bodies the frost table data for each site visit was analyzed. Each electrode location at each site was examined for the normal progression of the frost table (i.e. deeper frost depth in August 2010 than in June and July 2011) and classified as either a logical frost table or as indeterminate. The frost tables for August 2010 were graphed in order to analyze the sites when the active layer was at its thickest.

5.0 RESULTS

This section presents the results from the examination of each of the ten study sites, and is separated into two main subsections. The first section is the intra-site analysis of data for each site. The results are presented from the southern-most research site along the Alaska Highway (MP 178.0) to the northern-most (MP 844.1). In this section, the air temperature, ground surface temperature, and snow cover relationships are examined. The ground temperature data are presented and compared to different locations along the study site's profile. If available, a site's borehole data are also analyzed. Lastly, each site's ERT data are summarized and presented in a profile image, permafrost classification image, virtual borehole figure and percent change image.

The second section is the inter-site comparison of the results. In this section the temperature data for each site is compared in order to obtain a better understanding of the general climate in the study area. Temperature characteristics are calculated and compared, including the surface offsets, thermal offsets, n-factors and SDD. Lastly, the ERT data for all sites are compared.

5.1 Intra-site analysis

For each site, there were three locations along the profile where climate data were collected; one central climate station and two subsidiary stations. In order to present consistent results, the colours red, green, and blue were used from the front to the back of a profile regardless of the station type. All ten study sites had at least five ground surface temperature loggers installed. In order to avoid the display of similar data, any loggers with less than 0.5 °C difference in annual temperature were not included.

5.1.1 MP 178.0

MP 178.0 is located approximately 150 km south-southwest of Fort Nelson at an elevation of 1098 m asl. The topography at this site is slightly sloped upwards towards the back of the profile, however there is less than 1.5 m in elevation change from the highest point along the profile (31 m) to the lowest (0 m). In May 2011 there were large patches of snow present, as seen in Figure 11a,

and no standing water. More water was introduced to the profile after water-jet drilling was attempted in June 2011 which saturated the moss at 20 m and 29 m. These areas were still highly saturated in July 2011 and August 2011. The site is hummocky, with mosses, lichen, and Labrador tea present (James 2010). The area has spruce trees approximately 9 m in height (James 2010). The vegetation is shown in Figure 11b.

a)  b) 

Figure 11 – MP 178.0 site photos a) Taken in May 2011 from approximately 5 m looking towards the back of the profile, this photo shows the large snow patches that were present; b) Taken in June 2011 from approximately 3 m looking towards the back of the profile, this photo shows the vegetation.

Figure 12 displays the daily ground and air temperature values and daily snow depth values for MP 178.0 from August 2010 to August 2011. The daily air temperature values showed much greater variation in the winter months than in the summer months, which is typical of a continental climate. This pattern was seen at all of the study sites. At this site, some mid-winter air temperatures reached values just above 0 ºC. The daily air temperature range for this site was 50.7 ºC, with a mean air temperature of -3.0 ºC. The maximum hourly temperature was 26.1 ºC which occurred on August 18, 2010 at 14:00, the same day as the maximum daily temperature (14.9 ºC). The minimum

daily and hourly temperature value occurred on the same day, January 14, 2011. The minimum daily value was -35.8 °C and the minimum hourly value was -41.7 °C, which occurred at 08:00. Every site had the minimum daily and hourly air temperature on January 14, 2011.

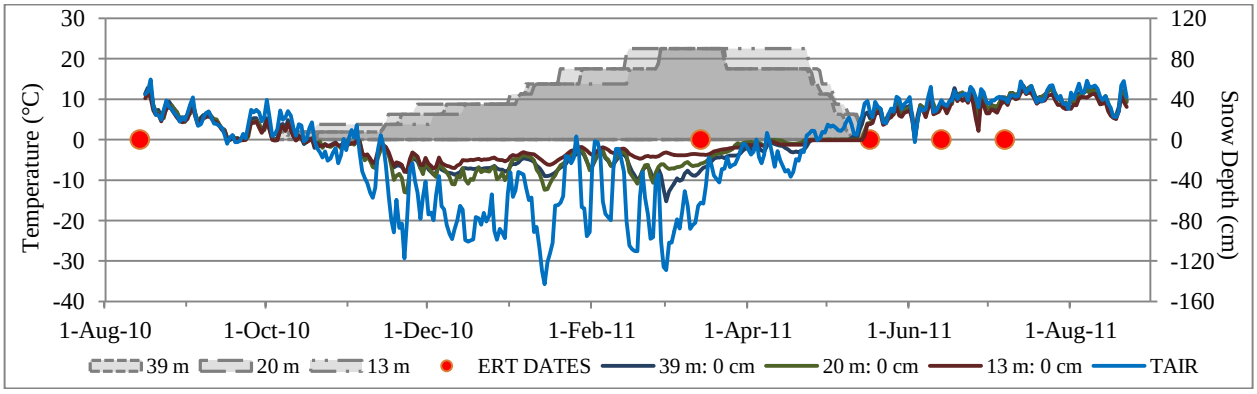

Figure 12 - Daily ground and air temperature values and daily snow depth values for MP 178.0 from August 2010 to August 2011. The red dots symbolize ERT collection days at this site.

The annual ground surface temperatures at this site varied from 0.3 to 0.9 °C. The largest difference in mean values occurred between a logger located at 13 m (0.9 °C) and one at 39 m (0.3 °C). As shown in Figure 12, the difference in ground temperatures between these loggers occurred mostly within the winter. This trend is common for all ground loggers present at every site. The loggers present at 13 m had a mean daily temperature range of 20.3 °C and 21.3 °C, and also had the warmest minimum daily value (-8.0 °C) which occurred on November 22, 2010. The loggers at 39 m had a temperature range of 23.6 °C to 28.7 °C, and had the coldest minimum daily value (-15.3 °C) on March 1, 2011. The minimum daily temperatures occurred between November 22 and 23, 2010 for the loggers at 13 m and 20 m, but occurred on March 1, 2011 for the 39 m loggers. The zero curtain at this site lasted for approximately 20 days.

Snow began to accumulate in early October, and continued to accumulate until mid-February when snow depth reached a maximum of 90 cm. In total, MP 178.0 had a 224 day snow season, which was calculated from the first day snow was observed until the last day snow was identified. The SDD at the front, centre and back of the profile were 10535, 11093 and 10171. The difference in SDDs for each snow stake was 9%, which accounts for approximately a 4 cm difference in annual

snow cover from the snow stake with the lowest SDD, 39 m, and the snow stake with the highest SDD, 20 m.

Table 3 shows the daily ground temperature summary statistics for MP 178.0. The ground temperature profile is consistent throughout the site, with less than 1 °C difference in mean annual values at every location at every depth.

Table 3 - Daily ground temperature summary statistics for MP 178.0, August 2010-August 2011.

Depth	9 m				20 m				39 m			
(m)	x̄	Max	Min	Range	x̄	Max	Min	Range	x̄	Max	Min	Range
0.00	0.7 0.9	12.2 12.4	-9.1 -8.0	21.3 20.3	0.4	13.3	-13.1	26.4	0.3 0.3	13.4 13.3	-15.3 -10.2	28.7 23.6
0.40	0.2	2.4	-0.1	2.5	--	---	--	--	0.3	2.2	-0.5	2.7
0.90	0.0	0.2	-0.1	0.3	--	--	--	--	-0.1	-0.1	-0.2	0.1
Cells with dashes indicate temperature sensors that failed.												

The apparent resistivity data at MP 178.0 had a mean of 377 Ωm, excluding the June and July surveys which were not completed due to problems with the terrameter. The spatial mean apparent resistivities from August 2010 to May 2011 were 343 Ωm, 398 Ωm, and 389 Ωm. The inverted resistivity data had a mean measurement of 511 Ωm. The minimum resistivity value was 22 Ωm, which occurred in May. The maximum resistivity was 14.1 kΩm and occurred in the March survey.

Figure 13 shows the inverted ERT profile, the frost depth, and the classified Surfer image for the August 2010 survey. The measured, calculated, and inverse profiles for each survey at MP 178.0 are presented in Appendix D.

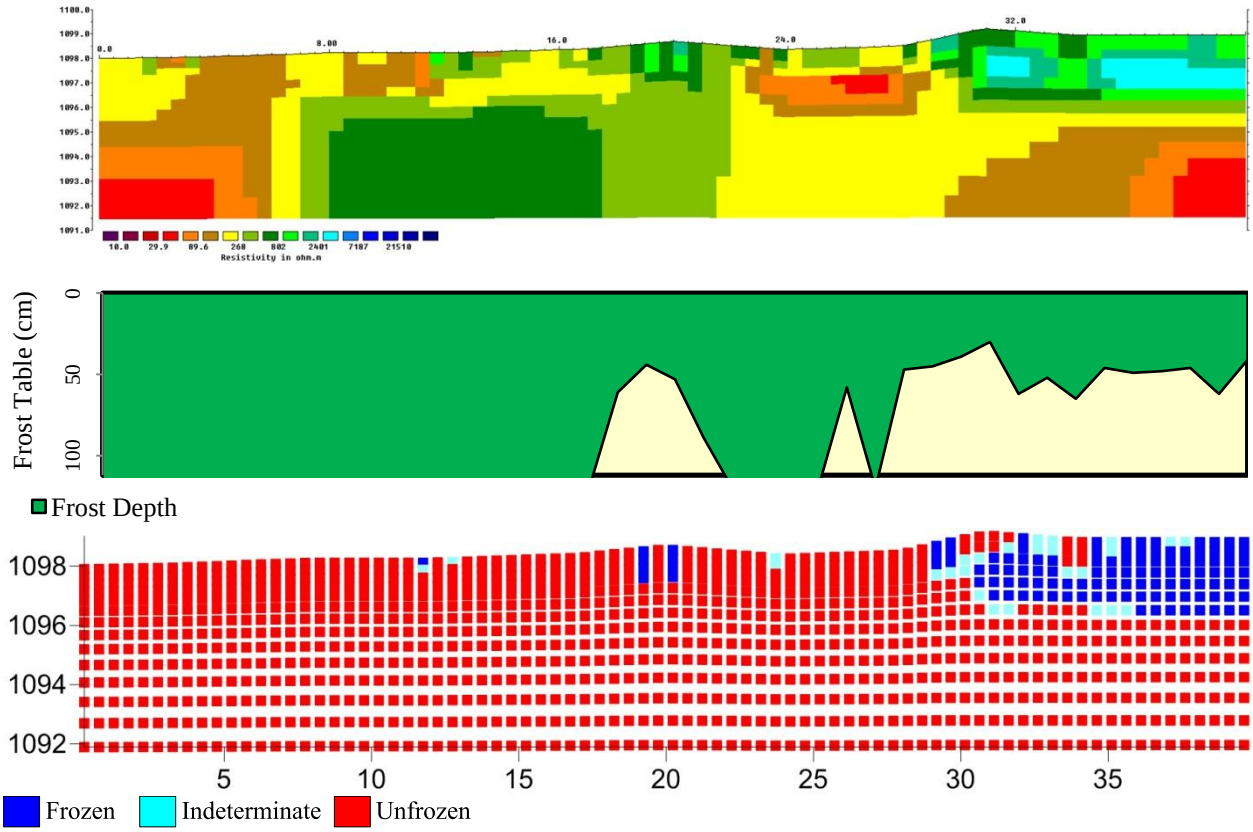

Figure 13 – Inverted ERT profile, frost table depths and permafrost classification image for MP 178.0 for the August 2010 survey. Legends for each of the images are in the bottom left corner. For the permafrost classification image unfrozen is 0 to 750 Ωm, indeterminate is 750 to 1000 Ωm, and frozen is all model blocks greater than 1000 Ωm. All images have identical horizontal scales in meters. The inverted ERT profile and permafrost classification image have vertical scale in meters.

At this site all of the frost probing measurements were logical and there were no indications of gravel or rocks. Based on the frost probing and temperature data the upper boundaries for frozen and indeterminate were 750 Ωm and 1000 Ωm, respectively. It should be noted that the climate station at 20 m was more elevated than the ERT profile. The ground temperature data from the 20 m station was unable to be collected, so the difference in elevation is not significant for this annual cycle.

Figure 14 shows the virtual borehole values for each climate station at MP 178.0.

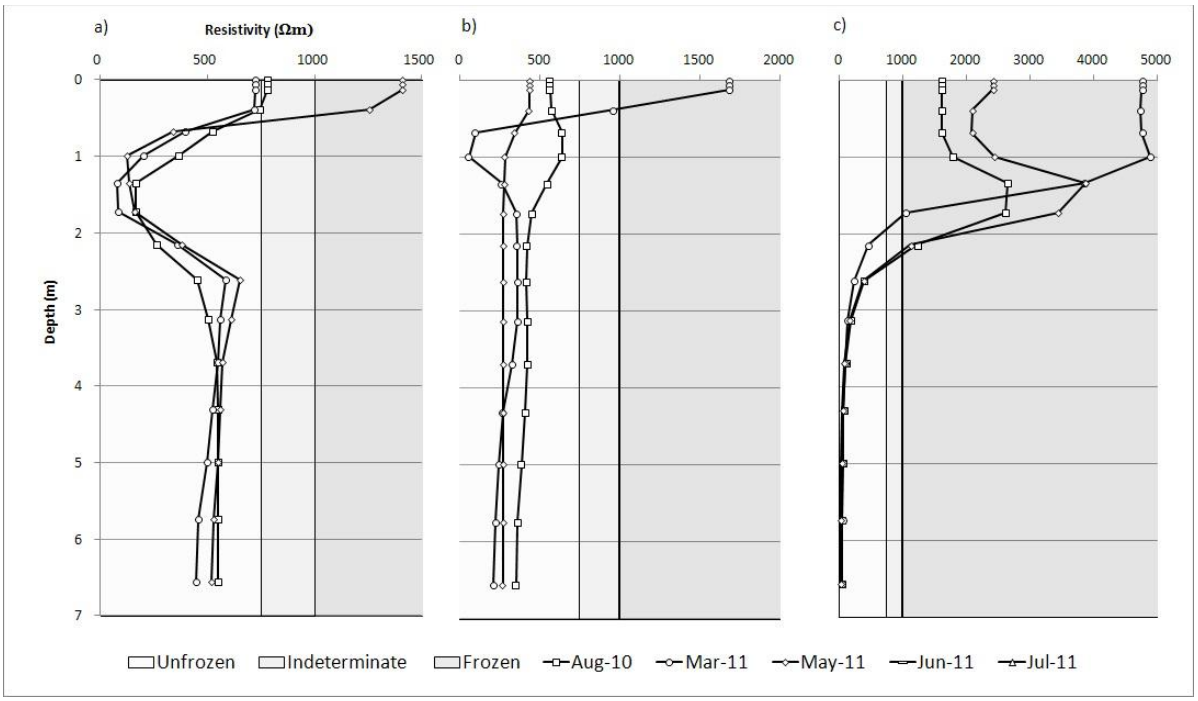

Figure 14 - Virtual boreholes for MP 178.0 at a) 13 m; b) 20 m; c) 39 m along the profile length. Note the difference in scale for each of the x axes.

At 13 m, the virtual borehole showed seasonally frozen ground to approximately 0.5 m, with no permafrost present. The August survey did not appear to have any frozen ground at this location. A frost table was not identified in this area in August 2011. The temperature sensors at 40 cm and 90 cm both had a mean annual temperature above 0 °C. These sensors were below 0 °C for both the March and May surveys. This temperature change was only reflected in the March resistivity values.

At 20 m there was no permafrost present. The seasonally frozen ground was approximately 50 cm thick. In July 2011 there was no frozen ground present within 115 cm of the surface at this climate station, although there was a frost table at 53 cm and 35 cm in August 2010 and June 2011, respectively. There was no ground temperature data for this location.

The virtual borehole at 39 m is interpreted as showing permafrost that was approximately 2 m thick with no seasonally unfrozen ground. The ground temperature sensor at 90 cm was within permafrost, but the 40 cm sensor was only below 0 °C for the March survey. The frost probe data showed a maximum frost probe depth of 62 cm. Therefore, there was seasonally thawed ground

within the first 60 cm of the surface, but this was not reflected in the resistivity values, which are, however, right at the end of the profile.

The frost probe, temperature, and ERT data suggested that there was permafrost present at MP 178.0. The permafrost body began at approximately 28 m along the profile and continued beyond the end of the survey line. The depth of the permafrost varied from 1 – 2 m thick. Based on field notes taken during the site visits there was a clear relationship between the elevated topography and the presence of a detectable frost table at this site.

Figure 15 shows the relative change in inverted resistivity in relation to the August 2010 survey.

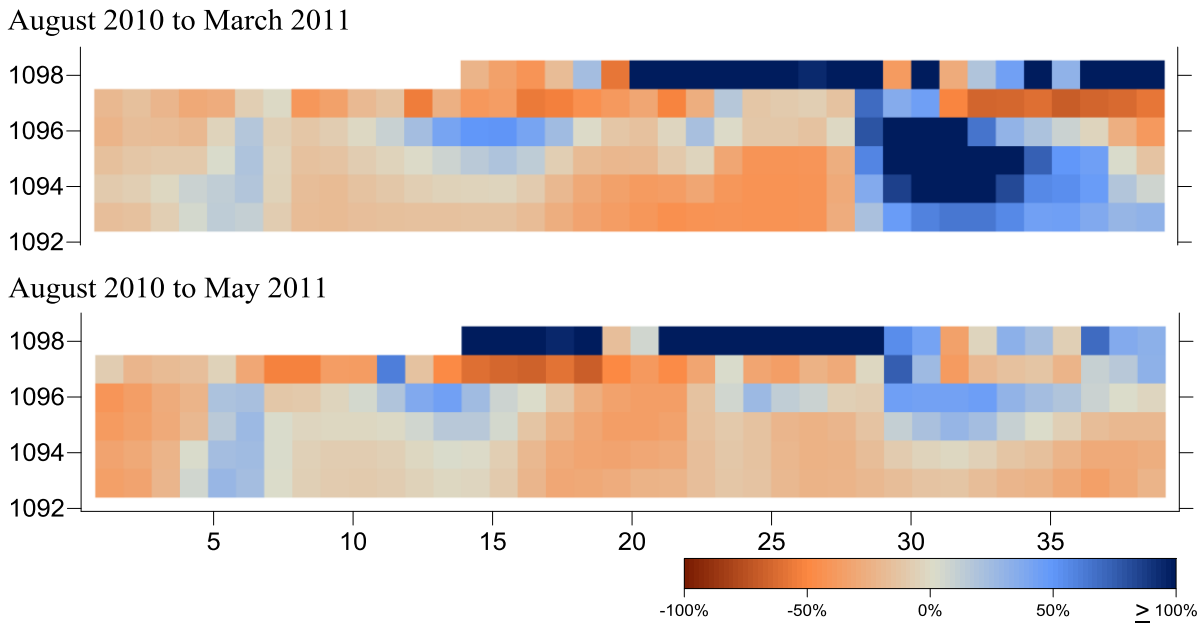

Figure 15 - Relative change in resistivity based on the August 2010 survey for MP 178.0.

Approximately 40% of the model blocks had their maximum values in March, and approximately 40% of the model blocks had their minimum values in August. Therefore, the largest relative change occurred from the August to March surveys. These blocks were distributed in the near-surface and at greater depths within the area classified as frozen or indeterminate. The high resistivity at greater depths may be an artefact due to the high resistivity in the near-surface. The August to May comparison had high resistivity increases in the near-surface.

5.1.2 MP 286.0

MP 286.0 is 14 km south-southwest of the Fort Nelson city boundary, and is approximately 417 m asl. The site is essentially flat, with less than 1 m in elevation change from the highest point (20 m) to the lowest (0 m). The site is approximately 70 m away from a large drainage ditch for the road but no standing water was present on the profile during any of the site visits. There was no snow cover present during the May 2011 visit (Figure 16a). The site is hummocky and is abundant in mosses, sphagnum, Labrador Tea, and lichens (Figure 16b) (James 2010). There are both spruce and tamarack present, and the former has a maximum height of 7.5 m (James 2010).

a)  b) 

Figure 16 – MP 286.0 site photos a) Taken in May 2011 at approximately 39 m looking towards the back of the profile, this photo shows the absence of snow cover; b) Taken in June 2011 at approximately 39 m looking towards the back of the profile, this photo shows the vegetation and tree species present in the profile.

Figure 17 displays the daily ground and air temperature values and daily snow depth values for MP 286.0 from August 2010 to August 2011. The daily air temperature values had a range of 59.1 °C, with the coldest daily value of -38.0 °C and the coldest hourly value of -42.8 °C (occurring at 10:00). The warmest daily value of 21.1 °C occurred on July 13, 2011, and the warmest hourly

value of 30.6 °C occurred on the same day at 16:00. The mean annual air temperature at this site was -1.6 °C. Unlike MP 178.0, daily air temperature values during the winter did not exceed nor come close to 0 °C.

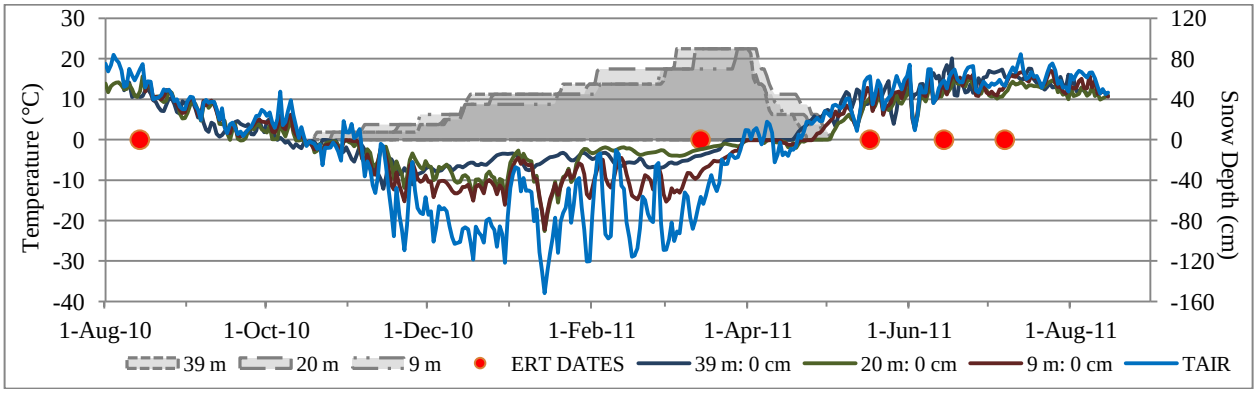

Figure 17 - Daily ground and air temperature values and daily snow depth values for MP 286.0 from August 2010 to August 2011. The red dots symbolize ERT collection days at this site.

Mean annual ground surface values varied from 0.7 °C to 2.4 °C for the loggers at MP 286.0. At 9 m, mean annual temperature were 0.7 °C to 1.0 °C, 1.5 °C for 20 m, and 1.7 °C to 2.4 °C for 39 m. The largest range in daily ground surface temperature was 39.3 °C and occurred at 9 m. As shown in Figure 17, this logger was the most affected by changes in the air temperature. The sensor at 39 m with the highest annual mean also had the lowest daily minimum temperature (-12.1 °C) and the lowest range in temperature, so it was least affected by changes in air temperature. The coldest daily temperature occurred on January 14, 2011 for the ground loggers at 9 m and 20 m, under deep snow cover. For 39 m, the coldest daily temperature was November 11, 2010, when snow cover was still thin. The spring zero curtain effect at this site began at the end of March and lasted approximately 28 days.

The snow cover began to accumulate at the end of October, and continued to build into March when snow depth reached 90 cm. Depths remained fairly consistent until snow melt, which began in April and ended in May. The SDD from the front to the back of the profile were 7397, 8680, and 7932. The difference in SDDs for each snow stake was approximately 7 cm in annual snow cover from the snow stake with the lowest SDD, 9 m, and the highest SDD, 20 m.

Table 4 shows the daily ground temperature summary statistics for MP 286.0. This site shows consistent results along the entire profile.

Table 4 - Daily ground temperature summary statistics for MP 286.0, August 2010- 2011.

Depth (m)	9 m				20 m				39 m			
	x̄	Max	Min	Range	x̄	Max	Min	Range	x̄	Max	Min	Range
0.00	0.7 1.0	17.1 17.4	-22.2 -18.6	39.3 36.0	1.5	15.2	-22.6	37.8	1.7 2.4	20.3 20.1	-15.9 -12.1	36.2 32.2
0.20					1.4	20.6	-27.2	47.9				
0.30					1.4	7.2	-5.3	12.4				
0.40					0.6	3.8	-2.0	5.8				
0.50	0.0	2.6	-1.7	4.3	0.0	2.6	-1.7	4.3	-0.1	1.1	-0.9	2.0
1.00	-0.1	-0.1	-0.2	0.1					-0.2	-0.2	-0.2	0.0
Grey cells indicate sensors that were not installed at that depth for that station.												

Figure 18 shows the minimum and maximum borehole temperature values for MP 286.0. This borehole is not located on the profile, but approximately 5 m away from the 20 m climate station. Due to logger failure the mean value for this borehole was unable to be calculated. There was no ground surface logger present at the borehole location so the ground logger at 20 m was used.

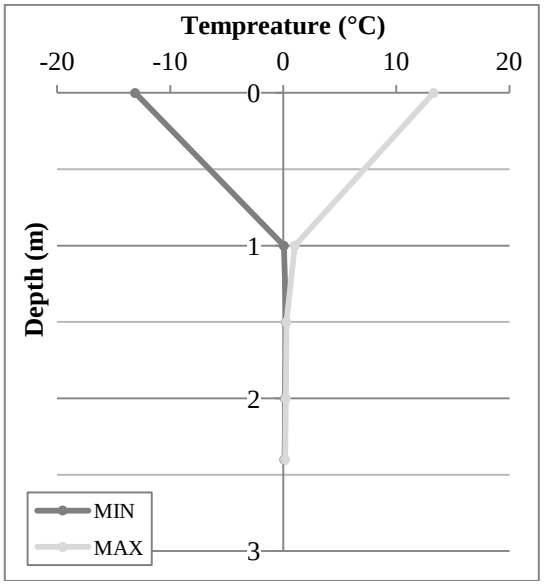

Figure 18 - Minimum and maximum borehole temperature values for MP 286.0, August 2010-2011.

The temperature envelope from this borehole suggests that permafrost is not present at this location. Minimum temperature values from 1 m to 2.4 m were all above 0 °C. The depth of zero

annual amplitude was at approximately 1.5 m in depth so the temperatures below this were mean ground values.

The apparent resistivity data at MP 286.0 had a mean of 385 Ωm, excluding the June survey, during which the terrameter malfunctioned. The spatial mean apparent resistivities from August 2010 to July 2011 were 327 Ωm, 489 Ωm, 379 Ωm and 344 Ωm. The inverted resistivity data had a mean of 457 Ωm, with the minimum resistivity value (3 Ωm) occurring in every survey except for August, and the maximum value (11.6 kΩm) occurring in March. The largest proportion of measurements (67% to 76%) were less than 500 Ωm, and 14% to 21% of the measurements were between 500 – 1000 Ωm.

Figure 19 shows the inverted ERT profile, frost table, and permafrost classification image for the August 2010 survey. The measured, calculated, and inverse profiles for each survey at MP 286.0 are presented in Appendix E.

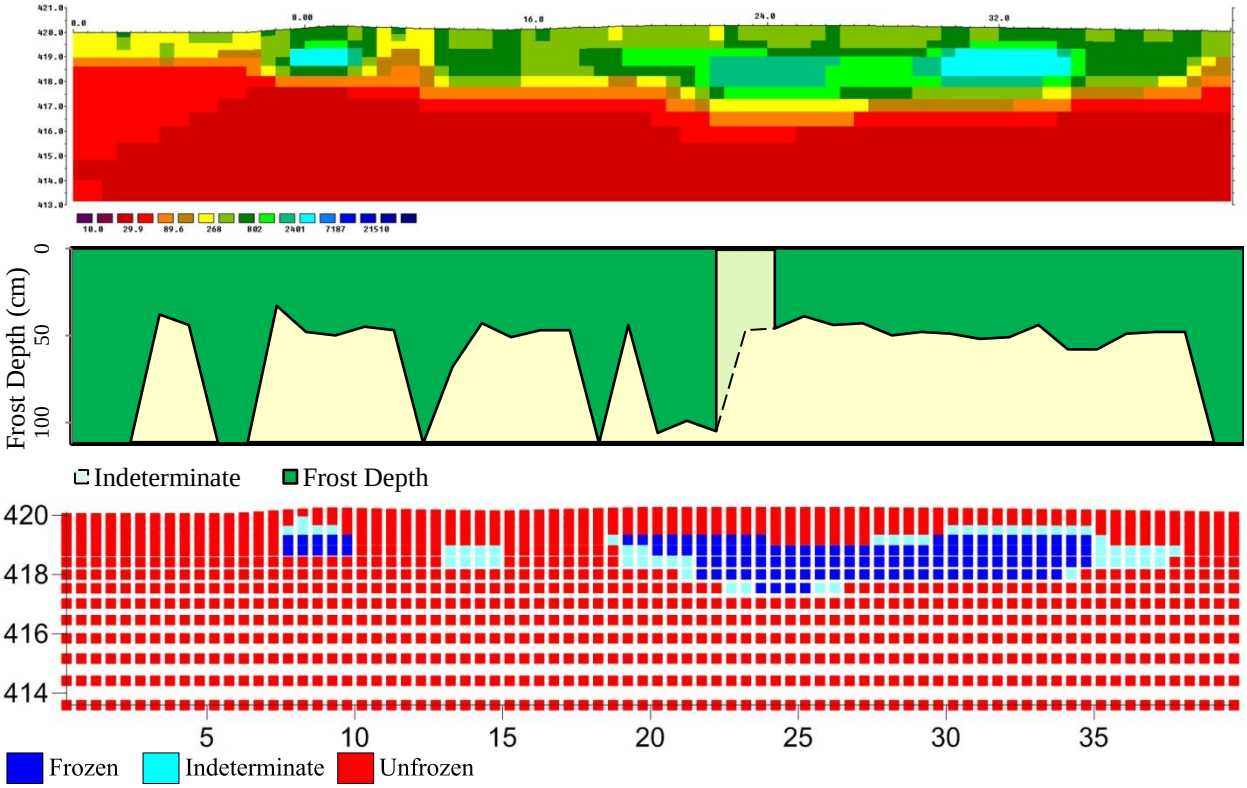

Figure 19 - Inverted ERT profile, frost table depths and permafrost classification image for MP 286.0 for the August 2010 survey. Legends for each of the images are in the bottom left corner. For the frost table image, areas of light green with dashed lines had an annual frost progression that was not logical. For the permafrost classification image unfrozen is 0 to 700 Ωm, indeterminate is 700 to 900 Ωm, and frozen is all model blocks greater than 900 Ωm. All images have identical horizontal scales in meters. The inverted ERT profile and permafrost classification image have vertical scale in meters.

All areas of the profile, with the exception of the electrode at 23 m, followed a logical annual frost table progression. The upper boundaries used for unfrozen and indeterminate are 700 Ωm and 900 Ωm, respectively. These values were chosen based on the data available at each climate station.

Figure 20 shows the virtual borehole values for each climate station at MP 286.0.

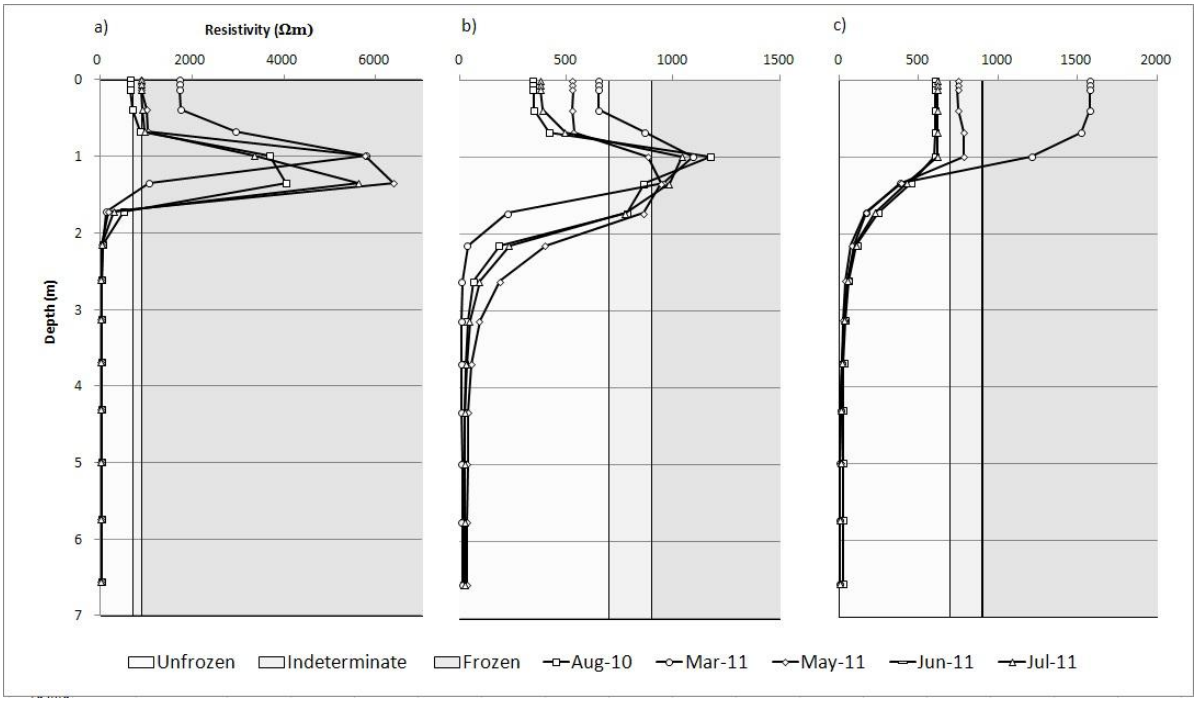

Figure 20 - Virtual boreholes for MP 286.0 at a) 9 m; b) 20 m; c) 39 m along the profile length. Note the difference in scale for each of the x axes.

The virtual borehole at 9 m showed 0.5 m of seasonally thawed ground with permafrost approximately 1.5 m thick. The frost table at 9 m in August 2010 and July 2011 was at approximately 50 cm which was consistent with the resistivity results. The 1 m temperature sensor was within permafrost and the 0.5 m logger was within seasonally frozen ground, which was also consistent with the resistivity results.

At 20 m there was 1 m thick permafrost overlain by a layer of seasonally thawed ground approximately 0.5 to 0.75 m thick. The frost probing showed a maximum thawed layer thickness of 105 cm in August 2010. The logger data showed each sensor (i.e., 20 cm, 30 cm, 40 cm and 50 cm) went above 0 °C, but they were below 0 °C for the March survey. It is possible that the resistivity boundaries for this location should be slightly lower in comparison to the other virtual borehole locations.

At 39 m there was a layer of seasonally frozen ground approximately 1 m to 1.25 m thick. There was no permafrost present at this location. The resistivity data were consistent with the frost

probing data, which did not include a detectable frost table in August 2010. The temperature data were not consistent with the resistivity data since the logger at 100 cm never went above 0 ºC.

Based on the available data, there was permafrost present at MP 286.0. The largest permafrost body occurred from 17 m to 39 m, was approximately 3 m thick and began 1 – 2 m below the surface. There were also three small frozen areas that occurred at 7 – 9 m, and 14 m. Based on field notes taken during the site visits there was a clear relationship between the elevated topography and the presence of a probable frost table at this site

Figure 21 shows the relative inverted resistivity based on the August 2010 survey.

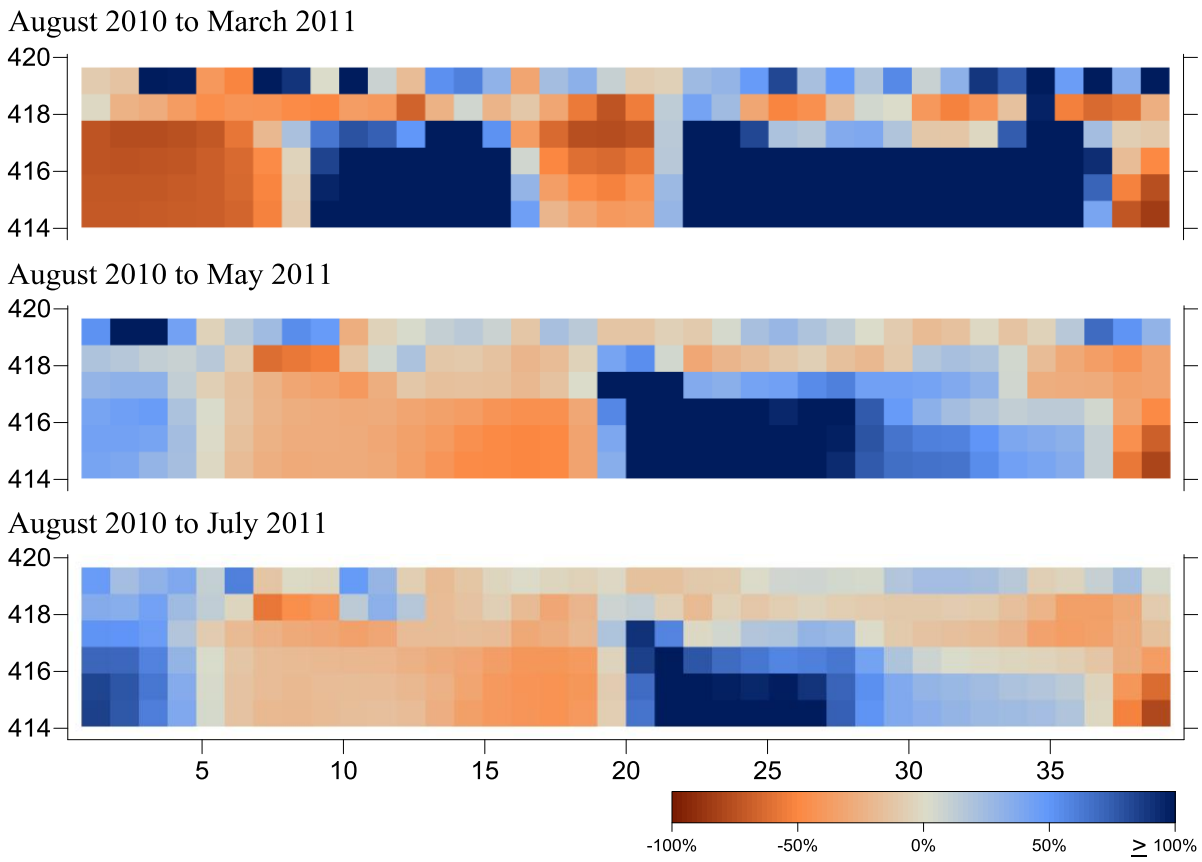

Figure 21 - Relative change in resistivity based on the August 2010 survey for MP 286.0.

The August to March survey comparison showed an increase in resistivity within parts of the lower portion of the profile, as well as a decrease in resistivity in others. The March survey had the highest percentage of maximum model blocks (51%), but it also had the highest percentage of

minimum model blocks as well (41%). Therefore, there are both large increases and decreases in resistivity in the August to March comparison. For all of the surveys there were large resistivity increases in the bottom portion of the profiles. These areas were classified as unfrozen, and some of them occur underneath areas that were classified as unfrozen or indeterminate. This pattern may be due to changes in the near-surface affecting resistivity measurements at greater depths.

5.1.3 MP 341.3

MP 341.3 is 50 km west of Fort Nelson and approximately 460 m asl. The site slopes downward towards the back of the profile but there is less than 1 m of elevation change between the front of the profile and the back of the profile. There was no standing water present during any of the surveys, and no snow cover was visible within or around the profile at the time of the May 2011 survey (Figure 22a). The site has small spruce approximately 4.5 m in height, as well as some tamarack (James 2010). The vegetation cover (Figure 22b) is predominantly mosses, lichen, sphagnum, Labrador tea, and some dwarf birch (James 2010). The soil is mostly organic to the frost table (James 2010).

a)  b) 

Figure 22 – MP 341.3 site photos a) Taken in May 2011 from approximately 65 m looking towards the back of the profile taken from approximately 25 m looking towards the back of the profile, this photo shows the absence of snow cover; b) Taken in July 2011, this photos shows the vegetation.

Figure 23 shows the daily ground temperature values and snow depth values for MP 341.3. The air temperature logger at this site malfunctioned, and no suitable location was available to correlate the air temperature with.

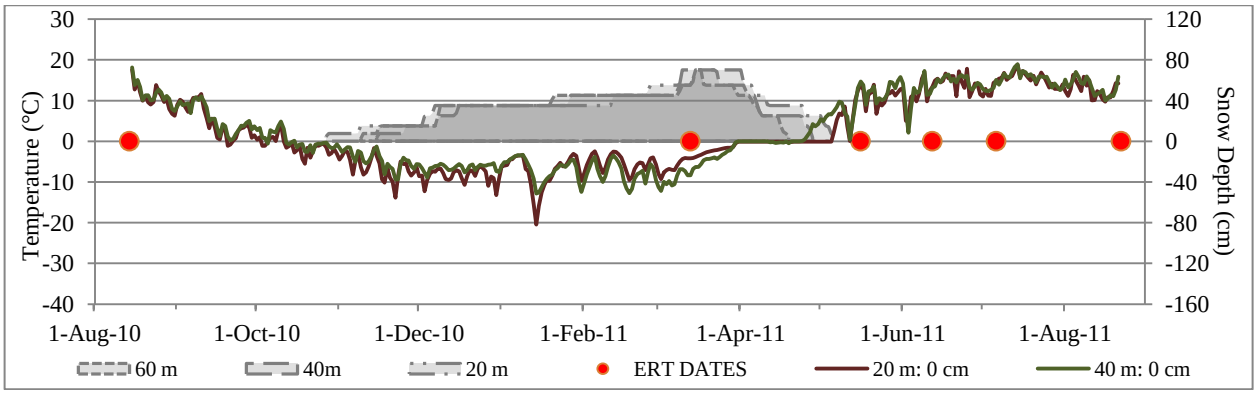

Figure 23 - Daily ground temperature and daily snow depth values for MP 341.3 from August 2010 to August 2011. Air temperature logger malfunctioned at this site. The red dots symbolize ERT collection days at this site.

The mean annual ground surface temperature at MP 341.3 varied from 1.7 °C to 2.2 °C at different locations along the profile. The largest difference in annual temperatures of 0.5 °C occurred

at 20 m. The two loggers had daily minimum, daily maximum, and temperature ranges that were all within 1.0 ºC. For all the loggers, the maximum daily temperature occurred on July 14, 2011. The minimum daily temperature occurred on January 14, 2011 for all but one logger at 60 m, which had its lowest daily temperature on November 22, 2010. At 40 m, the annual ground surface temperature was 2.2 ºC. This location had the coldest daily minimum temperature and the warmest daily maximum temperature, therefore having the greatest range. This location along the profile was most affected by air temperature, which can also be seen from the spring zero curtain effect which began at this site at the end of March and lasted approximately ten days shorter than at 20 m. At 60 m, the annual ground surface temperatures varied by only 0.2 ºC (i.e., 2.0 ºC and 1.8 ºC). This area of the plot had the logger with the lowest maximum daily temperature, which was 16.8 ºC, and the smallest temperature range, which was 28.9 ºC. Since both loggers at this location have small temperature ranges, this area may have been more affected by snow cover than other parts of the profile. The duration of the zero curtain at 60 m was similar to that at 20 m.

The snow cover at MP 341.3 began in late October, and accumulated until mid-March where it reached a maximum height of 45 cm. Snow cover began to decrease in late March until it disappeared at the beginning of May, which was a 192 day snow season. The SDD from the front to the back of the profile were 6836, 6129, and 5851. The difference in SDDs for each snow stake was 17%, which accounts for approximately a 5 cm difference in annual snow cover from the snow stake with the lowest SDD, 60 m, and the highest SDD, 40 m.

The daily ground temperature summary statistics for MP 341.3 are shown in Table 5. Temperatures were consistent at different locations at similar depths.

Table 5 – Daily ground temperature summary statistics for MP 341.3, August 2010-2011.

Depth (m)	20 m				40 m				60 m			
	x̄	**Max**	**Min**	**Range**	**x̄**	**Max**	**Min**	**Range**	**x̄**	**Max**	**Min**	**Range**
0.00	1.7 2.2	18.9 18.5	-20.5 -13.8	39.4 32.2	2.2	18.9	-12.9	31.8	1.8 2.0	16.8 17.7	-12.0 -12.0	28.8 29.7
0.25					1.5	10.45	-3.6	14.1				
0.50	0.4	4.0	-0.2	4.3	0.1	2.1	-1.3	3.5	-0.2	0.0	-1.7	1.7
0.75					-0.1	-0.1	-0.2	0.1				
1.00	0.1	0.9	0.9	0.0	-0.1	-0.1	-0.1	0.0	-0.2	-0.1	-0.4	0.2
Grey cells indicate sensors that were not installed at that depth for that station.												

The apparent resistivity data at MP 341.3 had a mean of 179 Ωm. This value excludes the July 2011 survey when the terrameter malfunctioned. The spatial mean apparent resistivities from August 2010 to June 2011 were 138 Ωm, 258 Ωm, 167 Ωm and 154 Ωm. The inverted resistivity data had a mean of 188 Ωm. The minimum resistivity value was 2 Ωm and the maximum resistivity value was 9.1 kΩm. Both of these measurements were from the March survey. The greatest proportion of resistivity values (86% to 88%) were less than 500 Ωm for each survey executed.

Figure 24 shows the August 2010 ERT survey, frost depth, and permafrost classification images. The measured, calculated, and inverse profiles for each survey at MP 341.3 are presented in Appendix F.

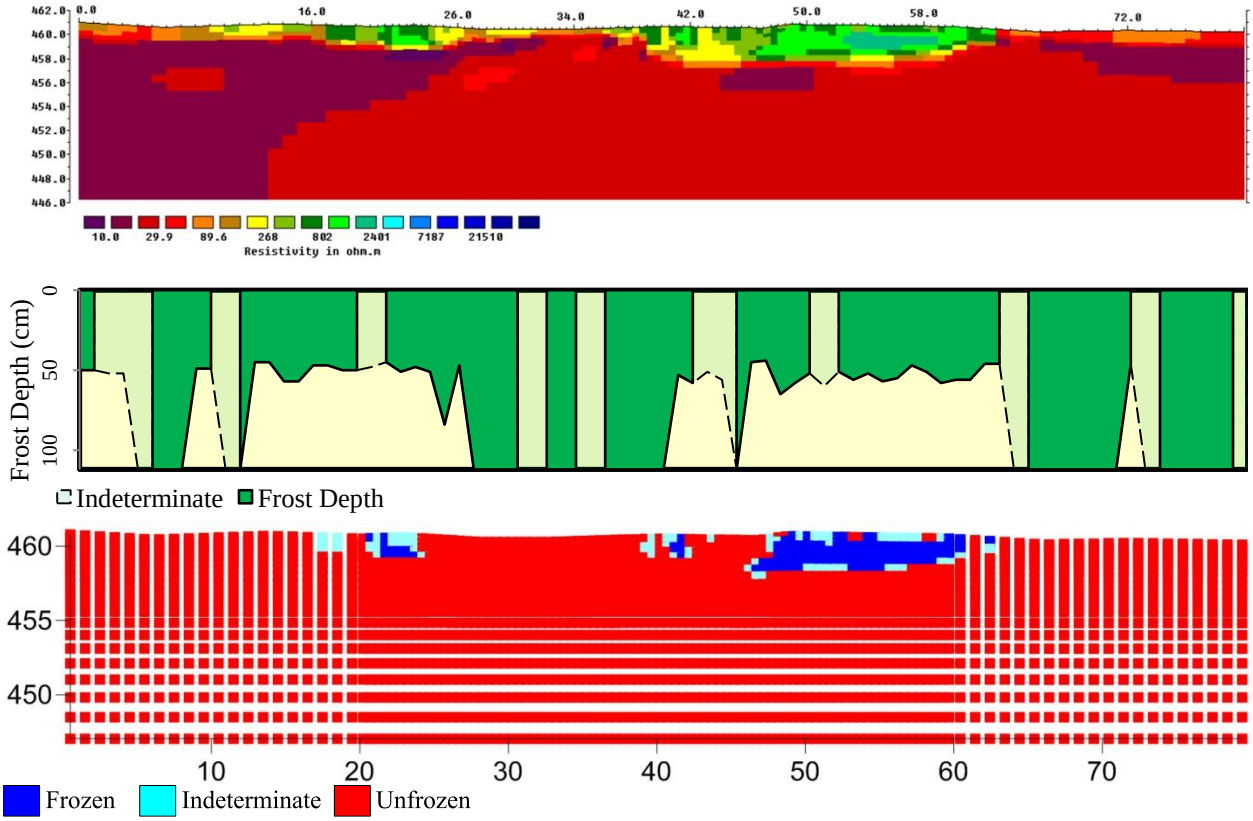

Figure 24 - Inverted ERT profile, frost table depths and permafrost classification image for MP 341.3 for the August 2010 survey. Legends for each of the images are in the bottom left corner. For the frost table image, areas of light green with dashed lines had an annual frost progression that was not logical. For the permafrost classification image unfrozen is 0 to 500 Ωm, indeterminate is 500 to 800 Ωm, and frozen is all model blocks greater than 800 Ωm. All images have identical horizontal scales in meters. The inverted ERT profile and permafrost classification image have vertical scale in meters.

There were several sections along the profile that did not follow a logical frost table progression. The upper boundaries of unfrozen and indeterminate were interpreted to be 500 Ωm and 800 Ωm, respectively. These values best suited all available data.

Figure 25 shows the virtual boreholes for each climate station at the site.

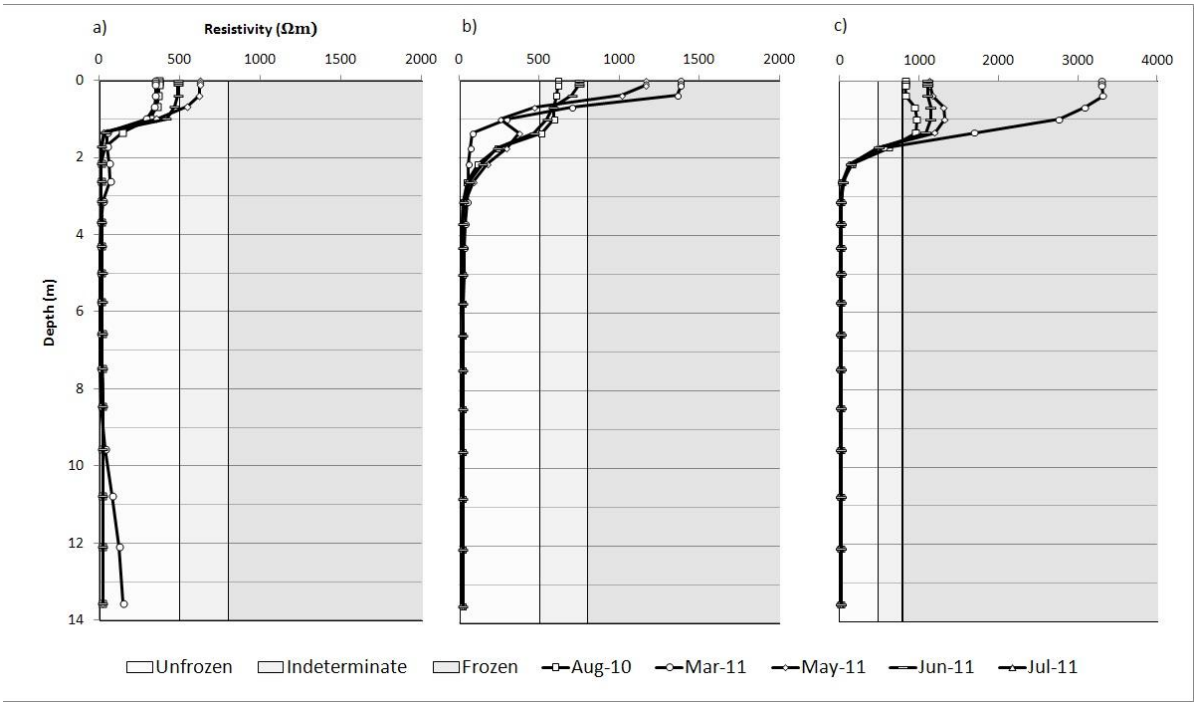

Figure 25 - Virtual boreholes for MP 341.3 at a) 20 m; b) 40 m; c) 60 m along the profile length. Note the difference in scale for c).

At 20 m, the virtual borehole showed seasonally freezing to approximately 1 m. This trend was inconsistent with frost probing data, which was able to identify an active layer during every survey conducted. However, the temperatures at 50 cm and 100 cm both went above 0 °C during the year.

The virtual borehole at 40 m shows possible permafrost that was roughly 1 m thick. There was no evidence of seasonally thawed ground. The deeper temperature sensors at this location (75 cm and 100 cm) both stayed below 0 °C, which was consistent with the resistivity data. There was no identifiable frost table in August 2010, which means there was some seasonal thawing at this location.

At 60 m there was permafrost within the top 1.75 m of the ground surface. Based on the resistivity values there was no seasonally thawed ground present. However, the temperature data and frost probe data showed there should be seasonally frozen ground. The 50 cm logger went above 0 °C, and a frost table was always able to be identified from 20 – 56 cm depth. It is possible that this area of the survey needed different resistivity boundaries in order for it to become more reflective of the actual conditions.

Based on the frost probe, temperature, and ERT data there was permafrost present at this study site. It was very thin, approximately 2 m maximum, and was only present discontinuously from 18 m to 25 m and 40 m to 60 m.

Figure 26 shows the relative inverted resistivity based on the August 2010 survey.

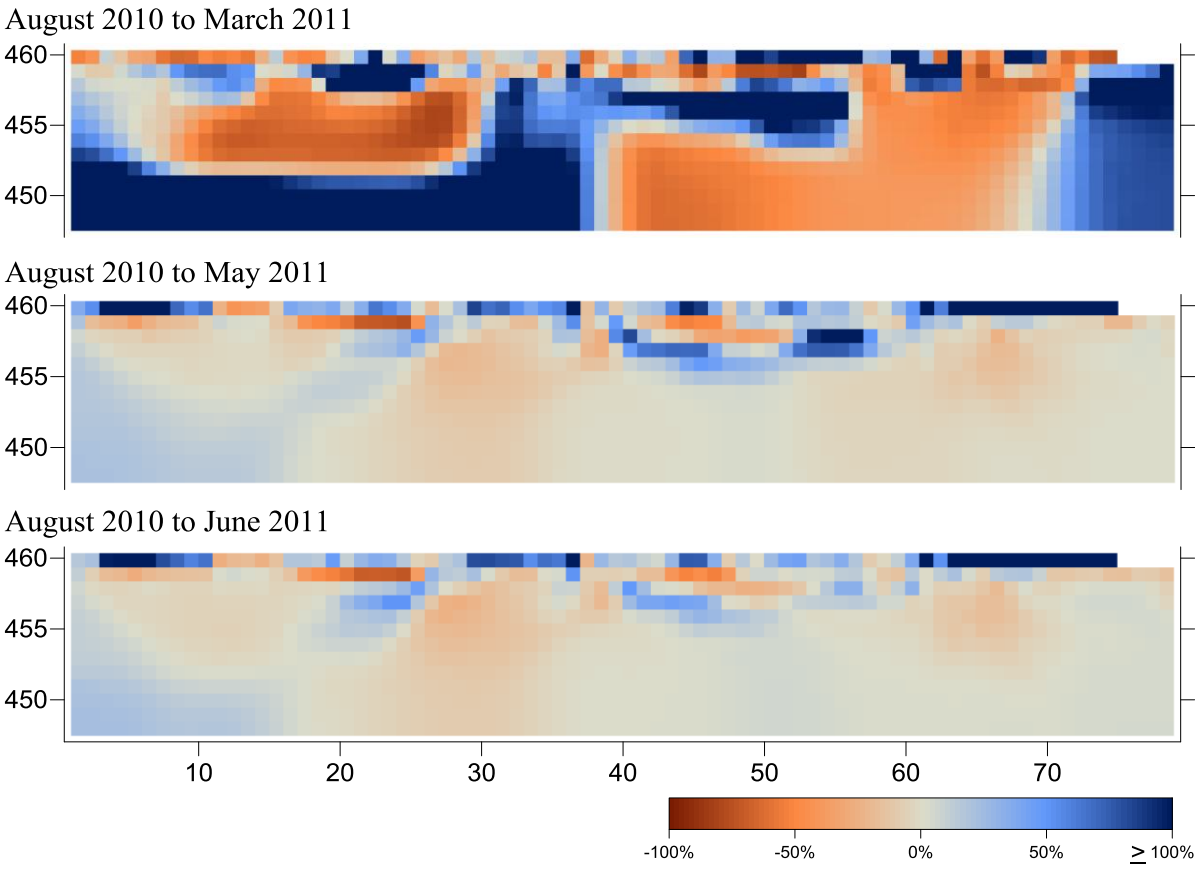

Figure 26 - Relative change in resistivity based on the August 2010 survey for MP 341.3.

The March survey had the highest proportion of both maximum (48%) and minimum (46%) model blocks. Therefore, the August to March survey had both areas of large resistivity increase and of resistivity decrease. The August to May and August to June comparisons showed relatively small increases in resistivity in the near-surface and very stable resistivity values at greater depths.

5.1.4 MP 400.5

MP 400.5 is approximately 130 km west-southwest of Fort Nelson and has an elevation of 1043 m asl. The site is sloped upward towards the back of the profile and has over 6 m of elevation change. Over half of this elevation change occurs in the last 20 m of the profile. Figure 27a was taken from 80 m along the profile facing towards the front. The elevation at 0 m is approximately that of the highway. Also visible in Figure 27a is a small snow patch. Several of these were present in May 2011 but none were substantial. There were also small patches of standing water present in May at 23 m and 33 - 34 m. MP 400.5 has predominantly spruce trees, which are approximately 6 m in height but become taller near the end of the profile (James 2010). The site is hummocky, with non-sphagnum and sphagnum mosses, grasses, lichens, Labrador tea, sedges, and birch shrub (Figure 27b). The soil is composed of cohesive clay and peat (James 2010).

a) 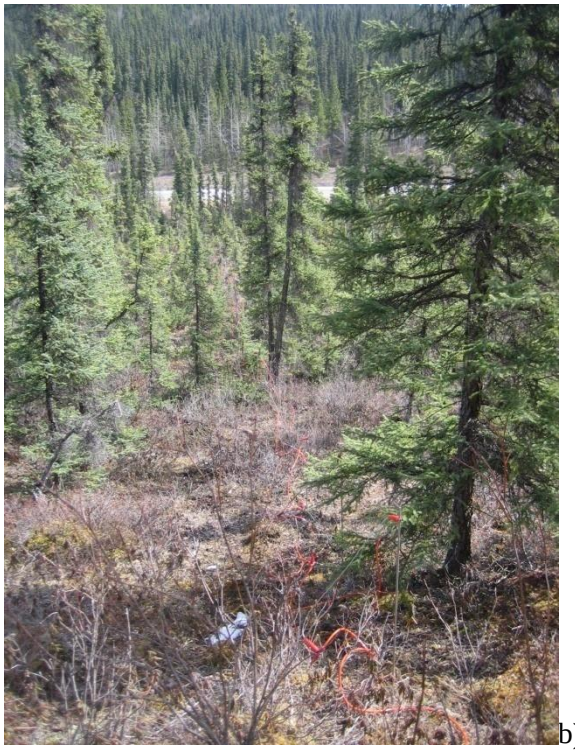 b) 

Figure 27 –MP 400.5 site photos a) Taken in May 2011 from 80 m looking towards the front of the profile, this photos shows a small snow patch and the change in elevation from the back to the front of the profile; b) Taken in June 2011 from approximately 20 m looking towards the back of the profile, this photo shows trees and microtopography.

Figure 28 shows the daily ground and air temperature values and daily snow depth values for MP 400.5 from August 2010 to August 2011. Air temperature variation within the winter months was considerable, with large fluctuations between one daily temperature and the next. Some daily winter temperatures exceeded 0 ºC. The daily air temperatures varied from -34.7 ºC to 16.7 ºC, which is a range of 51.4 ºC. The maximum hourly value was 27.4 ºC, which occurred on July 13, 2011 at 17:00. The minimum hourly value was -40.5 ºC, which occurred at 08:00 on January 14, 2011. The maximum and minimum daily temperate also occurred on these days. The mean annual air temperature for MP 400.5 was -2.7 ºC.

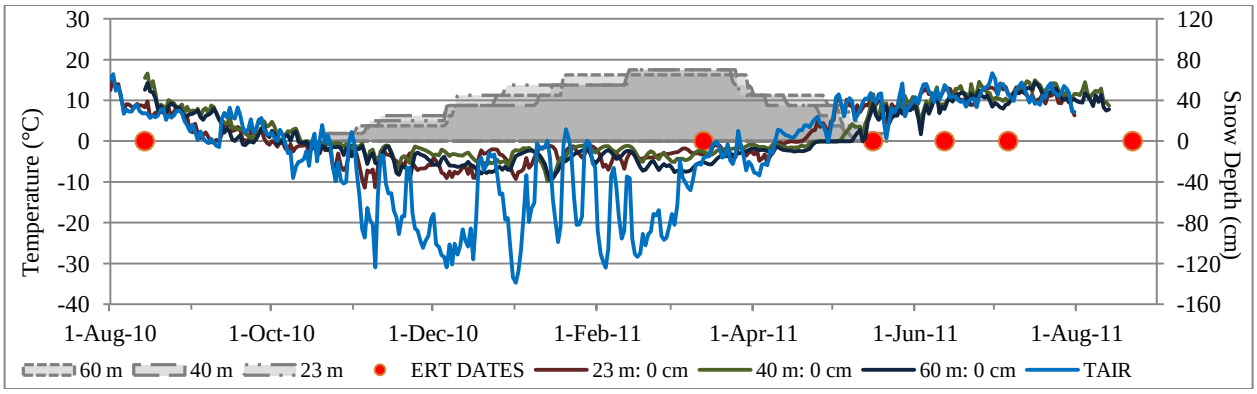

Figure 28 - Daily ground and air temperature values and daily snow depth values for MP 400.5 from August 2010 to August 2011. The red dots symbolize ERT collection days at this site. The 60 cm ibutton malfunctioned at the 60 m snow stake, and the 20 cm ibutton malfunctioned at the 23 m snow stake.

At MP 400.5 the mean annual ground surface varied from 0.9 °C to 2.3 °C, but was fairly consistent at each monitoring station along the profile. At 23 m, the mean annual temperature was 1.5 °C. This logger had the lowest minimum daily value (-11.4 °C), the highest maximum daily value (27.0 °C) and the largest temperature range (38.4 °C). This area was most affected by air temperatures in the winter season. At 40 m the mean annual ground surface temperature was 2.2 °C to 2.3 °C. Loggers at this location had the highest minimum daily temperature (-8.8 °C) and the lowest maximum daily temperature (16.6 °C). The maximum daily temperature for the loggers at 23 m and 40 m occurred on August 15, 2010, while for the loggers at 60 m this occurred on July 16, 2011. At 60 m, the annual ground temperature was 0.9 °C for both loggers. The spring zero curtain at this site began on approximately April 24th and lasted for 15 days.

The snow depth at MP 400.5 was fairly consistent at the three stakes. Snow cover began on approximately October 20, 2010 and depths gradually increased until a March maximum, then decreased through to the end of May. Snow accumulation began first at 23 m, and then continued to the middle and back of the profile. The snow at 23 m also remained the longest at the site, which gave it the largest snow depth day value for the site. From the front of the profile to the back the SDD are 8678, 8211, and 8384. The difference in SDDs for each snow stake equates to a 2 cm difference in annual snow cover from the snow stake with the lowest SDD, 60 m, and the highest SDD, 40 m.

Table 6 shows the daily ground temperature summary statistics for MP 400.5. Temperatures were consistent throughout different locations on the profile.

Table 6 – Daily ground temperature summary statistics for MP 400.5, August 2010-2011.

Depth (m)	23 m				40 m				60 m			
	x̄	**Max**	**Min**	**Range**	**x̄**	**Max**	**Min**	**Range**	**x̄**	**Max**	**Min**	**Range**
0.00	1.5	15.6	-11.4	27.0	2.2 2.3	16.0 16.6	-8.8 -9.9	24.8 26.5	0.9 0.9	15.3 14.4	-10.7 -9.4	26.0 23.9
0.10	2.0	13.5	-6.5	20.0								
0.25	1.1	8.2	-2.7	10.9								
0.40	0.2	5.8	-1.5	7.3								
0.50	0.1	5.0	-0.6	5.6	--	--	--	--	-0.2	0.5	-1.2	1.7
1.00					0.1	2.0	-0.9	3.0	-0.2	-0.1	-0.2	0.1

Cells with dashes indicate temperature sensors that failed. Grey cells indicate sensors that were not installed at that depth for that station.

The apparent resistivity data at MP 400.5 had a mean of 806 Ωm. The spatial mean apparent resistivities from August 2010 to July 2011 were 629 Ωm, 1.0 kΩm, 913 Ωm, 789 Ωm and 684 Ωm. The inverted resistivity data had a mean of 1.3 kΩm. The maximum resistivity value of 21.1 kΩm occurred in May, and the minimum resistivity value of 14 Ωm occurred in March. 33% to 46% of the resistivity measurements were less than 1000 Ωm, and 85% to 95% were less than 2000 Ωm.

Figure 29 shows the ERT profile and permafrost classification image for MP 400.5 based on the August 2010 survey. The measured, calculated, and inverse profiles for each survey at MP 400.5 are presented in Appendix G.

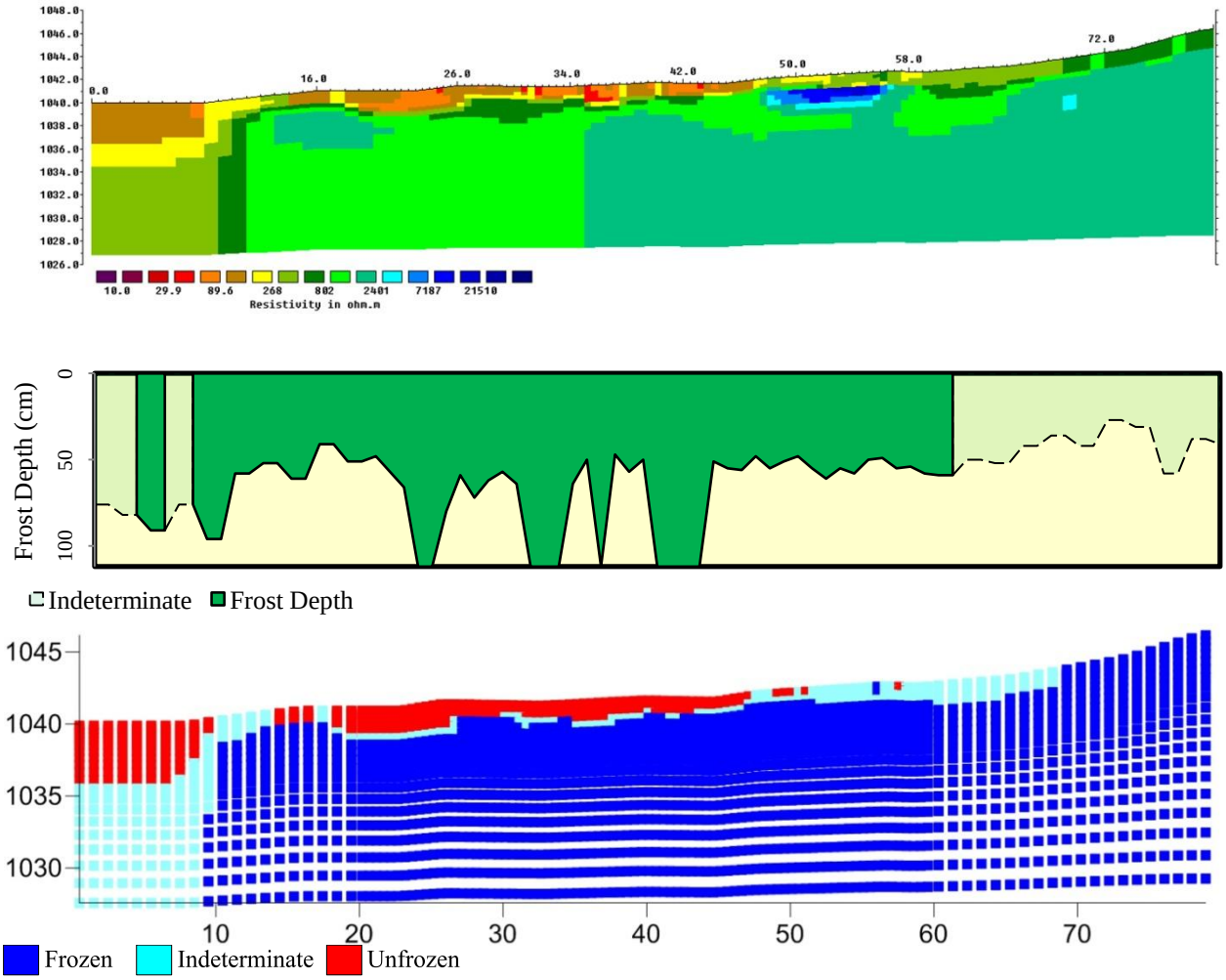

Figure 29 – Inverted ERT profile, frost table depths and permafrost classification image for MP 400.5 for the August 2010 survey. Legends for each of the images are in the bottom left corner. For the frost table image, areas of light green with dashed lines had an annual frost progression that was not logical. For the permafrost classification image unfrozen is 0 to 200 Ωm, indeterminate is 200 to 500 Ωm, and frozen is all model blocks greater than 500 Ωm. All images have identical horizontal scales in meters. The inverted ERT profile and permafrost classification image have vertical scale in meters.

Sections at the beginning and end of the profile had gravel present, which affected the frost table results. The upper boundaries for unfrozen and indeterminate were assessed as 200 Ωm and 500 Ωm, respectively.

Figure 30 displays the virtual borehole at each climate station for the surveys conducted.

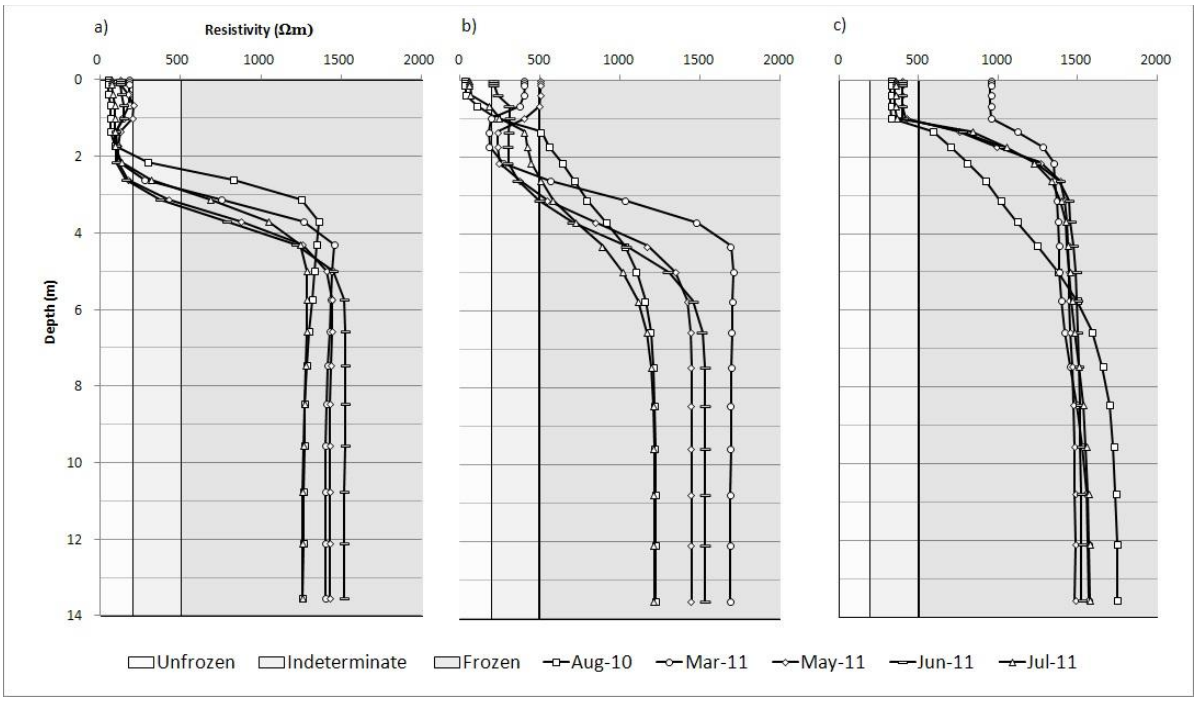

Figure 30 - Virtual boreholes for MP 400.5 at a) 23 m; b) 40 m; c) 60 m along the profile length.

The virtual borehole at 23 m showed seasonally thawed ground that was approximately 2 m thick and permafrost that appears to extend to the base of the survey profile. The deepest logger at this location was 50 cm, and its temperature rose above 0 ºC. The frost table was unable to be probed in August 2010. Both the temperature and frost table data are consistent with the ERT results but the presence of permafrost at depth indicated by the ERT could not be independently confirmed.

At 40 m the permafrost again appeared to extend to the base of the survey and was overlain by a layer of seasonally thawed ground that was approximately 2 m thick. In the March survey there was an area below the seasonally frozen ground that did not appear to be frozen which could have been a supra-permafrost talik. This anomaly was consistent with the frost probe and temperature data. The frost table was not able to be probed in August 2010, and the 100 cm sensor at this location was not within permafrost.

The virtual borehole at 60 m showed permafrost that was thicker than the penetration depth of the survey and seasonally thawed ground to a depth of 1 m. The 1 m temperature sensor did not go

above 0 ºC whereas the 50 cm one did; this is consistent with the possible active layer thickness. However, the frost table was not identified at this location due to gravel.

The ERT, frost probe, and ground temperature data indicate that MP 400.5 had thick permafrost with a thick layer of thawed ground in places, some of which may have remained thawed throughout the year. The permafrost was present throughout the entire profile, and the active layer thickness varied from 0 to 2 m.

Figure 31 shows the relative change in inverted resistivities based on the August 2010 survey.

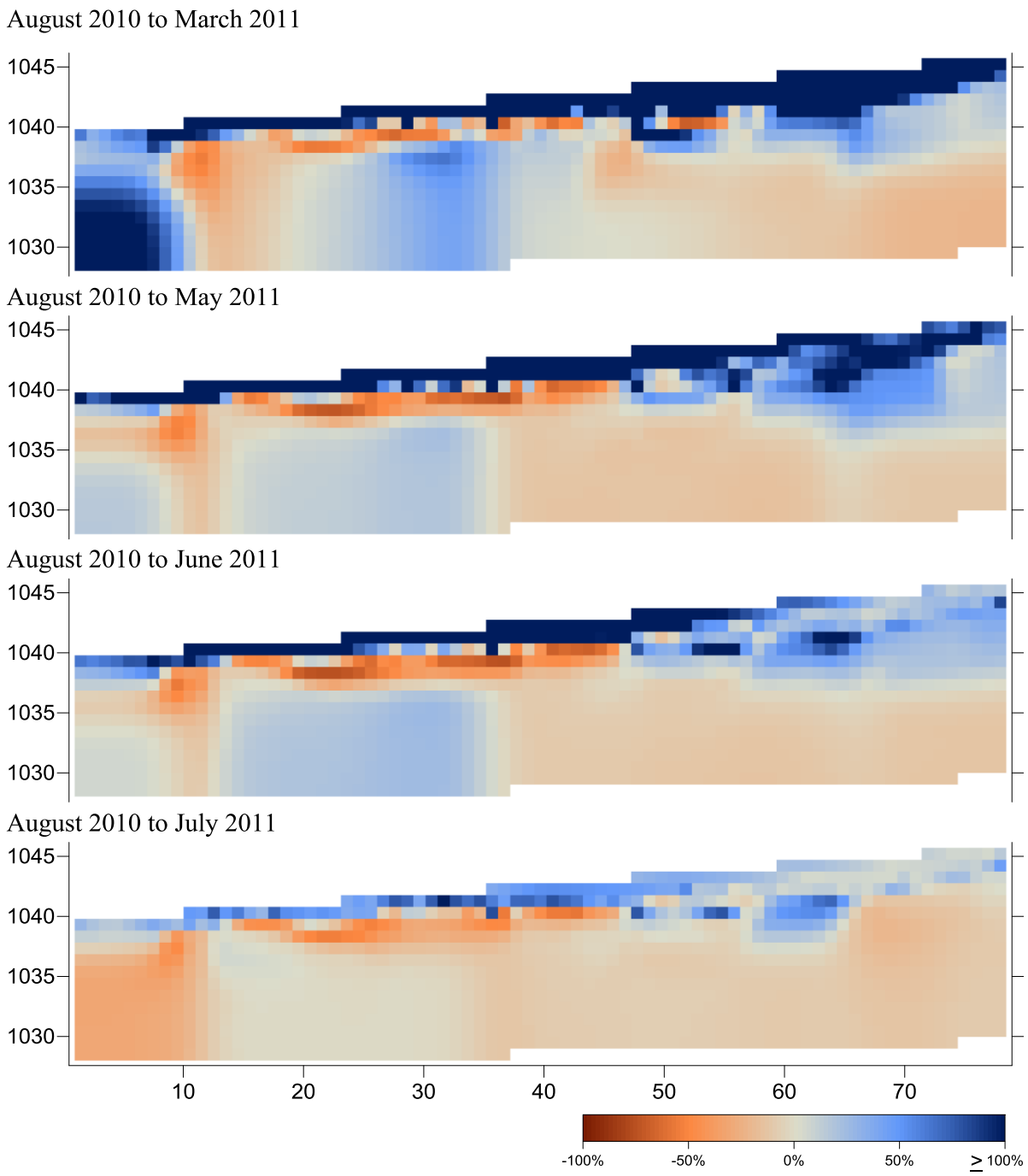

Figure 31 - Relative change in resistivity based on the August 2010 survey for MP 400.5.

The August to March survey comparison showed a large increase in resistivity in the near-surface, as well as in a permafrost body from approximately 0 to 10 m at the bottom of the profile. However, this body was near the edge of the profile and was therefore subject to considerable uncertainty. The successive profiles showed lesser near-surface resistivity increases. The July and

August surveys exhibited relatively equal amounts of minimum model blocks, approximately 28%. The similarity between these two surveys was evident in the August to July comparison. For all of the comparisons the lower portion of the profiles remained fairly consistent. The near-surface resistivity change was greatest from 50 to 80 m along the profile for each comparison. This area was classified as indeterminate or frozen.

5.1.5 MP 579.1

MP 579.1 is located 70 km east-southeast of Watson Lake, and is approximately 725 m asl. This site has less than 0.5 m in elevation change, and is located down a steep slope from the Alaska Highway. Due to this steep slope there was standing water present at the beginning of the profile in May 2011 (Figure 32a). Standing water was also present at 55 m and 70 m along the profile in May 2011. All standing water was gone by the June 2011 survey. The microtopography (Figure 32b) is hummocky, with non-sphagnum mosses, Labrador tea, sphagnum mosses, lichen, and dwarf birch (James 2010). Spruce trees are present along the profile. The soil is moderately cohesive with peat and sandy silt (James 2010).

a)  b) 

Figure 32 – MP 579.1 site photos a) Taken in March 2011 from 0 m looking in front of the profile, this photo shows the large embankment from the Alaska Highway to the site (shown by the parked white vehicle) and the standing water present near the first electrode of the profile; b) taken in July 2011 from approximately 75 m looking towards the back of the profile, this photos shows the microtopography of the profile.

Figure 33 displays the daily ground temperature and snow depth values for MP 579.1. The air temperature logger at this site malfunctioned in December 2012, which did not allow for a suitable number of measurements to be correlated with another location.

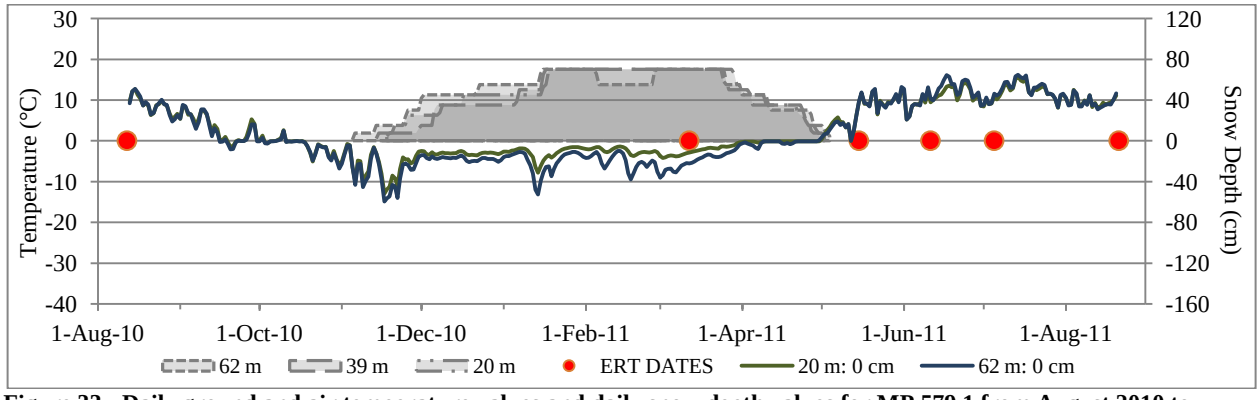

Figure 33 - Daily ground and air temperature values and daily snow depth values for MP 579.1 from August 2010 to August 2011. The red dots symbolize ERT collection days at this site. The air temperature malfunctioned, as did the 20 cm ibutton at the 39 m snow stake.

The mean annual ground surface temperature at MP 579.1 varied from 1.3 to 2.1 ºC. Although there was a 0.8 ºC range in annual temperature, the loggers located at the same location along the plot had differences of less than 0.3 ºC. At 20 m, the mean temperatures were 1.7 ºC to 2.1 ºC, and at 62 m the means were 1.3 ºC to 1.5 ºC. The loggers at 20 m had higher minimum daily temperatures, lower maximum daily temperatures, and lower temperature ranges in comparison to the loggers at 62 m. The temperatures at 20 m were less affected by snow cover, which can be seen in Figure 33. The spring zero curtain at this site started on approximately April 8th and lasted for 22 days.

The snow cover at MP 579.1 began in early November and the pack continued to accumulate until mid-March. The snow cover then began to thin until the beginning of May. The snow began to accumulate first at the 62 m station and subsequently at the 20 m station and then at the central 39 m station. This central snow stake had 8243 SDD, which is greater than 39 m (7850 SDD) and less than 62 m (8590 SDD). The 9% difference between the 39 m SDD and the other locations may be an effect of the 20 cm ibutton malfunctioning. The difference in SDDs for each snow stake equates to a 4 cm difference in annual snow cover from the snow stake with the lowest SDD, 39 m, and the highest SDD, 62 m.

The daily ground temperature summary statistics for MP 579.1 are shown in Table 7. Ground temperatures were consistent at different locations along the profile.

Table 7- Daily ground temperature summary statistics for MP 579.1, August 2010-2011.

Depth (m)	20 m				39 m				62 m			
	x̄	Max	Min	Range	x̄	Max	Min	Range	x̄	Max	Min	Range
0.00	1.8 2.1	15.2 15.8	-13.4 -12.9	28.6 28.7					1.6 1.3	17.1 16.2	-17.2 -14.9	34.4 31.1
0.25					0.6	6.0	-2.6	8.6				
0.50	0.2	2.4	-0.7	3.0	0.1	1.0	-0.3	1.3	-0.3	0.6	-0.8	1.4
0.75					0.1	0.6	0.0	0.7				
1.00	0.0	1.3	-0.3	1.6	0.0	0.4	-0.1	0.5	-0.1	0.2	-0.2	0.4
Grey cells indicate sensors that were not installed at that depth for that station.												

The apparent resistivity data at MP 579.1 had a mean of 404 Ωm. The spatial mean apparent resistivities from August 2010 to July 2011 were 251 Ωm, 555 Ωm, 460 Ωm, 412 Ωm and 341 Ωm.

The inverted resistivity data had a mean of 460 Ωm. The highest resistivity measurement was 20.1 kΩm and occurred in March, the lowest resistivity measurement was 21 Ωm and occurred in August. The largest percentage of measurements (70 – 93%) were less than 500 Ωm for each survey at this site.

Figure 34 shows the August 2010 ERT survey, frost table depth and permafrost classification map for MP 579.1. The measured, calculated, and inverse profiles for each survey at this site are presented in Appendix H.

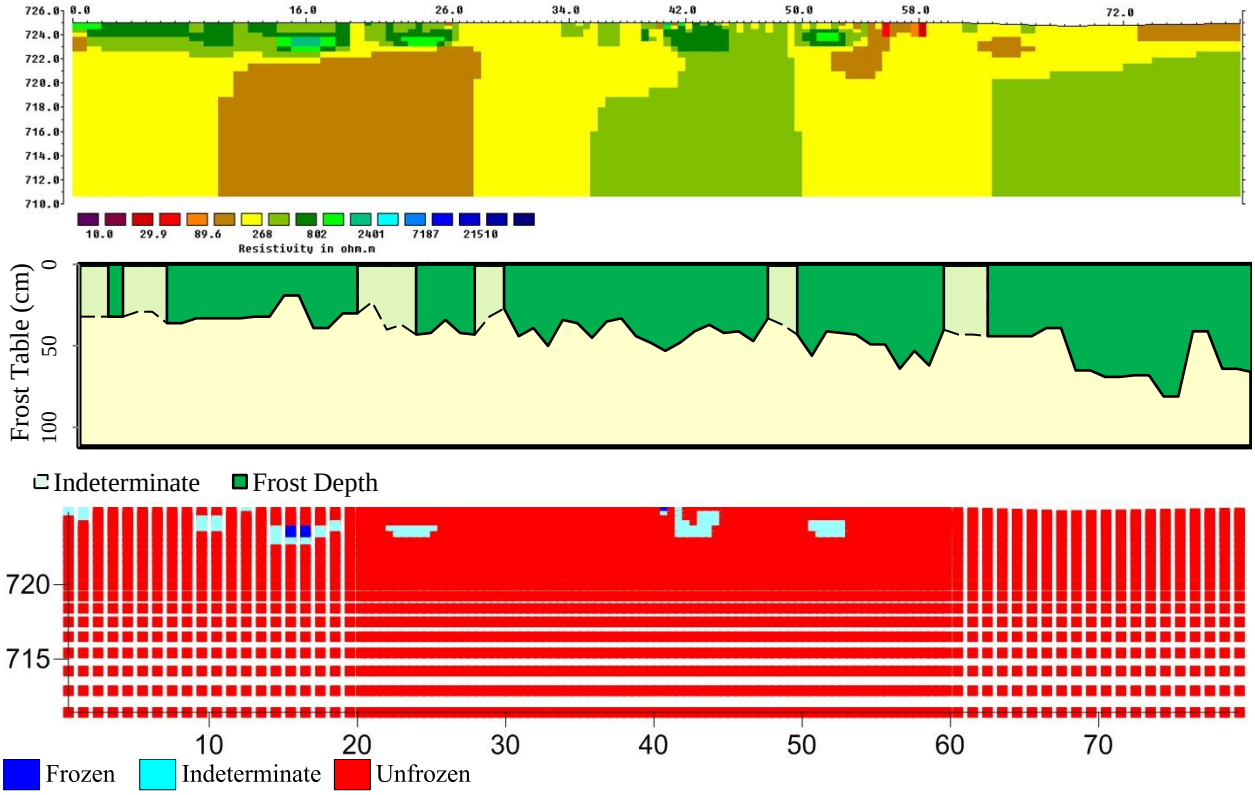

Figure 34 - Inverted ERT profile, frost table depths and permafrost classification image for MP 579.1 for the August 2010 survey. Legends for each of the images are in the bottom left corner. For the frost table image, areas of light green with dashed lines had an annual frost progression that was not logical. For the permafrost classification image unfrozen is 0 to 600 Ωm, indeterminate is 600 to 1,300 Ωm, and frozen is all model blocks greater than 1,300 Ωm. All images have identical horizontal scales in meters. The inverted ERT profile and permafrost classification image have vertical scale in meters.

There were several small sections along the profile that were identified as having gravel and others where there was very cohesive stiff soils, both of which could have affected the frost table

probing results. The upper boundaries for unfrozen and indeterminate are 600 Ωm and 1,300 Ωm, respectively.

Figure 35 shows the virtual borehole measurements for each climate station.

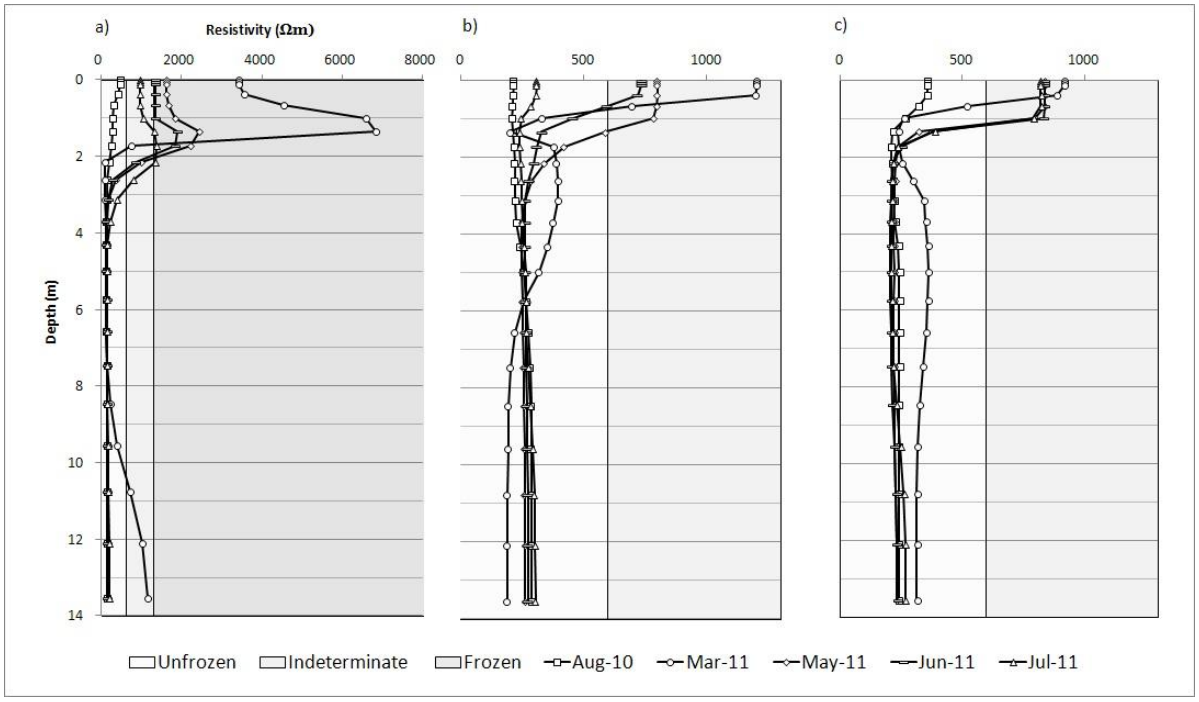

Figure 35 - Virtual boreholes for MP 579.1 at a) 20 m; b) 39 m; c) 62 m along the profile length. Note the difference in scale in a).

The virtual borehole at 20 m showed seasonally frozen ground approximately 2.0 m to 2.5 m thick. The August 2010 survey indicated no frozen ground present at this location. The temperature data for this location also suggested there was no permafrost present as the temperature sensors at 50 cm and 100 cm both went above 0 ºC. The 50 cm logger was below 0 ºC for the March and May surveys, and the 100 cm logger was below 0 ºC for every survey except for the one in August 2010. This pattern was consistent with the resistivity values and the classified permafrost boundaries. The frost probing in this area was inconclusive due to the presence of gravel.

At 39 m, the virtual borehole showed seasonally frozen ground that was 1 – 1.5 m thick. The August 2010 and July 2011 surveys indicated that no frozen ground present. The frost table data at this location was inconsistent with the virtual borehole. The temperature loggers present all went

above 0 ºC. In March all of the temperature sensors, to a depth of 100 cm, were below 0 ºC, which is consistent with the virtual borehole.

At 62 m there was a layer of seasonally frozen ground 1.50 m to 1.75 m thick. There was a frost table of 44 cm in August 2010, which was inconsistent with the virtual borehole findings. The 50 cm and 100 cm temperature sensors both went above 0 ºC, however they only did this after the July 2011 survey. Therefore, the August 2010 survey should have had higher resistivity values in the near-surface.

Based on the results from the August 2010 ERT survey alone it is possible to conclude that there is no permafrost present at MP 579.1. However, based on the other available data, and the surveys conducted throughout 2011 (Appendix H), it is more probable that there is permafrost present at this site. Temperature and frost probe data indicate very warm permafrost at least at 62 m. It is possible that the ground at this site was so dry that the transition from frozen to unfrozen ground did not exponentially change the resistivity values. It is also possible that coarser soil was present at this site, which caused the unfrozen moisture content to decrease more rapidly within a smaller range of temperature.

Figure 36 shows the relative inverted resistivity changes based on the August 2010 survey.

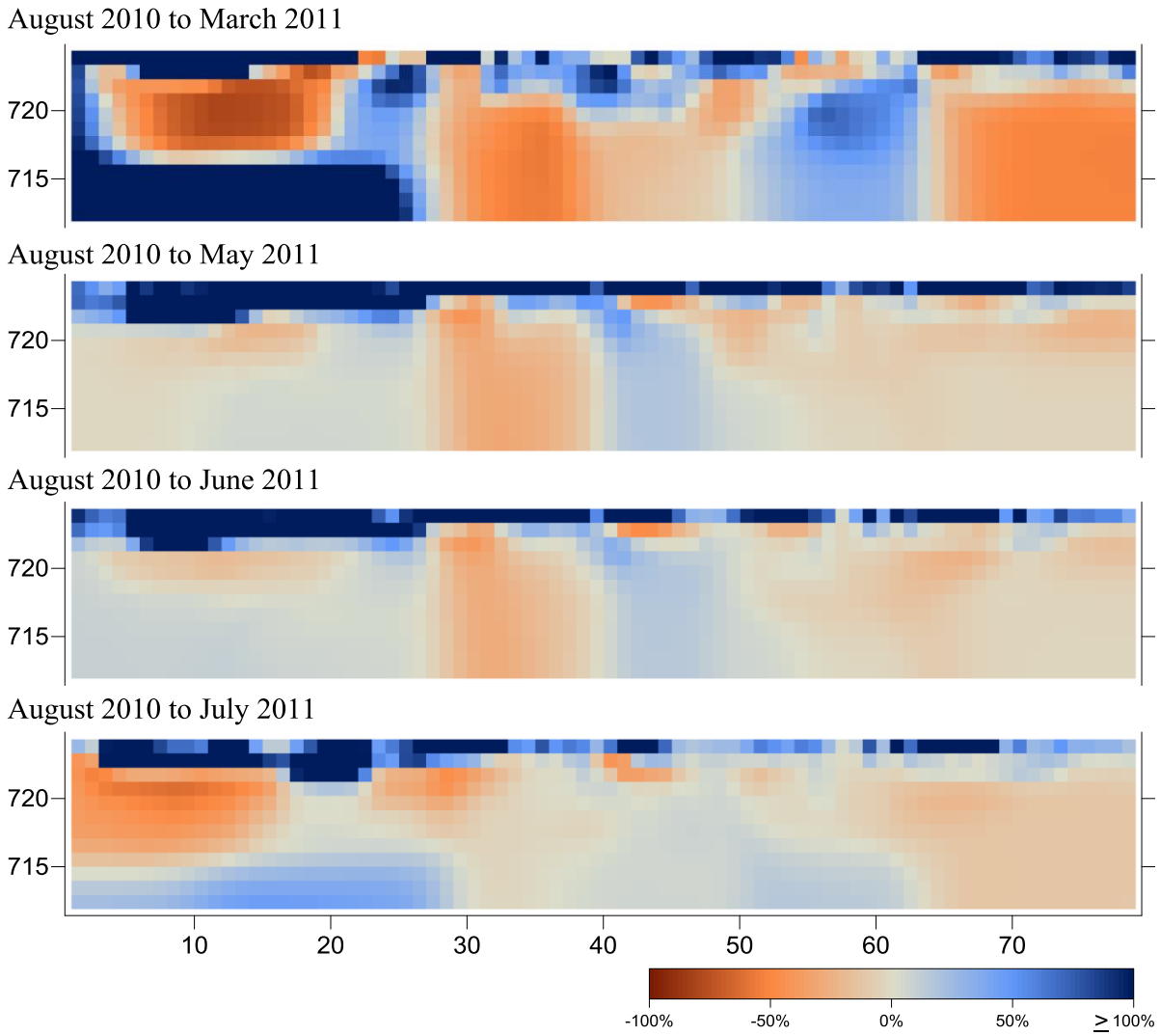

Figure 36 - Relative change in resistivity based on the August 2010 survey for MP 579.1.

The August to March profile showed high resistivity change within the near-surface. Approximately 37% of the model blocks had their minimum values in August and 46% of the model blocks had their maximum values in March. These percentages are the largest proportion of minimum and maximum values; therefore, the maximum amount of change occurred between August and March. There was also substantial resistivity increases in the August to May, August to June, and August to July comparisons. The near-surface resistivity increases were greatest from 0 to 20 m, where small patches of ground classified as indeterminate were present.

5.1.6 MP 597.5

MP 597.5 is located approximately 45 km southeast of Watson Lake, and is at approximately 682 m asl. The site gradually slopes downward towards the end of the profile, with a difference of 2.7 m from the front of the profile to the back. In May 2011 no snow or standing water was present at this site. Soils are peaty and the site has spruce, tamarack, lichen, Labrador tea, sphagnum moss, dwarf birch, and non-sphagnum mosses (James 2010). The soil is organic with sand, silt, and some stones (James 2010). The vegetation can be seen in Figure 37 a and b.

a)  b) 

Figure 37 – Site photos for MP 597.5, both showing the vegetation a) taken June 2011 from approximately 45 m looking towards the back of the profile; b) Taken in July 2011from approximately 10 m looking towards the back of the profile.

Figure 38 displays the daily air temperature, ground temperature, and snow depth measurements for MP 597.5. There was a large range of variability in daily air temperatures at this site, but temperatures remained well below 0 °C throughout the winter. The air temperature at this site had an annual mean of -2.9 °C, with a daily temperature range of 64.3 °C. The minimum daily value was -45.0 °C and the minimum hourly value was -48.0 °C and occurred at 10:00 on January

14, 2011. The maximum daily value was 19.3 °C and occurred on July 14, 2011, while the maximum hourly value was 32.4 °C and occurred on August 5, 2010 at 1400.

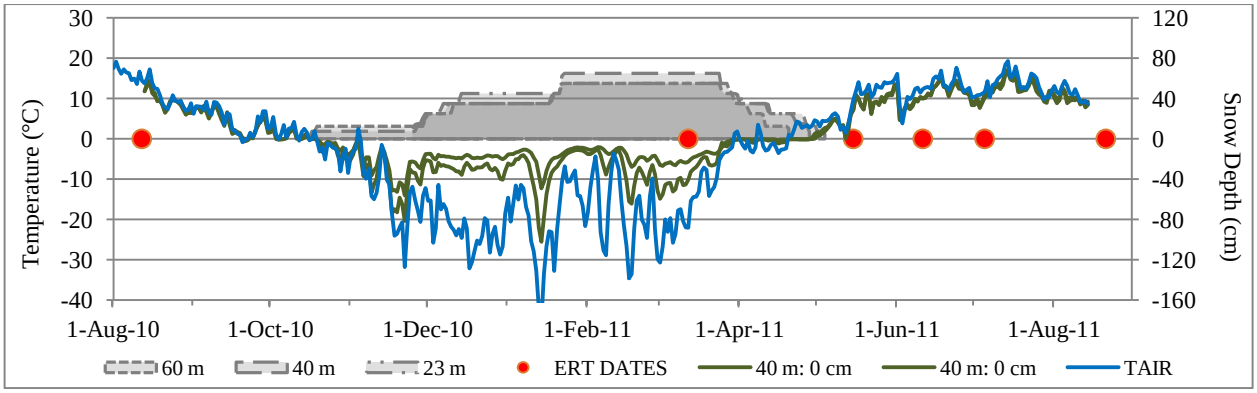

Figure 38 - Daily ground surface and air temperature values and daily snow depth values for MP 597.5 from August 2010 to August 2011. The red dots symbolize ERT collection days at this site. The 60 cm ibutton at the 40 m station and the 10 cm ibutton at the 60 m station malfunctioned.

The mean annual ground surface temperature at MP 597.5 varied from 0.3 °C to 1.8 °C. There was variation in temperature throughout the site and at each station. At 23 m, the ground temperature was 1.2 °C. At 40 m the annual ground temperature varied from 0.3 °C to 1.8 °C. This area had both the lowest and highest temperature range (i.e., 31.2 °C to 42.0 °C) and the lowest and highest daily minimum daily minimum temperature (i.e., -14.0 °C and -25.6 °C). At 60 m, the annual ground surface temperature was 1.1 °C to 1.6 °C. The spring zero curtain for this site began at the end of March and continued for approximately 30 days until the end of April.

The snow at MP 597.5 began to cover the ground in mid-October, and continued to build until the end of January when each snow stake experienced its maximum snow depth. This depth was maintained until the end of March, when the snow cover decreased until the beginning of May. At 23 m, the snow began more than a month after the other locations. It reached a maximum snow depth of 55 cm, and had 6744 SDD. In contrast, the snow at 40 m began the earliest and was interpreted as reaching a maximum depth of 65 cm. This difference in maximum snow depth related in part to the malfunctioning of the 60 cm ibutton. Once the 50 cm ibutton had been covered, the level was set as mid-way to the next button on the stake at 80 cm. There were 7344 SDD at the 40 m stake, the highest SDD value. At 60 m, the snow cover began at approximately the same time as the 40 m, but

only reached a maximum snow depth of 55 cm. It was the first location to lose its snow cover and had 6451 SDD. The difference in SDDs for each snow stake was 14%, which accounts for approximately a 4 cm difference in annual snow cover from the snow stake with the lowest SDD, 60 m, and the highest SDD, 40 m.

Table 8 shows the daily ground temperature summary statistics for MP 597.5. Ground temperatures were consistent throughout the plot.

Table 8 – Daily ground temperature summary statistics for MP 597.5, August 2010-August 2011.

Depth (m)	23 m				40 m				60 m			
	x̄	Max	Min	Range	x̄	Max	Min	Range	x̄	Max	Min	Range
0.00	1.1	25.8	-19.2	45.0	0.3 1.8	16.4 17.2	-25.6 -14.0	42.0 31.2	1.1 1.6	18.2 17.2	-22.1 -15.5	40.3 32.7
0.10	0.9	14.7	-12.6	27.2								
0.25	1.0	11.5	-6.7	18.2								
0.40	0.0	4.3	-2.4	6.7								
0.50	-0.4	2.4	-2.0	4.4	-0.2	-0.1	-0.9	0.9	-0.2	0.2	-1.3	1.5
1.00					-0.1	-0.1	-0.4	0.4	-0.3	-0.2	-0.5	0.3
Grey cells indicate sensors that were not installed at that depth for that station.												

The apparent resistivity data at MP 597.5 had a mean of 1.9 kΩm. The spatial mean apparent resistivities from August 2010 to July 2011 were 1.4 kΩm, 3.0 kΩm, 1.7 kΩm, 1.7 kΩm and 1.5 kΩm. The inverted resistivity data had a mean of 2.4 kΩm. The maximum value was 39.5 kΩm and the minimum value was 36 Ωm; both values occurred in March. 70% to 93% of the resistivity measurements were less than 500 Ωm for the surveys conducted at this site.

Figure 39 shows the inverted ERT profile, frost table depth, and classified permafrost image for August 2010 for MP 597.5. The measured, calculated, and inverse profiles for each survey for this site are presented in Appendix I.

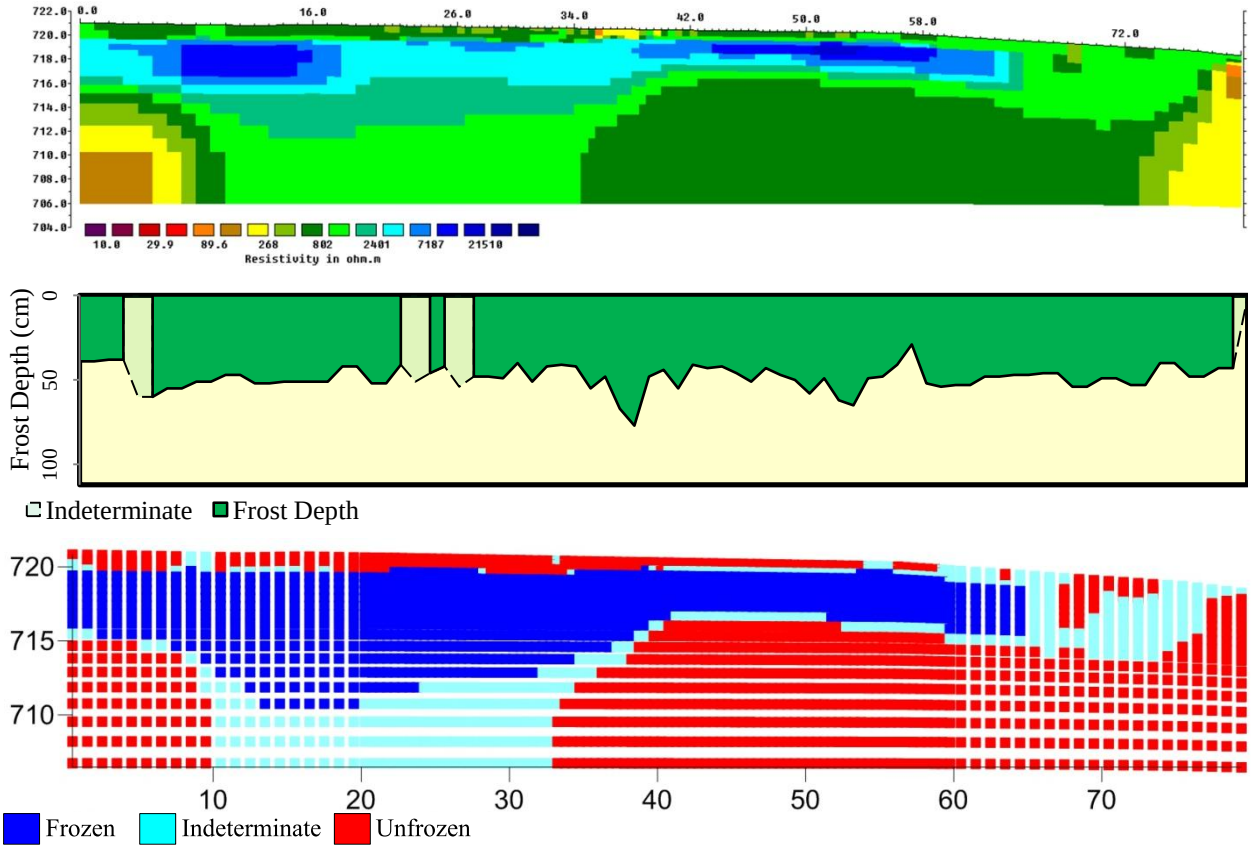

Figure 39 - Inverted ERT profile, frost table depths and permafrost classification image for MP 597.5 for the August 2010 survey. Legends for each of the images are in the bottom left corner. For the frost table image, areas of light green with dashed lines had an annual frost progression that was not logical. For the permafrost classification image unfrozen is 0 to 900 Ωm, indeterminate is 900 to 1,300 Ωm, and frozen is all model blocks greater than 1,300 Ωm. All images have identical horizontal scales in meters. The inverted ERT profile and permafrost classification image have vertical scale in meters.

Small areas in the first half of the profile had illogical frost table progressions. The upper boundaries for unfrozen and indeterminate were 900 Ωm and 1,300 Ωm, respectively. These values were based on all of the available data from the climate stations at this site.

Figure 40 displays the virtual boreholes for the three climate stations at MP 597.5.

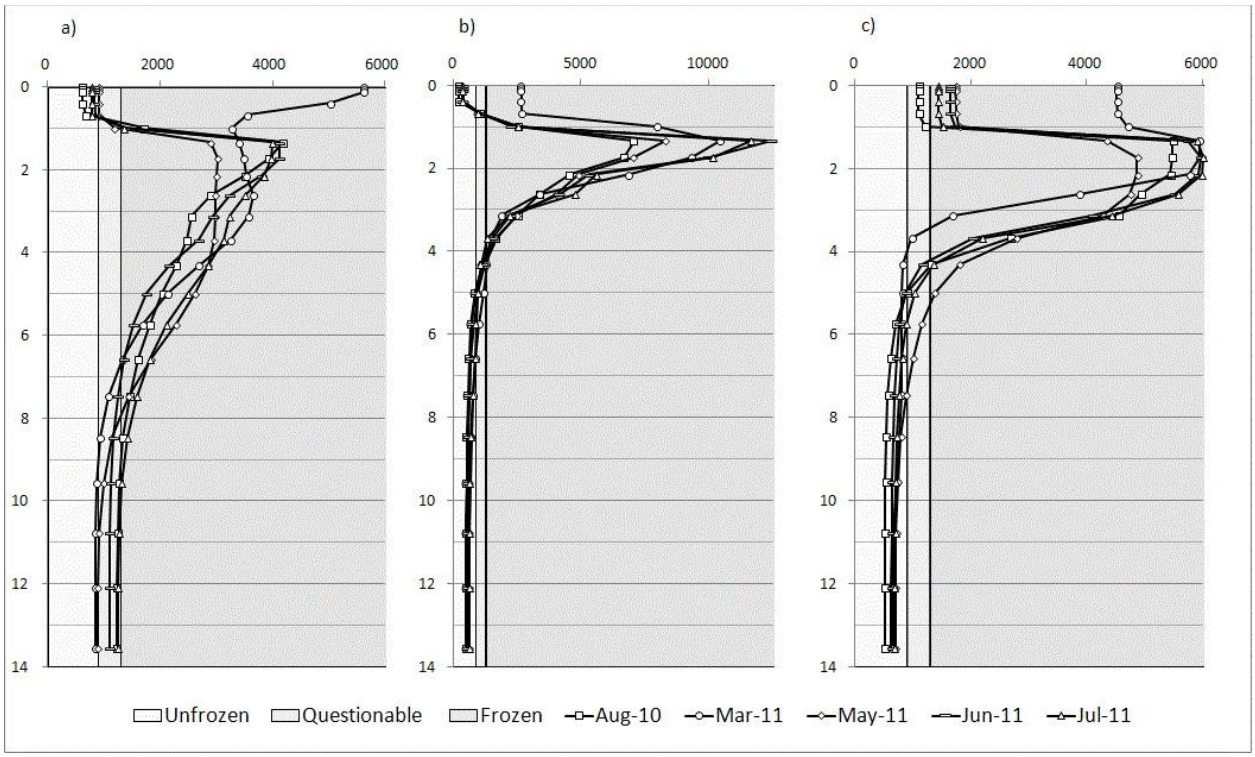

Figure 40 - Virtual boreholes for MP 597.5 at a) 23 m; b) 40 m; c) 60 m along the profile length. Note the difference in scale in b).

The virtual borehole at 23 m showed seasonally thawed ground that was approximately 1 m thick over permafrost that was approximately 7 m thick. The frost probing at this location was never deeper than 51 cm, which is somewhat consistent with resistivity data. The temperature sensors present at this location (i.e., 10 cm, 25 cm, 40 cm and 50 cm) all went above 0 °C, which was consistent with the frost probing data.

At 40 m, the resistivity values showed an active layer of 50 cm with permafrost extending to a depth of approximately 4 m. The frost probing was consistent with the resistivity data and had a maximum frost probe depth of 49 cm in August 2011. In addition, the temperature sensors at 50 cm and 100 cm were both within permafrost.

At 60 m, the virtual borehole showed an active layer of approximately 1 m and permafrost that was approximately 3.5 m thick. The active layer resistivity values were never low enough to regard the near-surface as ‘unfrozen’, however the consistent resistivity values between 0 – 1 m

depths during each survey, and the large difference between the resistivities at 1 m and 1.3 m indicated that a transition from thawed to frozen was present.

The frost probing, temperature, and ERT data suggested there was permafrost present at MP 597.5. This body of permafrost begins before the start of the profile and may end at beyond 65 – 80 m. The thickness of this body ranges from 5 – 13 m, with the thickest portion from 10 – 35 m along the profile.

Figure 41 shows the relative inverted resistivity changes based on the August 2010 survey.

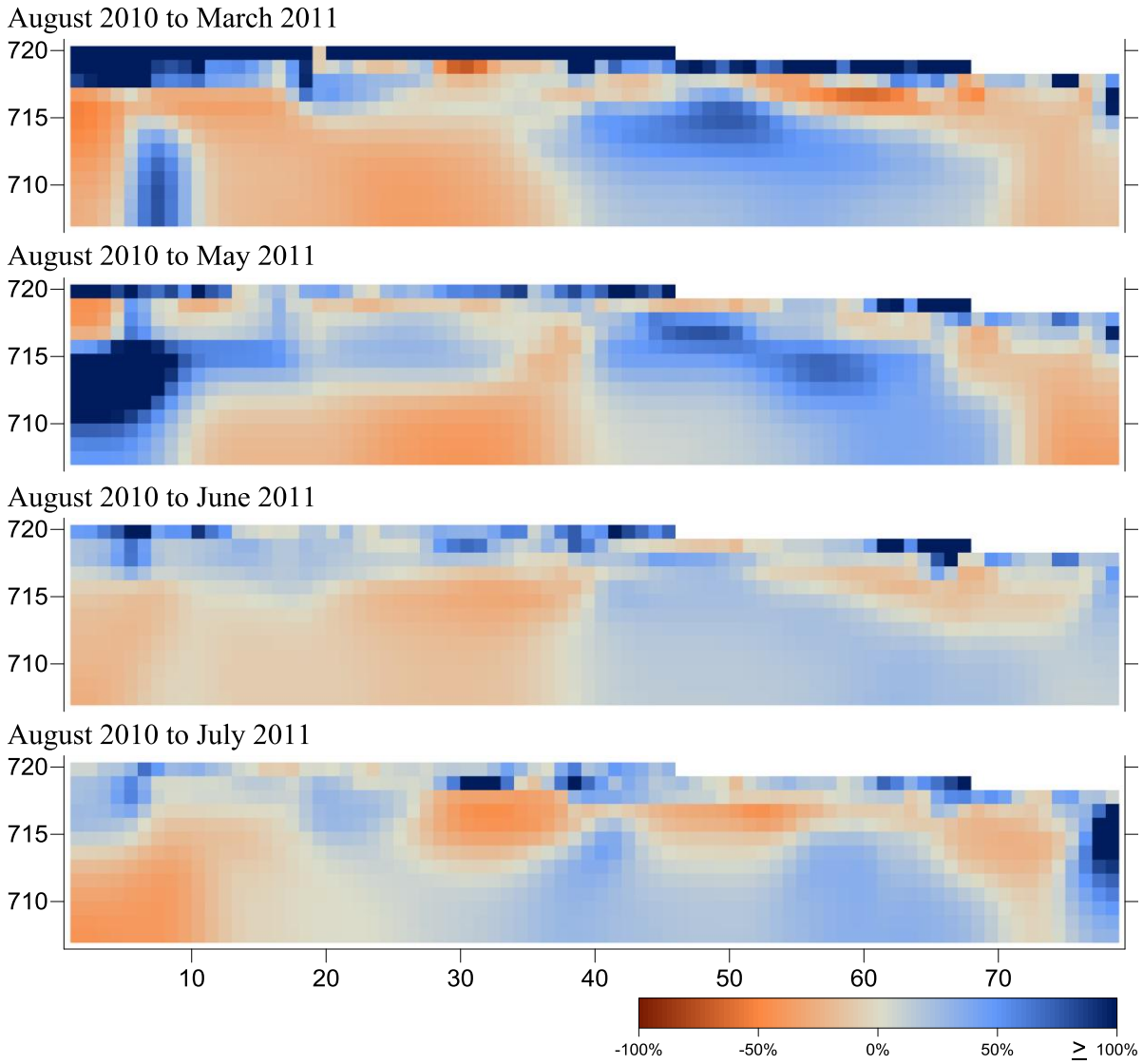

Figure 41 - Relative change in resistivity based on the August 2010 survey for MP 597.5.

Approximately 40% of the model blocks had their maximum resistivity values in March and their minimum resistivity values in August. This trend can be seen in the August to March comparison, which has large changes in the near-surface and in the first 5 m of the profile. The near-surface percent change decreases from each comparison plot to the next. This pattern may be due to the fact that MP 597.5 has a visible active layer in the ERT surveys from 0 – 60 m, and the seasonal freezing and thawing can be seen more prominently than in other surveys. In general, the percent changes at this site do not appear to be as extreme as the other sites (excluding MP 400.5).

5.1.7 MP 681.1

MP 681.1 is located approximately 65 km northwest of Watson Lake at an elevation of 849 m asl. The profile topography is fairly flat, with less than 1 m in elevation change from the front of the profile to the back, and associated with hummocky topography. In May 2010 there were small patches of snow present throughout the profile. In addition to the snow, there were large areas of standing water from 59 – 70 m and 74 – 80 m. These water bodies were present up to and including the July 2011 site visit. Figure 42 shows the area from 59 – 70 m in both May 2011 (Figure 42a) and July 2011 (Figure 42b). Spruce, tamarack, and willow are present at this site, with maximum tree height being approximately 15 m for spruce (James 2010). Mosses, lichen, Labrador tea and birch shrubs are also present (James 2010). The soil is moderately cohesive with silt and organics (James 2010).

a)  b) 

Figure 42 – MP 681.1 site photos a) Taken in May 2011 from approximately 59 m looking towards the back of the profile, this photo shows a patch of snow and standing water; b) Taken in July 2011 from approximately 59 m looking towards the back of the profile, this photo shows the vegetation and the remains of the standing water.

Figure 43 shows the daily air and ground temperature and snow depth values for MP 681.1. The mean annual air temperature at MP 681.1, which was partially obtained by correlation with nearby Watson Lake, was -3.3 ºC. The daily temperature range was 60.2 ºC, with the minimum daily temperature of -42.6 ºC and a minimum hourly value of -46.1 ºC which occurred at 08:00. The maximum daily temperature (17.6 ºC) occurred on July 13, 2011, and the maximum hourly temperature (24.7 ºC) occurred at 1600 on that day. Daily air temperatures in the winter remained well below 0 ºC at this site.

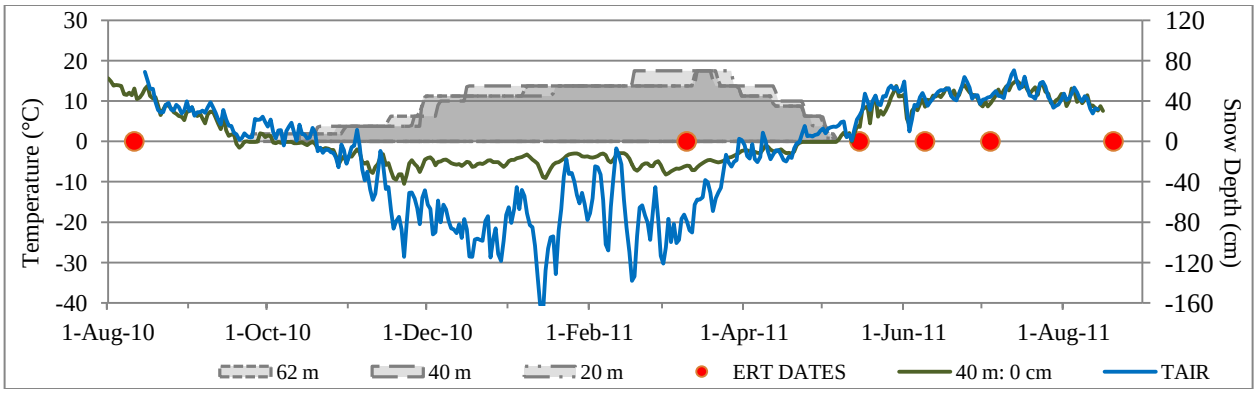

Figure 43 - Daily ground and air temperature values and daily snow depth values for MP 681.1 from August 2010 to August 2011. The red dots symbolize ERT collection days at this site. The air temperature at this site is correlated from Watson Lake.

The mean annual ground surface temperature varied from 0.7 ºC to 1.5 ºC. The lowest daily minimum was -18.5 ºC and occurred on January 13, 2011. The highest daily maximum was 16.2 ºC and occurred on July 12, 2011. The spring zero curtain at this site lasted for approximately 14 days, from April 21 to May 4, 2011.

Snow began to accumulate at MP 681.1 in late September and the pack continued to build until mid-March. Snow depths then began to decrease and snow was no longer present by the beginning of May. At 20 m, snow cover began on October 12, 2010 and continued to build until March 14, 2011 when it reached 70 cm. It had 8148 SDD which is less than at 50 m (8892 SDD) or 62 m (8456 SDD). At 50 m the snow began on October 13, 2010, but reached 70 cm on February 18, 2011, which is a month earlier than the other locations. At 62 m the snow began much earlier than the other two locations, on September 24, 2010. The difference in SDDs for each snow stake was 9%, which accounts for approximately a 4 cm difference in annual snow cover from the snow stake with the lowest SDD, 20 m, and the highest SDD, 50 m.

The daily ground temperature summary statistics for MP 681.1 are shown in Table 9. Temperatures were consistent at similar depths along the profile.

Table 9 – Daily ground temperature summary statistics for MP 681.1, August 2010-2011.

Depth (m)	20 m				50 m				62 m			
	x̄	Max	Min	Range	x̄	Max	Min	Range	x̄	Max	Min	Range
0.00	0.7 1.0	14.0 15.1	-12.5 -10.6	26.4 25.6	1.0	15.1	-10.6	25.6	1.0 1.5	16.2 15.3	-18.5 -14.6	34.7 29.8
0.25	0.2	3.4	-2.3	5.6	-0.3	4.1	-5.5	9.7	0.5	8.7	-5.4	14.0
0.50					-0.5	0.1	-3.8	3.9				
0.65	-0.3	-0.2	-1.1	0.9					0.6	5.4	-1.1	6.5
Grey cells indicate sensors that were not installed at that depth for that station.												

The apparent resistivity data at MP 681.1 had a mean of 3.3 kΩm. The spatial mean apparent resistivities from August 2010 to July 2011 were 1.5 kΩm, 7.0 kΩm, 3.1 kΩm, 2.6 kΩm and 2.1 kΩm. The inverted resistivities had a mean of 5.1 kΩm. The maximum value of 158 kΩm occurred in March while the minimum of 51 Ωm occurred in August. The resistivity values had a large range, but 44% to 65% of the measurements were less than 2000 Ωm.

Figure 44 shows the ERT profile, frost probe depth and permafrost classification image for MP 681.1 from the August 2010 survey. The measured, calculated, and inverse profiles for each survey at MP 681.1 are presented in Appendix J.

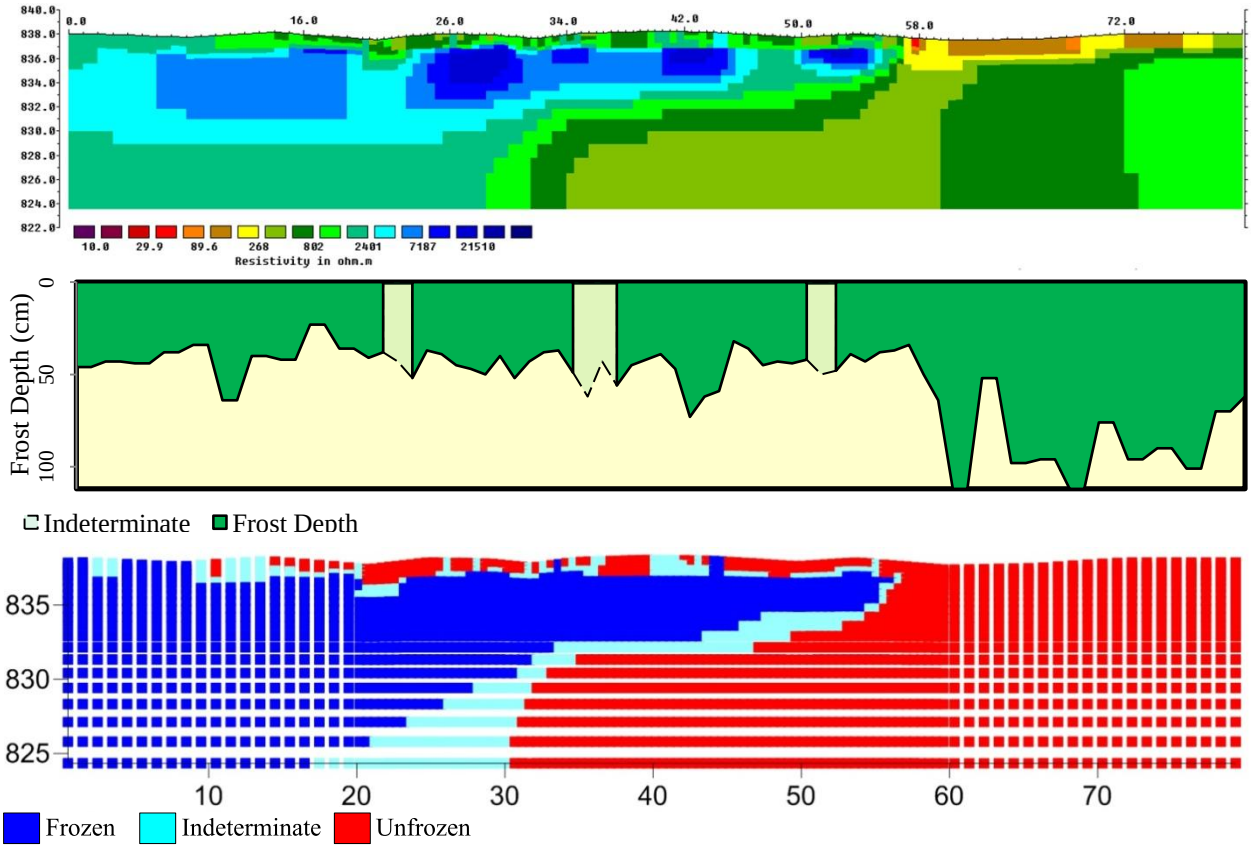

Figure 44 - Inverted ERT profile, frost table depths and permafrost classification image for MP 681.1 for the August 2010 survey. Legends for each of the images are in the bottom left corner. For the frost table image, areas of light green with dashed lines had an annual frost progression that was not logical. For the permafrost classification image unfrozen is 0 to 1,000 Ωm, indeterminate is 1,000 to 1,900 Ωm, and frozen is all model blocks greater than 1,900 Ωm. All images have identical horizontal scales in meters. The inverted ERT profile and permafrost classification image have vertical scale in meters.

Small sections near the centre of the profile did not have logical frost table progressions. The upper limits for unfrozen and indeterminate were assessed as 1,000 Ωm and 1,900 Ωm, respectively. Figure 45 shows the virtual boreholes for each climate station at this site.

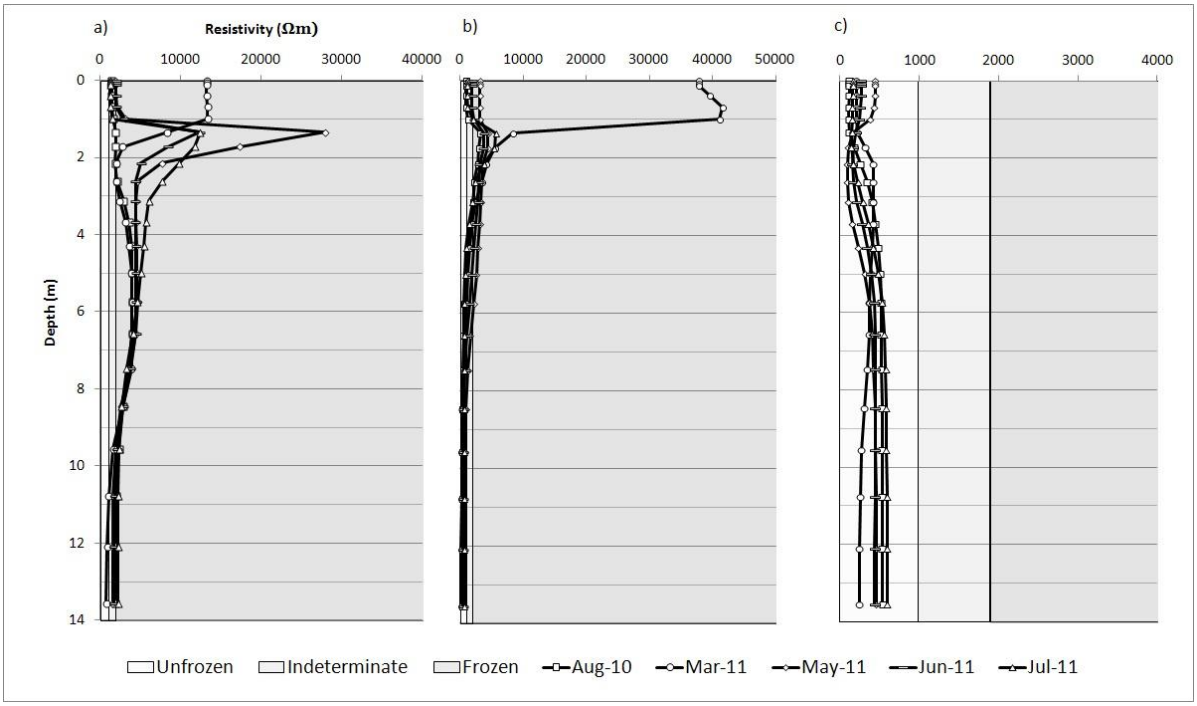

Figure 45 - Virtual boreholes for MP 681.1 at a) 20 m; b) 50 m; c) 62 m along the profile length. Note the differences in scale.

At 20 m, the virtual borehole suggested an active layer approximately 1 m thick overlying permafrost that was 9 – 10 m thick and possibly extended to the base of the profile. The frost probing at this location showed a maximum frost table depth of 41 cm in August 2010. This is less than the virtual borehole suggests but is supported by the temperature data because the sensor at 65 cm was within permafrost. Therefore, it was possible that the active layer at this location was less than 1 m. However, the resistivity values are too consistent from 0 m to 1 m to see a thinner active layer within the virtual borehole.

The virtual borehole at 50 m showed an active layer of 1 m with a permafrost layer of 5 m to 6 m. The temperatures sensors at 25 cm and 50 cm were both not within permafrost, which was consistent with the virtual borehole. However, the maximum frost probing depth at this location was 44 cm, which was thinner than the thawed layer inferred in Figure 45.

At 62 m, the virtual borehole showed an area of no permafrost and no seasonally frozen ground. Frost probing at this location was 52 m in August 2010, which is inconsistent with the

virtual borehole. The sensors at 25 cm and 65 cm both had an annual temperature above 0 °C, but were both below 0 °C during the March and May surveys. Therefore, the near-surface resistivity values seem to have been impacted by the low resistivity values beneath.

Based on the available data, the permafrost at MP 681.1 was present from 0 m to 57 m along the profile. The thickness of the permafrost ranged from beyond the penetration depth of the survey to approximately 6 m. The area beyond 57 m was unfrozen, most likely due to the standing water that was present for the majority of the annual cycle.

Figure 46 shows the relative inverted resistivity changes based on the August 2010 survey.

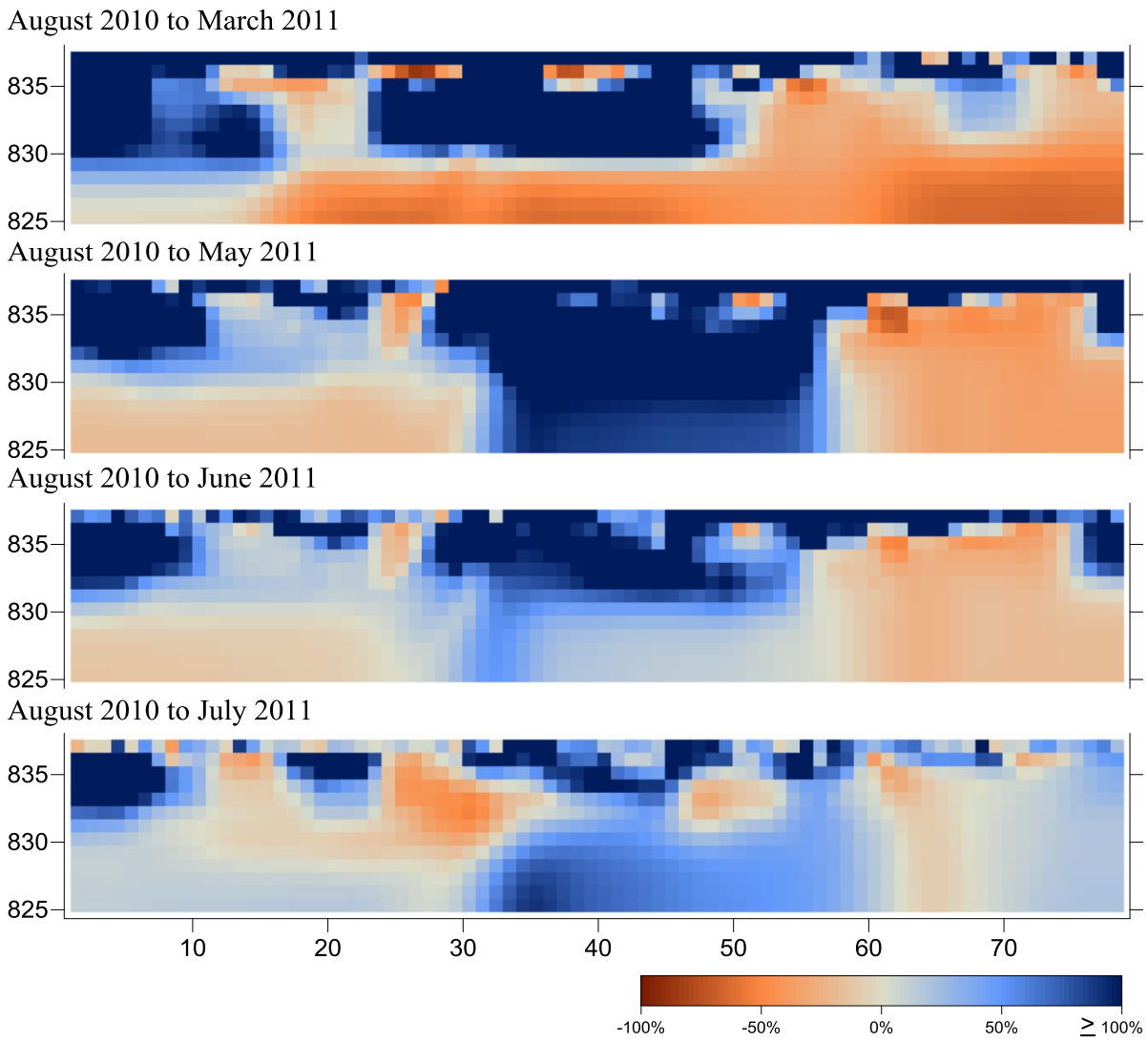

Figure 46 - Relative change in resistivity based on the August 2010 survey for MP 681.1.

The August to March survey had the largest change within the near-surface. This difference is because the August survey had the highest percentage of minimum model blocks (40%) and the March survey had the highest percentage of maximum model block (42%). The majority of the minimum and maximum blocks occurred in the near-surface. The increases in resistivity appeared to decrease with each survey, with the August to July survey having the least amount of percent change in the near-surface and at greater depths. Within all of the surveys there was a large increase in resistivity in the deeper portions of the profile from 0 – 10 m and from 30 – 60 m. These values also coincided with high resistivity values in the near-surface and may be artefacts.

5.1.8 MP 788.5

MP 788.5 is located 170 km southeast of Whitehorse and is at approximately 760 m asl. The first 24 m of the profile are within a grassy area with few hummocks and mosses. The rest of the profile is on a hummocky peat plateau with mosses, lichens, and Labrador tea (James 2010). Spruce have a maximum height of approximately 12 m in the area (James 2010). The change in vegetation can be seen in Figure 47b. The topography of the profile is, generally, sloping downward from the front of the profile to the back. However, there are many undulations and only 1.8 m difference from the highest point (0 m) to the lowest (80 m). In May 2011 there was no snow cover present but a large area of standing water from 20 – 24 m. This area is just before the beginning of the peat plateau. There was also continued saturation until July 2011. Figure 47 shows this area in a) March 2011 and in b) July 2011.

a)  b) 

Figure 47 – MP 788.5 site photos a) Taken in May 2011 from approximately 18 m looking towards the back of the profile, this photo shows the area of standing water; b) Taken in July 2011 from approximately 18 m looking towards the back of the profile, this photo shows the vegetation present at the site and the beginning of the peat plateau.

Figure 47 displays the daily ground and air temperature values and daily snow depth values for MP 788.5 from August 2010 to August 2011. The mean annual air temperature at this site was -2.0 ºC, with a temperature range of 57.9 ºC. The minimum daily temperature was -39.9 ºC and the minimum hourly temperature was -45.7 ºC, which occurred at 1000 on January 14, 2011. The maximum daily temperature was 18.0 ºC and occurred on July 13, 2011, while the maximum hourly temperature was 27.1 ºC and occurred from 1500 to 1600 on July 12, 2011.

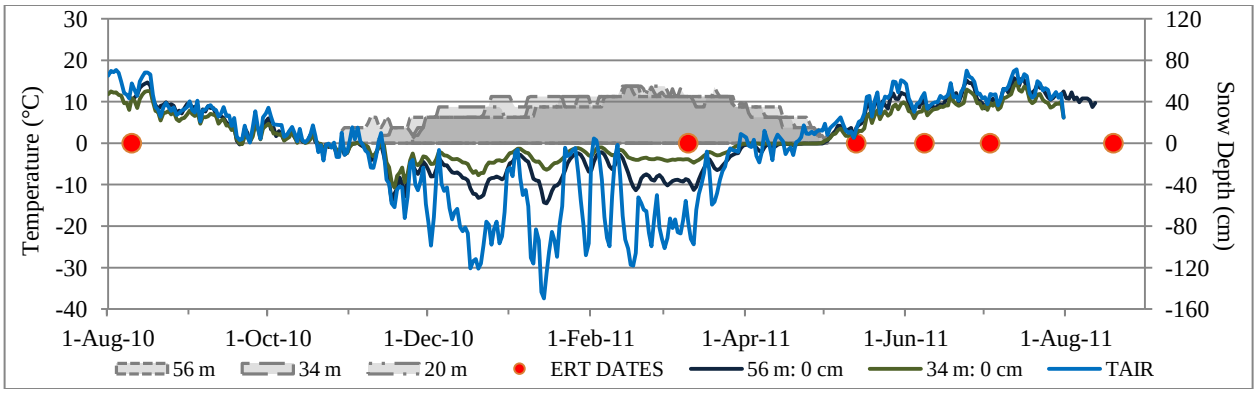

Figure 48 - Daily ground and air temperature values and daily snow depth values for MP 788.5 from August 2010 to August 2011. The red dots symbolize ERT collection days at this site.

The mean annual ground temperature varied from 1.8 °C to 3.8 °C. The large range in temperature was due to the loggers at 20 m where the ground temperatures were 3.3 °C and 3.8 °C. This area had the highest minimum daily temperature (-7.4 °C), the highest maximum daily temperature (15.9 °C), and the smallest range (23.2 °C). The stations at 40 m and 60 m had a mean annual temperature range from 1.8 - 1.9 °C. In addition to different annual temperatures, these stations had different zero curtains. The zero curtain began at the end of March for the 20 m logger and ended approximately a month later. The 60 m logger had a zero curtain that began in mid-April and finished at the beginning of May.

The snow cover at MP 788.5 began at the beginning of November and continued to build until mid-March when all the snow depths reached their maximum. The snow cover then began to decrease in the beginning of April, disappearing from the site by mid-May. At 20 m, the snow began at roughly the same time, with a long period of high snow cover after the beginning of April. This location had 6062 SDD, which is the lowest amount for this site. At 40 m, there were 6150 SDD, and at 60 m there were 6840 SDD. The difference in SDDs for each snow stake equates to a 4 cm difference in annual snow cover from the snow stake with the lowest SDD, 20 m, and the highest SDD, 60 m.

The daily ground temperature summary statistics for MP 788.5 are shown in Table 10. There is a notable temperature difference between the loggers at 20 m and the loggers present at the other

stations at this site. Temperatures at ground surface and 1.0 m depths are warmer at 20 m than at 40 and 60 m.

Table 10 – Daily ground temperature summary statistics, MP 788.5, August 2010-2011.

Depth (m)	20 m				40 m				60 m			
	x̄	Max	Min	Range	x̄	Max	Min	Range	x̄	Max	Min	Range
0.00	3.4 3.8	15.9 15.7	-7.4 -8.0	23.2 23.6	1.9	17.7	-12.1	29.8	1.8 1.9	13.9 13.9	-11.4 -10.2	25.4 24.0
0.50	--	--	--	--					-0.1	0.1	-0.9	1.0
1.00	1.2	5.4	-1.0	6.3	0.0	0.0	-0.2	0.2	-0.1	-0.1	-0.3	0.2
Cells with dashes indicate temperature sensors that failed. Grey cells indicate sensors that were not installed at that depth for that station.												

Figure 49 displays the temperature envelope for the borehole present at 40 m at MP 788.5. The temperature sensors at 0 m and 0.3 m both had a mean annual temperature above 0 °C. From 0.5 m to 1.5 m the mean annual temperature was below 0 °C, and once the borehole had stabilized thermally following drilling, the temperature remained less than 0 °C. The temperature range below 1 m in depth was less than 0.1 °C. Therefore, the depth of zero annual amplitude was only slightly greater than the depth of the active layer.

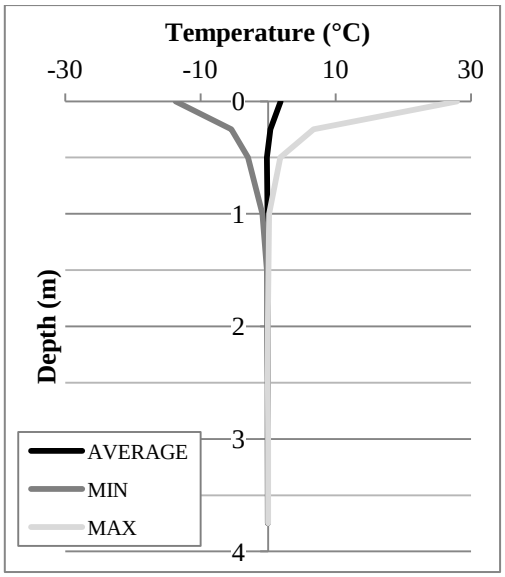

Figure 49 – Temperature envelope for MP 788.5 borehole, August 2010-2011.

The apparent resistivity data at MP 788.5 had a mean of 572 Ωm. The spatial mean apparent resistivities from August 2010 to July 2011 were 448 Ωm, 765 Ωm, 573 Ωm, 542 Ωm and 530 Ωm.

The inverted resistivity data had a mean resistivity value of 756 Ωm. The maximum value occurred in March (16.4 kΩm) and the minimum value occurred in August (16 Ωm). A large proportion of the resistivity values (i.e, 65 – 81%) were less than 1,000 Ωm.

Figure 50 shows the August 2010 ERT survey, frost probe depths and the corresponding permafrost classification image. The measured, calculated, and inverse profiles for each survey at MP 788.5 are presented in Appendix K.

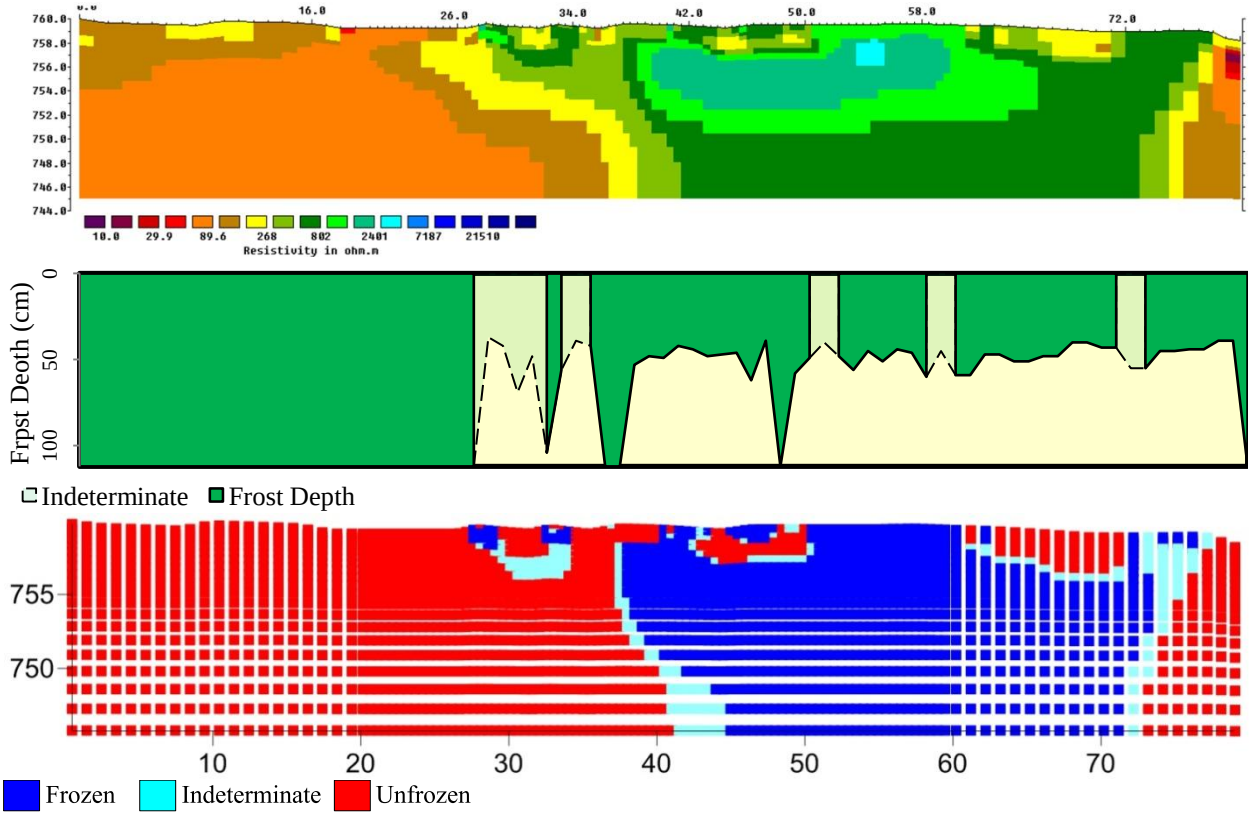

Figure 50 - Inverted ERT profile, frost table depths and permafrost classification image for MP 788.5 for the August 2010 survey. Legends for each of the images are in the bottom left corner. For the frost table image, areas of light green with dashed lines had an annual frost progression that was not logical. For the permafrost classification image unfrozen is 0 to 450 Ωm, indeterminate is 450 to 600 Ωm, and frozen is all model blocks greater than 600 Ωm. All images have identical horizontal scales in meters. The inverted ERT profile and permafrost classification image have vertical scale in meters.

Several sections along the profile had illogical frost probing which may have been due to gravel. The upper boundaries for unfrozen and indeterminate are 450 Ωm and 600 Ωm. Figure 51 shows the virtual boreholes for each climate station at MP 788.5.

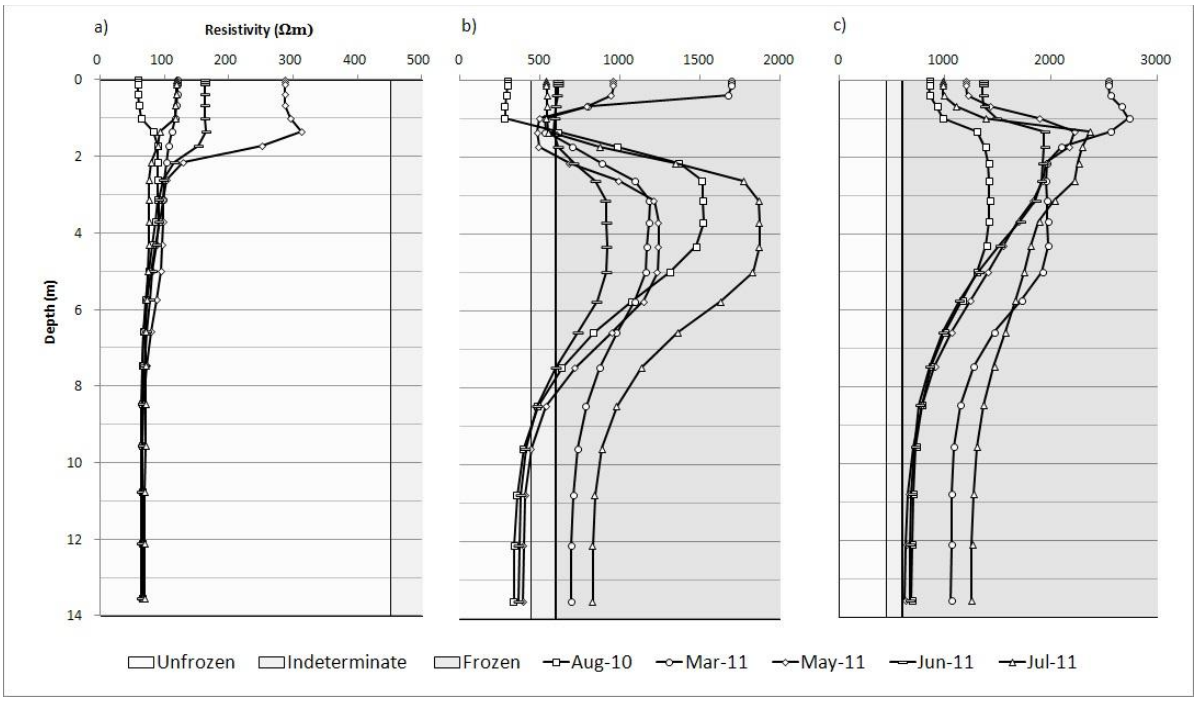

Figure 51 - Virtual boreholes for MP 788.5 at a) 20 m; b) 40 m; c) 60 m along the profile length. Note the difference in scale for each of the x axes.

The 20 m virtual borehole showed no permafrost and no seasonally frozen ground. This trend is consistent with frost probing conducted in August 2010, July 2011 and August 2011 which was unable to find a frost table to 112 cm in depth. The climate data for 100 cm in depth had an annual mean above 0 ºC, however there was freezing at this depth in March. There was a large increase in resistivity in the near-surface in March, but the boundaries chosen for this site still classify this as 'unfrozen'. Therefore, it is possible the low resistivity values at depth were affecting the values in the near-surface.

The 40 m virtual borehole showed a 2 m active layer with permafrost approximately 6 m thick. The frost probing data showed an active layer of approximately 40 cm, which was slightly inconsistent with the depth shown in Figure 51. The sensors in the borehole from 1.0 m to 3.75 m have maximum temperature values of less than 0 ºC, which was consistent with the virtual borehole.

At 60 m, the ground appeared to be frozen to below the penetration depth of the ERT survey. There also appeared to be no seasonal thawing. Frost probing at this location had a maximum thaw depth of 59 cm, which is inconsistent with the resistivity values. In addition, the logger at 50 cm in

depth did go above 0 °C and was therefore not within permafrost. The near-surface values in this virtual borehole appear to have been affected by the high resistivity values below, which is the opposite of what occurred at 20 m.

Based on the available data, the permafrost at MP 788.5 began at approximately 38 m, which is at the start of the peat plateau, and ended at 78 m along the profile. The thickness of the permafrost varied from approximately 4 m to a maximum depth that was beyond the penetration depth of the survey. The maximum depth occurred from 41 – 72 m.

Figure 52 shows the relative inverted resistivity change based on the August 2010 survey.

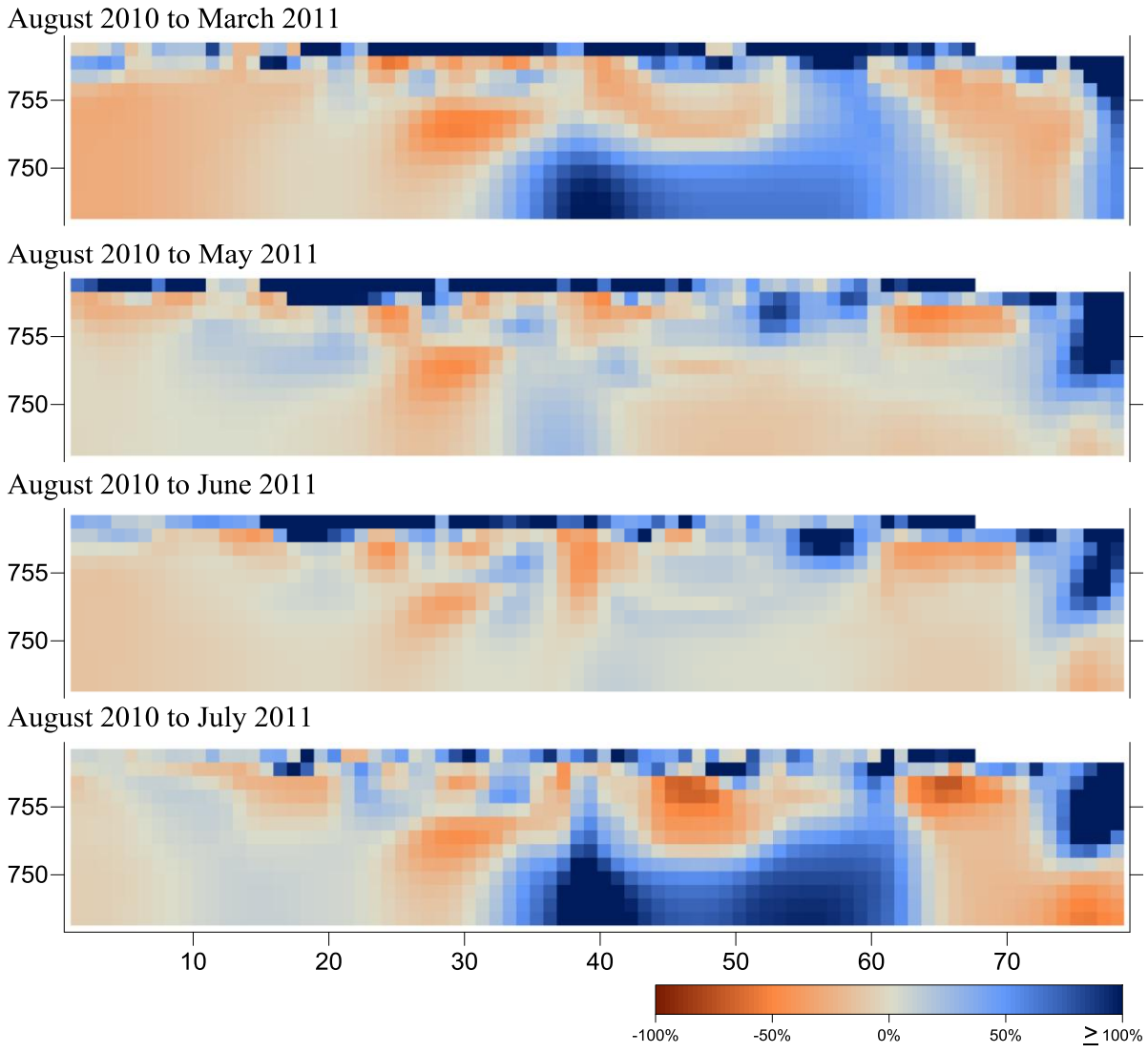

Figure 52 - Relative change in resistivity based on the August 2010 survey for MP 788.5.

The August to March profile had the largest increase in resistivity in the near-surface. There was also an increase at the bottom of the profile from 35 m to 65 m, which may have been an artefact from the high resistivity surface. The August to May and August to July profiles appeared to have very little change below the surface and moderate change in the near-surface. The August to July profile had a large increase in resistivity in the deeper portions of the profile, which was similar to the August to March profile. Approximately 30% of the model blocks at MP 788.5 had maximum measurements occur in July, the majority of which were in the lower portion of the profile. With all of the profiles, the majority of the near-surface appeared to have an increase in resistivity values in comparison to August. August had the highest percentage of minimum model blocks, and the majority of them were within the near-surface.

5.1.9 MP 825.2

MP 825.2 is approximately 120 km southeast of Whitehorse, and at approximately 720 m asl. The profile begins relatively flat, then climbs onto a hummocky surface that continues upwards towards the end of the profile. There is a 4 m difference in elevation from the front of the profile to the back. Figure 53b shows the upwards slope towards the borehole and central climate station. In May 2011 there was standing water present at 8 m along the profile (Figure 53a). This water remained until the June 2011 site visit. The site is hummocky, with spruce, mosses, lichen, and Labrador Tea present (James 2010). The soil is cohesive and composed of silt and sand, with some stones present (James 2010).

a)  b) 

Figure 53 – MP 825.2 site photos a) Taken in March 2011 from beside the profile looking at 8 m, this photo shows the standing water present. This photo also shows the relatively flat area at the beginning of the profile; b) Taken in July 2011 from approximately 27 m looking towards the back of the profile, this photo shows the rise in elevation from the beginning of the profile to the end.

Figure 54 shows the daily ground and air temperature and snow depth values for MP 825.2. The mean annual air temperature for this site was -1.4 ºC, with a daily temperature range of 55.2 ºC. The minimum daily temperature was -37.4 ºC and minimum hourly temperature (-42.6 ºC) occurred at 08:00. The maximum daily temperature was 17.8 ºC and occurred on July 13, 2011. The maximum hourly temperature was 27.9 ºC and occurred on August 15, 2010 at 17:00.

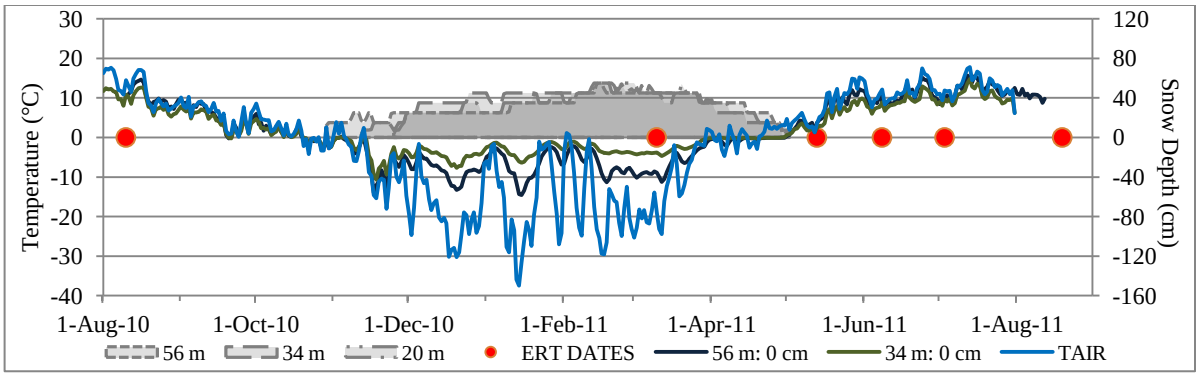

Figure 54 - Daily ground and air temperature values and daily snow depth values for MP 825.2 from August 2010 to August 2011. The red dots symbolize ERT collection days at this site. Note malfunctioning 5 cm ibutton at 56 m station.

The mean annual ground surface temperature at MP 825.2 varied from 1.0 °C to 1.8 °C. The difference in mean values related to different stations. At 34 m, the annual temperature was 1.8 °C, with a mean daily temperature range of 25.5 °C. At 56 m, two loggers had a mean annual ground surface temperature of 1.0 °C. The zero curtain at this site began at the end of March and was finished by the beginning of May, after approximately 32 days.

Snow cover at this site began in late October, and continued to build until the middle of February. The snow cover then began to decrease at the beginning of March, until there was no snow left at the beginning of May. The station at 20 m was the last location on the plot to begin to accumulate snow. It had 5504 SDD, the smallest value at MP 825.2. The snow began to accumulate almost two weeks earlier at 34 m and resulted in 5931 SDD. Lastly, the snow at 56 m began to accumulate a full two weeks before there was snow at 34 m, and had 5785 SDD. The difference in SDDs for each snow stake was 8%, which accounts for approximately a 2 cm difference in annual snow cover from the snow stake with the lowest SDD, 20 m, and the highest SDD, 34 m.

Table 11 shows the daily ground temperature summary statistics for MP 825.2. Ground temperatures were consistent for similar depths at different areas along the profile. The loggers at 20 m malfunctioned due to surface meltwater in that location on the profile.

Table 11 – Daily ground temperature summary statistics for MP 825.2, August 2010-2011.

Depth (m)	20 m				34 m				56 m			
	x̄	Max	Min	Range	x̄	Max	Min	Range	x̄	Max	Min	Range
0.00	--	--	--	--	1.4	14.8	-10.7	25.5	1.0	15.7	-14.6	30.3
0.50	--	--	--	--	0.4	4.0	-1.8	5.8	0.3	2.3	-0.1	2.4
1.00	--	--	--	--	0.1	0.1	0.0	0.1	0.1	1.2	-0.1	1.3
Cells with dashes indicate temperature sensors that failed.												

Figure 55 shows the temperature envelope for the borehole present at 34 m at MP 825.2. From 0 m to 0.5 m the mean annual temperatures were above 0 ºC. Below 0.5 m the mean annual temperatures are very close to 0 ºC; 0.1 ºC, 0.0 ºC, 0.1 ºC, 0.0 ºC, -0.1 ºC for the depths 1 m, 1.5 m, 1.75, 2 m, and 4 m, respectively. The temperature range for 1 m was 0.1 ºC and every logger below 1 m had a temperature range of 0 ºC. Therefore, the depth of zero annual amplitude and the depth of the active layer were most likely between 1 m and 1.5 m in depth.

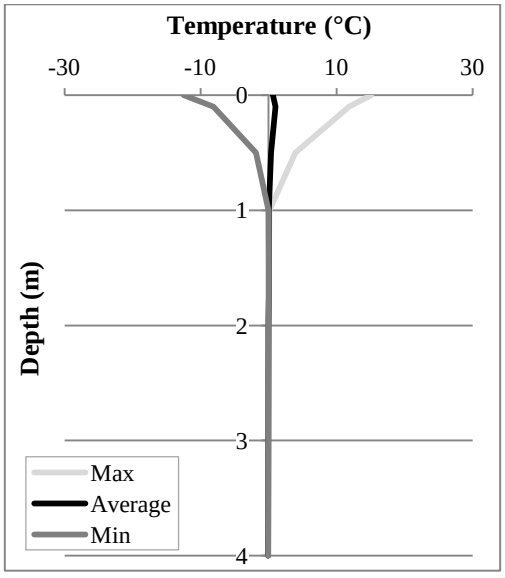

Figure 55 – Temperature envelope for MP 825.2, August 2010-2011.

The apparent resistivity data at MP 825.2 had a mean of 274 Ωm. The spatial mean apparent resistivities from August 2010 to July 2011 were 230 Ωm, 310 Ωm, 294 Ωm, 275 Ωm and 261 Ωm. The inverted resistivity data had a mean resistivity of 357 Ωm. The resistivity values ranged from 26 Ωm, which occurred in August, and 20.3 kΩm, which occurred in March. 75% to 80% of the

resistivity values were between 0 and 500 Ωm, and no more than 11% of measurements were above 1000 Ωm for each survey executed.

Figure 56 shows the ERT survey, frost table depths and permafrost classification image that occurred in August 2010. The measured, calculated, and inverse profiles for each survey at MP 825.2 are presented in Appendix L.

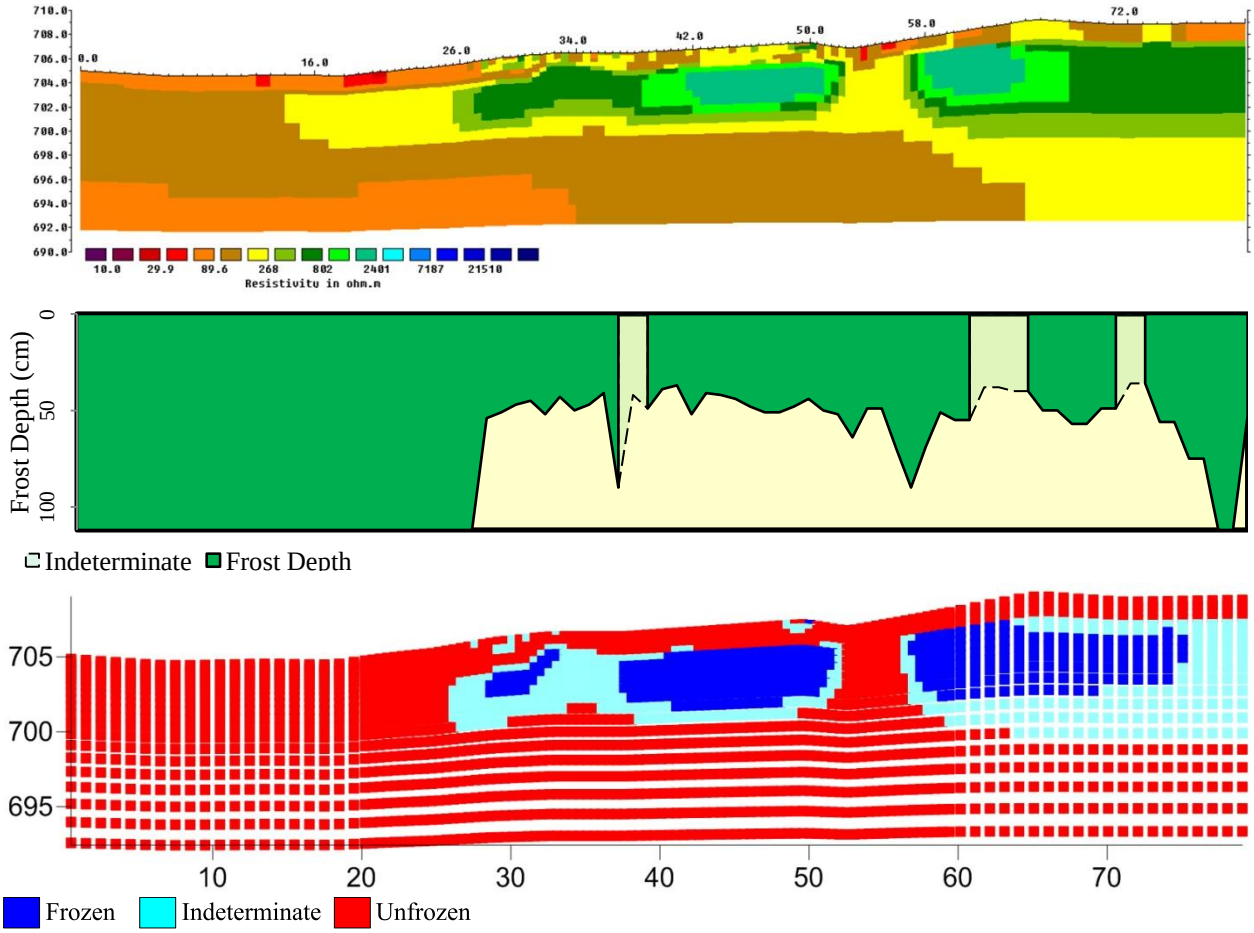

Figure 56 - Inverted ERT profile, frost table depths and permafrost classification image for MP 825.2 for the August 2010 survey. Legends for each of the images are in the bottom left corner. For the frost table image, areas of light green with dashed lines had an annual frost progression that was not logical. For the permafrost classification image unfrozen is 0 to 300 Ωm, indeterminate is 300 to 700 Ωm, and frozen is all model blocks greater than 700 Ωm. All images have identical horizontal scales in meters. The inverted ERT profile and permafrost classification image have vertical scale in meters.

Three locations along the profile had illogical frost table progressions. The upper limits for the unfrozen and indeterminate classification are 300 Ωm and 700 Ωm, respectively. These limits were based on all the available data from the study site.

Figure 57 shows the virtual borehole measurements for each climate station at MP 825.2.

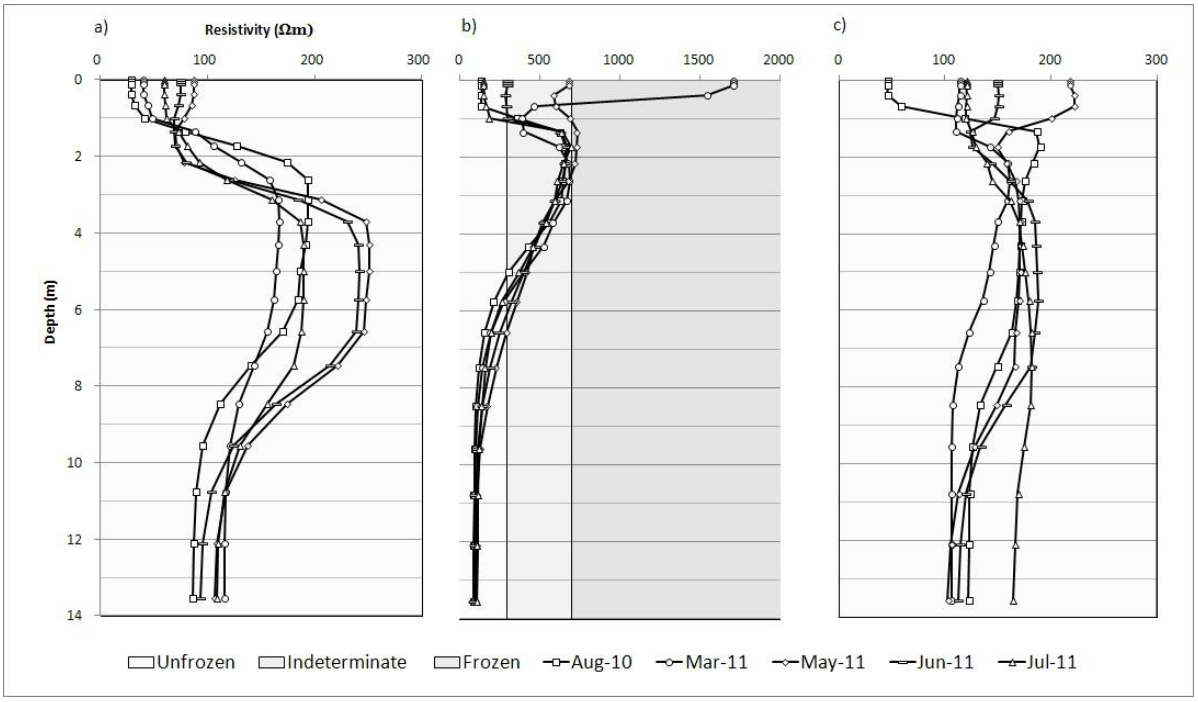

Figure 57 - Virtual boreholes for MP 825.2 at a) 20 m; b) 34 m; c) 56 m along the profile length. Note the difference in scale in b).

At 20 m, the virtual borehole showed no permafrost and no seasonally frozen ground. This was consistent with frost probing conducted in August 2010 and July 2011, which was unable to find a frost table to a depth of 112 cm. However, it is unlikely that this area did not undergo seasonal freezing since there was a frost table during some surveys. It is more likely that the near-surface measurements in March and May were affected by the low resistivity values below. It should be noted that the March survey had the highest resistivity in the near-surface, and the August survey had the lowest. No temperature data were available for this area.

At 34 m, the virtual borehole showed a layer of seasonally frozen ground of approximately 1 m, with permafrost that was approximately 4 – 5 m thick. The depth of the seasonally frozen ground was fairly consistent with the frost probing data that showed a maximum frost depth of only 50 cm. The borehole present at this location had mean ground temperatures within 0.1 °C of 0 °C for depths of 1 m, 1.5 m, 1.75 m, and 2 m, respectively. Although some of these values are above 0.0 °C, the

shapes of the resistivity values are more consistent with a permafrost area than a seasonally frozen one. The curve from 2 m to 6 m in depth is indicative of permafrost. Therefore, it appears that the contradiction is due to imprecision in the temperature measurements.

At 56 m, the virtual borehole showed no permafrost and no seasonally frozen ground present. This location, like 20 m, was inconsistent with the frost probing data. The maximum frost probing depth was 70 cm. The temperature data showed both sensors at 50 cm and 100 cm were not within permafrost. However, the logger at 100 cm was only thawed for the August survey, and the 50 cm logger was only thawed from November 2010 to August 2011. Therefore, the near-surface data from this virtual borehole appears to have been affected by the low resistivity values at greater depths.

Based on the available data there were bodies of permafrost present at MP 825.2. One body occurred from 28 m to 50 m, was 3 m to 5 m thick, and began 1 m to 1.5 m below the surface. The second permafrost body started at 58 m and continued beyond the profile, was approximately 6 m thick and occurred 1 m to 4 m below the surface.

Figure 58 shows the relative inverted resistivity change based on the August 2010 survey.

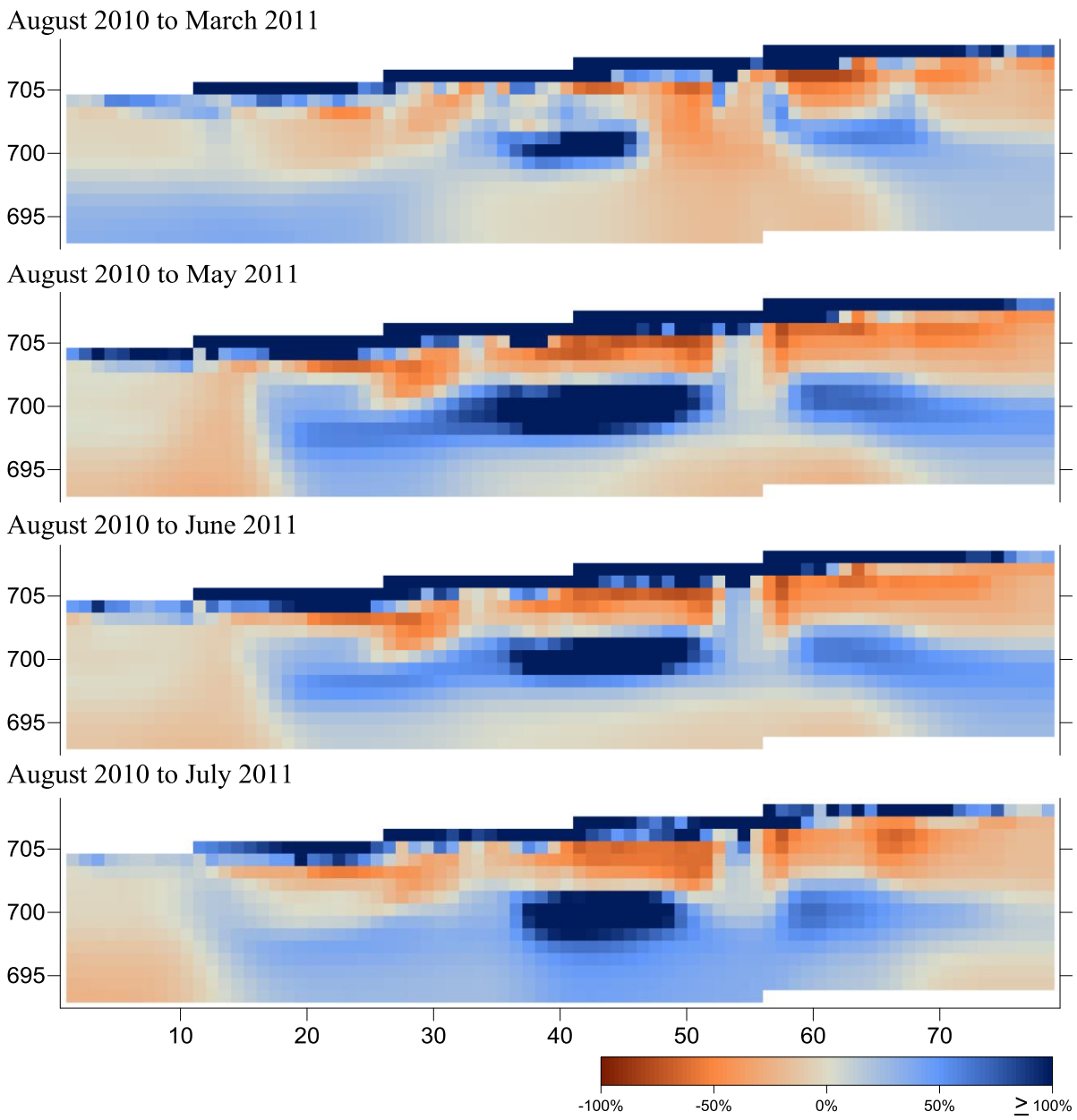

Figure 58 - Relative change in resistivity based on the August 2010 survey for MP 825.2.

The August to March profile showed a large increase in resistivity in the near-surface, however the August to May profile showed the largest percentage change in the near-surface. Approximately 33% of the model blocks reached their maximum values in the May survey. The August to June and August to July surveys also showed some changes in the near-surface, although they were not as great as for the March and May surveys. The August survey had approximately

40% of the minimum model block values, and a majority of them were within the near-surface, which was why all of the profiles showed an increase in resistivity when compared to the August survey. Within all of relative change comparisons there was also an increase within the bottom portion of the profiles, in particular areas that were classified as indeterminate. This change may be due to the high resistivity values in the near-surface affecting the values at greater depths.

5.1.10 MP 844.1

MP 844.1 is 95 km southeast of Whitehorse and is at 813 m asl. The site is relatively flat, with a small downward slope towards the centre of the plot and a small upward slope over the last 15 m. The lowest point (60 m) and the highest point (0 m) have a 1.2 m difference in elevation. In May 2011 a large snow patch was present within the centre of the plot (Figure 59a). This area was thawed before the June 2011 survey. No standing water was ever present at this site. MP 844.1 has both spruce (with a maximum height of 9 m) and willow (with a maximum height of 2 m) (James 2010). The site is not hummocky, but does have non-sphagnum mosses and Labrador tea (Figure 59b). The soil is silty, with rocks and gravel present (James 2010).

a)  b) 

Figure 59 – MP 844.1 study site photos a) This photo was taken in May 2011 from approximately 20 m looking towards the back of the profile, and shows the snow cover present at the centre of the plot; b) This photo was taken in July 2011 from approximately 35 m looking towards the back of the profile and shows the vegetation.

Figure 60 shows the daily ground and air temperature values and daily snow depth values for MP 844.1. Air temperature at this site, which was correlated from MP 825.2, had an annual mean of -2.6 °C and a range of 55.6 °C. The minimum daily temperature was -38.8 °C, and the minimum hourly temperature was -44.0 °C (which occurred at 0800).

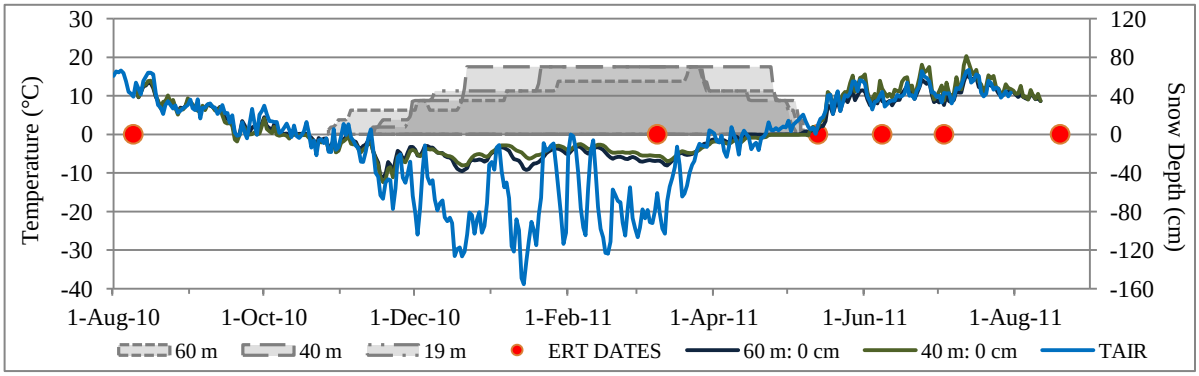

Figure 60 - Daily ground and air temperature values and daily snow depth values for MP 844.1 from August 2010 to August 2011. The red dots symbolize ERT collection days at this site. Note 50 cm, 60 cm, and 80 cm ibuttons malfunctioned at 40 m station. Air temperature was correlated from MP 825.2.

At MP 844.1, the mean annual ground surface temperature varied from 1.0 – 1.6 ºC. The largest difference in annual values occurred at different locations along the profile. At 19 m, the mean was 1.2 – 1.3 ºC. At 40 m, the mean was 1.3 - 1.6 ºC. This location had the lowest minimum daily temperature of -14.7 ºC which occurred on November 18, 2010. All of ground surface loggers at this site had minimum daily temperatures on this day. At 60 m, the mean annual temperature was 1.0 ºC. This location had the lowest temperature range (24.9 ºC) the lowest minimum daily temperature (-10.2 ºC) and the lowest maximum daily temperature (14.7 ºC). The zero curtain began in mid-April and ended approximately 3 weeks later.

The snow cover at MP 844.1 began in late-October and continued to build until the end of January when maximum snow depth was reached for each station. The snow season lasted for 193 days, with snow cover no longer present by mid-May, soon after the survey on May 13. From the front to the back of the profile, the SDD for MP 844.1 were 8449, 10063, and 7818. The difference in SDDs for each snow stake was 28%, which accounts for approximately a 12 cm difference in annual snow cover from the snow stake with the lowest SDD, 60 m, and the highest SDD, 40 m. A portion of this variation in SDD was due to the malfunction of multiple ibuttons on the 40 m snow stake.

Table 12 shows the daily ground temperature summary statistics for MP 844.1. Ground temperatures were consistent through the entire plot.

Table 12 – Daily ground temperature summary statistics for MP 844.1.

Depth (m)	19 m				40 m				60 m			
	x̄	**Max**	**Min**	**Range**	**x̄**	**Max**	**Min**	**Range**	**x̄**	**Max**	**Min**	**Range**
0.00	1.3	17.4	-14.2	31.6	1.3	17.6	-12.7	30.3	1.0	15.5	-11.1	26.6
					1.6	20.3	-12.4	32.6	1.0	14.7	-10.2	24.9
0.10	1.7	19.3	-16.3	35.7								
	1.1	15.7	-13.0	9.3								
0.25	1.6	15.7	-13.0	28.6								
	0.8	7.7	-2.8	10.5								
0.50	0.3	2.6	-1.2	3.8	0.0	1.4	-1.7	3.1	0.7	6.4	-4.1	10.4
0.75	0.1	1.3	-0.5	1.8	0.0	1.2	-1.3	2.4	0.4	3.7	-2.9	6.6
1.00	0.0	1.0	-0.6	1.7								

Grey cells indicate sensors that were not installed at that depth for that station.

The apparent resistivity data at MP 844.1 had a mean of 2.9 kΩm. The spatial mean apparent resistivities from August 2010 to July 2011 were 1.5 kΩm, 9.6 kΩm, 1.1 kΩm, 1.0 kΩm and 1.2 kΩm. The inverted resistivity data had a mean of 2.2 kΩm, with the maximum value of 88.6 kΩm and the minimum value of 71 Ωm both occurring in March. More than 50% of the values within each survey were between 0 – 500 Ωm and there was also a high percentage of values (i.e., 22% to 35%) that were above 2000 Ωm.

Figure 61 shows the ERT profile, frost table depth, and permafrost classification image for MP 844.1 for the August 2010 survey. The measured, calculated, and inverse profiles for each survey at this site are presented in Appendix M.

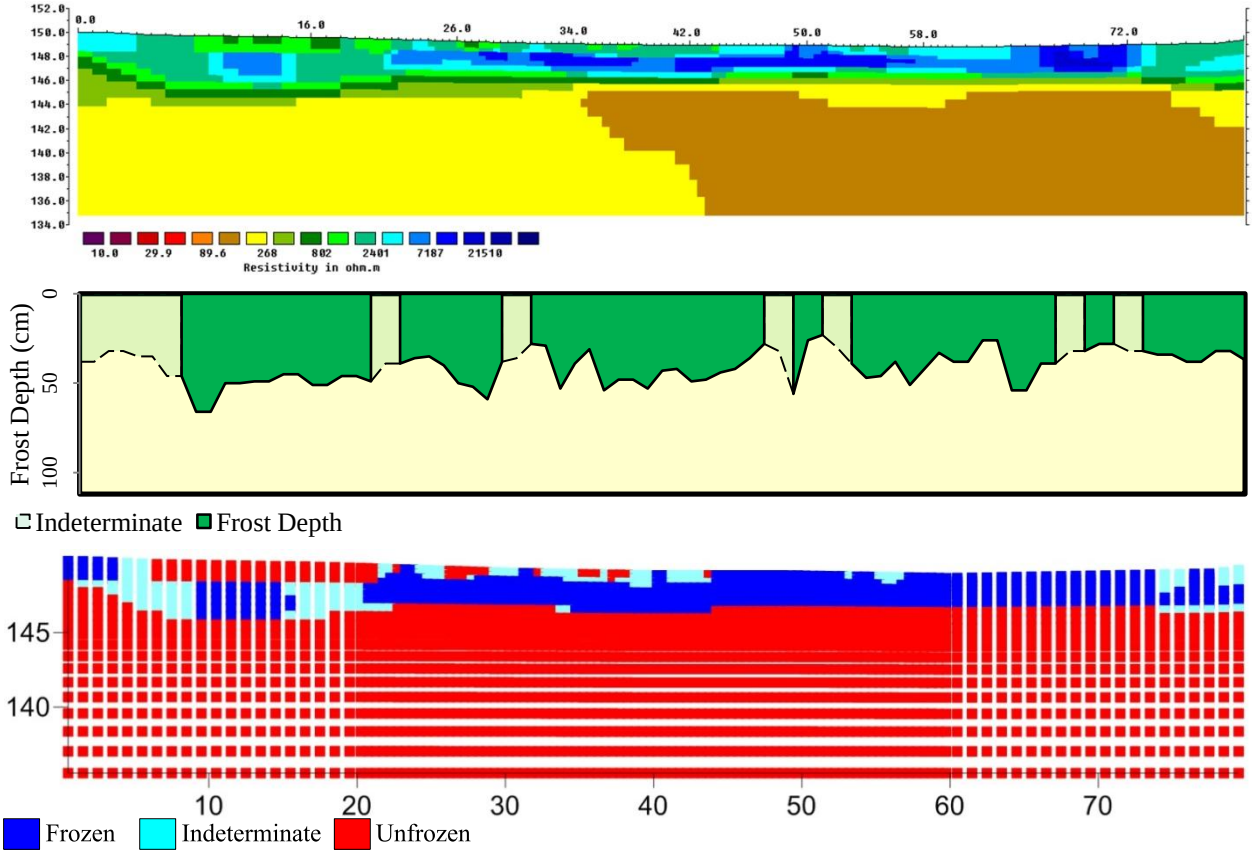

Figure 61 - Inverted ERT profile, frost table depths and permafrost classification image for MP 844.1 for the August 2010 survey. Legends for each of the images are in the bottom left corner. For the frost table image, areas of light green with dashed lines had an annual frost progression that was not logical. For the permafrost classification image unfrozen is 0 to 1,500 Ωm, indeterminate is 1,500 to 2,000 Ωm, and frozen is all model blocks greater than 2,000 Ωm. All images have identical horizontal scales in meters. The inverted ERT profile and permafrost classification image have vertical scale in meters.

Several sections of the profile had gravel and a proper frost table depth was not measureable. The upper limits for unfrozen and indeterminate were 1,500 Ωm and 2,000 Ωm, respectively. These values were assigned based on the available data from MP 844.1.

Figure 62 shows the virtual borehole for each climate station this study site.

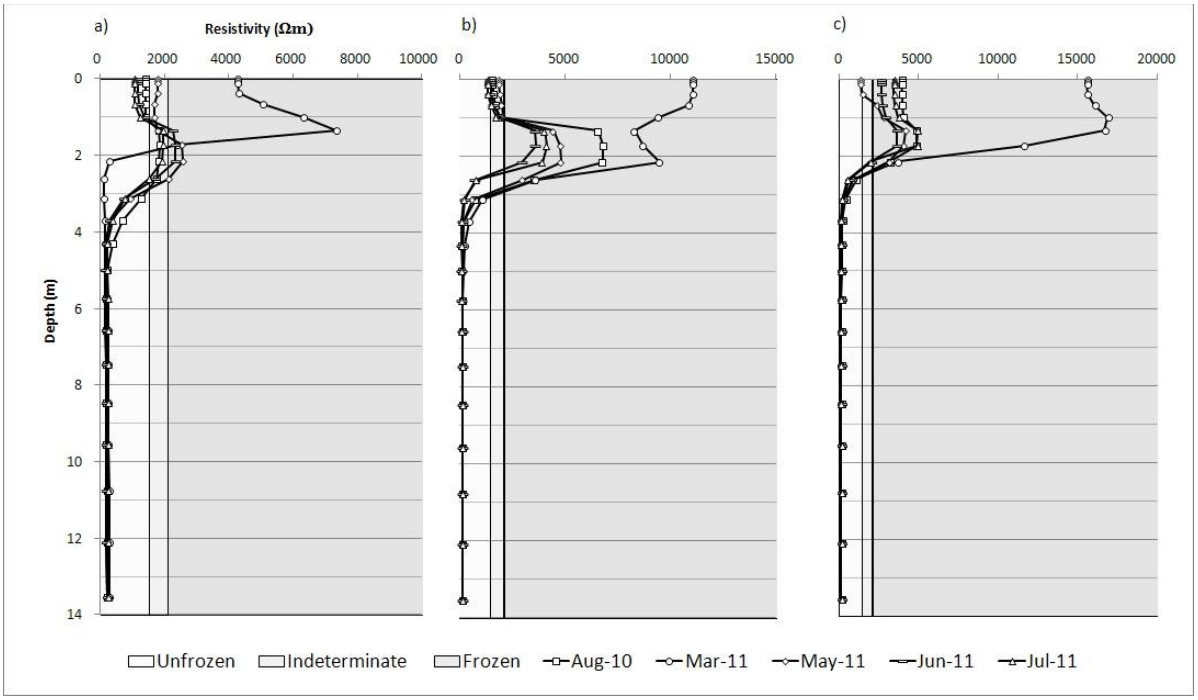

Figure 62 - Virtual boreholes for MP 844.1 at a) 19 m; b) 40 m; c) 60 m along the profile length. Note the difference in scale for each of the x axes.

At 19 m the virtual borehole showed an active layer of approximately 1 m and a permafrost layer of 2 m. The 100 cm logger at that location was not within permafrost, but was below 0 °C for the March and May surveys. This trend was consistent with the borehole, which showed higher resistivity values in the near-surface in those months. The sensors at 10 cm, 25 cm, and 50 cm were below 0 °C for the March survey, which was also shown in the resistivity measurements. The frost table at this location was 46 cm in August 2010, which was thinner than what was expected from the ERT survey.

At 40 m there was an active layer of approximately 1 m with approximately 2 m of permafrost below. Frost probing in August 2010 and 2011 showed an active layer of 40 cm, less than

the virtual borehole indicates. The temperature sensors at 50 cm and 75 cm were within seasonally frozen ground. The 75 cm logger was below 0 °C for the March and May surveys, which was consistent with the resistivity measurements.

At 60 m the virtual borehole showed an active layer of approximately 50 cm that only thawed in the May survey. The permafrost at this station was approximately 1.5 m thick. Frost probing at this station reached a maximum depth of 56 cm in August 2011, which consistent with the estimated active layer thickness in the virtual borehole but inconsistent with the date of the depth. The sensors at 25 cm and 50 cm were within the seasonally frozen ground and were only frozen for the March and May surveys.

Based on all available data, the permafrost at MP 844.1 appears to be approximately 1.5 – 3 m thick with an active layer of 0.5 – 1 m. The permafrost is consistent throughout the entire profile.

Figure 63 shows the relative inverted resistivity change based on the August 2010 survey.

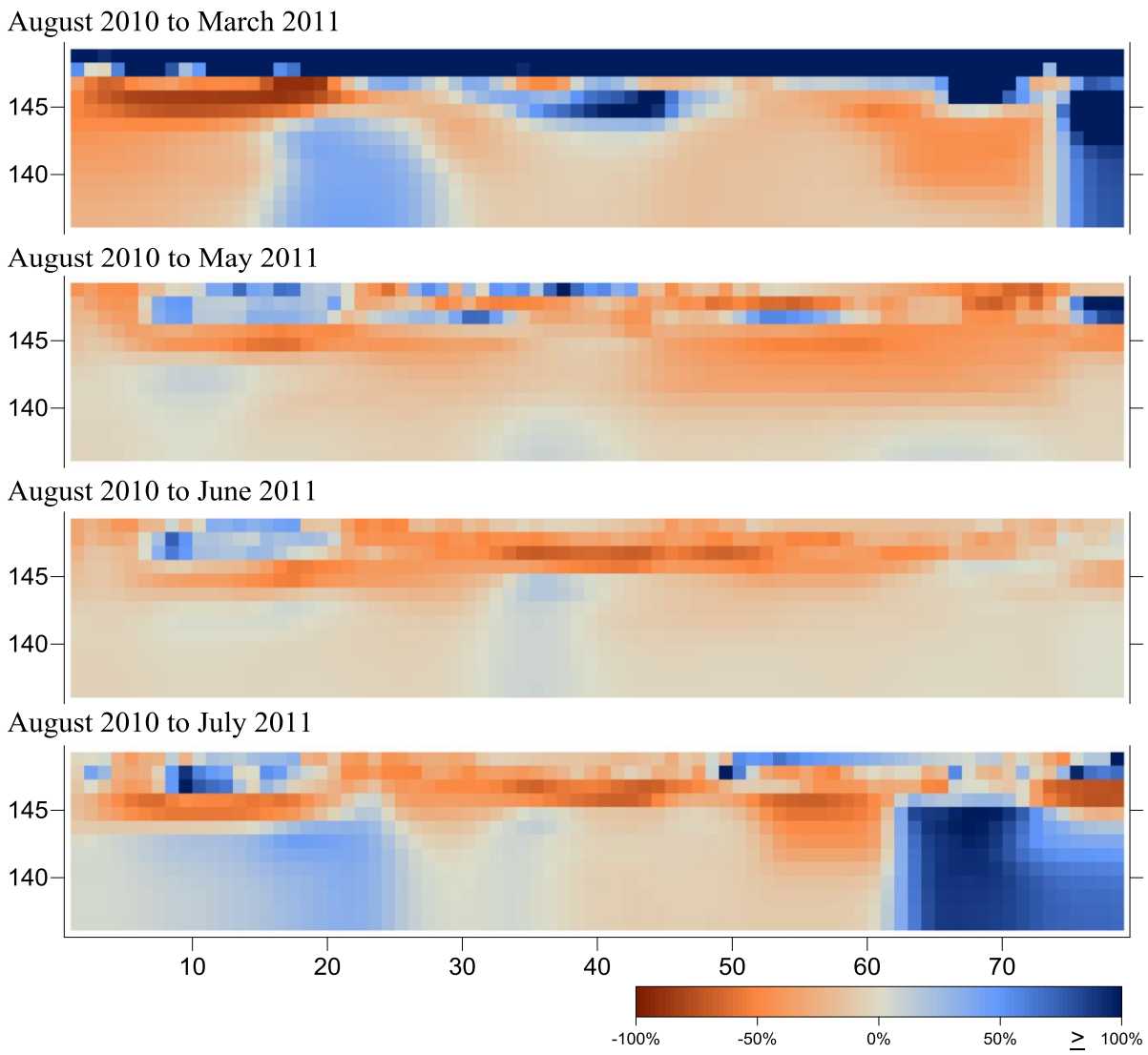

Figure 63 – Relative change in resistivity based on the August 2010 survey for MP 844.1.

The August to March survey showed a large increase in resistivity in the near-surface, which was due to the high percentage (47%) of maximum model blocks in the March survey. The August to May showed very little change within the entire profile. The August to June survey showed very little increase in resistivity and some areas of decrease. This pattern was because the June survey had the lowest percentage of minimum model blocks (4%) and August had the second lowest percentage (27%). The August to July survey had areas of resistivity increase in the lower portions of the

profile. These areas were within the edges of the profile and were therefore more prone to incorrect interpretation.

5.2 Inter-site Comparison

5.2.1 Temperature Data

Table 13 shows the mean annual air, ground surface, and ground temperatures for each study site. Mean annual air temperatures for the study sites varied from -3.3 ºC to -1.4 ºC. MP 681.1 had the lowest mean annual air temperature, as well as the lowest maximum hourly value. These annual data are consistent with results from 2007-2008 (James 2010). The Liard Basin, located north of MP 681.1, can have Arctic air pooling during the winter months which can cause prolonged cold periods (Wahl et al. 1987). MP 579.5 and MP 178.0 both had the second lowest mean annual air temperature of -3.0 ºC. MP 579.5 also the largest temperature range, the lowest daily and hourly temperatures, and the highest hourly temperature. MP 178.0 had the lowest maximum daily value, as well as the smallest range in temperature.

MP 825.2 had the highest mean annual air temperature and the highest minimum daily value. This elevated temperature may be due to this site's proximity to the Pacific Ocean, which can moderate cooler temperatures in the winter (Wahl et al. 1987). In 2007 – 2008 the warmest MAAT occurred at MP844, just 23 km north-west of MP 825.2 (James 2010). MP 400.5 had the warmest minimum hourly value, and MP 286.0 had the warmest maximum daily value.

Table 13 - Mean Annual air, ground surface, and ground temperatures for study sites, August 2010-2011.

	Elevation	T_{AIR}	Front Station		Middle Station		Back Station	
	(m asl)	(°C)	Depth (m)	Temperature (°C)	Depth (m)	Temperature (°C)	Depth (m)	Temperature (°C)
MP 178.0	1098	-3.0	0.00	0.7-0.9	0.00	0.4	0.00	0.3
			0.40	0.2			0.40	0.3
			0.90	0.0			0.90	-0.1
MP 286.0	417	-1.6	0.00	0.7-1.0	0.00	1.5	0.00	1.7-2.4
					0.20	1.4[b]		
					0.30	1.4[b]		
					0.40	0.6[b]		
			0.50	0.0	0.50	0.0[b]	0.50	-0.1
			1.00	-0.1			1.00	-0.2
MP 341.3	461		0.00	1.7-2.2	0.00	2.2	0.00	1.8-2.0
					0.25	1.5		
			0.50	0.4	0.50	0.1	0.50	-0.2
					0.75	-0.1		
			1.00	0.1	1.00	-0.1	1.00	-0.2
MP 400.5	1043	-2.7	0.00	1.5	0.00	2.2-2.3	0.00	0.9
			0.10	2.0[b]				
			0.25	1.1[b]				
			0.40	0.2[b]				
			0.50	0.1[b]			0.50	-0.2
					1.00	0.1	1.00	-0.2
MP 579.1	725		0.00	1.8-2.1			0.00	1.3-1.6
					0.25	0.6		
			0.50	0.2	0.50	0.1	0.50	-0.1
					0.75	0.1		
			1.00	0.0	1.00	0.0	1.00	-0.3
MP 597.5	682	-2.9	0.00	1.1	0.00	0.3-1.8	0.00	1.1-1.6
			0.10	0.9[b]				
			0.25	1.0[b]				
			0.40	0.0[b]				
			0.50	-0.4[b]	0.50	-0.1	0.50	-0.2
					1.00	-0.2	1.00	-0.3
MP 681.1	849	-3.3[a]	0.00	0.7-1.0	0.00	1.0	0.00	1.0-1.5
			0.25	0.2	0.25	-0.3	0.25	0.5
					0.50	-0.5		
			0.65	-0.3			0.65	0.6
MP 788.5	760	-2.0	0.00	3.4-3.8	0.00	1.9	0.00	1.8-1.9
							0.50	-0.1
			1.00	1.2	1.00	0.0	1.00	-0.1
MP 825.2	721	-1.4			0.00	1.4	0.00	1.0
					0.50	0.4	0.50	0.3
					1.00	0.1	1.00	0.1
MP 844.1	813	-2.6[a]	0.00	1.3	0.00	1.3-1.6	0.00	1.0
			0.10	1.1-1.7				
			0.25	0.8-1.6				
			0.50	0.3	0.50	0.0	0.50	0.7
			0.75	0.1	0.75	0.0	0.75	0.4
			1.00	0.0				

[a] Air temperature was correlated from a nearby study site or community [b] Data were collected with a four-channel logger

Mean annual ground surface temperatures averaged from each site varied from 0.5 ºC to 2.6 ºC. MP 178.0 had the lowest annual ground surface mean temperature, as well as the lowest

maximum daily temperature (12.9 ºC) and smallest temperature range (24.1 ºC). MP 788.5 had the highest mean annual ground surface temperature, which was more than 1.0 ºC higher than any other logger at any site. MP 788.5 also had the highest minimum daily temperature of -9.8 ºC. MP 579.5 had the lowest minimum daily temperature, which was -19.0 ºC. MP 400.5 had the highest maximum daily temperature (23.7 ºC) and MP 286.0 had the largest temperature range (36.3 ºC). On average there was a 1.1 °C range of mean annual ground surface temperatures for different loggers at the same site. Six of the ten sites had ranges that were less than 0.8 °C, and MP 341.3 had the most consistent mean temperatures (within 0.5 °C of each other). Four of the ten sites had annual variations that were more than 1.4 ºC, and MP 788.5 had the highest intra-site variation of 2.0 ºC.

The mean annual ground temperatures were similar at every site, with no site was consistently warmer or colder at every monitored depth. At any depth, the mean annual temperature varied less than 2.0 ºC from the minimum to maximum value. The one notable anomaly in ground temperature occurred at 20 m at MP 788.5 at 100 cm depth. The mean annual temperature of 1.2 ºC was more than 1 ºC higher than any other logger at that depth. This higher ground temperature was also seen in the mean annual ground surface temperature and reflects persistent standing water and absence of permafrost at this location.

Table 14 displays the SDD for each station location of the study sites. This table also displays the mean SDD for each site, and the number of snow days for each site.

Table 14 - SDD for study sites, winter 2010-2011.

	Front Station (SDD)	Middle Station (SDD)	Back Station (SDD)	Mean (SDD)	Snow Season (days)
MP 178.0	10535	11093	10171	10600	224
MP 286.0	7397	8680	7932	8003	196
MP 341.3	6836	6129	5851	6272	192
MP 400.5	8678	8211	8384	8242	215
MP 579.1	8243	7850	8590	8228	181
MP 597.5	6744	7344	6451	6846	201
MP 681.1	8148	8892	8458	8499	225
MP 788.5	6062	6150	6840	6351	187
MP 825.2	5504	5931	5785	5740	186
MP 844.1	8449	10063	7818	8777	193

The mean snow season at the ten sites was 200 days long. The shortest season occurred at MP 579.1 and the longest at MP 681. MP 178.0 had the highest mean SDD as well as the highest SDD for each station. MP 825.2 had the lowest mean SDD as well as the lowest SDD for each station. Considering the mean snow season, the difference in snow depth from MP 178.0 and MP 825.2 was 24 cm.

James (2010) calculated SDD for MP 286.0, MP 400.5, MP 597.5, MP 681.1, and MP 844.4. MP 286.0, MP 400.5, and MP 844.4 had an increase of less than 24 cm in snowcover from 2010-2011 to 2007-2008. These sites are close to communities that experienced an increase in snowcover when compared to the climate normals. MP 597.5 and MP 681.1 had a decrease of less than 12 cm in snowcover from 2010-2011 to 2007-2008. These two sites are close to Watson Lake, which also experienced decreased snowcover when compared to the climate normal.

5.2.2 Surface and Thermal Offsets

Table 15 shows the surface and thermal offsets for each of the study sites.

Table 15 – The surface the thermal offsets for the study sites, August 2010 to August 2011.

	Surface Offset (°C)	Thermal Offset (°C)
MP 178.0	3.3 to 3.9	-0.4 to -0.9
MP 286.0	2.3 to 4.0	-0.9 to -2.5
MP 341.3		-1.9 to -2.1
MP 400.5	3.6 to 5.0	-1.1 to -2.2
MP 579.1		-1.6 to -2.3
MP 597.5	3.2 to 4.7	-0.6 to -2.1
MP 681.1	4.0 to 4.8	-0.9 to -1.0
MP 788.5	3.8 to 5.8	-1.9 to -2.6
MP 825.2	2.4 to 2.8	-0.9 to -1.3
MP 844.1	3.6 to 4.2	-1.0 to -1.6
Grey cells indicate study sites where the thermal offset could not be calculated due to logger failure.		

The surface offsets ranged from 2.3 °C to 5.8 °C, and the values within a site varied by 0.4 °C to 2.0 °C. The largest range in surface offset occurred at MP 788.5 due to the high ground surface temperatures at 20 m. The surface offset values were generally equal to or greater than the values calculated by James in 2007-2008 (James 2010). This difference may be an effect of the higher snow depth in 2010-2011. The only site with a smaller mean surface offset in comparison with 2007-

2008 was MP 597.5. MP 597.5 also had less snow in 2010-2011 in comparison to the earlier measurements.

All mean surface temperatures exceeded 0 °C so it is the thermal offset that allows permafrost to persist at the study sites. The thermal offsets ranged from -0.4 °C to -2.6 °C, and the values within a site varied by from 0.1 °C to 1.7 °C. The site with the largest range in thermal offsets was MP 286.0 due to the large range of mean annual ground surface temperatures. For sites with pre-existing climate stations, the 2010-2011 thermal offsets varied less than 0.2 °C from the 2007-2008 values (James 2010).

Under equilibrium conditions, the thermal offset is controlled by the difference in a soil's ability to transmit heat when it is frozen or thawed, which differs depending on soil type, density, moisture, and vegetation. The high thermal offsets at each site are most likely due to the presence of mosses, sphagnum, lichen, and peat (Brown 1967). The thermal conductivity of peat can range from 0.05 – 2.00 W/m K depending on its temperature and moisture content (French 2007). This large range in thermal conductivity would prevent heat from penetrating the ground during the summer and allow cold to penetrate the ground in the winter. Therefore, it is the thermal offset that is controlling the presence or absence of permafrost within these study sites. It is also very likely that the permafrost is not in equilibrium. The long-term existence of permafrost at these locations is not possible with the current climate, so the TTOP temperatures are producing the high thermal offset values (Lewkowicz et al. 2011). This phenomenon is common for areas at the southern limit of permafrost (Smith and Riseborough 2002; James 2010; Bonnaventure and Lewkowicz 2011).

5.2.3 N Factors

The freezing n-factors (n_f) were calculated for the winter of 2010-2011. These values ranged from 0.06 to 0.57, and were similar to previous measurements conducted at the study sites (as seen in Table 16).

Table 16 – Freezing n-factors for each study site.

	2007-2008	2008-2009	2009-2010	2010-2011
MP 178.0				0.27 to 0.43
MP 286.0	0.51	0.37	0.45	0.33 to 0.57
MP 341.3				--
MP 400.5	0.56	0.42	0.39	0.22 to 0.38
MP 579.1				--
MP 597.5	0.29	0.26	0.36	0.27 to 0.45
MP 681.1	0.46	0.45	--	0.28 to 0.36
MP 788.5				0.06 to 0.30
MP 825.2			0.25	0.25 to 0.48
MP 844.1	0.36	--	--	0.33 to 0.36

Grey cells indicate study sites where the climate stations were not yet installed. Cells with dashes indicate study sites where the n_f could not be calculated due to logger failure.

The n_f is closely influenced by snow conditions, and is expected to have an inverse correlation to mean annual snow depth but is also influenced by MAAT through the rate of freezing (Smith and Riseborough 1996; Smith and Riseborough 2002; Karunaratne and Burn 2004). The values calculated for winter 2010-2011 did not correlate with snow depth, and the majority were much higher than predicted by Smith and Riseborough's (2002) relationships (Figure 64). This is most likely due to the low moisture content and the thin active layer depths at these sites (Throop et al. 2012). During the late fall, the active layer freezes rapidly which then allows the surface temperature to fall (Throop et al. 2012).

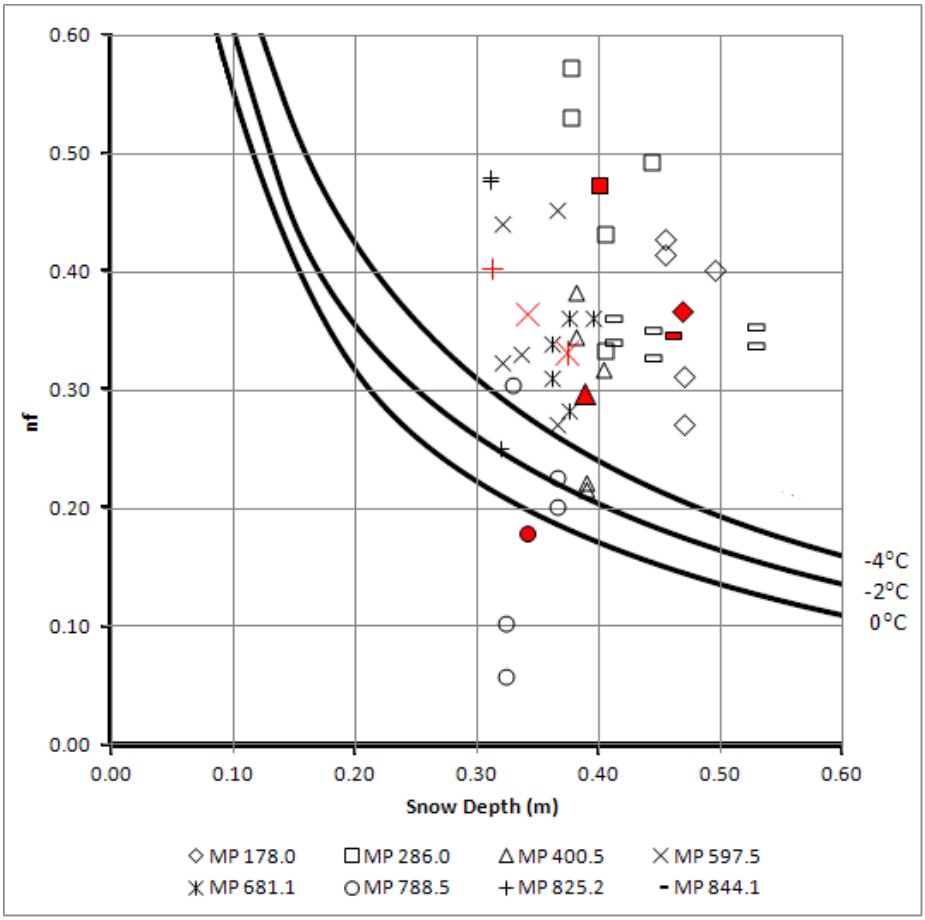

Figure 64 – N-factor values for all ground temperature loggers at every study site. Mean n-factor values are in red. N-factors as a function of snow depth for the MAATs 0 °C, -2 °C, and -4 °C are also shown (adapted from (Smith and Riseborough 2002)). Snow depth was calculated by dividing each climate station's SDD by the site's snow season.

Although snow depth is considered the major influence on n_f, the presence or absence of permafrost can also affect it due to the effects of latent heat (Karunaratne and Burn 2004). When an area with permafrost undergoes freezing, latent heat is released until the active layer has frozen, which then allows the ground surface temperature to cool (Karunaratne and Burn 2004). In an area without permafrost, or with a supra-permafrost talik, the surface continues to stay warm during the freezing season due to the constant release of latent heat from the ground (Karunaratne and Burn 2004). This release causes the n_f to be low, which likely explains the very low values at MP 788.5.

5.2.4 Electrical Resistivity Tomography Data

MP 341.3 had the lowest mean apparent resistivity of 179 Ωm. The model block resistivity values for MP 341.3 ranged from 1 Ωm to 6 kΩm, both of which occurred in March. MP 681.1 had the highest mean apparent resistivity of 3.3 kΩm. The resistivity values ranged from 155 Ωm (which occurred in August) to 81 kΩm (which occurred in March).

The trends in the apparent resistivity values were similar to those found in the inverted resistivity values. MP 341.3 had the lowest mean inverted resistivity value of 188 Ωm. In addition to the lowest mean inverted resistivity, MP 341.3 also had the lowest minimum and maximum model block resistivity values, 2 Ωm and 9 Ωm, respectively. MP 681.1 had the highest mean inverted resistivity value of 5 kΩm. This site did not have the most permafrost within the profile, but it did have the highest minimum (51 Ωm) and maximum (158.4 kΩm) model block resistivity values. Therefore, the permafrost at MP 681.1 was either cooler or more ice-rich than the other nine sites. This observation was consistent with the site's low MAAT and the presence of cold air pooling (Wahl et al. 1987). There were numerous hummocky and elevated surfaces at MP 681.1, which suggests the permafrost at that site could have higher ice content.

The mean variation between each survey was 127%. This value was affected by two sites that had a percentage change that exceeded 300% and one site that had more than 100%. These sites were MP 579.1, MP 681.1 and MP 844.1. As seen in Figure 65a, these sites also had the largest range for 'indeterminate' ground, meaning there was a larger range of resistivities that were unable to be identified conclusively as unfrozen or frozen. These sites also had gravel present. MP 597.5 was also noted to have gravel but it was not identified during frost probing (Brown 1967). The presence of gravel may explain the slightly larger range for 'indeterminate' at MP 597.5.

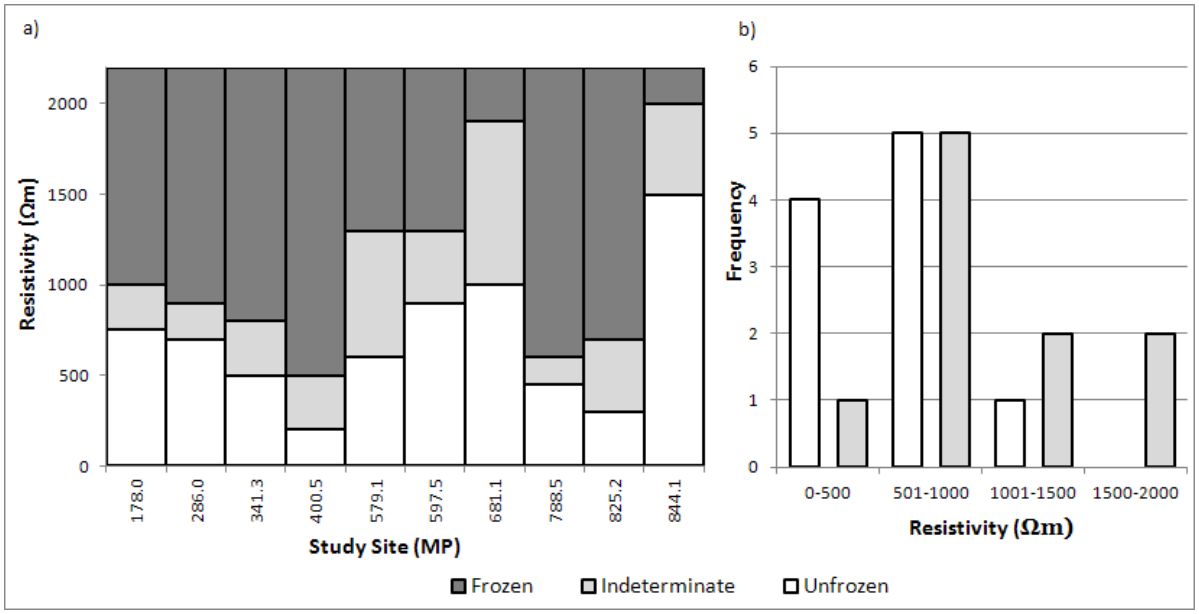

Figure 65 – The distribution of ERT classifications by site and frequency a) A bar graph displaying the upper and lower limits of each ERT classification for each of the ten sites. Note that the upper limit or frozen is not shown since it depends on the highest value recorded; b) frequency distribution of the upper limits of the 'unfrozen' and 'indeterminate' classifications.

Figure 65b shows the distribution of the classifications developed for each site. The majority of sites had their upper limit of unfrozen ground at or less than 1,000 Ωm and their upper limit of indeterminate ground at or less than 2,000 Ωm. All resistivity values above 2,000 Ωm were classified as frozen. However, there are significant variations among the sites.

Figure 66a displays the relationship between available mean annual air temperatures at each site and the mean resistivity. The R^2 value is 0.58 when an exponential trendline is used. This type of trendline is reasonable because of the physical exponential relationship between resistivity and soil temperature (Hauck and Kneisel 2008). It is important to note that the R^2 value would increase to 0.95 if MP 178.0 was removed. MP 178.0 had the highest SDD and lowest thermal offset value; therefore, it is possible that this site's MAAT had the least effect on its resistivity.

Figure 66b displays the relationship between the ground temperature values during each survey taken and the corresponding model block resistivity value. There appears to be no relationship between these two values, most likely due to the very small temperature range in the ground temperatures.

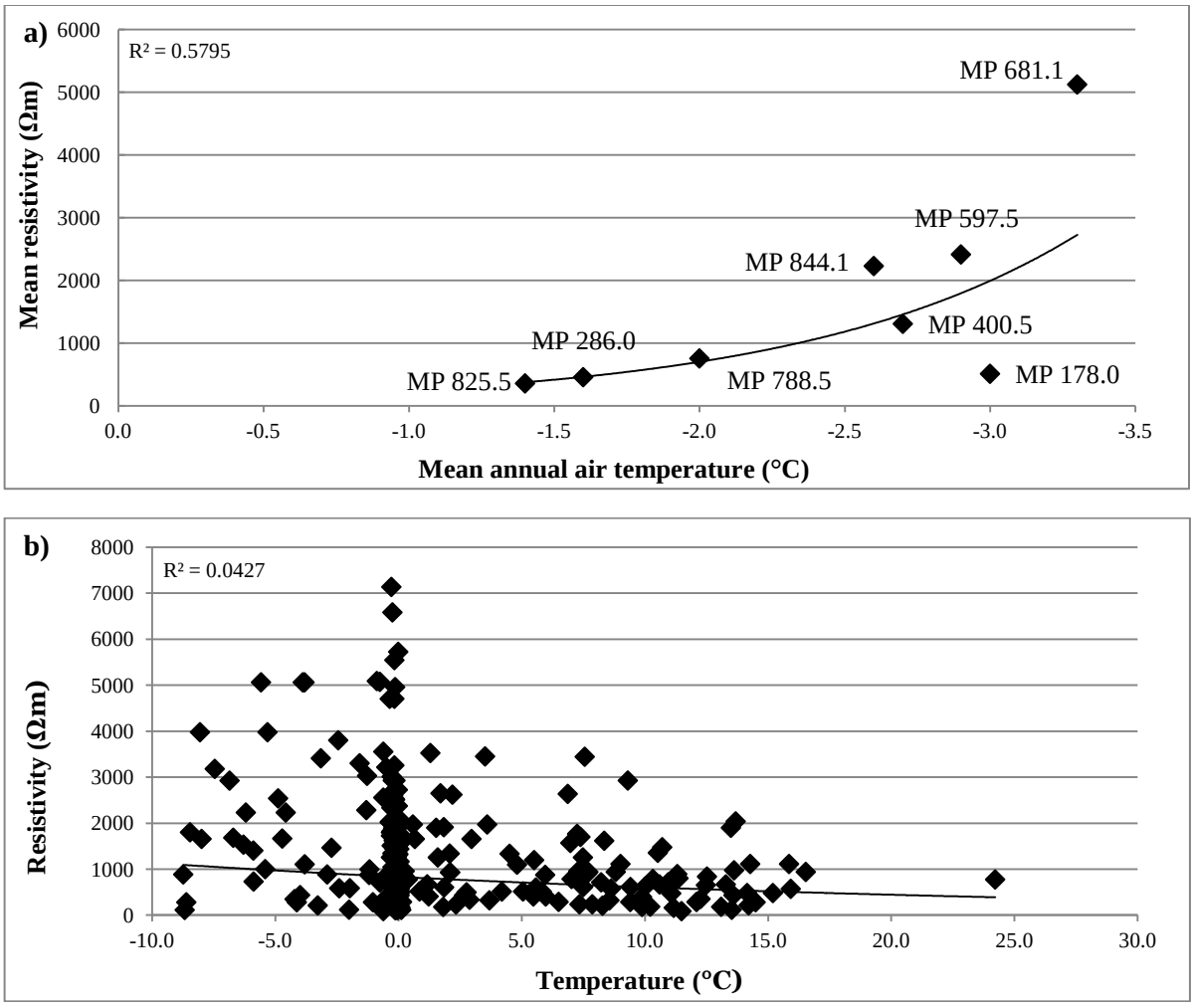

Figure 66 – The relationship between resistivity and temperature; a) Mean annual air temperature and mean resistivity for each of the study sites. The exponential trendline has an R^2 value of 0.58; b) Model block resistivity values and the ground temperature for each survey at each study site. The exponential trendline has an R^2 value of 0.04 and is not statistically significant.

6.0 DISCUSSION

6.1 Current and Predicted Permafrost Conditions

All of the sites had characteristics that are common within the sporadic discontinuous and isolated patches permafrost zones, which is consistent with research previously conducted in the area (Brown 1967; James 2010; Lewkowicz et al. 2011). However, the ten study sites investigated had different frozen ground and permafrost characteristics when compared with each other.

The study sites can be subdivided based on their ERT profiles: those with three-layer permafrost systems and those with two-layer permafrost systems. A three-layer permafrost system has a visible active layer, permafrost body, and a sub-permafrost talik (James 2010). A two-layer permafrost system has a visible active layer and permafrost body and the depth of the permafrost cannot be determined (James 2010). MP 400.5 was the only site with a two-layer permafrost system while all the rest had three-layer permafrost. The permafrost at these three-layer sites had distinct permafrost bodies alternating with seasonally frozen ground, thin continuous layers of permafrost, or a combination of the two.

Based on the permafrost classification by Shur and Jorgenson (2007), the permafrost at each of the sites is Ecosystem-protected. Permafrost likely developed in the Little Ice Age, when temperatures were cooler than at present (Vitt et al. 1994; Halsey et al. 1995; Shur and Jorgenson 2007). If the current climate continues, permafrost in these areas can persist only if undisturbed by hydrologic processes, such as lake expansion or groundwater flow (Shur and Jorgenson 2007) or by fire (Burn 1998). There were several sites which had areas where surface ponding occurred in the spring, namely MP 825.2, MP 788.5, MP 681.1 and MP 579.1. These areas along the profile did not have permafrost, most likely due to this hydrologic disturbance. Ecosystem-protected permafrost will also degrade if the area is affected by forest fire. Signs of past fire were noted by James (2010) for MP 844.1, but no damage was observed at other sites.

The persistence of permafrost at these sites is also related to the thermal offset and possibly to cold air pooling. The thermal offset is an extremely important factor for permafrost persistence at

the southern limits of discontinuous permafrost (Smith and Riseborough 1996; Smith and Riseborough 2002; Shur and Jorgenson 2007). The high thermal offset at the study sites is due to the presence of mosses, lichens, and peat (Brown 1967; Brown 1968; Shur and Jorgenson 2007). Peat becomes dry during the summer due to increased evapotranspiration (Brown 1968). This lowered water content decreases the thermal conductivity, which allows lower temperature permafrost below to remain cool (Brown 1968). In the autumn, increased moisture and lower temperatures allow the peat to freeze, which increases the thermal conductivity (Brown 1968). This increase allows further decreases in ground temperatures to occur (Brown 1968).

Cold air pooling has been reported in two areas within or close to the study area (Harris 1982; Wahl et al. 1987). Near Summit Lake, west of Fort Nelson, air temperature differences of 33 ºC were observed in January 1982 between one site at 1,524 m asl (-38 ºC) and another site located at 1,170 m asl (-71 ºC) (Harris 1982). This temperature inversion may have affected MP 400.5 and MP 341.3, which are located to the east and west of where these temperatures were recorded in 1982. Cold air pooling is also present in the Central Yukon Basin, north of MP 681.1 (Wahl et al. 1987). There is a possibility that MP 681.1 is affected by this cold air drainage as shown by its low MAAT. Cold air pooling can have a large effect on permafrost presence and thickness (Harris 1982).

Ecosystem-protected permafrost will degrade if there is a large increase in temperature (Halsey et al. 1995; ACIA 2005; Shur and Jorgenson 2007). As seen in Figure 5, the climate within the study area has warmed since the 1970s, which followed 30 years of fairly consistent temperatures (James 2010; Environment Canada 2012a). From 1971 to 2010, climate has warmed by a rate of 0.5 ºC/decade in Whitehorse and Watson Lake and 0.3 ºC/decade in Fort Nelson and Fort St. John. These rates are similar to those within the Arctic, typically 0.4 ºC/decade from 1966 to 2003 (ACIA 2005). If the study sites have experienced similar rates their MAATs were 1.4 ºC to 2.3 ºC colder in 1964 when Roger Brown investigated permafrost in the area. All sites south of and including MP 341.3 have warmed by a rate of 0.3 ºC/decade and all sites north of and including MP 400.5 have warmed by a rate of 0.5 ºC/decade. If this rate of change continues, permafrost in the study area

could decrease in thickness, increase in temperature, or thaw. Although permafrost can form rapidly under cold temperatures, several warm years are required in order for it to thaw (Riseborough and Smith 1993; Romanovsky et al. 2010). Changes in permafrost thickness due to climate change are expected to be observed over years to decades (Kwong and Gan 1994).

There is evidence of permafrost thaw within the study area. The southern limit of discontinuous permafrost appears to have moved approximately 75 km northward since Brown's permafrost survey (Heginbottom et al. 1995; James 2010). Additionally, there is evidence that the permafrost within the study sites is not in equilibrium and is susceptible to thaw. Ecosystem-protected permafrost can begin to thaw from the surface. When this occurs, an unfrozen area can develop between the base of the active layer and the permafrost body. This supra-permafrost talik may continue to increase in depth until the permafrost has thawed. Evidence of supra-permafrost taliks were seen in the permafrost classification profiles for MP 597.5, MP 681.1, MP 788.5 and MP 825.2 (Figure 11 in each of Appendices I, J ,K and L).

6.2 Electrical Resistivity Tomography Results

In order to determine the effectiveness of the ERT in thin permafrost over an annual cycle, it is important to compare the anticipated results with the results that were observed. The anticipated results, described in Section 1.2, were modified from Hilbich et al. (2011).

For each survey, the apparent and inverted resistivities were analyzed. The apparent resistivity can be useful when analyzing multiple surveys at the same site (Hilbich et al. 2008). In Hilbich et al. (2011), the minimum apparent resistivity occurred when the active layer was at its deepest. For this research, the maximum active layer thickness was in the August 2010 survey. Figure 67 shows the apparent and inverted resistivity values for each study site for each survey. The resistivity values for MP 597.5, MP 681.1 and MP 844.1 are grouped into Figure 67b and Figure 67d for scaling purposes.

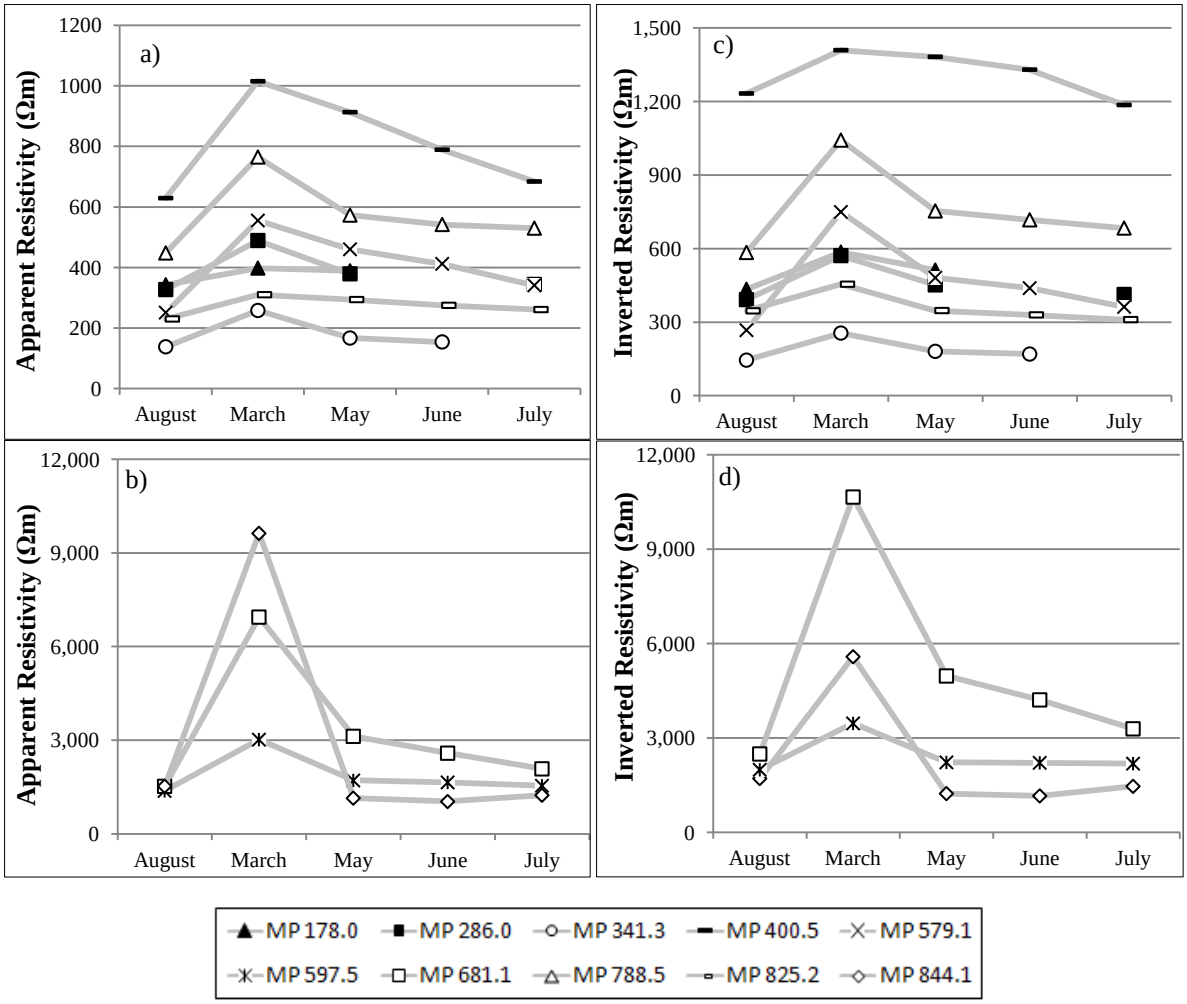

Figure 67 - Apparent and inverted resistivity summary graphs a) Apparent mean resistivity values for MP 178.0, MP 286.0, MP 341.3, MP 400.5, MP 579.1, MP 788.5 and MP 825.2; b) Apparent mean resistivity values for MP 597.5, MP 681.1 and MP 844.1; c) Inverted mean resistivity values for MP 178.0, MP 286.0, MP 341.3, MP 400.5, MP 579.1, MP 788.5 and MP 825.2; d) Inverted mean resistivity values for MP 597.5, MP 681.1 and MP 844.1.

As seen in Figure 67a and b, nine of the ten study sites had minimum mean apparent resistivities in the August 2010 survey. MP 844.1 had its minimum apparent resistivity value in June, which is fairly consistent with the expected results, since June is expected to have a thick active layer and high ground surface temperatures. All ten sites had mean minimum temperatures in March, which was also an expected result since this was the only survey conducted during the winter. Therefore, the apparent resistivity values behaved as expected.

The mean monthly inverted resistivity values are shown in Figure 67c and d. All sites had the maximum mean inverted resistivity values in March, and seven sites had minimum mean resistivity values in August. MP 400.5 and MP 825.2 had their minimum mean resistivity values in July. The difference in mean resistivities between these site's July and August surveys are both less than 150 Ωm, so it is possible this small difference is due to the inversion process. MP 844.1 has its minimum mean resistivity value in June. There was a 544 Ωm difference between MP 844.1's August and June survey. It is unclear what caused this high average in August, but this was not consistent with the expected results.

There should be a visible difference in apparent resistivity values within the active layer between surveys due to the changes in active layer thickness. Although mean apparent resistivity is a good measure of seasonal resistivity fluctuations, it takes the whole profile into account. In order to determine if seasonal cycling is occurring in the active layer, the mean apparent resistivity was calculated for the first full layer of model blocks for each survey at each site (Table 17).

Table 17 - Mean apparent resistivity for the near-surface for each survey at each study site. Note that the August 2010 survey is placed at the end of the table. For the 40 m surveys, the near-surface is defined as the first layer of model blocks that span the entire length of the profile. For the 80 m surveys, the near-surface is defined as the first layer of higher concentrated model blocks that span from 20 – 55 m.

	Mean apparent resistivity for each survey (Ωm)					Mean apparent resistivity (Ωm)
	March 2011	May 2011	June 2011	July 2011	August 2010	
MP 178.0	850	707	--	--	475	677
MP 286.0	986	623	--	519	446	643
MP 341.3	1,027	562	518	--	400	627
MP 400.5	943	541	374	265	203	465
MP 579.1	1,682	932	747	463	276	820
MP 597.5	5,530	1,380	1,282	1,077	869	2,028
MP 681.1	16,191	2,461	1,786	1,274	949	4,532
MP 788.5	2,193	930	793	683	547	1,029
MP 825.2	595	415	335	261	164	354
MP 844.1	30,981	2,266	1,984	2,352	2,753	8,067
Cells with dashes indicate study sites where the resistivity survey malfunctioned						

Based on the results of Hilbich et al.(2011), the surveys should have decreasing mean resistivity values from March 2011, when the active layer is expected to be frozen over permafrost, or seasonal freezing is at its maximum where permafrost is absent, to August 2010, when the active layer is its thickest. As shown in Table 17, nine out of the ten sites produced expected results. MP 844.1 had

high near-surface resistivity values in August 2010, which affected the progression of resistivity values.

The inverted resistivity percent change based on the August 2010 survey should have shown maximum change in the near-surface compared to the March survey due to changes in the active layer. All of the sites showed large resistivity differences in the near-surface, and the majority of them showed maximum percent change in the near-surface in March. The largest difference between the percent change figures in Hilbich et al. (2011) and the results obtained here are the magnitude of percent change values. Many of the model blocks underwent greater than 100% percent change from the August 2010 survey to subsequent surveys. This extreme change was not seen in the monitoring station at Schilthorn, which shows percent change of approximately ±50% as extremes. However, the apparent resistivity ranged from 600 to 3507 Ωm in Schilthorn, which was a much smaller range than was found in this study (Hilbich et al. 2011). The larger range in this study is most likely due to the variation in soil type, vegetation, and permafrost thickness. In contrast to Hilbich et al. (2011), this research took place in fine-grained thin permafrost with no known bedrock outcropping within the ERT surveys. The variation in soil type and grain size may have caused the large difference in seasonal change. In addition, there was no vegetation or organic mat at the Schilthorn site, in contrast to the ten study sites. Organic surface layers are usually highly conductive when thawed and highly resistive when frozen.

6.3 Electrical Resistivity Tomography Weaknesses

The results of the ERT surveys were expected to be insightful and predictable in their seasonal behavior. The former appears to be true: the bodies of permafrost at each study site were delineated and their thickness and length could be determined. However, the overall predictability of the ERT surveys is less concrete. The majority of the results from the apparent and inverted resistivity analysis were what was expected, but there were greater discrepancies when analyzing the virtual boreholes and the inverted percent change figures. There are several reasons why the results were not always as consistent as those achieved by Hilbich et al. (2011).

Firstly, and most important, is the presence of three-layer permafrost. This difference is most obvious when comparing the inverted percent change and virtual borehole figures of MP 400.5 to the other nine study sites. MP 400.5 was mostly predictable and consistent, and the results of any other study site. It is well known that areas below high resistivity bodies are less accurate (Hauck and Mühll 2003). Therefore, when the majority of the profile is below a high resistivity layer, it is probable that accuracy will decrease. In addition to areas below high resistivity bodies, there are also probable errors in the near-surface that are above areas of low resistivity. For example, when examining the virtual boreholes there were a number of areas that had no permafrost and no seasonally frozen ground, even within the March survey. This observation is most likely an error since ground surface temperatures were below 0 ºC in the winter. Since Hilbich et al. (2011) studied a two-layer permafrost system, these weaknesses were not discussed. Previous research has been conducted in three-layer systems (Vanhala et al. 2009; Lewkowicz et al. 2011) however none of these performed multi-temporal surveys.

It is possible that a higher accuracy can be rectified in the inversion procedure. For this project, the inversion routine was taken from Hilbich et al. (2011), which did not need take into account three-layer systems. The purpose of this thesis was not to create an idealized inversion routine for three-layer permafrost, but rather to evaluate the procedures that are commonly used. Therefore, the knowledge of an individual better versed in geophysics might have aided in improving the accuracy of the results.

Lastly, there may have been inaccuracy due to the malfunctioning of a relay switchboard in the terrameter, which began in approximately June 2011. Although the majority of the surveys were useable up until July, it is possible the machine was not in optimal condition and therefore not collecting optimal results. This malfunction was especially evident for the surveys from MP 341.3, MP 286.0 and MP 178.0 that were unable to be included due to instrument error. The switchboard completely malfunctioned in August 2011, which is why a full annual cycle was unable to be collected. This was also a weakness of the project, since the inverted resistivity percent change from

August 2010 to August 2011 surveys would have been valuable in determining the effectiveness of ERT.

6.4 Future Research

The study sites used for this project are ideal for continual monitoring and research. Permafrost observations exist for these sites from 1964, when Roger J.E. Brown classified the southern limit of permafrost for the Division of Building Research, National Research Council. From 2007-2010, climate stations, boreholes, and ERT arrays were installed at all of the sites. This infrastructure is easily accessible by road from the Alaska Highway, making them cost-effective and practical for annual, seasonally independent visits. Lastly, the four major communities (i.e., Whitehorse, Watson Lake, Fort Nelson, and Fort St. John) provide additional climate data along the highway.

Future research has already been planned for these study sites. In August 2012, temperature stations will undergo maintenance and ERT surveys will be conducted at each of the study sites. The ERT surveys will be particularly useful since an annual cycle was not achieved for this study.

In addition to the scheduled future research, additional projects could be undertaken at these sites in order to fully comprehend the relationship between resistivity and ground conditions. Soil samples could be collected from each site to determine their specific resistivity measurements and moisture properties. These measurements are important since changes in soil moisture can mask the relationship between temperature and resistivity (Hilbich et al. 2008). By obtaining soil and moisture information there would be better classification of the unfrozen/indeterminate/frozen ground.

There are also numerous potential projects that can be undertaken with the ERT equipment. A longer ERT survey at MP 400.5 could be conducted to see if the depth of permafrost could be determined. Three-dimensional ERT surveys could be conducted in order to identify in greater detail the areal extent of specific permafrost bodies. This would provide additional insight into the specific conditions that are conducive to sustaining permafrost. Different electrode arrays could be used at

the same location to compare the results. Three-layer permafrost may react better to different arrays due to the different measurement configurations. Lastly, electrode spacing could be decreased in areas of thin permafrost in order to gain a clear perspective on active layer freeze-thaw processes.

7.0 CONCLUSIONS

The communities along the Alaska Highway within southern Yukon and northern British Columbia are experiencing a rate of warming of 0.3 to 0.5 ºC/decade. After a lag period, the permafrost in this area will be affected by this increase in air temperature.

The majority of permafrost at the ten study sites was thin, and occupied only parts of the landscape. The permafrost was also very warm, with the mean annual TTOP values no colder than -0.3 °C. Therefore, the permafrost within the study sites can be classified as sporadic discontinuous and isolated patches. This permafrost is vulnerable to thaw, which is evident by the absence of permafrost in areas of hydrologic disturbance.

ERT allowed for the delineation of permafrost in both two- and three-layer systems. Active layer delineation was most successful in areas with thick active layers. Multiple surveys were able to identify the two surveys with the greatest active layer change (i.e., August 2010 to March 2011), and, conversely, the two surveys of least active layer change (i.e., August 2010 to June or July 2011).

Due to the inability to acquire a full annual cycle, it is not completely certain if longer term, not just seasonal, permafrost change can be identified by ERT. However, there is evidence to suggest that using ERT to evaluate change is possible, since surveys conducted in June and July 2011 appeared to be 'returning' to values similar to those obtained in August 2010. It should be noted that there are also additional weaknesses when ERT is being undertaken in three-layer permafrost. Resistivities obtained for areas below high resistivity layers are known to be less accurate (Hilbich et al. 2008), and observations in this study have also shown that areas of low surface resistivity due to seasonal freezing may also affect values in the underlying unfrozen soils. The modification of inversion techniques or the use of different arrays may be the solutions needed

in order for ERT surveys to be as reliable and predictable in three-layer systems as they are in two-layer systems.

Apparent and inverted resistivity values both appear to be useful and predictable. However, conducting surveys in three-layer systems may increase the number of artefacts, which would affect the inverted percent change when comparing multiple surveys of the same location.

Most importantly, the results from this project show that in order to effectively use ERT, it is imperative that it is not used as a stand-alone method. The more auxiliary information within the profile, the more accurate the classification of frozen ground will occur. These methods could include climate monitoring, snow depth monitoring, soil specific moisture and resistivity measurements, and borehole monitoring. Lastly, the input of a geophysical professional might help in the precise interpretation of frozen and unfrozen model blocks.

ERT can be an effective method for monitoring long-term climate change. However, seasonal changes may be inaccurately interpreted as long-term permafrost change. In order to receive the most accurate information regarding permafrost extent and thickness, it seems ideal to conduct ERT surveys annually during the same season, preferably the same month. The annual repeat of ERT surveys, in combination with the continuation of additional monitoring, will aid in determining the effects that climate change will have on the southern limit of permafrost.

REFERENCES

ACIA (2005). Impacts of a Warming Arctic. New York, N.Y., Cambridge University Press**:** 1042.

Bond, J., E. Fuller, et al. (2004). Soils. In: Ecoregions of the Yukon Territory: Biophysical properties of Yukon landscapes, C.A.S. Smith, J.C. Meikle and C.F. Roots (eds.), Agriculture and Agri-Food Canada, PARC Technical Bulletin No. 04-01, Summerland, British Columbia, p. 27-31.

Bond, J. D. (2003). "Late Wisconsinan McConnell glaciation of the Whitehorse map area (105D), Yukon." Yukon Exploration and Geology: 73-88.

Bonnaventure, P. and A. Lewkowicz (2011). "Modelling climate change effects on the spatial distribution of mountain permafrost at three sites in northwest Canada." Climatic Change **105**(1): 293-312.

Brown, J., F. J. Sidlauskas, et al. (1997). International Permafrost Association Circum-Arctic map of permafrost and ground ice conditions. Reston, Va.

Brown, R. (1967). Permafrost investigations in British Columbia and Yukon Territory. Ottawa, National Research Council of Canada, Division of Building Research.

Brown, R. (1968). Occurence of Permafrost in Canadian Peatlands. Third international peat congress, Quebec, Canada, National Research Council of Canada.

Burn, C. R. (1998). "The response (1958-1997) of permafrost and near-surface ground temperatures to forest fire, Takhini River valley, southern Yukon Territory." Canadian Journal of Earth Sciences **35**(2): 184-199.

Canadian Digital Elevation Data (1998). Sherbrooke, Quebec, Canada, Government of Canada, Natural Resources Canada, Earth Sciences Sector, Mapping Information Branch, Centre for Topographic Information - Ottawa**:** 094a, 094b, 094g, 094h, 094j, 094k, 094l, 094m, 094n, 094o, 095d, 104n, 104o, 104p, 105a, 105b, 105c, 105d, 105e, 105f, 105g, 105h.

Duk-Rodkin, A. (2004). "Glacial History, In: Ecoregions of the Yukon Territory: Biophysical properties of Yukon landscapes, landscapes, C.A.S. Smith, J.C. Meikle and C.F. Roots (eds.), Agriculture and Agri-Food Canada, PARC Technical Bulletin No. 04-01, Summerland, British Columbia, p. 24-26.".

Environment Canada. (2012a, 2012-02-06). "National Climate Data and Information Archive." Retrieved 2012-03-05, from http://www.climate.weatheroffice.gc.ca/climateData/canada_e.html.

Environment Canada. (2012b, 2012-02-06). "Canadian Climate Normals 1971-2000 " Retrieved 2012-03-05, from http://www.climate.weatheroffice.gc.ca/climate_normals/index_e.html.

Environment Canada. (2012c, 2012-03-14). "Canadian Climate Normals or Averages 1961-1990." Retrieved 3/25/2012, from http://www.climate.weatheroffice.gc.ca/climate_normals/index_1961_1990_e.html.

French, H. M. (2007). The periglacial environment. Chichester, England; Hoboken, NJ, John Wiley and Sons.

French, H. M. and I. E. Egorov (1998). 20th Century Variations in the Southern Limit of Permafrost Near Thompson, Northern Manitoba, Canada. Seventh International Permafrost Conference, Yellowknife, Canada, Collection Nordicana.

Gądek, B. and J. Leszkiewicz (2010). "Influence of snow cover on ground surface temperature in the zone of sporadic permafrost, Tatra Mountains, Poland and Slovakia." Cold Regions Science and Technology **60**(3): 205-211.

Goodrich, L. E. (1982). "The influence of snow cover on the ground thermal regime." Canadian Geotechnical jrounal **19**: 421-432.

Halsey, L. A., D. H. Vitt, et al. (1995). "Disequilibrium response of permafrost in boreal continental western Canada to climate change." Climatic Change **30**(1): 57-73.

Harris, S. A. (1982). "Cold air drainage west of Fort Nelson, British Columbia." Arctic **35**(4): 537-541.

Hauck, C. (2002). "Frozen ground monitoring using DC resistivity tomography." Geophys. Res. Lett. **29**(21): 2016.

Hauck, C. and C. Kneisel (2008). Applied Geophysics in Periglacial Environments, Cambridge University Press.

Hauck, C. and D. V. Mühll (2003). "Inversion and interpretation of two-dimensional geoelectrical measurements for detecting permafrost in mountainous regions." Permafrost and Periglacial Processes **14**(4): 305-318.

Hauck, C., D. Vonder Mühll, et al. (2003). "Using DC resistivity tomography to detect and characterize mountain permafrost." Geophysical Prospecting **51**(4): 273-284.

Heginbottom, J. A., M. A. Dubreuil, et al. (1995). Canada -- Permafrost in National Atlas of Canada, 5th edition, Plate 2.1 (MCR 4177).

Hilbich, C., C. Fuss, et al. (2011). "Automated time-lapse ERT for improved process analysis and monitoring of frozen ground." Permafrost and Periglacial Processes **22**(4).

Hilbich, C., C. Hauck, et al. (2008). "Monitoring mountain permafrost evolution using electrical resistivity tomography: A 7-year study of seasonal, annual, and long-term variations at Schilthorn, Swiss Alps." J. Geophys. Res. **113**(F1): F01S90.

Hilbich, C., L. Marescot, et al. (2009). "Applicability of electrical resistivity tomography monitoring to coarse blocky and ice-rich permafrost landforms." Permafrost and Periglacial Processes **20**(3): 269-284.

IPCC (2007). Climate Change 2007: The Physical Science Basis. Contribution of Working Group I to the Fourth Assessment Report of the Intergovernmental Panel on Climate Change. S. Solomon, D. Qin, M. Manning, Z. Chen, M. Marquis, K.B. Averyt, M. Tignor and H.L. Miller. Cambridge, United Kingston and New York, NY, USA**:** 996.

Ishikawa, M. (2003). "Thermal regimes at the snow–ground interface and their implications for permafrost investigation." Geomorphology **52**(1–2): 105-120.

Jackson, L. E., B. Ward, et al. (1991). "The Last Cordilleran Ice Sheet in Southern Yukon Territory." Géographie physique et Quaternaire **45**(3): 341-354.

James, M. (2010). Historic Change in Permafrost Distribution in Northern British Columbia and Southern Yukon Territory, Canada. M.Sc., University of Ottawa.

Karunaratne, K. C. and C. R. Burn (2004). "Relations between air and surface temperature in discontinuous permafrost terrain near Mayo, Yukon Territory." Canadian Journal of Earth Sciences **41**(12): 1437-1451.

Kaufman, D. S., T. A. Ager, et al. (2004). "Holocene thermal maximum in the western Arctic (0–180°W)." Quaternary Science Reviews **23**(5–6): 529-560.

Klene, A. E., F. E. Nelson, et al. (2001). "The N-Factor in Natural Landscapes: Variability of Air and Soil-Surface Temperatures, Kuparuk River Basin, Alaska, U.S.A." Arctic, Antarctic, and Alpine Research **33**(2): 140-148.

Kneisel, C., C. Hauck, et al. (2008). "Advances in geophysical methods for permafrost investigations." Permafrost and Periglacial Processes **19**(2): 157-178.

Kneisel, C., C. Hauck, et al. (2000). "Permafrost below the Timberline Confirmed and Characterized by Geoelectrical Resistivity Measurements, Bever Valley, Eastern Swiss Alps." Permafrost and Periglacial Processes **11**(4): 295-304.

Kuhry, P., E. Dorrepaal, et al. (2010). "Potential remobilization of belowground permafrost carbon under future global warming." Permafrost and Periglacial Processes **21**(2): 208-214.

Kwong, Y. T. J. and T. Y. Gan (1994). "Northward migration of permafrost along the Mackenzie highway and climatic warming." Climatic Change **26**(4): 399-419.

Lewkowicz, A. G. (2008). "Evaluation of miniature temperature-loggers to monitor snowpack evolution at mountain permafrost sites, northwestern Canada." Permafrost and Periglacial Processes **19**(3): 323-331.

Lewkowicz, A. G., P. P. Bonnaventure, et al. (2012). "Spatial and thermal characteristics of mountain permafrost, Northwest Canada." Geografiska Annaler: Series A, Physical Geography **94**(2): 195-213.

Lewkowicz, A. G., B. Etzelmüller, et al. (2011). "Characteristics of discontinuous permafrost based on ground temperature measurements and electrical resistivity tomography, southern Yukon, Canada." Permafrost and Periglacial Processes: n/a-n/a.

Loke, M. H. (1999). Electrical imaging surveys for environmental and engineering studies: A practical guide to 2-D and 3-D surveys. Malaysia.

Loke, M. H. (2011). "Tutorial : 2-D and 3-D electrical imaging surveys."

Lunardini, V. (1978). Theory of n-factors and correlation of data. Third International Conference on Permafrost, Edmonton, Alberta, National Research Council of Canada.

Maxim Integrated Products. (2012). "DS1921K Thermochron iButton Kit Overview." Retrieved 3/6/12, from http://www.maxim-ic.com/products/ibutton/ibuttons/1921Kit.cfm.

Noetzli, J., C. Hilbich, et al. (2008). Comparison of Simulated 2D temperature profiles with time-lapse electrical resistivity data at the Schilthorn crest, Switzerland. Ninth International Conference on Permafrost, Fairbanks, Alaska, Institute of Northern Engineering, University of Alaska Fairbanks.

NRCan. (2007, 2007-09-17). "Permafrost." Retrieved 2012-06-19, 2012, from http://www.nrcan.gc.ca/earth-sciences/climate-change/landscape-ecosystem/permafrost/230.

Onset HOBO Data Loggers. (2012). "HOBO U23 Pro v2 External Temperature Data Logger - U23-004." Retrieved 3/6/12, from http://www.onsetcomp.com/products/data-loggers/u23-004.

Outcalt, S. I. and K. M. Hinkel (1996). "The Response of Near-Surface Permafrost to Seasonal Regime Transitions in Tundra Terrain." Arctic and Alpine Research **28**(3): 274-283.

Parks Canada (2003). Terrestrial Ecozones of Canada. P. Canada.

RBR. (2012, 3/6/12). "Products." Retrieved 3/6/12, from http://www.rbr-global.com/products.

Riseborough, D. W. and M. W. Smith (1993). Modelling permafrost reponse to climate change and climate variability. 4th International Symposium on Thermal Engineering and Science of Cold Regions, Hanover, New Hampshire, US Army Cold Regions Research and Engineering Laboratory, Special Report.

Romanovsky, V. E., S. L. Smith, et al. (2010). "Permafrost thermal state in the polar Northern Hemisphere during the international polar year 2007–2009: a synthesis." Permafrost and Periglacial Processes **21**(2): 106-116.

Rowe, J. S. (1972). Forest regions of Canada. Ottawa, Information Canada.

Shur, Y. L. and M. T. Jorgenson (2007). "Patterns of permafrost formation and degradation in relation to climate and ecosystems." Permafrost and Periglacial Processes **18**(1): 7-19.

Smith, M. W. and D. W. Riseborough (1996). "Permafrost monitoring and detection of climate change." Permafrost and Periglacial Processes **7**(4): 301-309.

Smith, M. W. and D. W. Riseborough (2002). "Climate and the limits of permafrost: a zonal analysis." Permafrost and Periglacial Processes **13**(1): 1-15.

Smith, S. (2004). "Introduction, In: Ecoregions of the Yukon Territory: Biophysical properties of Yukon landscapes, landscapes, C.A.S. Smith, J.C. Meikle and C.F. Roots (eds.), Agriculture and Agri-Food Canada, PARC Technical Bulletin No. 04-01, Summerland, British Columbia, p. 3-7.".

Smith, S. (2004). Soils, In: Ecoregions of the Yukon Territory: Biophysical properties of Yukon landscapes, landscapes, C.A.S. Smith, J.C. Meikle and C.F. Roots (eds.), Agriculture and Agri-Food Canada, PARC Technical Bulletin No. 04-01, Summerland, British Columbia, p. 35-38.

Smith, S. L., V. E. Romanovsky, et al. (2010). "Thermal state of permafrost in North America: a contribution to the international polar year." Permafrost and Periglacial Processes **21**(2): 117-135.

Soil Classification Working Group (1998). The Canadian System of Soil Classification. Agriculture and Agri-Food Canada Publication**:** 187 pp.

Tarnocai, C., J. G. Canadell, et al. (2009). "Soil organic carbon pools in the northern circumpolar permafrost region." Global Biogeochem. Cycles **23**(2): GB2023.

Taylor, B. (1997). The Climates of British Columbia and Yukon. Responding to global climate change in British Columbia and Yukon: Volume I of the Canada Country Study: Climate impacts and adaptation. E. Taylor and B. Taylor. Ottawa, Canada Communication Group INC.

Throop, J., A. G. Lewkowicz, et al. (2012). "Climate and ground temperature relations at sites across the continuous and discontinuous permafrost zones, northern Canada." Canadian Journal of Earth Sciences.

UNEP (2007). "Global Outlook for Ice and Snow ".

Vanhala, H., P. Lintinen, et al. (2009). "Electrical resistivity study of permafrost on Ridnitsohhka Fell in Northwest Lapland, Finland." Geophysica **45**(1-2): 103-118.

Vitt, D. H., L. A. Halsey, et al. (1994). "The Bog Landforms of Continental Western Canada in Relation to Climate and Permafrost Patterns." Arctic and Alpine Research **26**(1): 1-13.

Vonder Mühll, D., C. Hauck, et al. (2002). "Mapping of mountain permafrost using geophysical methods." Progress in Physical Geography **26**(4): 643-660.

Wahl, H. E., D. B. Fraser, et al. (1987). Climate of the Yukon. Canada, Canadian Government Publishing Centre, Ottawa, Canada.

Williams, P. J. and M. W. Smith (1989). The Frozen Earth: Fundamentals of Geocryology. Cambridge, Cambridge University Press.

Zhang, T. (2005). "Influence of the seasonal snow cover on the ground thermal regime: An overview." Rev. Geophys. **43**(4): RG4002.

Zhang, Y., W. Chen, et al. (2006). "Temporal and spatial changes of permafrost in Canada since the end of the Little Ice Age." J. Geophys. Res. **111**(D22): D22103.

APPENDIX A

Site information

Table A1 - Site information, including GPS location, equipment, and date of installation

Site Name (Mile Post)	**Location** (Degrees, Minutes, Seconds)		**Elevation** (m asl)	**ERT Resistivity Length** (m)	**Central Station**		[a] **Subsidiary Station 1 Location** (m from beginning of plot)	[a] **Subsidiary Station 2 Location** (m from beginning of plot)	**Borehole**		
	Latitude	**Latitude**			**Location** (m from beginning of plot)	**Installation Date** (dd/mm/yy)			**Location** (m from beginning of plot)	**Depth** (m)	**Installation Date** (dd/mm/yy)
178.0	57° 25' 30"	-122° 51' 54"	1098	40	20	15/08/10	13	39			
286.0	58° 39' 47"	-122° 41' 35"	417	40	20	15/08/07	9	39	~20	2.4	01/08/09
341.3	58° 47' 20"	-123° 34' 23"	461	80	40	14/08/10	20	60			
400.5	58° 41' 35"	-124° 51' 32"	1043	80	23	13/08/07	40	60			
579.1	59° 57' 54"	-127° 31' 55"	725	80	39	12/08/10	20	62			
597.5	59° 59' 46"	-127° 57' 18"	682	80	23	13/08/07	40	60			
681.1	60° 11' 20"	-129° 53' 56"	849	80	50	11/08/07	20	62			
788.5	60° 05' 28"	-132° 22' 05"	760	80	40	10/08/10	20	60	2-21	3.75	10/08/10
825.2	60° 22' 19"	-133° 6' 40"	721	80	34	20/09/08	20	56	2-15	4	25/09/08
844.1	60° 28' 34"	-133° 29' 02"	813	80	19	09/08/07	40	60			

[a] All subsidiary stations were installed in August 2010. Grey cells indicate sites where the cell information is not applicable.

APPENDIX B

Field work schedule

Table B1 - Field work schedule

Date		Site	Field Work Executed
2010	August 9	MP 844.1	Installation of ERT array and subsidiary stations Downloading of previously installed loggers Execution of ERT survey and frost probing
	August 10	MP 825.2	Installation of ERT array and subsidiary stations Downloading of previously installed loggers Execution of ERT survey and frost probing
		MP 788.5	Installation of ERT array, central climate station, subsidiary stations, and borehole Execution of ERT survey and frost probing
	August 11	MP 788.5	Installation of ERT array, central climate station, subsidiary stations, and borehole Execution of ERT survey and frost probing
		MP 681.1	Installation of ERT array and subsidiary stations Downloading of previously installed loggers Execution of ERT survey and frost probing
	August 12	MP 597.5	Installation of ERT array and subsidiary stations Downloading of previously installed loggers Execution of ERT survey and frost probing
		MP 579.1	Installation of ERT array, central climate station, and subsidiary stations Execution of ERT survey and frost probing
	August 13	MP 597.5	Installation of ERT array and subsidiary stations Downloading of previously installed loggers Execution of ERT survey and frost probing
		MP 579.1	Installation of ERT array, central climate station, and subsidiary stations Execution of ERT survey and frost probing
		MP 400.5	Installation of ERT array and subsidiary stations Downloading of previously installed loggers Execution of ERT survey and frost probing
	August 14	MP 400.5	Installation of ERT array and subsidiary stations Downloading of previously installed loggers Execution of ERT survey and frost probing
		MP 341.3	Installation of ERT array, central climate station, and subsidiary stations Execution of ERT survey and frost probing
		MP 286.0	Installation of ERT array and subsidiary stations Downloading of previously installed loggers Execution of ERT survey and frost probing
	August 15	MP 286.0	Installation of ERT array and subsidiary stations Downloading of previously installed loggers Execution of ERT survey and frost probing
		MP 178.0	Installation of ERT array, central climate station, and subsidiary stations Execution of ERT survey and frost probing
2011	March 9	MP 844.1	Execution of ERT survey and snow depth probing
	March 10	MP 825.2	Execution of ERT survey and snow depth probing
		MP 788.5	Execution of ERT survey and snow depth probing
	March 11	MP 681.1	Execution of ERT survey and snow depth probing
	March 12	MP 597.5	Execution of ERT survey and snow depth probing
		MP 579.1	Execution of ERT survey and snow depth probing

	March 13	MP 400.5	Execution of ERT survey and snow depth probing
		MP 341.3	Execution of ERT survey and snow depth probing
	March 14	MP 178.0	Execution of ERT survey and snow depth probing
		MP 286.0	Execution of ERT survey and snow depth probing
	May 13	MP 844.1	Execution of ERT survey and frost probing
		MP 825.2	Execution of ERT survey and frost probing
	May 14	MP 788.5	Execution of ERT survey and frost probing
		MP 681.1	Execution of ERT survey and frost probing
	May 15	MP 597.5	Execution of ERT survey and frost probing
		MP 579.1	Execution of ERT survey and frost probing
	May 16	MP 400.5	Execution of ERT survey and frost probing
		MP 341.3	Execution of ERT survey and frost probing
	May 17	MP 286.0	Execution of ERT survey and frost probing
		MP 178.0	Execution of ERT survey and frost probing
	June 8	MP 844.1	Execution of ERT survey, frost probing, and logger downloading
		MP 825.2	Execution of ERT survey, frost probing, and logger downloading
	June 9	MP 788.5	Execution of ERT survey, frost probing, and logger downloading
		MP 681.1	Execution of ERT survey, frost probing, and logger downloading
	June 11	MP 597.5	Execution of ERT survey, frost probing, and logger downloading
		MP 579.1	Execution of ERT survey, frost probing, and logger downloading
	June 12	MP 400.5	Execution of ERT survey, frost probing, and logger downloading
		MP 341.3	Execution of ERT survey, frost probing, and logger downloading
	June 13	MP 178.0	Execution of ERT survey, frost probing, and logger downloading
	June 14	MP 286.0	Execution of ERT survey, frost probing, and logger downloading
	July 3	MP 844.1	Execution of ERT survey and frost probing
		MP 825.2	Execution of ERT survey and frost probing
	July 4	MP 788.5	Execution of ERT survey and frost probing
		MP 681.1	Execution of ERT survey and frost probing
	July 5	MP 597.5	Execution of ERT survey and frost probing
		MP 579.1	Execution of ERT survey and frost probing
	July 6	MP 400.5	Execution of ERT survey and frost probing
		MP 341.3	Execution of ERT survey and frost probing
	July 7	MP 286.0	Execution of ERT survey and frost probing
		MP 178.0	Execution of ERT survey and frost probing
	August 19	MP 844.1	Execution of ERT survey, frost probing, and logger downloading
		MP 825.2	Execution of ERT survey, frost probing, and logger downloading
	August 20	MP 788.5	Execution of ERT survey, frost probing, and logger downloading
		MP 681.1	Execution of ERT survey, frost probing, and logger downloading
	August 21	MP 597.5	Execution of ERT survey, frost probing, and logger downloading
		MP 579.1	Execution of ERT survey, frost probing, and logger downloading
	August 22	MP 400.5	Execution of ERT survey, frost probing, and logger downloading
		MP 341.3	Execution of ERT survey, frost probing, and logger downloading
	August 23	MP 286.0	Frost probing, and logger downloading
		MP 178.0	Frost probing, and logger downloading

APPENDIX C

ERT inversion information

```
Initial damping factor is 0.1000.
Minimum damping factor is 0.0050.
Line search is always used.
Convergence limit is 5.0000.
Minimum change in RMS error is 0.5000.
Number of iterations is 5.
Vertical to horizontal flatness filter ratio is 1.0000.
User defined increase in layer thickness.
Number of nodes between adjacent electrodes is 2.
Smoothness constrain is only used directly on model resistivity values.
Number of topographical datum points is not reduced.
Topographical modeling is to be carried out.
Average topographical trend to be removed.
Jacobian matrix is recalculated after each iteration.
Increase of damping factor with depth is 1.1500.
Finite element method is used for topographic modeling.
Robust data inversion constrain is used with cutoff factor 0.0500.
Robust model inversion constrain is used with cutoff factor 0.0050.
Extended model is used.
Effect of side blocks is severely reduced.
Normal mesh is used.
Damping factor is optimised at each iteration.
No inter-model constrain is used in time-lapse inversion.
Simultaneous time-lapse inversion is used.
Thickness of first layer is 0.5000.
Factor to increase thickness layer with depth is 1.1000.
Finite element method is used
Width of blocks used is 1 times the unit electrode spacing
All models blocks must have the same width
RMS convergence limit is 0.1 percent
Logarithm of apparent resistivity values are used for the inversion
Resistivity/IP data are inverted sequentially
Do not proceed automatically in sequential IP inversion
IP damping factor is 0.1000
Automatic IP damping factor is not used
Cutoff factor for borehole data is 0.00010
Standard cross-borehole model is used.
Upper resistivity cutoff limit is 50.00000
Lower resistivity cutoff limit is 0.02000
Average resistivity used.
Model refinement used.
Reference model with damping factor of 0.010 used.
```

Figure C1 – ERT parameters

APPENDIX D

MP 178.0

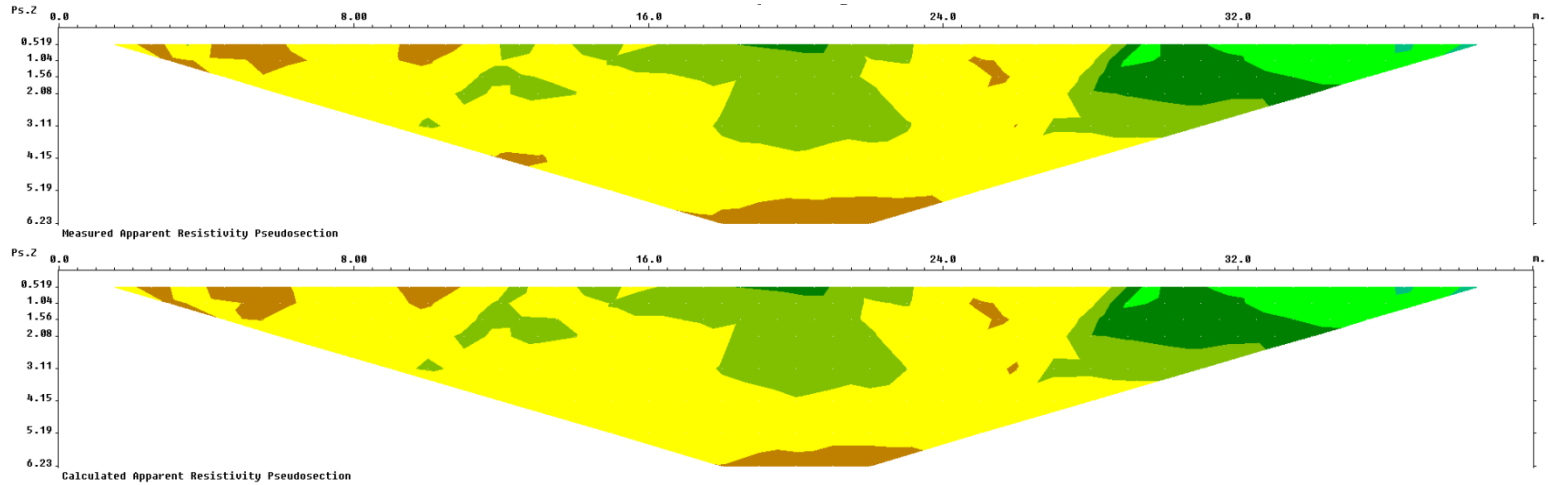

Figure D1 – Measured and calculated apparent resistivity for the August 2010 survey at MP 178.0

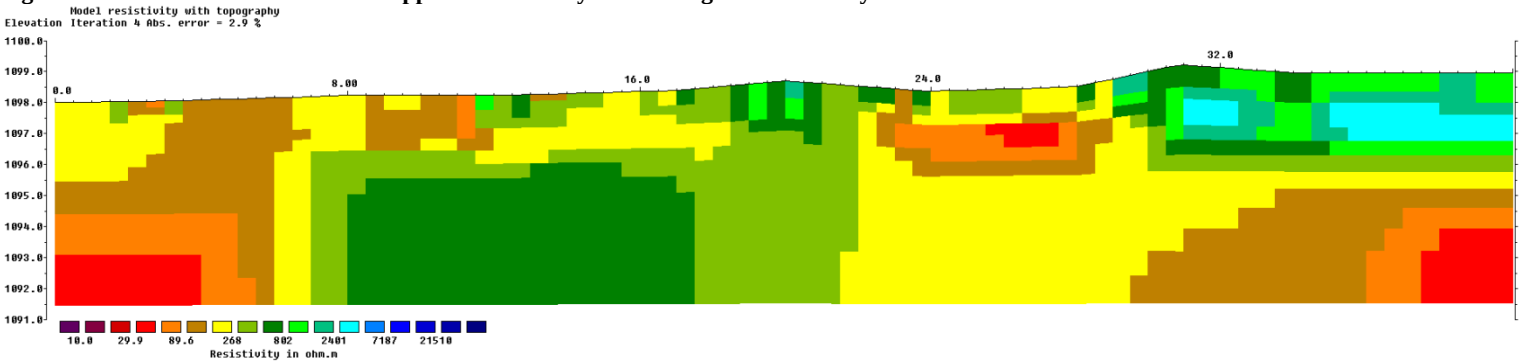

Figure D2 – Model resistivity with topography for the August 2010 survey for MP 178.0

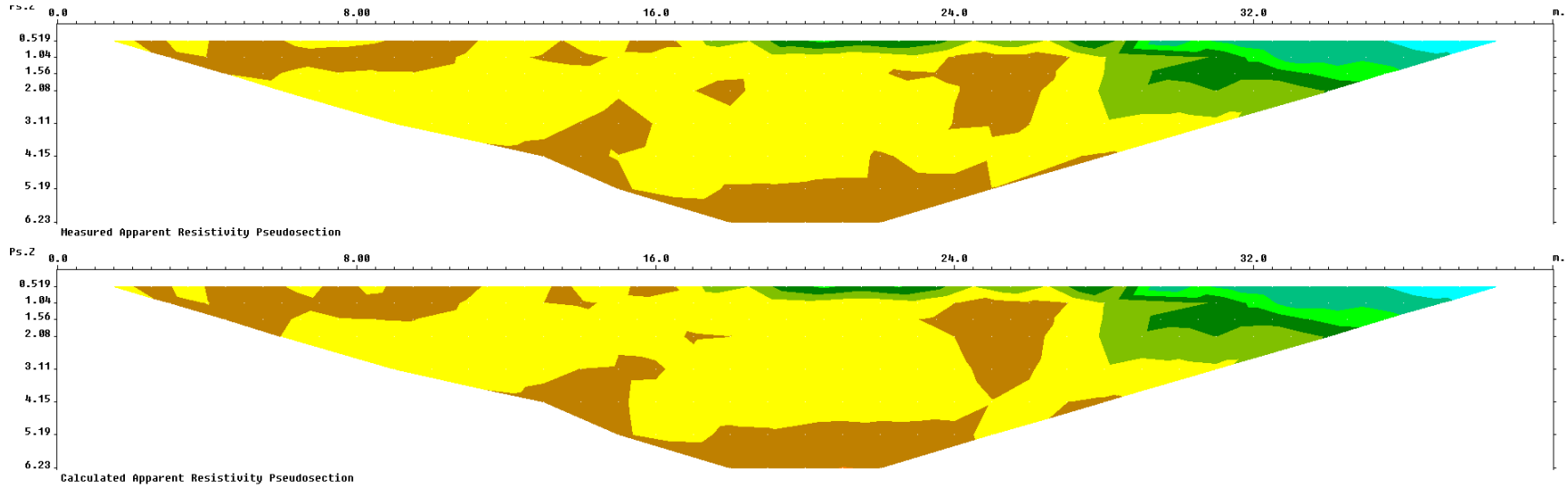

Figure D3 – Measured and calculated apparent resistivity for the March 2011 survey at MP 178.0

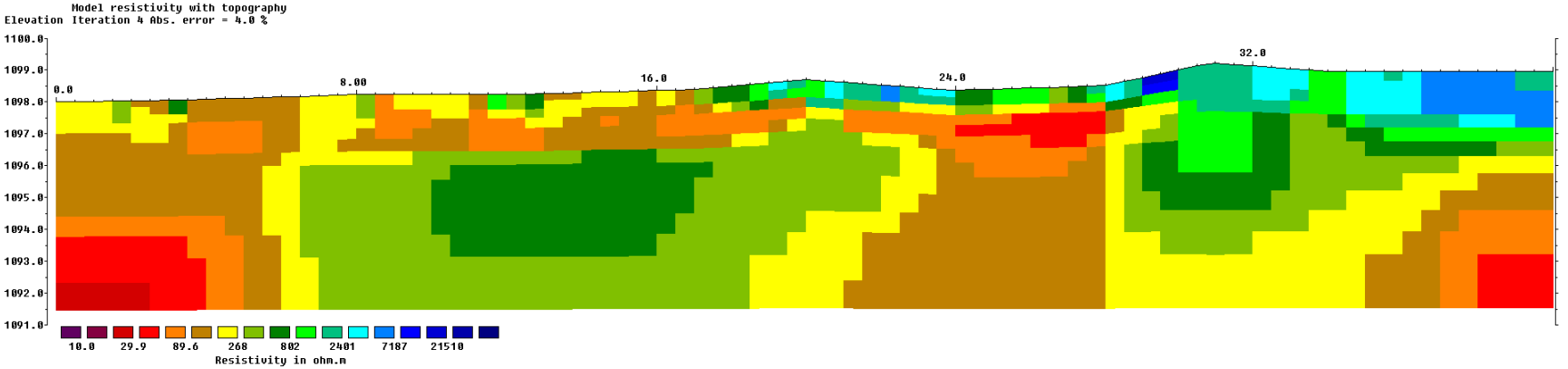

Figure D4 - Model resistivity with topography for the March 2011 survey for MP 178.0

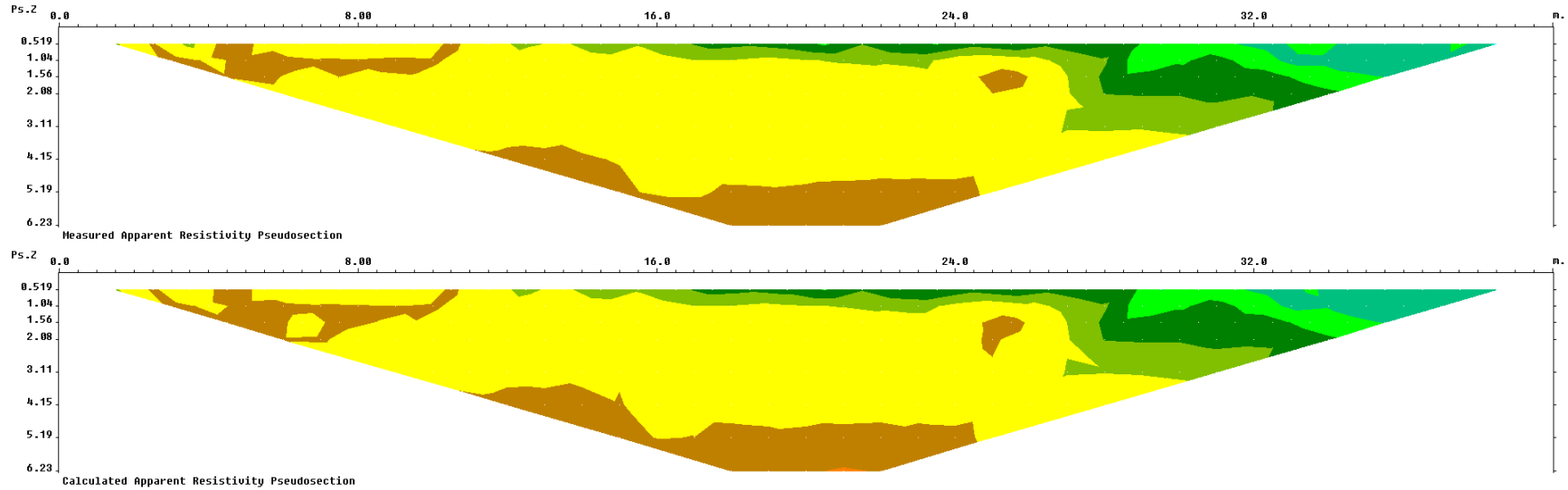

Figure D5 - Measured and calculated apparent resistivity for the May 2011 survey at MP 178.0

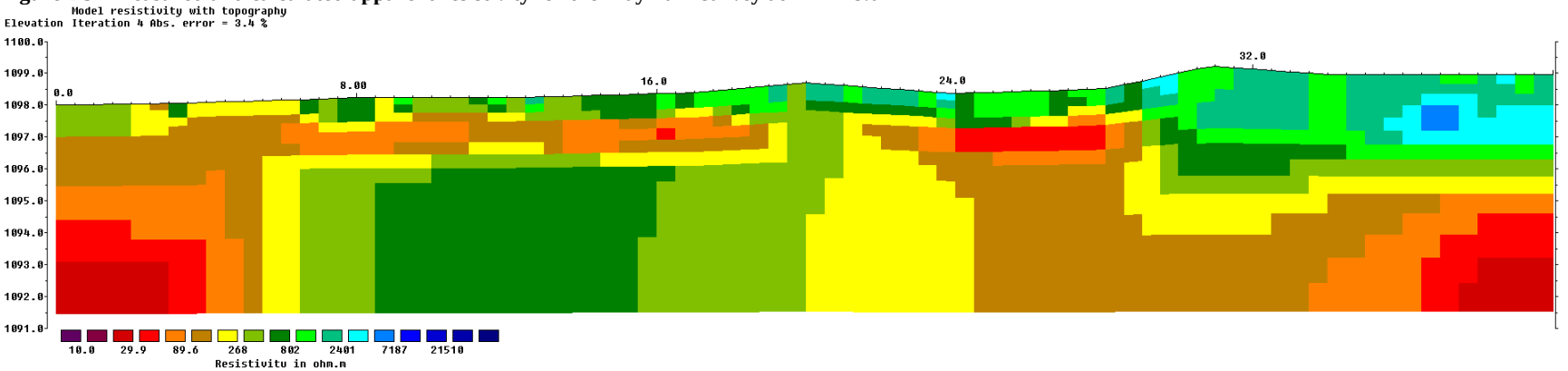

Figure D6 - Model resistivity with topography for the May 2011 survey for MP 178

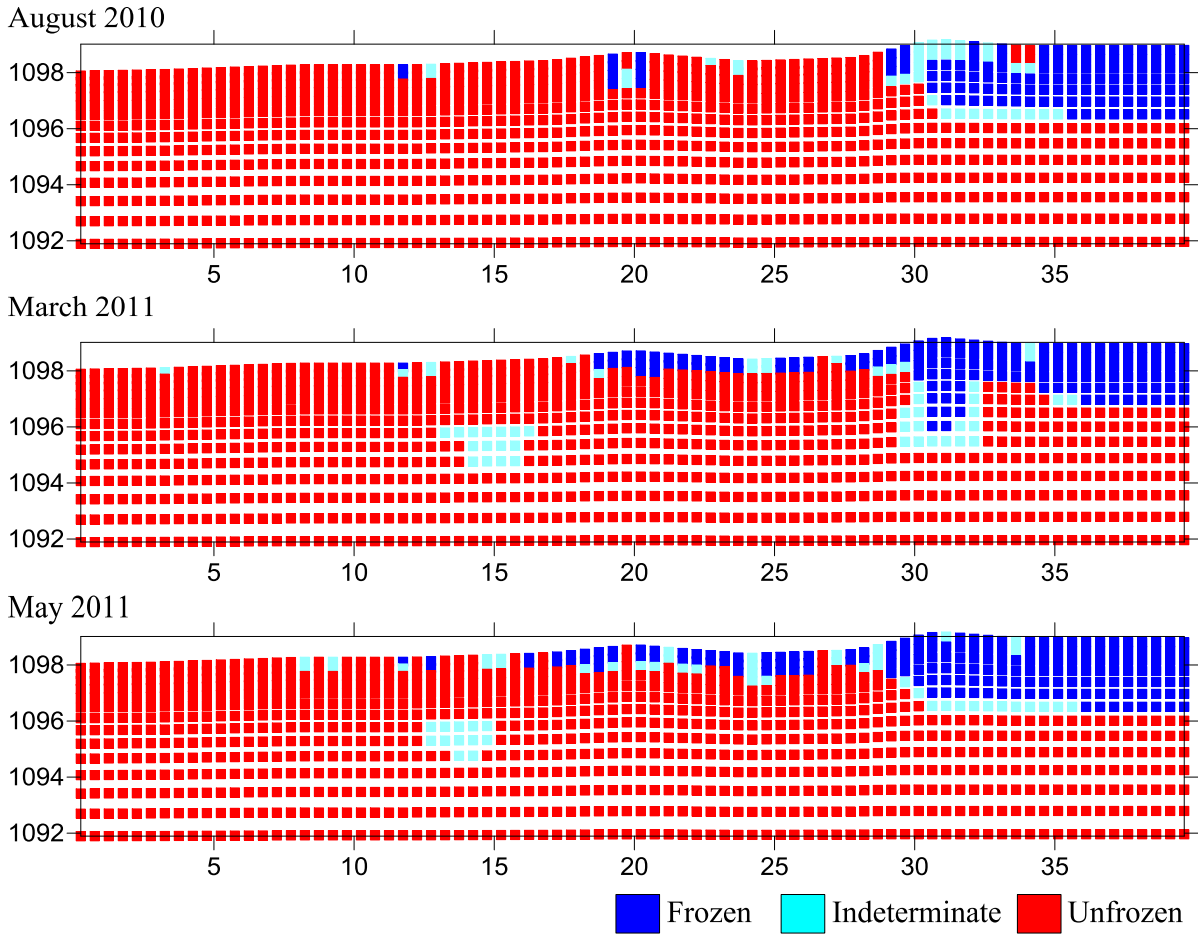

Figure D7 - Permafrost classification images for the surveys conducted at MP 178.0

APPENDIX E

MP 286.0

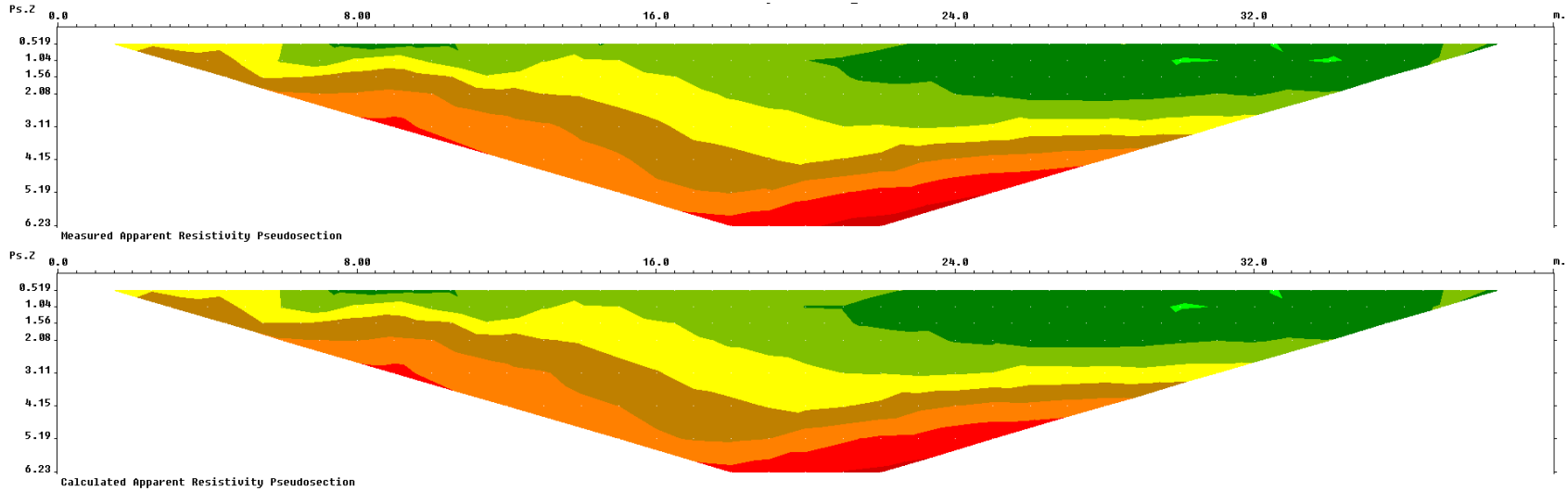

Figure E1 – Measured and calculated apparent resistivity for the August 2010 survey at MP 286.0

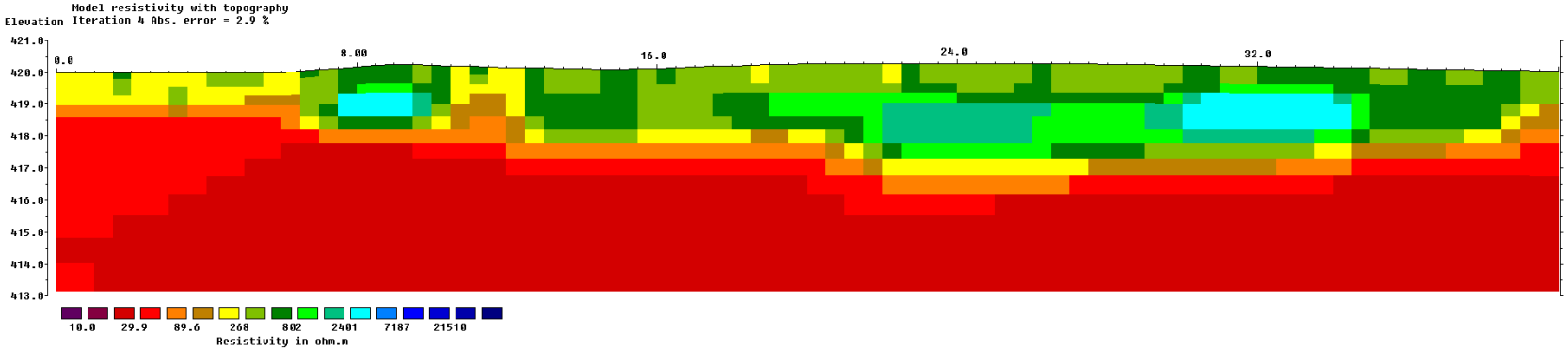

Figure E2 - Model resistivity with topography for the August 2010 survey for MP 286.0

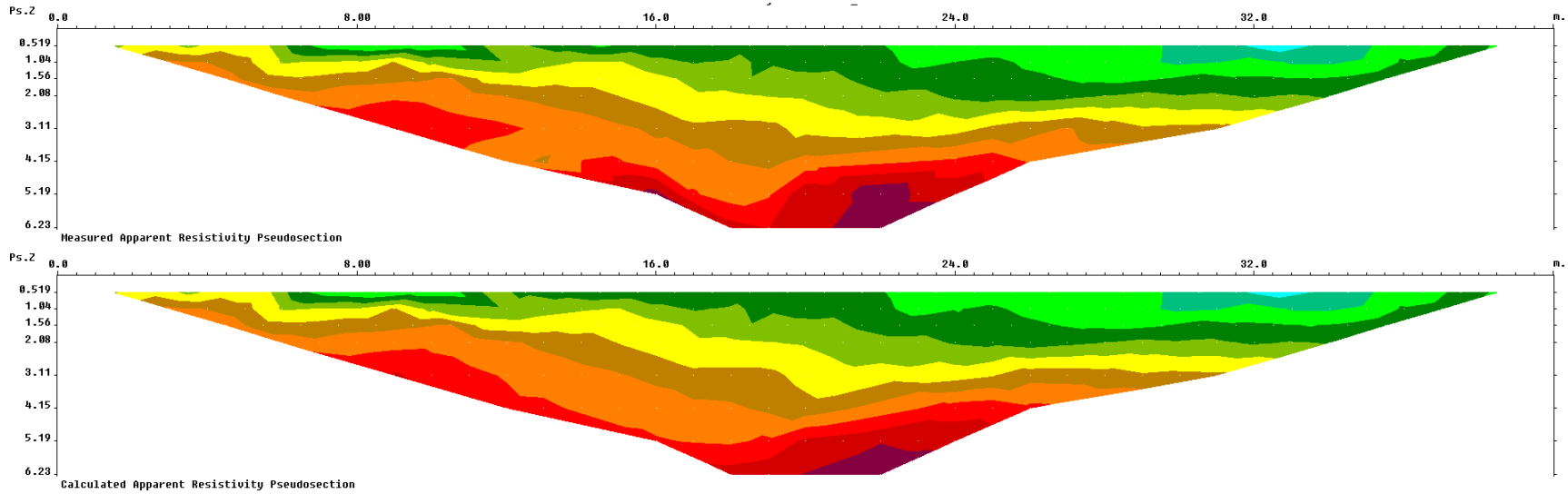

Figure E3 - Measured and calculated apparent resistivity for the March 2011 survey at MP 286.0

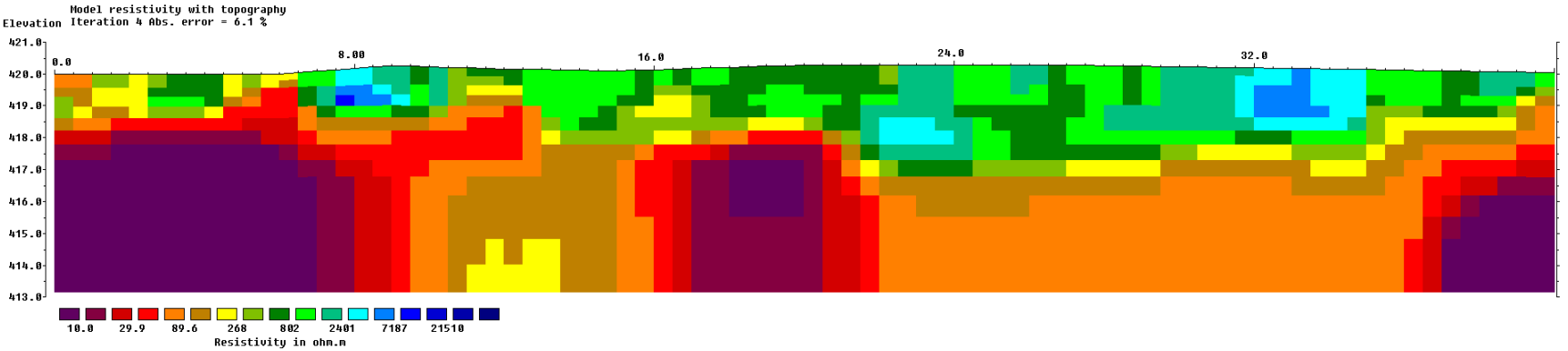

Figure E4 - Model resistivity with topography for the March 2011 survey for MP 286.0

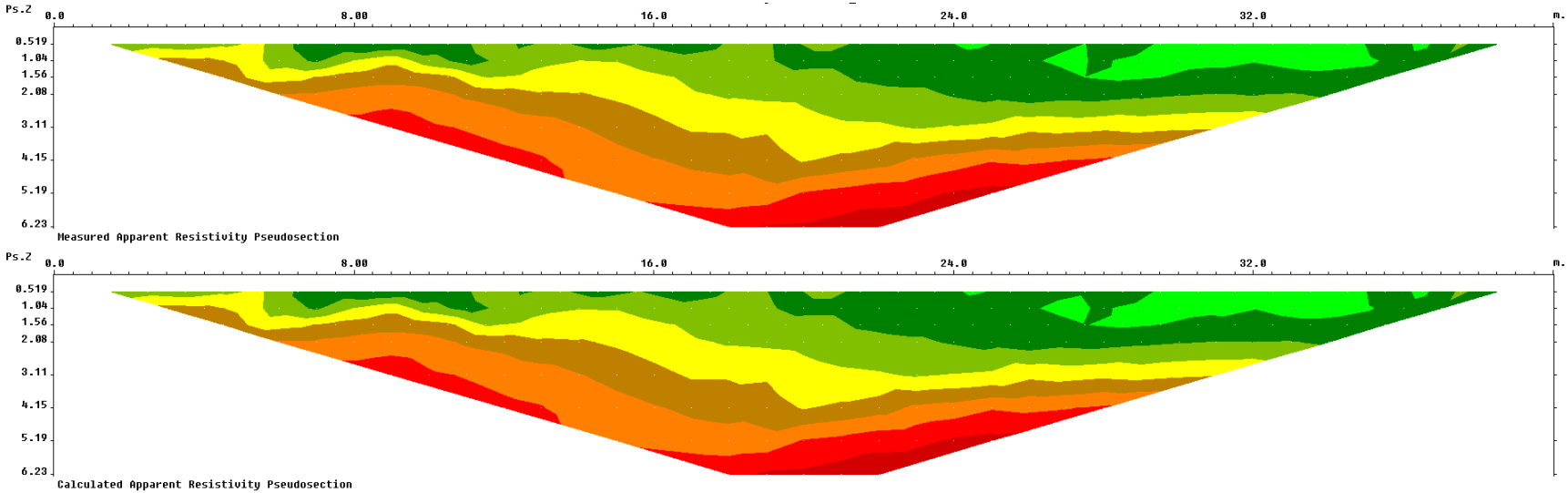

Figure E5 - Measured and calculated apparent resistivity for the May 2011 survey at MP 286.0

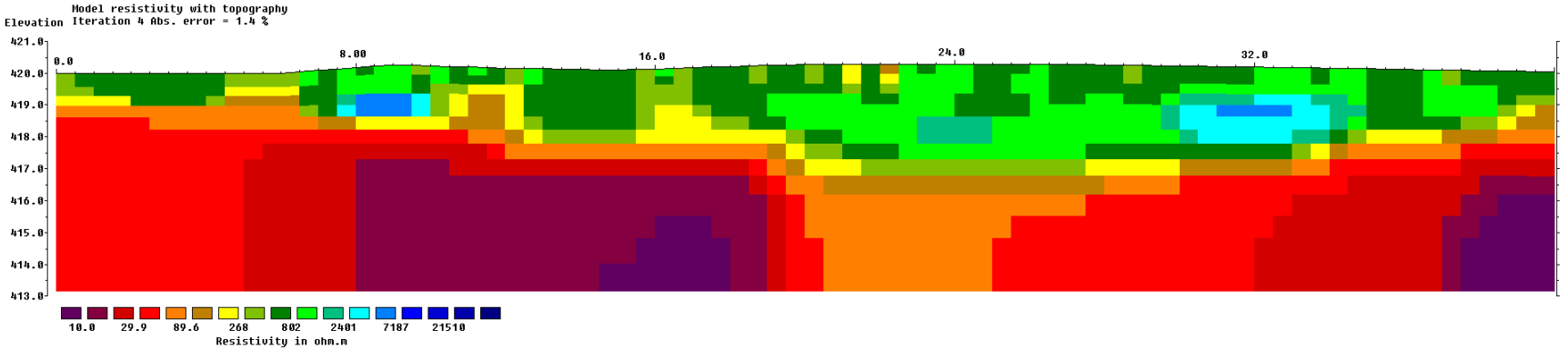

Figure E6 - Model resistivity with topography for the May 2011 survey for MP 286.0

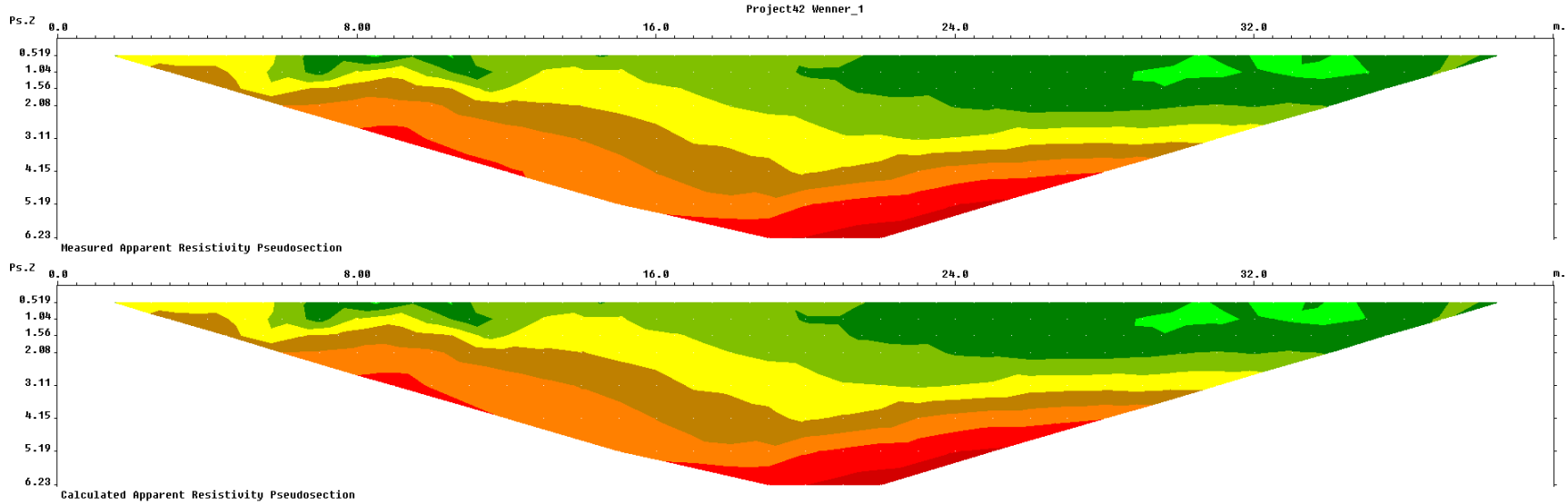

Figure E7 - Measured and calculated apparent resistivity for the July 2011 survey at MP 286.0.

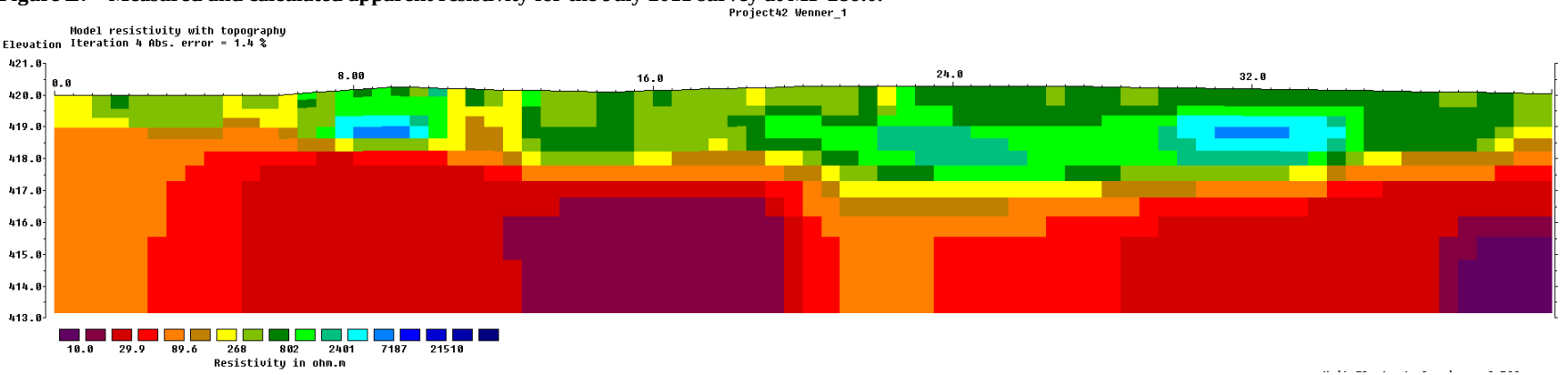

Figure E8 - Model resistivity with topography for the July 2011 survey for MP 286.0.

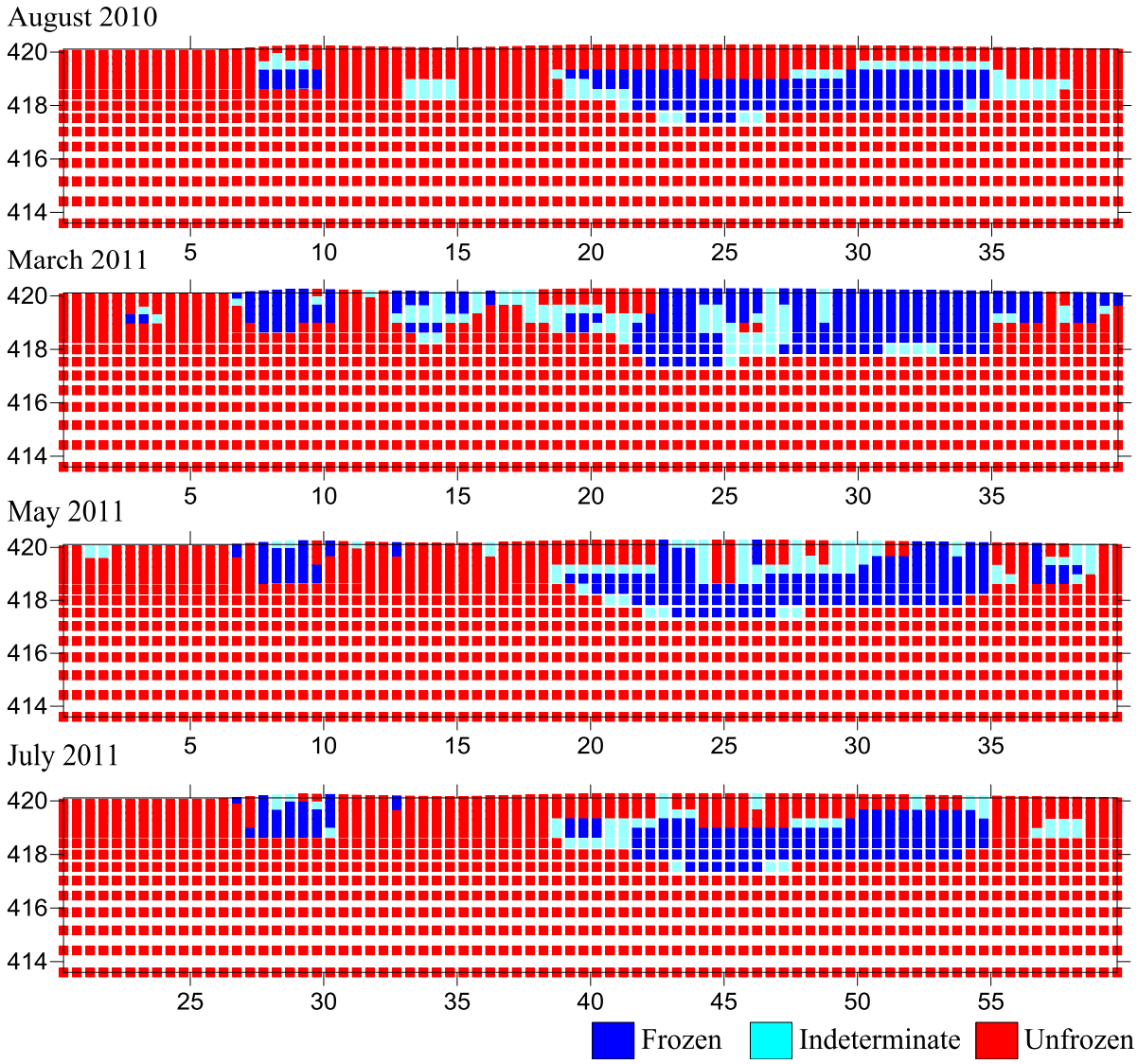

Figure E 9 - Permafrost classification images for the surveys conducted at MP 286.0. Note the incorrect profile length along the x-axis for the July 2011 survey.

APPENDIX F

MP 341.3

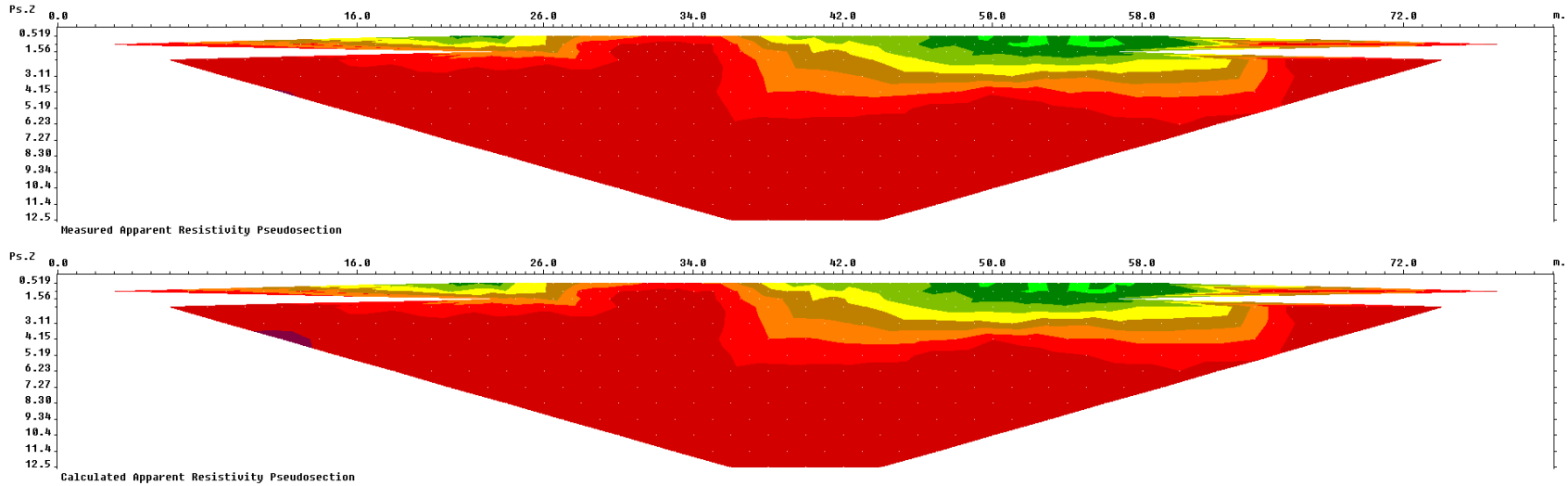

Figure F1 - Measured and calculated apparent resistivity for the August 2010 survey at MP 341.3

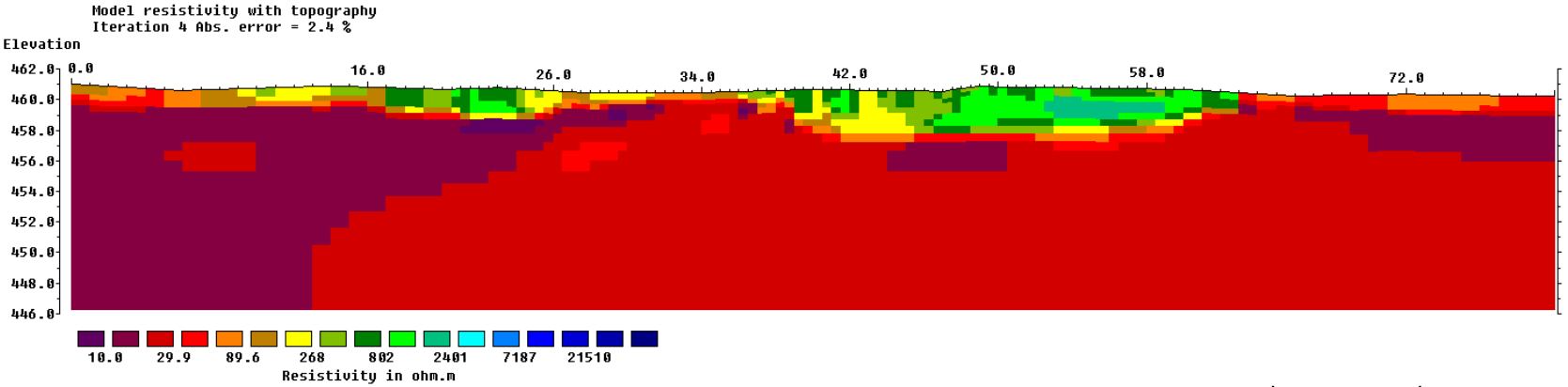

Figure F2 - Model resistivity with topography for the August 2010 survey for MP 341.3

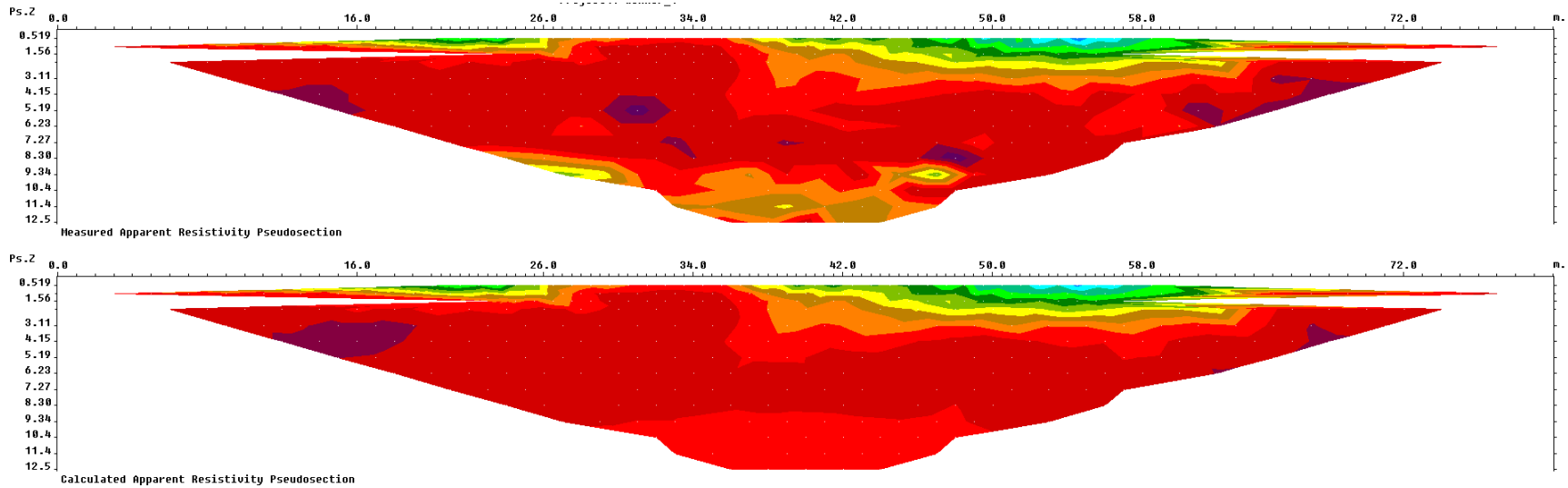

Figure F3 - Measured and calculated apparent resistivity for the March 2011 survey at MP 341.3

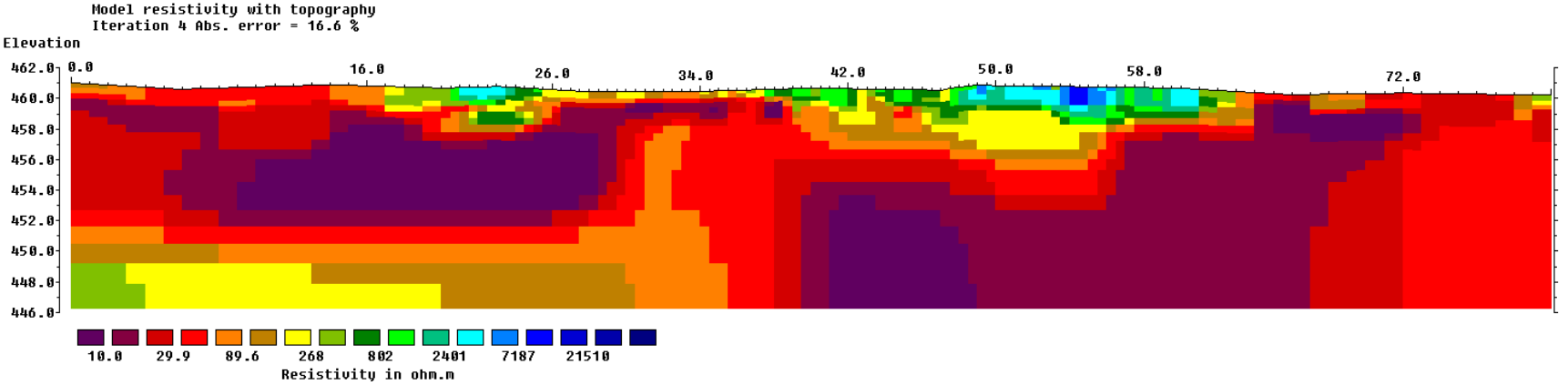

Figure F4 – Model resistivity with topography for the March 2011 survey for MP 341.3

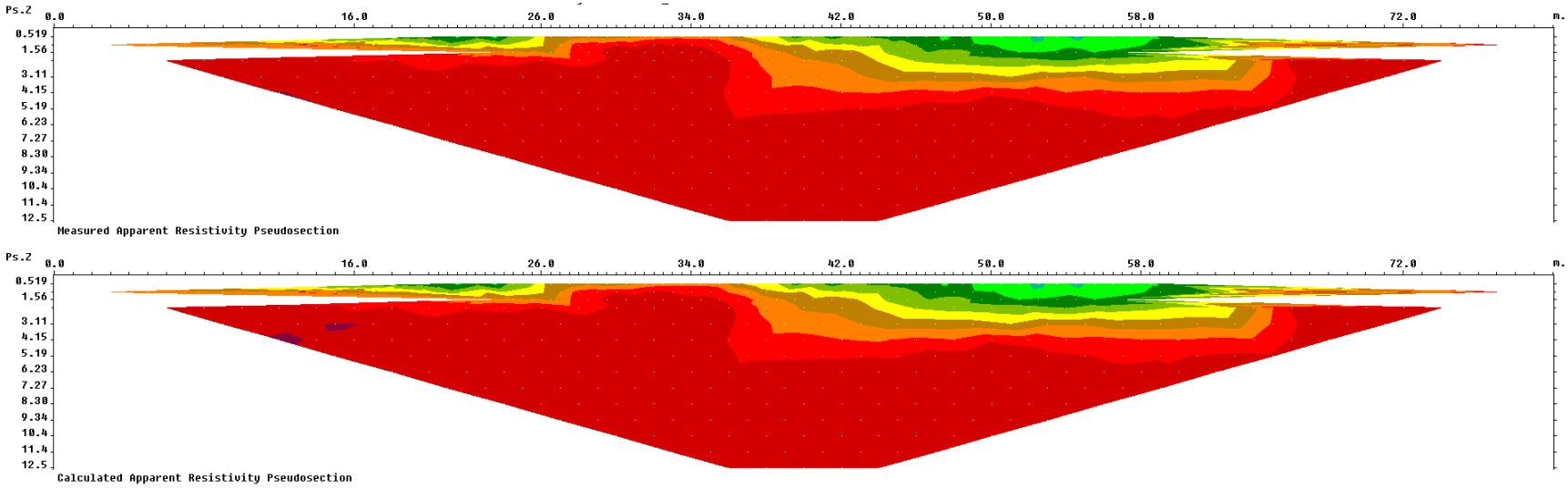

Figure F5 - Measured and calculated apparent resistivity for the May 2011 survey at MP 341.3

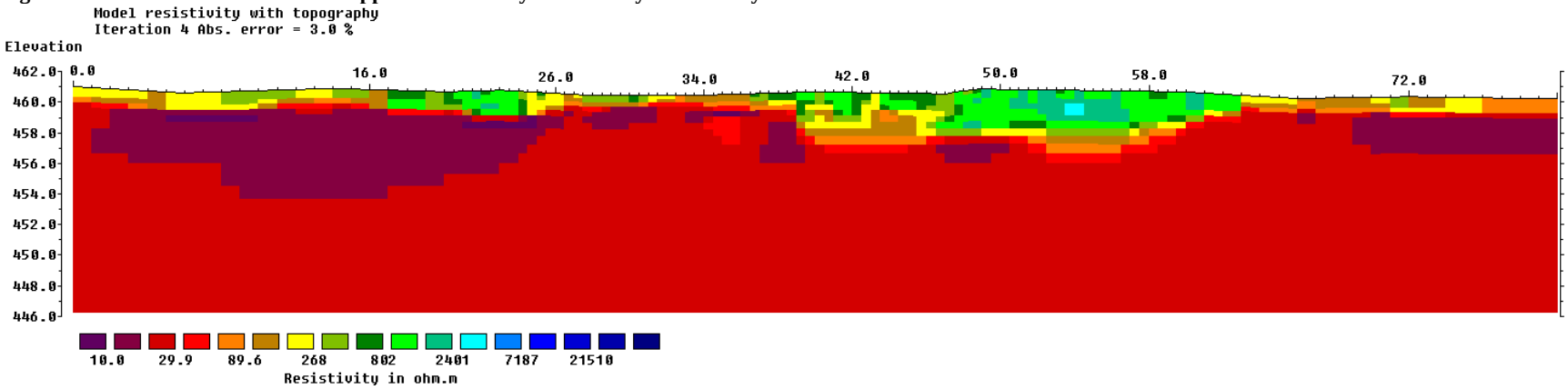

Figure F6 – Model resistivity with topography for the May 2011 survey for MP 341.3

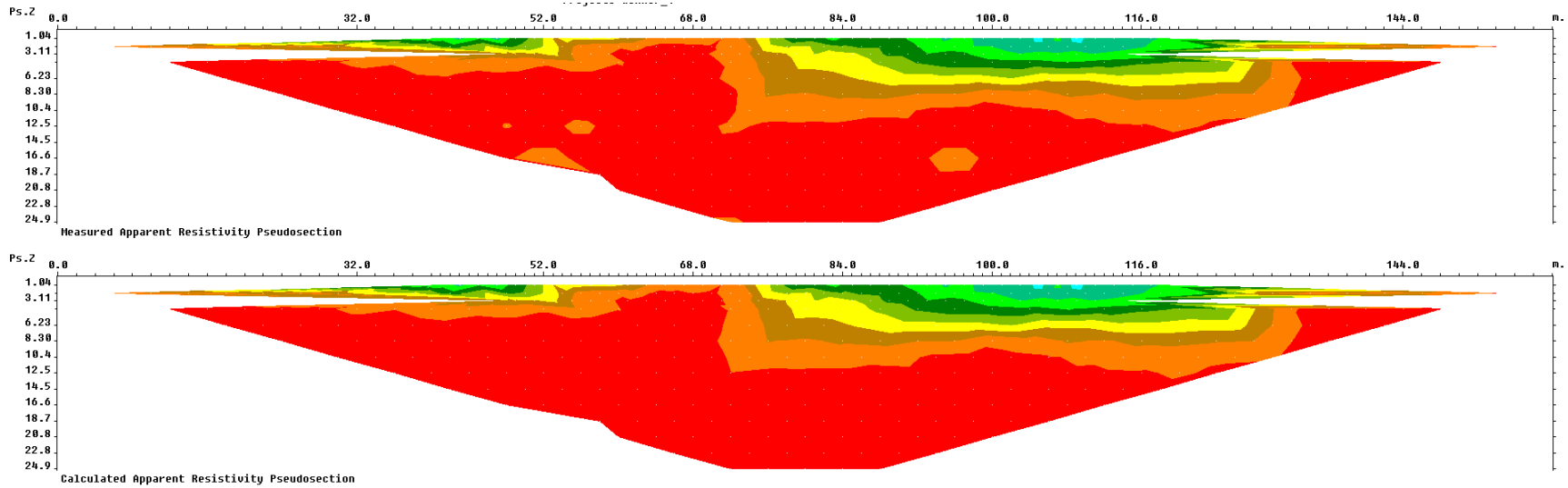

Figure F7 - Measured and calculated apparent resistivity for the June 2011 survey at MP 341.3

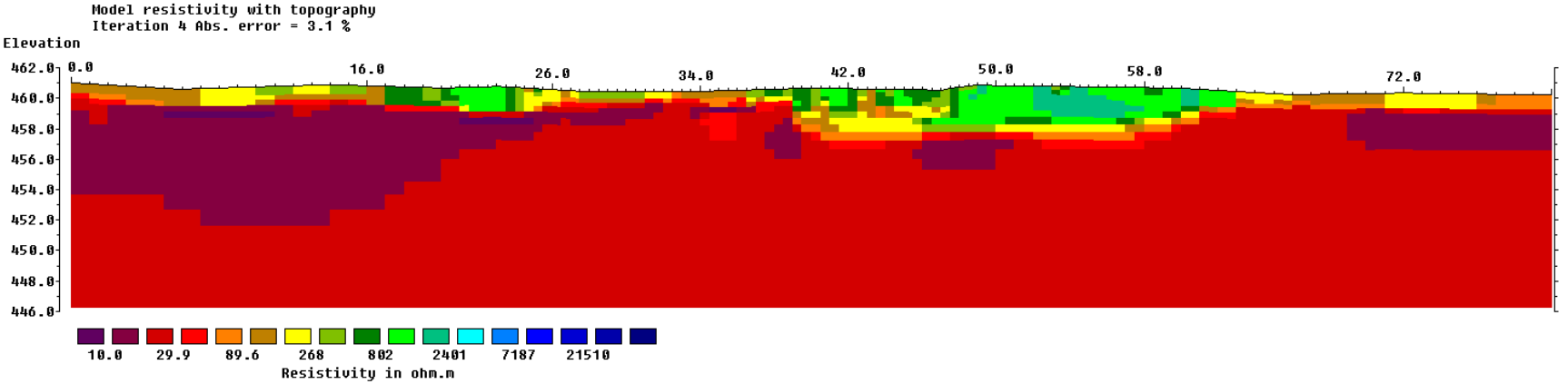

Figure F8 - Model resistivity with topography for the June 2011 survey for MP 341.3

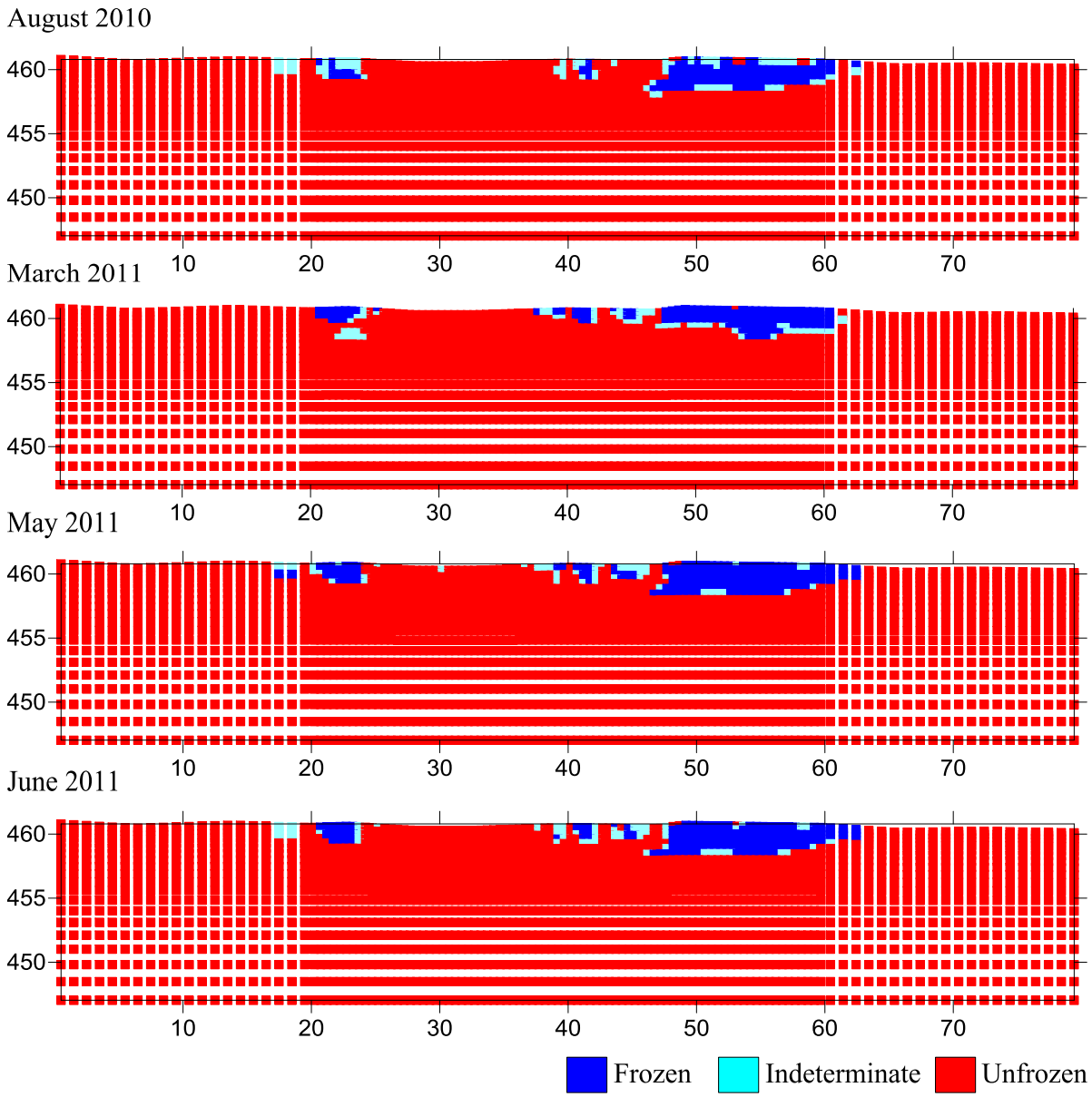

Figure F9 - Permafrost classification images for the surveys conducted at MP 341.3

APPENDIX G

MP 400.5

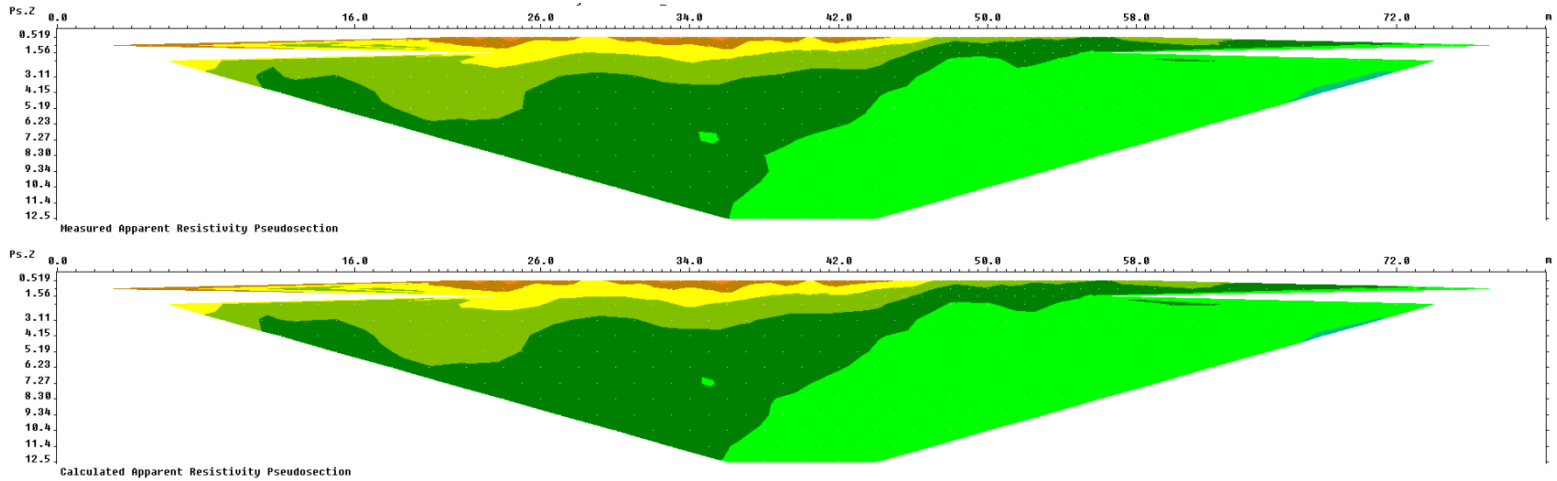

Figure G1 - Measured and calculated apparent resistivity for the August 2010 survey at MP 400.5

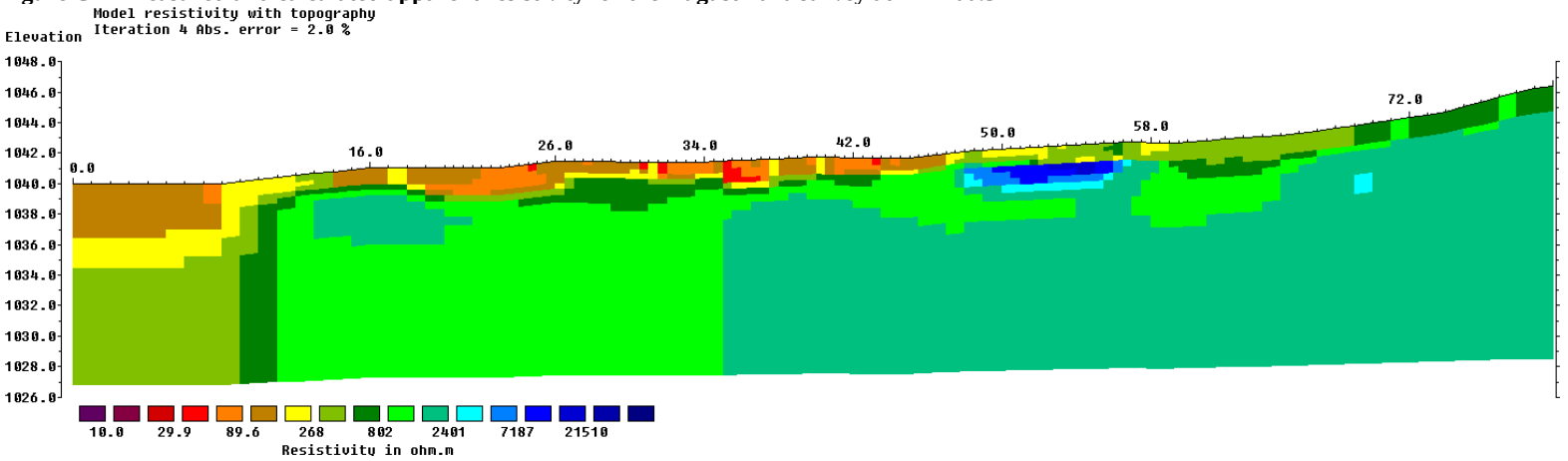

Figure G2 - Model resistivity with topography for the August 2010 survey for MP 400.5

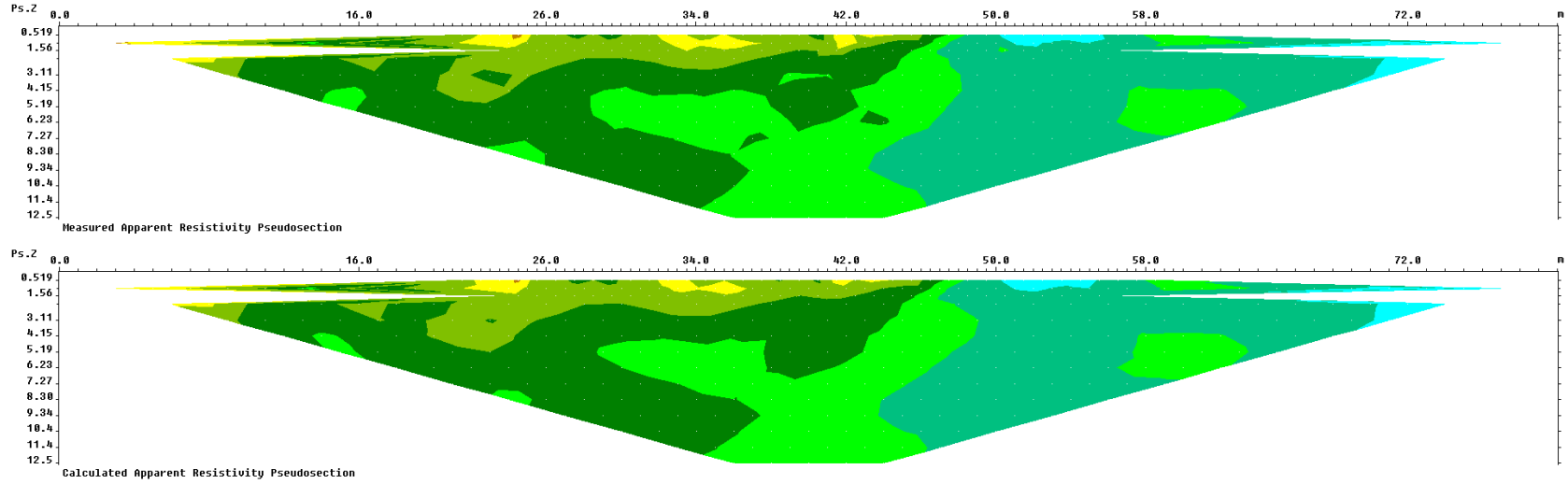

Figure G3 - Measured and calculated apparent resistivity for the March 2011 survey at MP 400.5

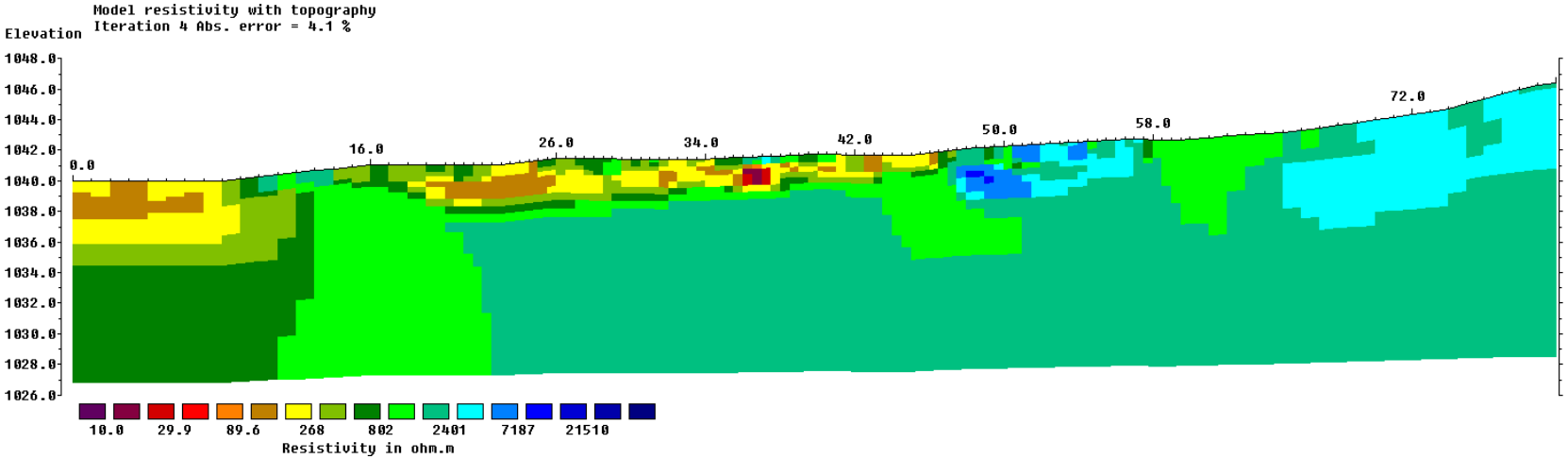

Figure G4 - Model resistivity with topography for the March 2011 survey for MP 400.5

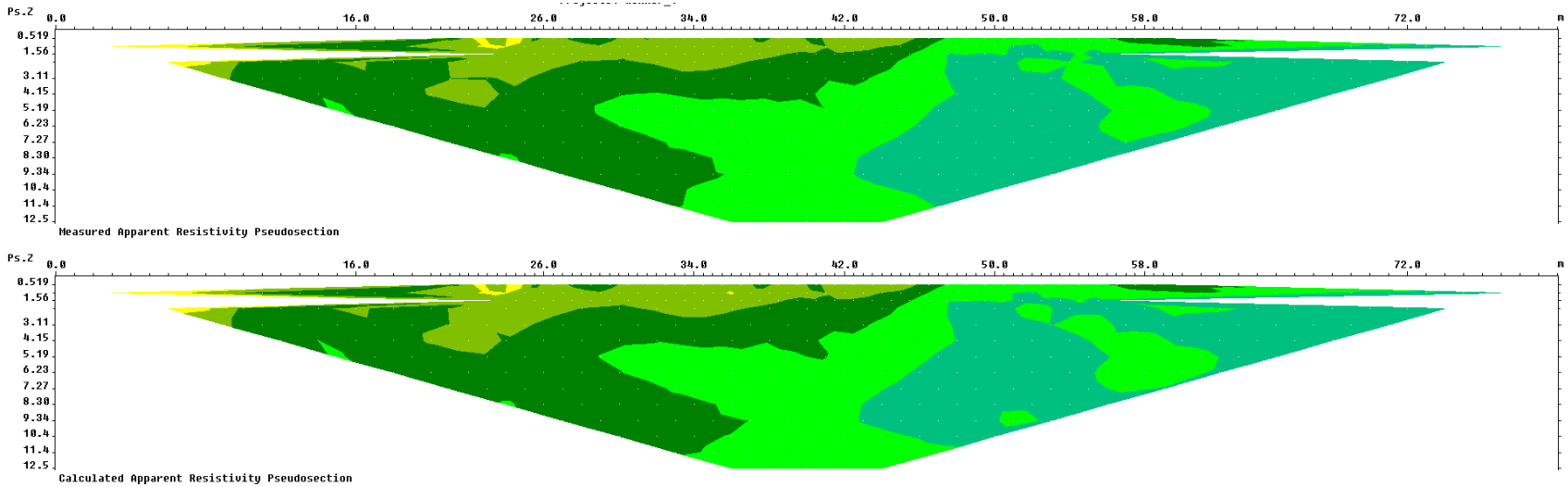

Figure G5 - Measured and calculated apparent resistivity for the May 2011 survey at MP 400.5

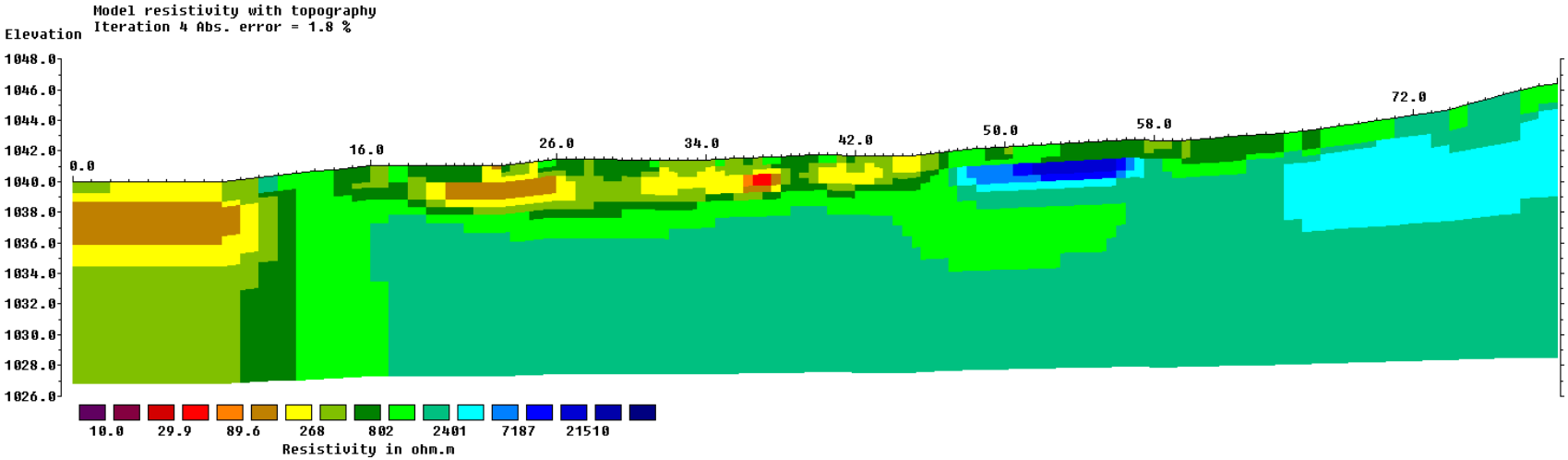

Figure G6 - Model resistivity with topography for the May 2011 survey for MP 400.5

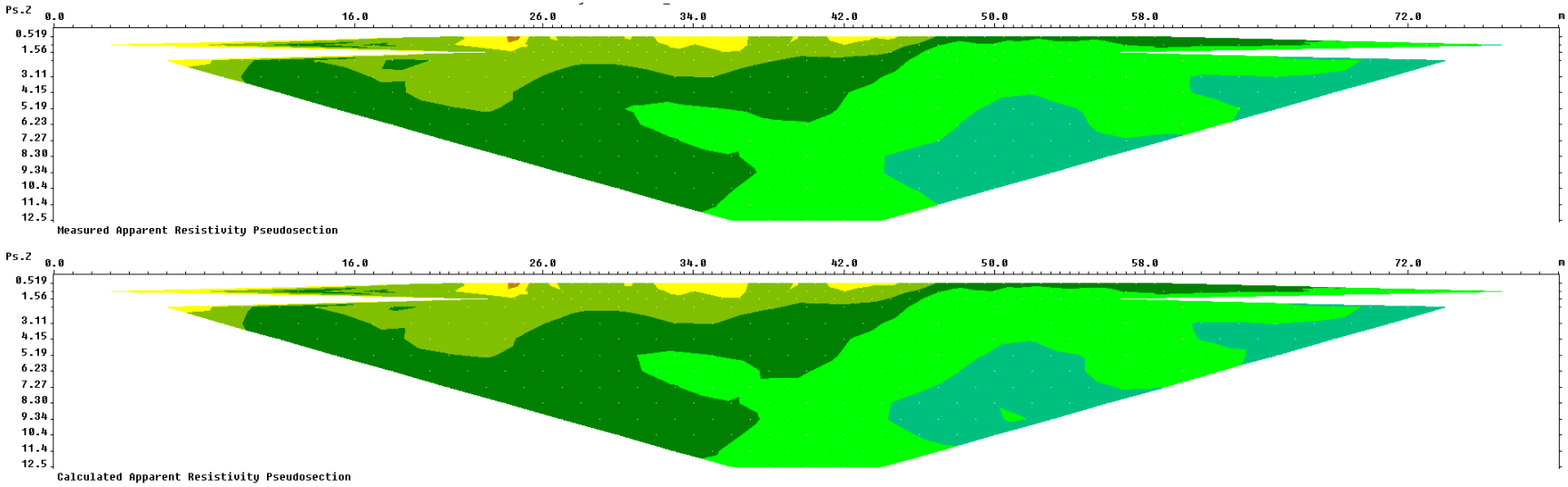

Figure G7 - Measured and calculated apparent resistivity for the June 2011 survey at MP 400.5

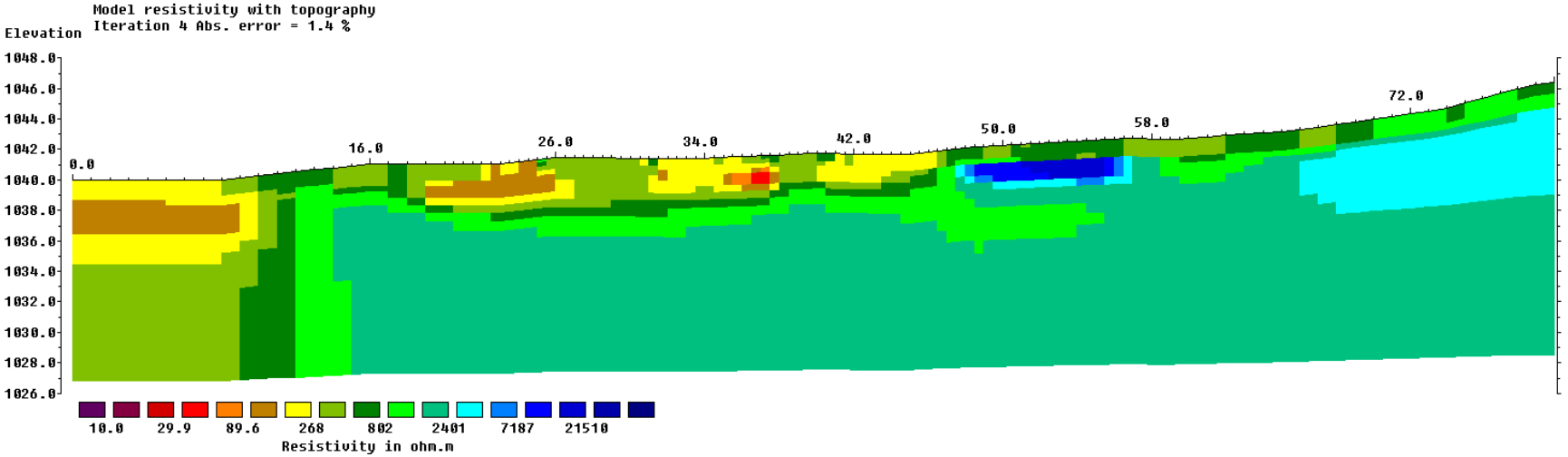

Figure G8 - Model resistivity with topography for the June 2011 survey for MP 400.5

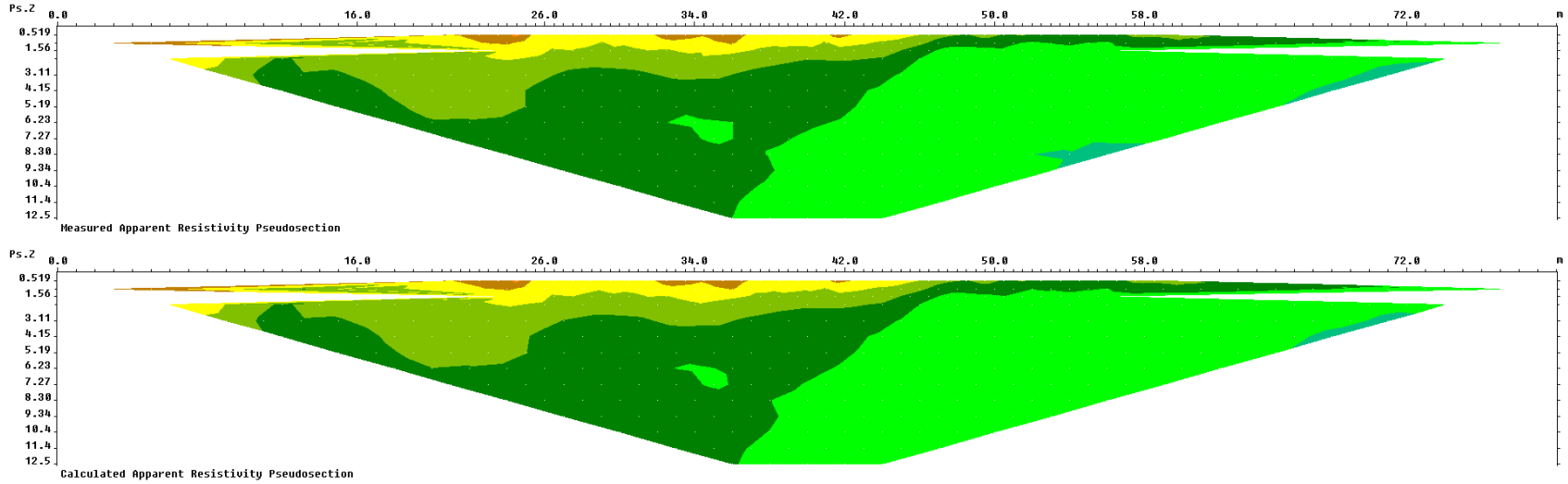

Figure G9 - Measured and calculated apparent resistivity for the July 2011 survey at MP 400.5

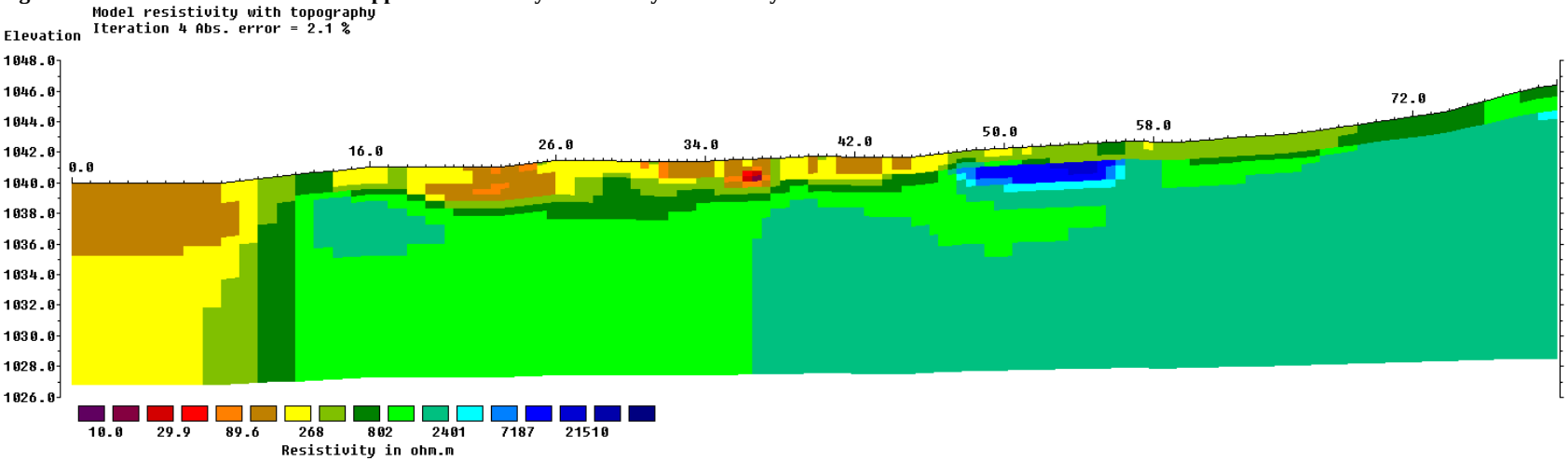

Figure G10 - Model resistivity with topography for the July 2011 survey for MP 400.5

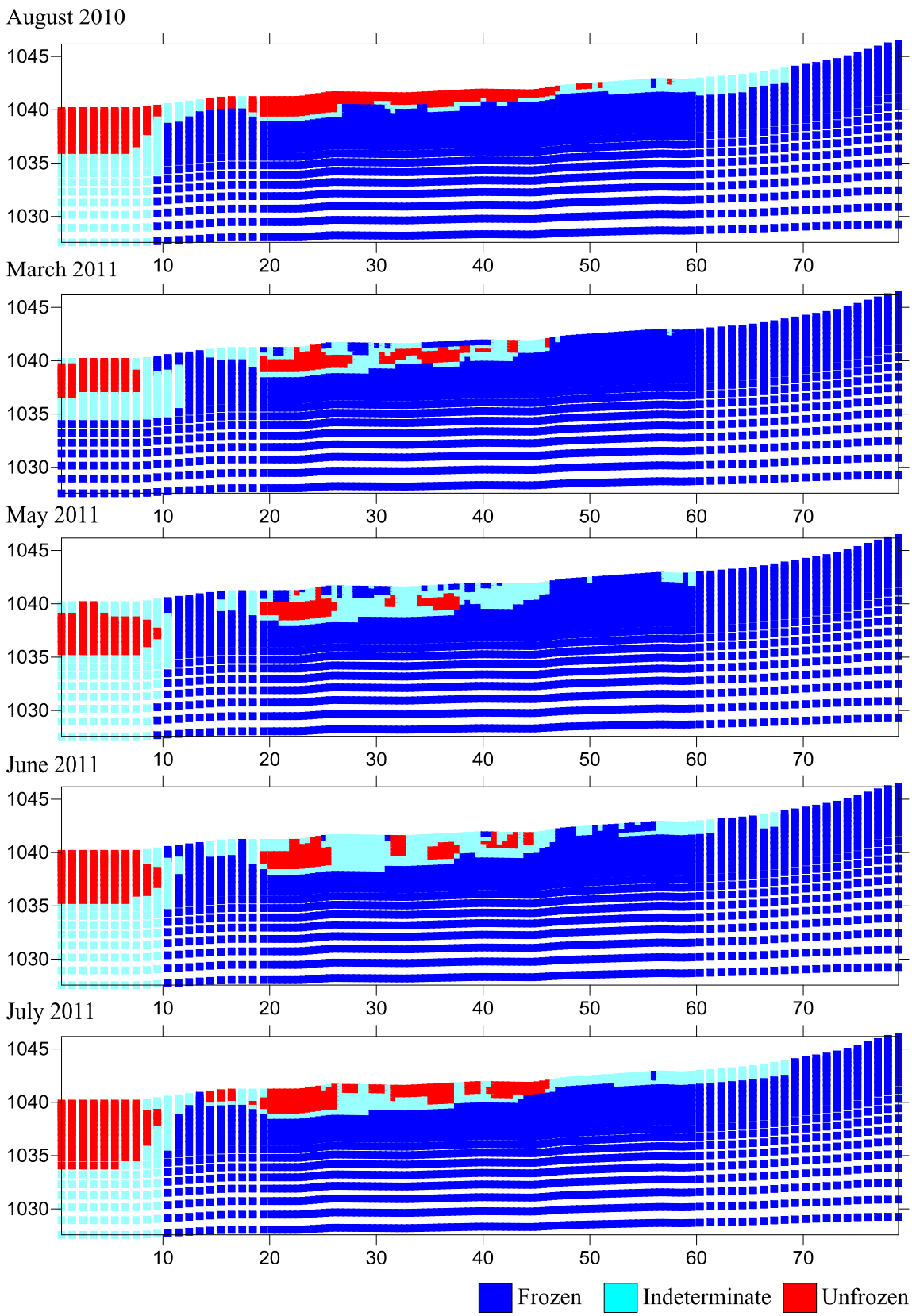

Figure G11 - Permafrost classification images for the surveys conducted at MP 400.5

APPENDIX H

MP 579.1

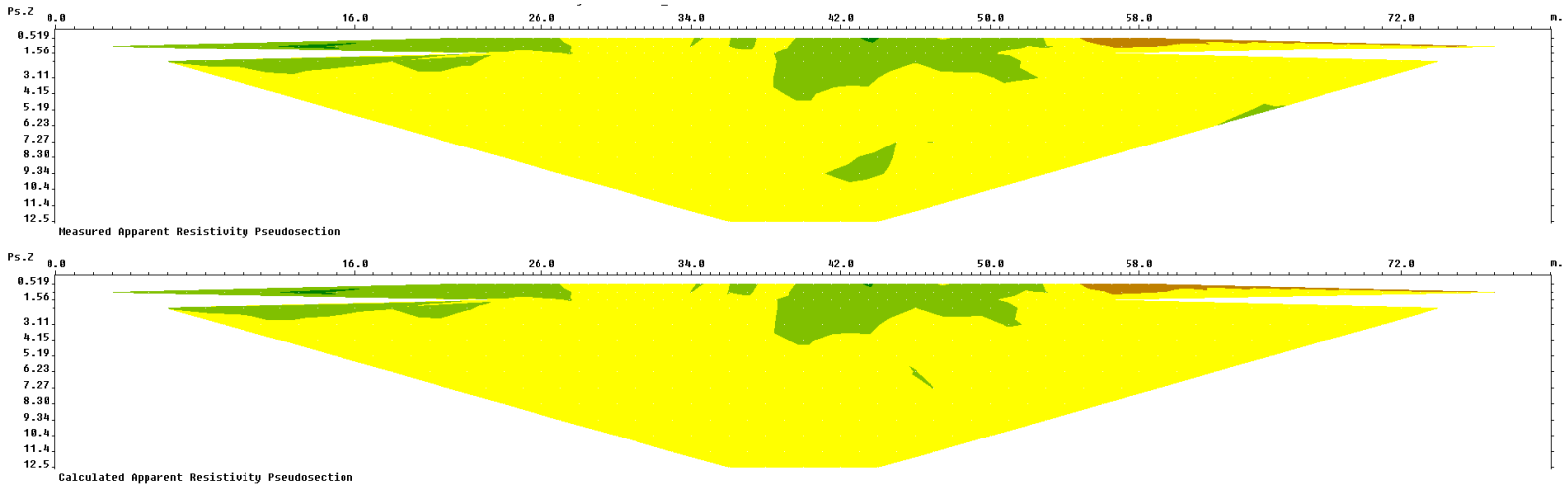

Figure H1 - Measured and calculated apparent resistivity for the August 2010 survey at MP 579.1

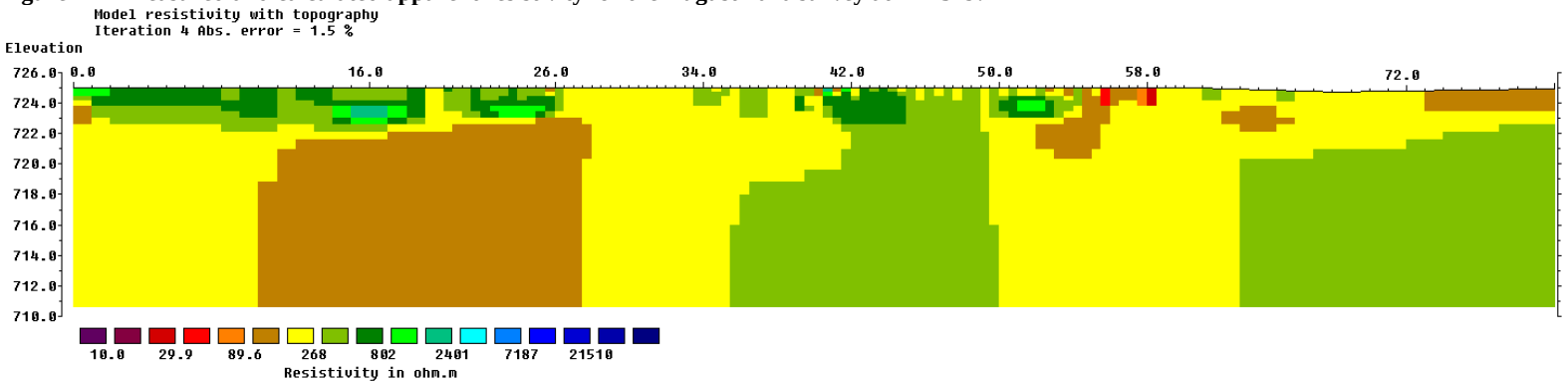

Figure H2 - Model resistivity with topography for the August 2010 survey for MP 579.1

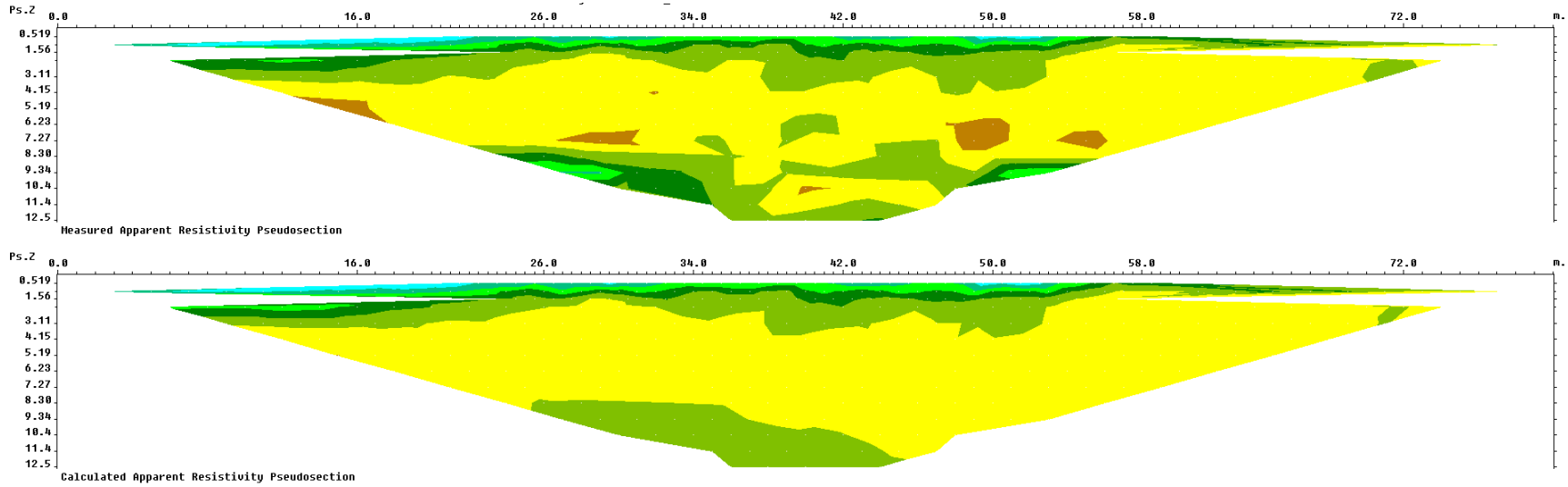

Figure H3 - Measured and calculated apparent resistivity for the March 2011 survey at MP 579.1

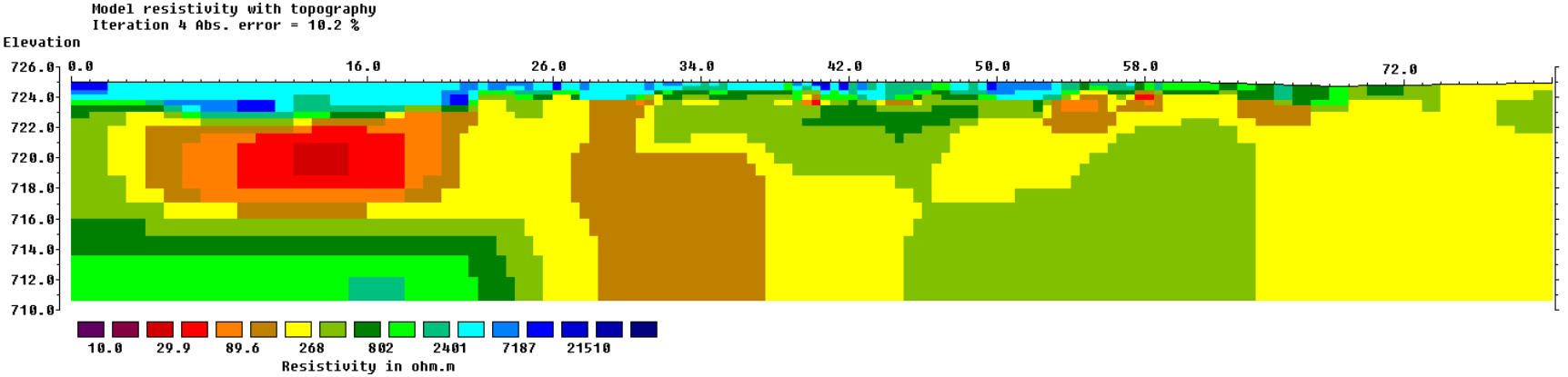

Figure H4 - Model resistivity with topography for the March 2011 survey for MP 579.1

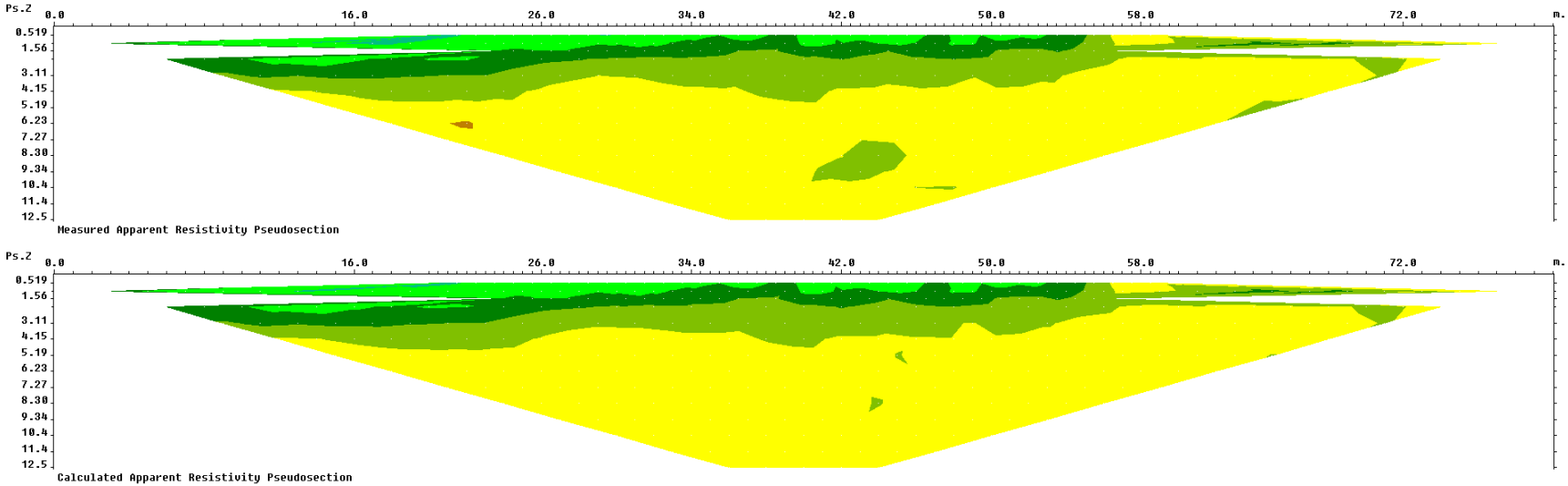

Figure H5 - Measured and calculated apparent resistivity for the May 2011 survey at MP 579.1

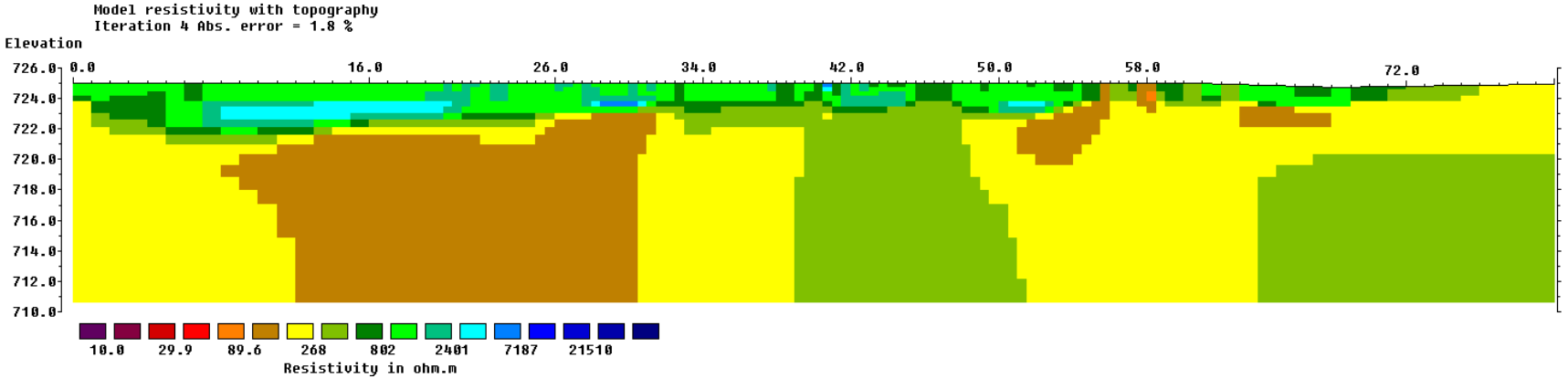

Figure H6 - Model resistivity with topography for the May 2011 survey for MP 579.1

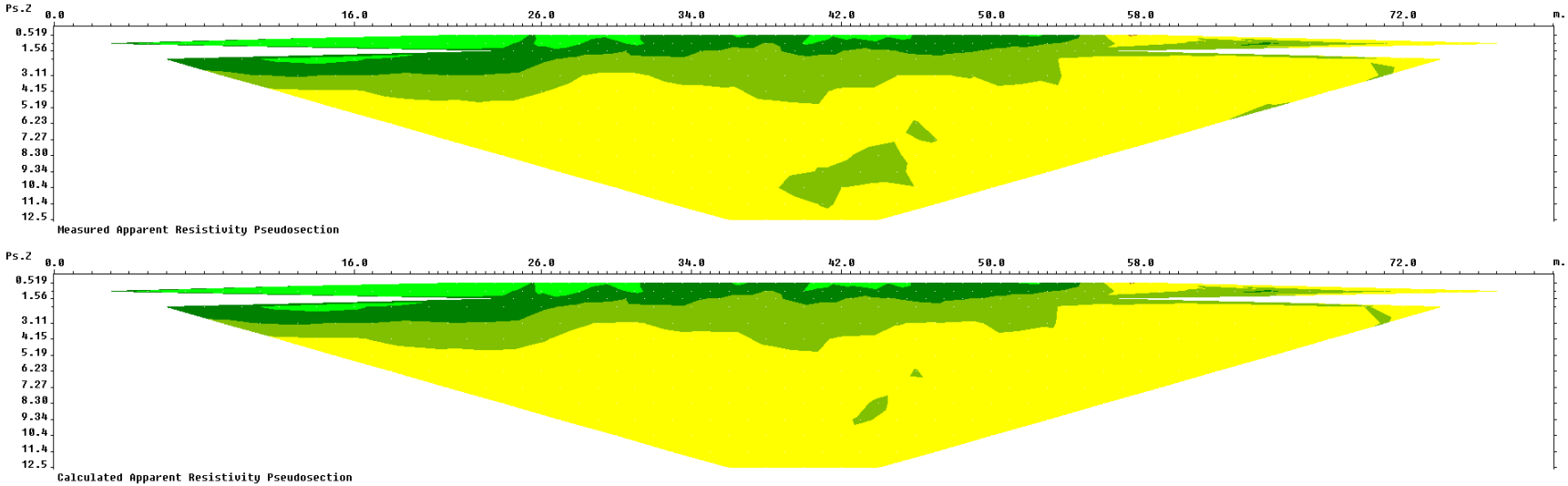

Figure H7 - Measured and calculated apparent resistivity for the June 2011 survey at MP 579.1

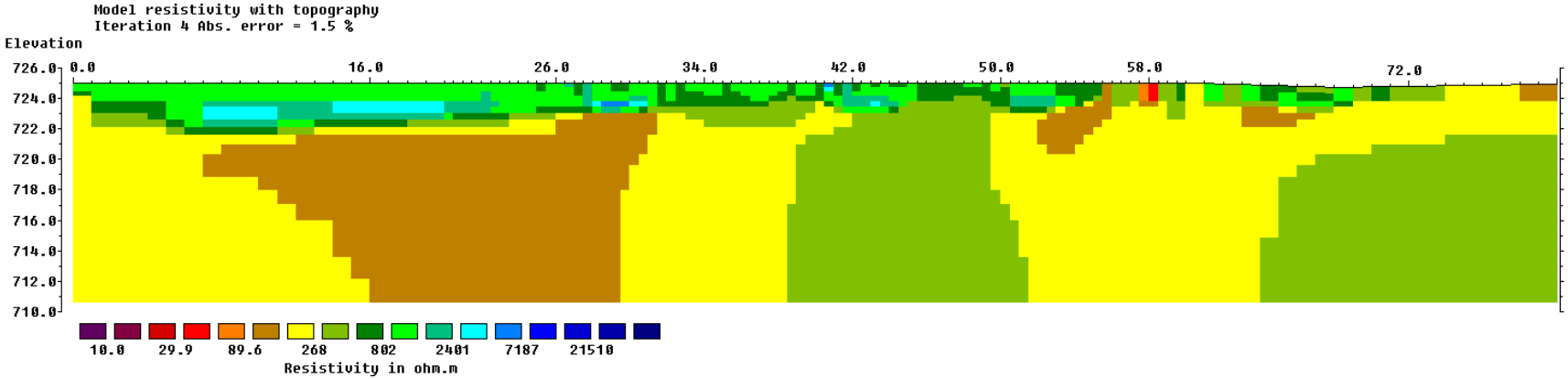

Figure H8 - Model resistivity with topography for the June 2011 survey for MP 579.1

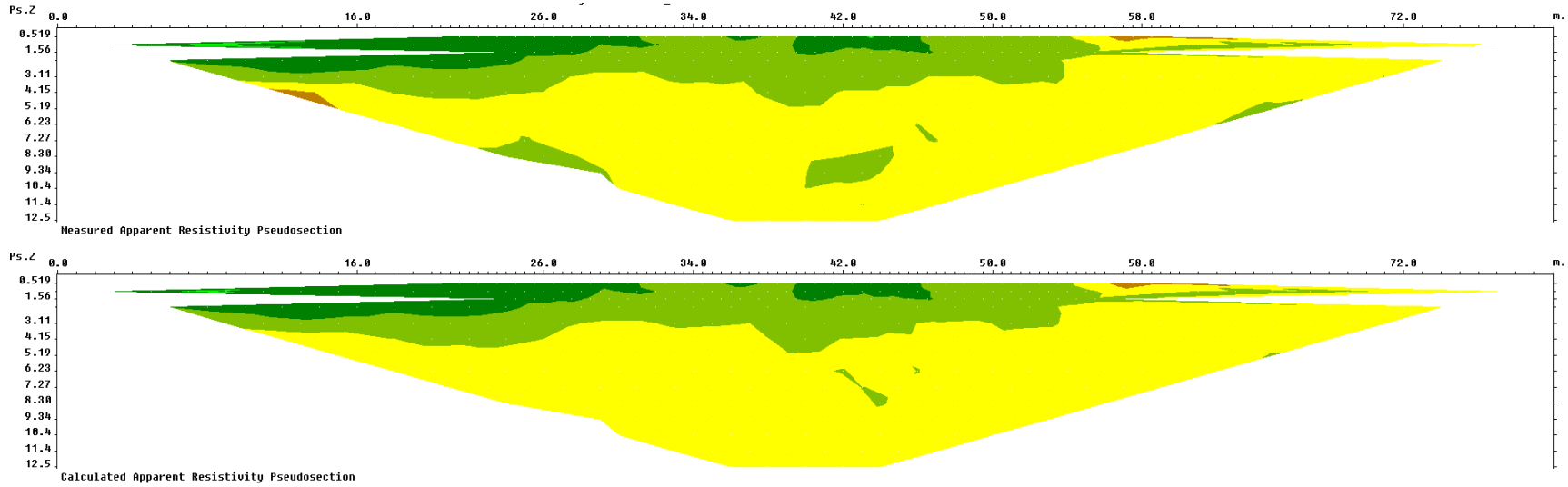

Figure H9 - Measured and calculated apparent resistivity for the July 2011 survey at MP 579.1

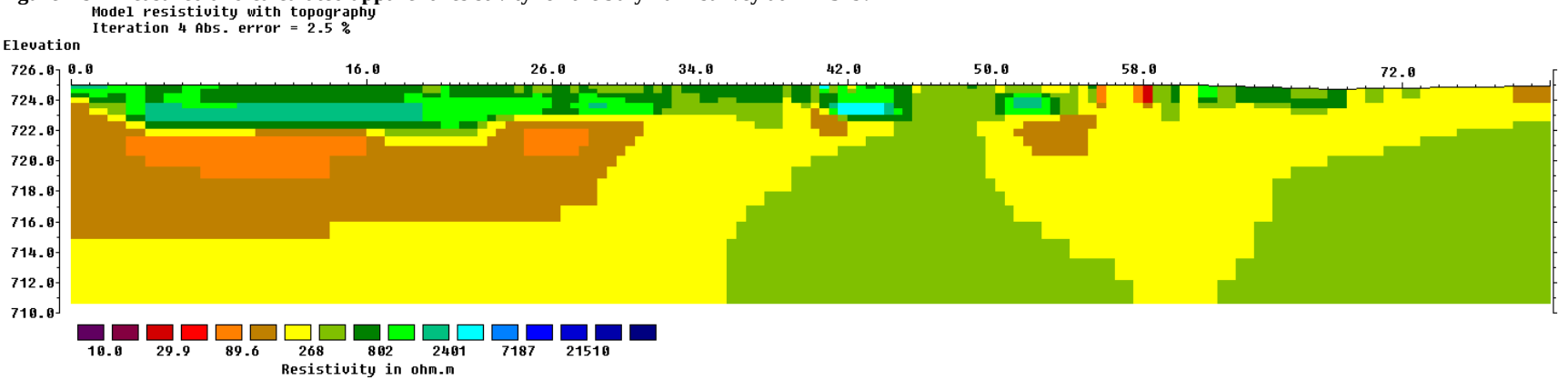

Figure H10 - Model resistivity with topography for the July 2011 survey for MP 579.1

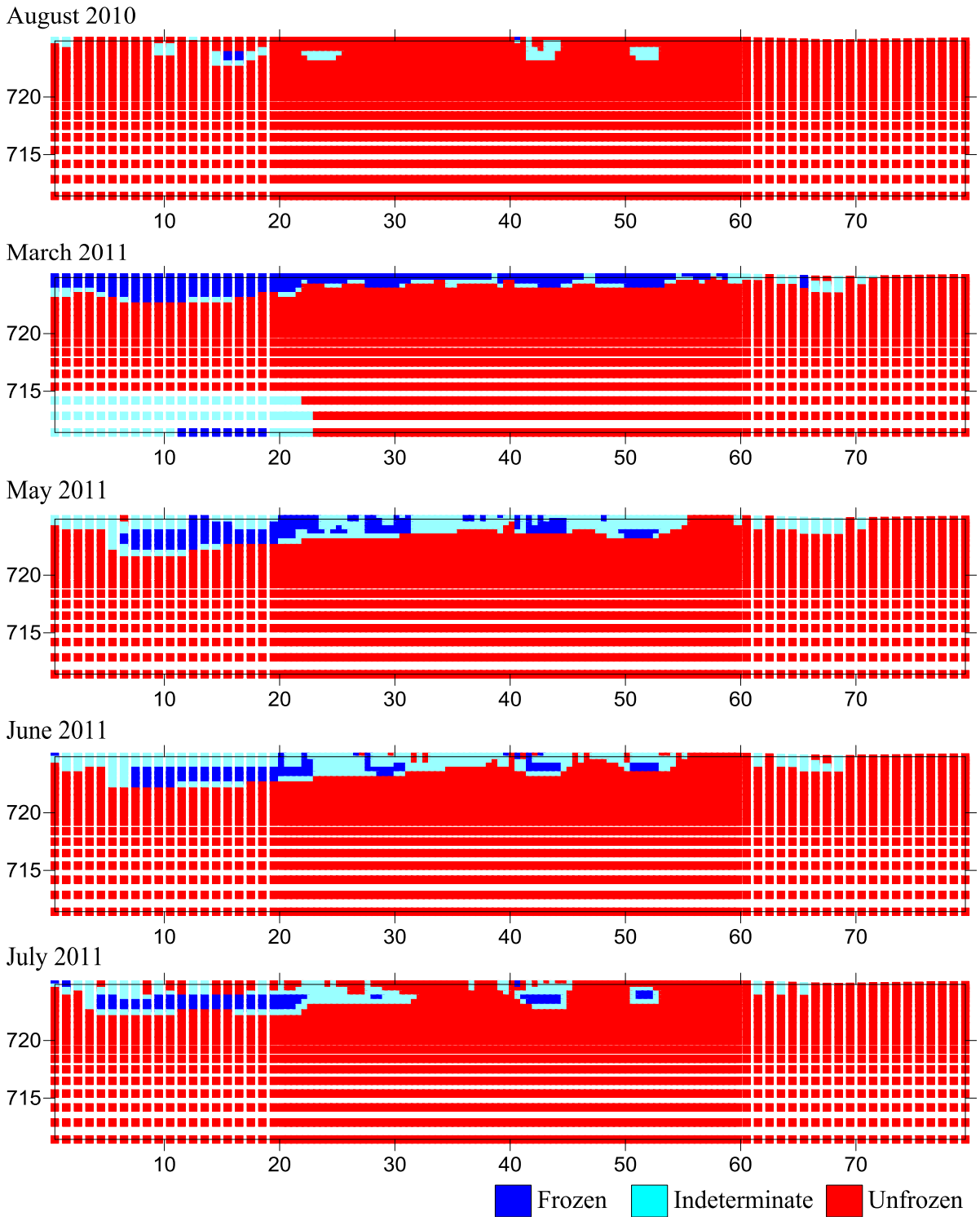

Figure H11 - Permafrost classification images for the surveys conducted at MP 579.1

APPENDIX I

MP 597.5

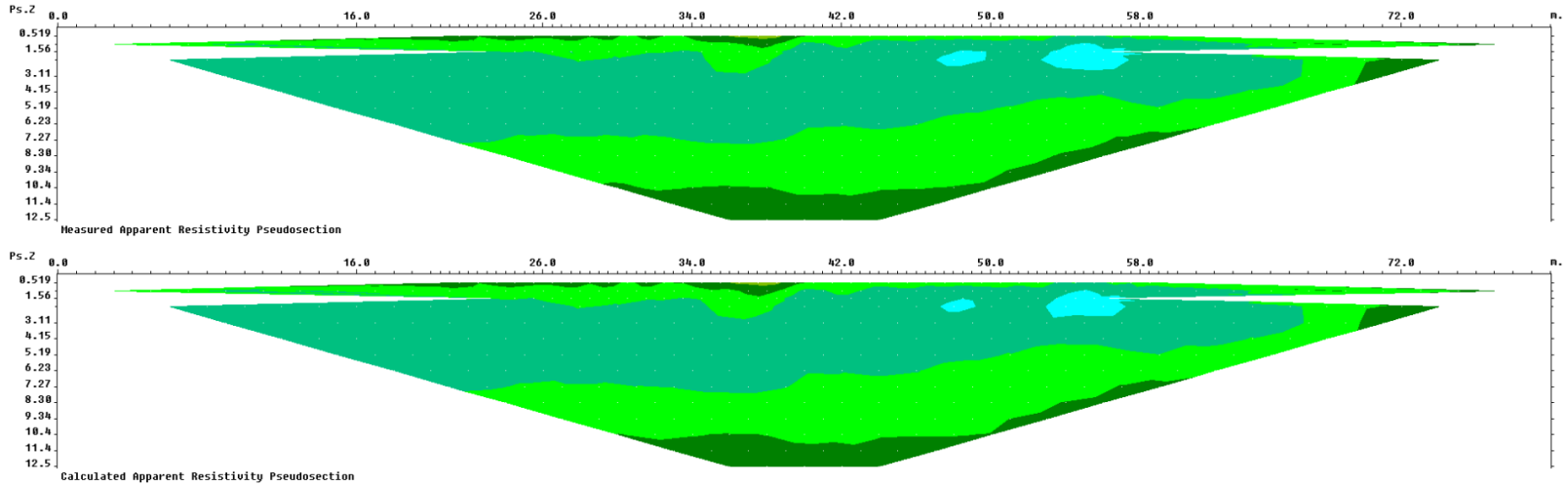

Figure I1 - Measured and calculated apparent resistivity for the August 2010 survey at MP 597.5

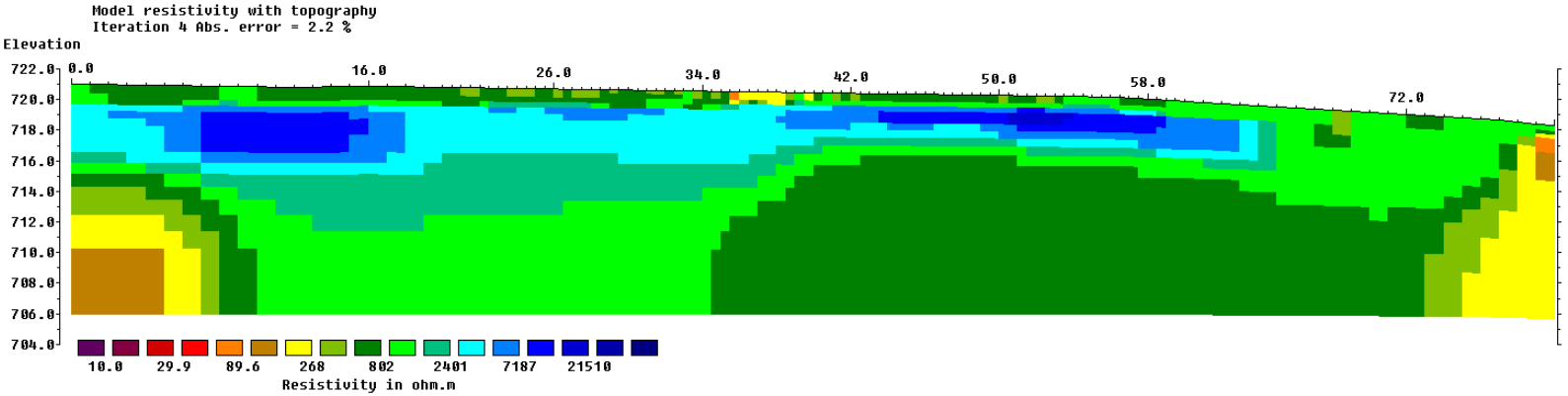

Figure I2 - Model resistivity with topography for the August 2010 survey for MP 597.5

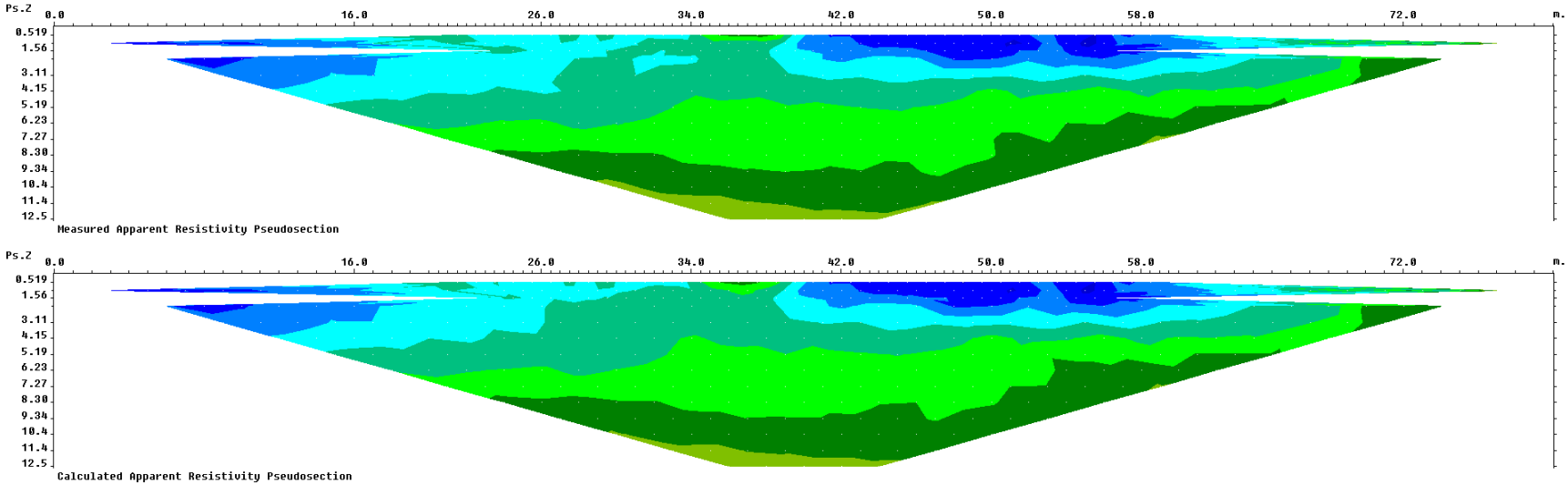

Figure I3 - Measured and calculated apparent resistivity for the March 2011 survey at MP 597.5

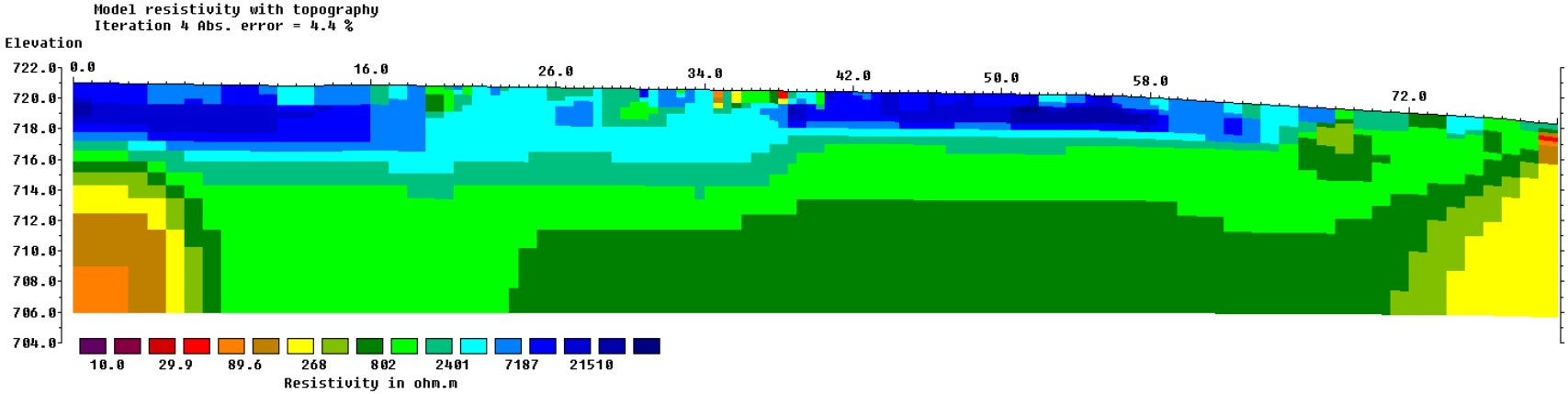

Figure I4 - Model resistivity with topography for the March 2011 survey for MP 597.5

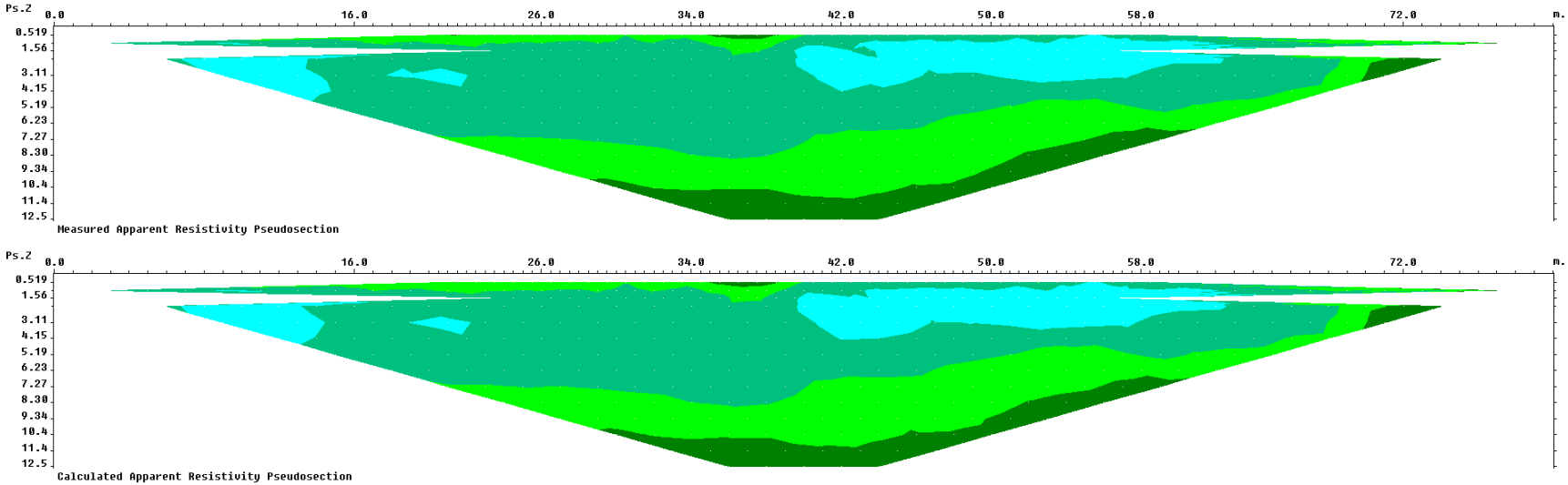

Figure I5 - Measured and calculated apparent resistivity for the May 2011 survey at MP 597.5

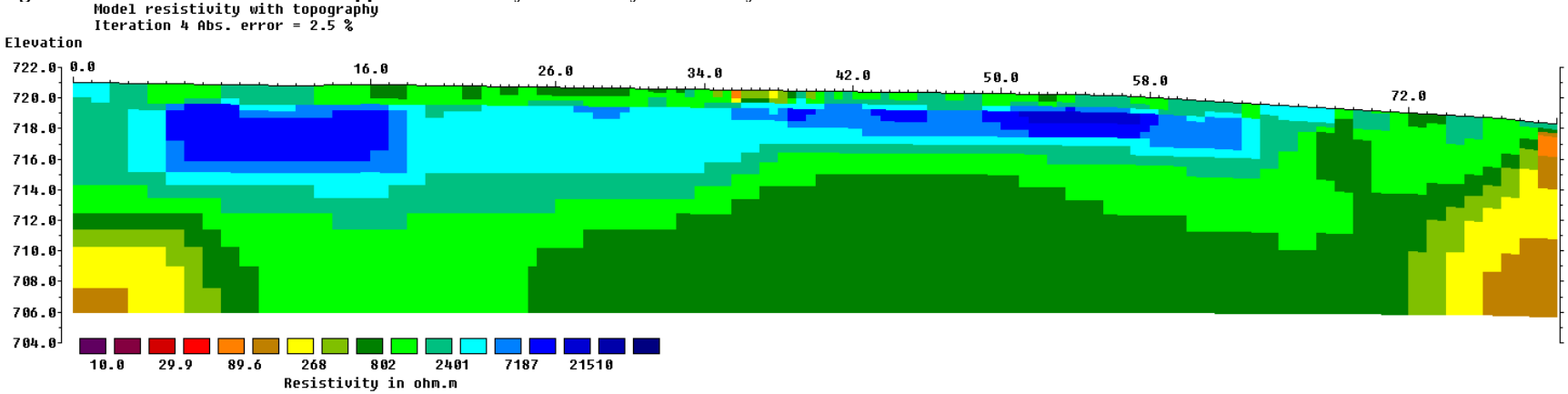

Figure I6 - Model resistivity with topography for the May 2011 survey for MP 597.5

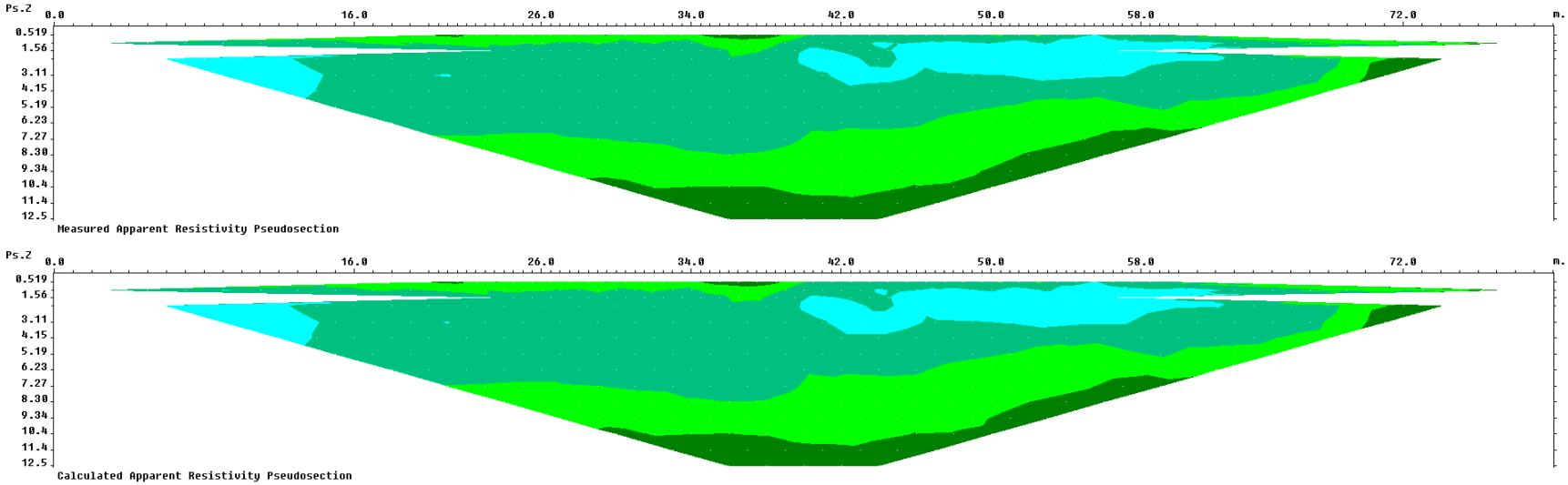

Figure I7 - Measured and calculated apparent resistivity for the June 2011 survey at MP 597.5

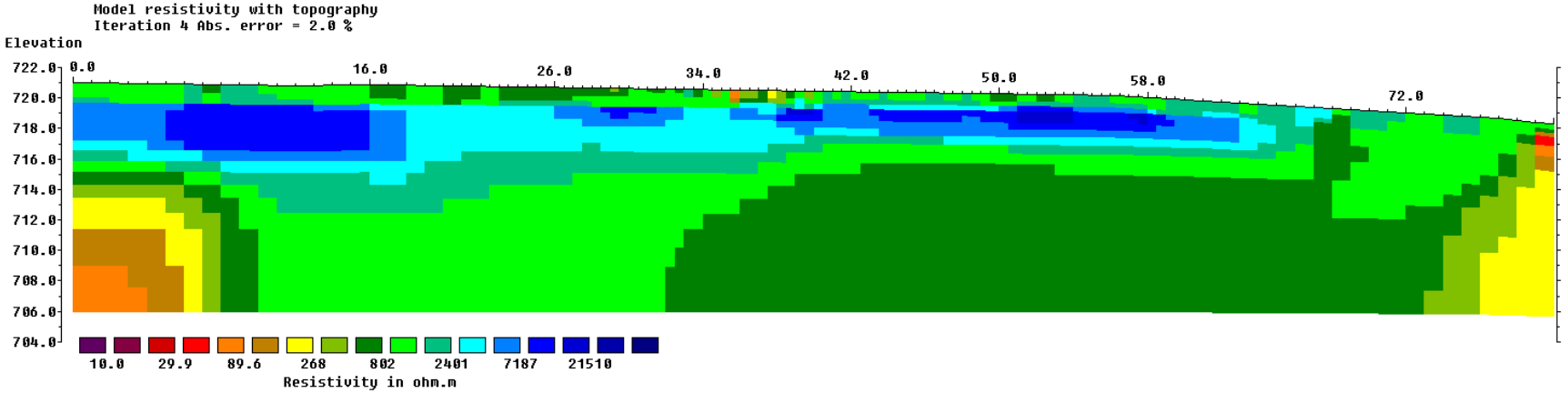

Figure I8 - Model resistivity with topography for the June 2011 survey for MP 597.5

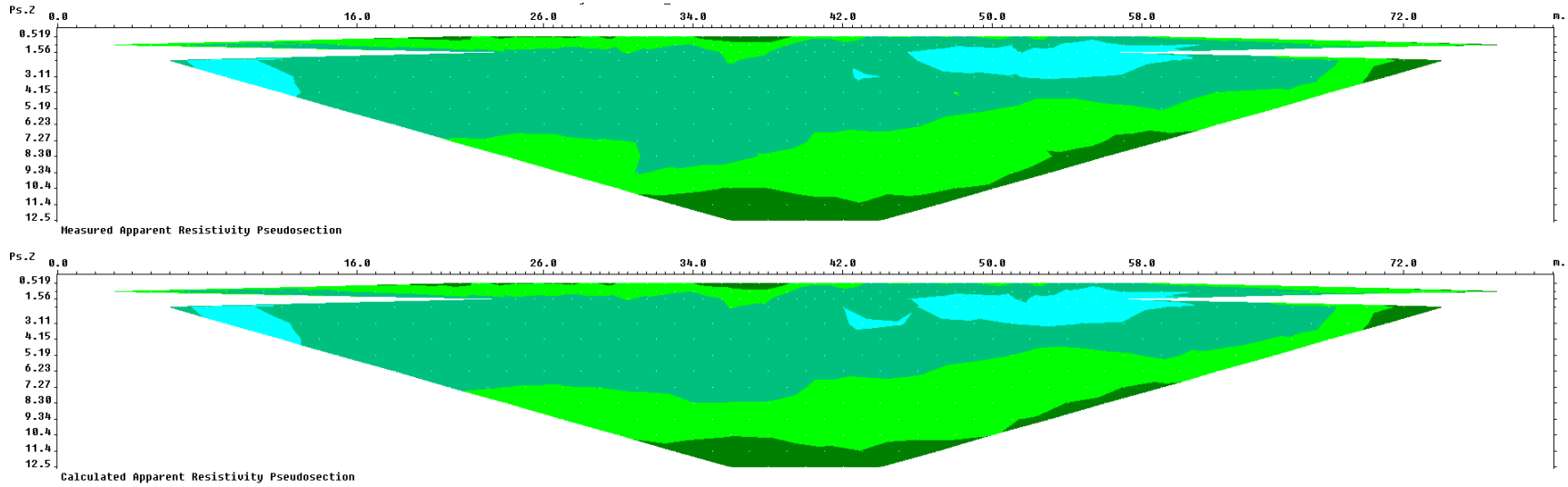

Figure I9 - Measured and calculated apparent resistivity for the July 2011 survey at MP 597.5

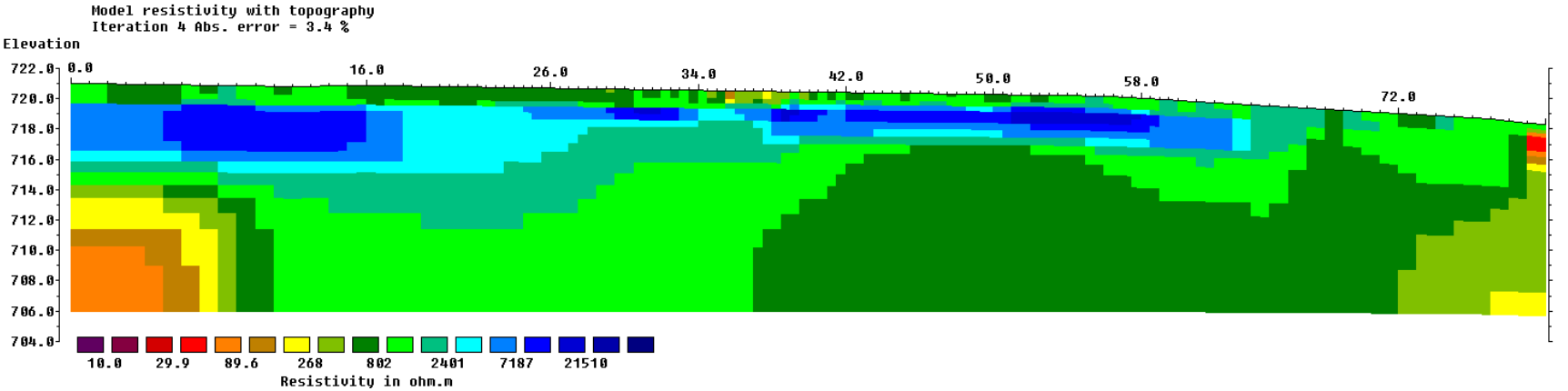

Figure I10 - Model resistivity with topography for the July 2011 survey for MP 597.5

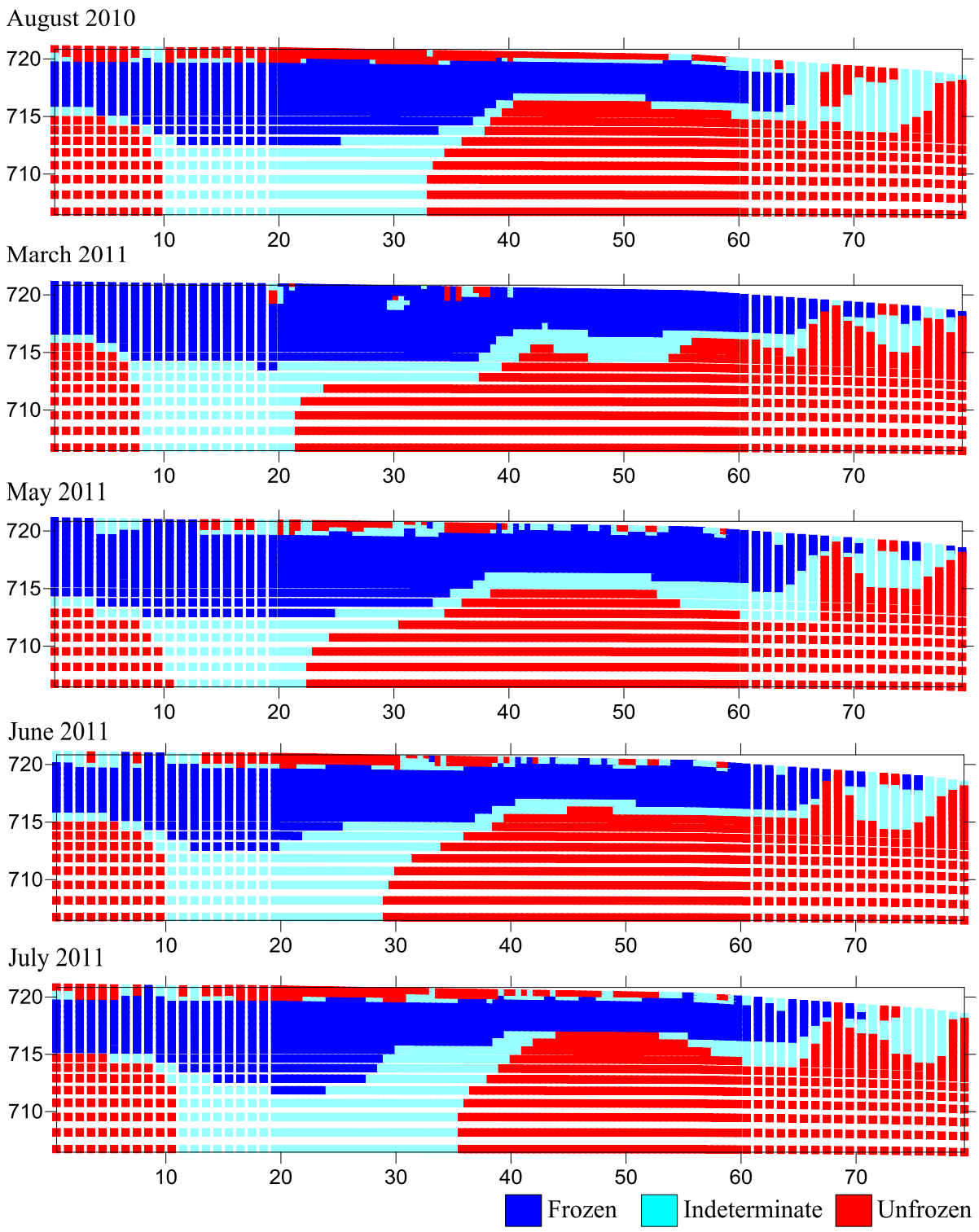

Figure I11 - Permafrost classification images for the surveys conducted at MP 597.5

APPENDIX J

MP 681.1

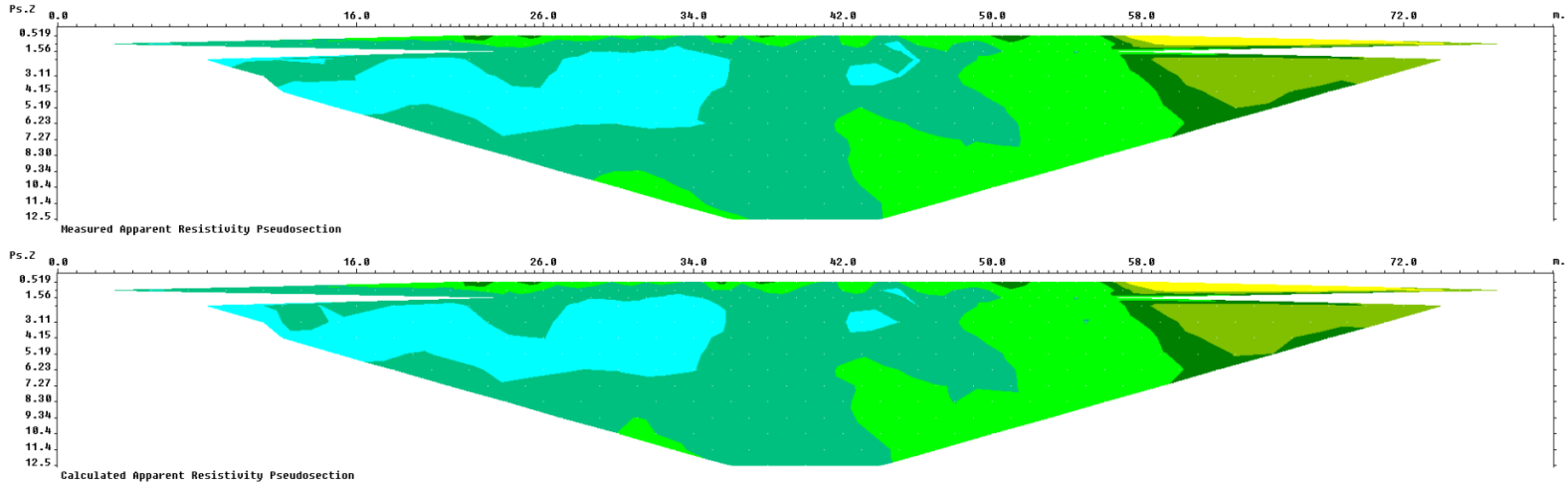

Figure J1 - Measured and calculated apparent resistivity for the August 2010 survey at MP 681.1

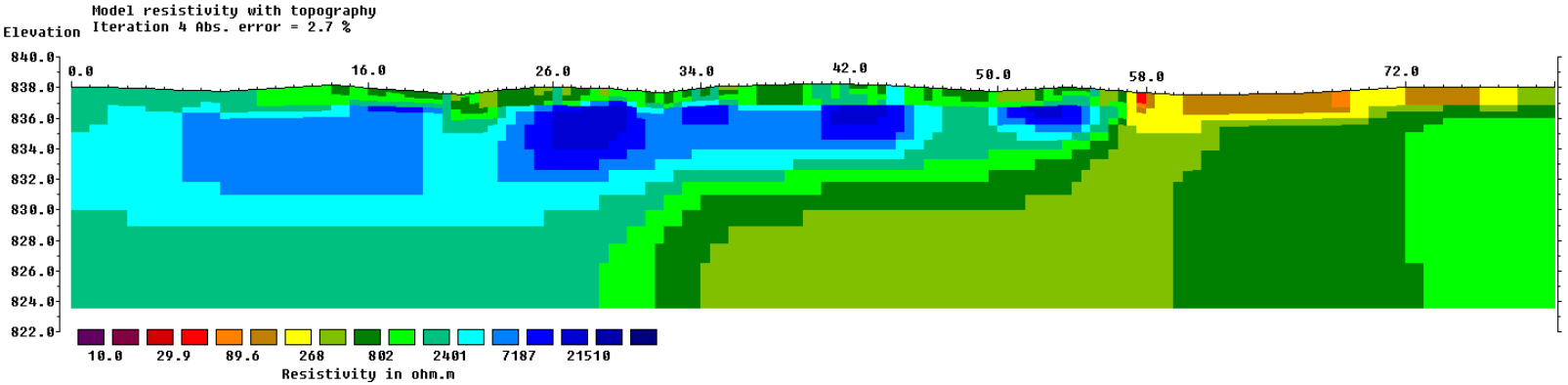

Figure J2 - Model resistivity with topography for the August 2010 survey for MP 681.1

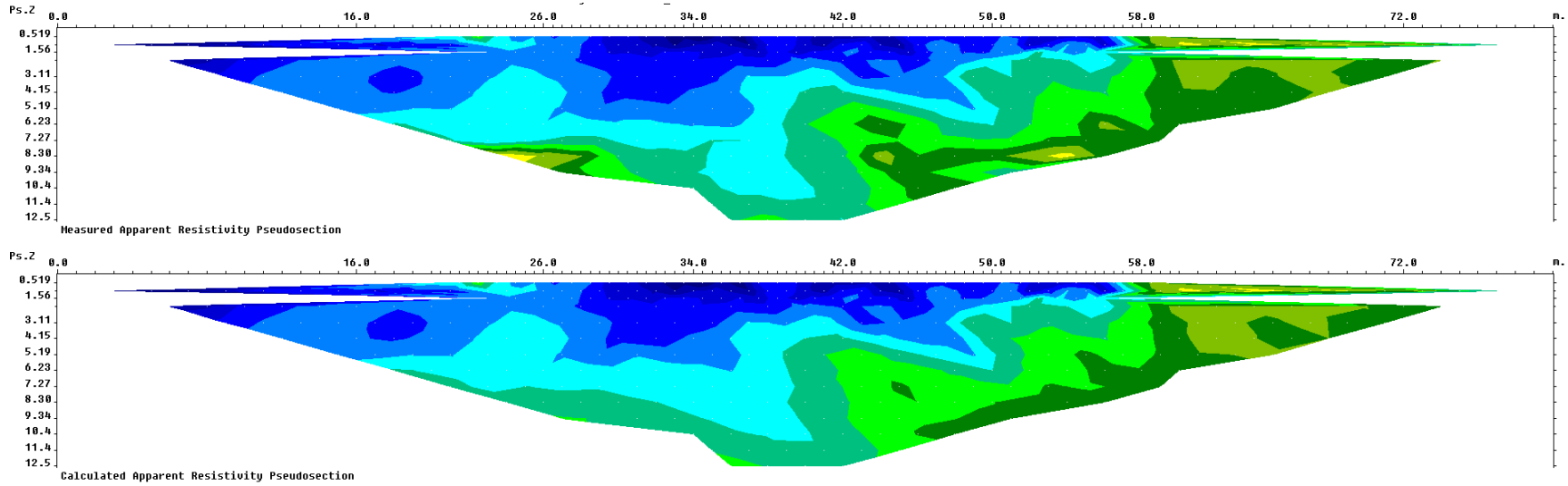

Figure J3 - Measured and calculated apparent resistivity for the March 2011 survey at MP 681.1

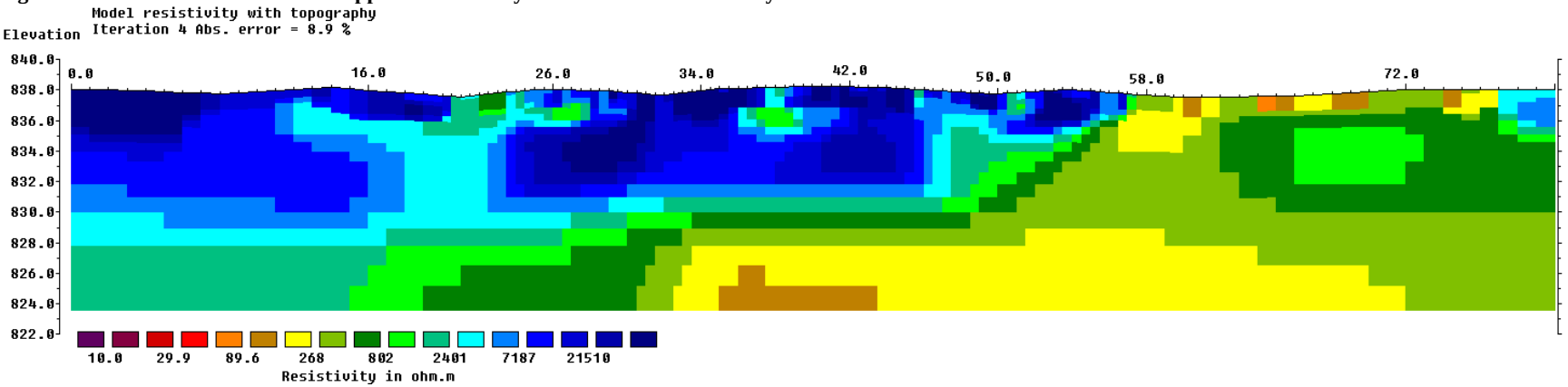

Figure J4 - Model resistivity with topography for the March 2011 survey for MP 681.1

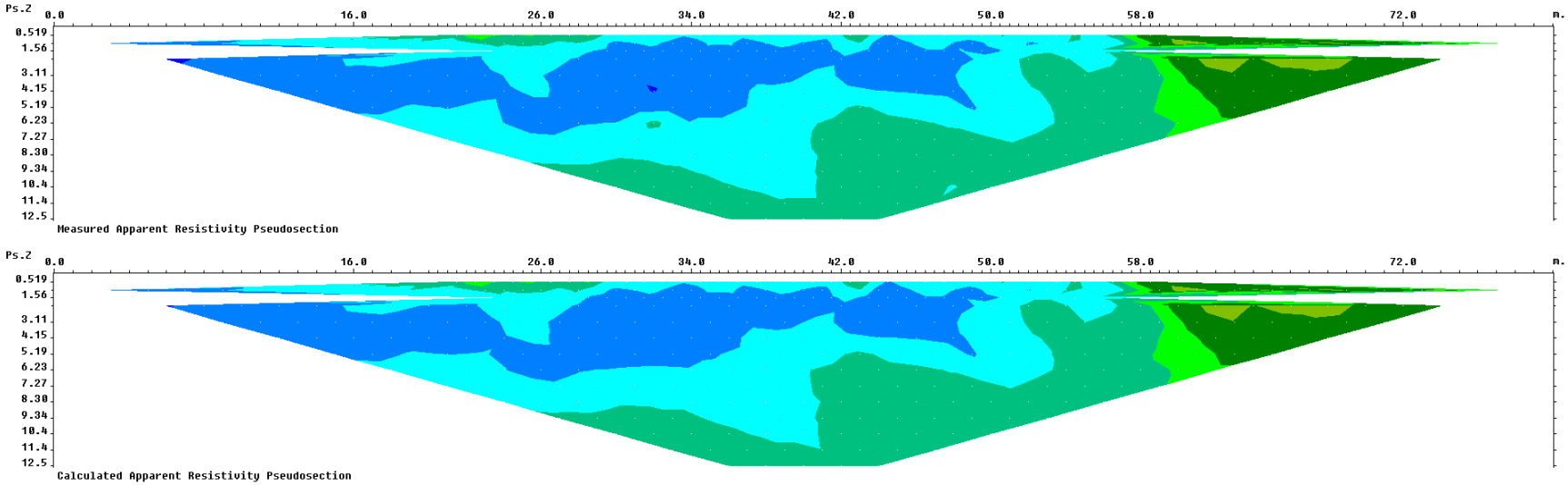

Figure J5 - Measured and calculated apparent resistivity for the May 2011 survey at MP 681.1

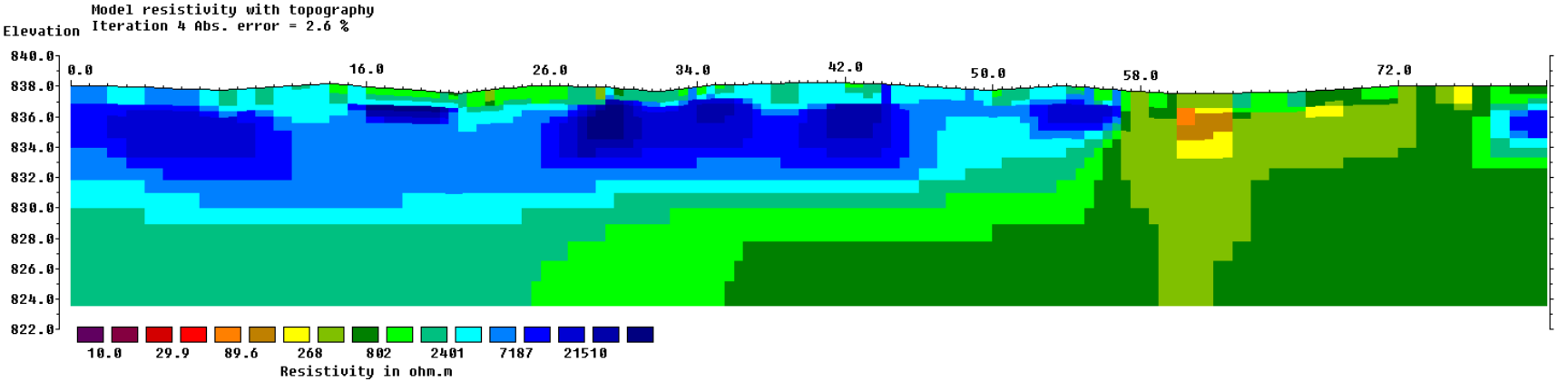

Figure J6 - Model resistivity with topography for the May 2011 survey for MP 681.1

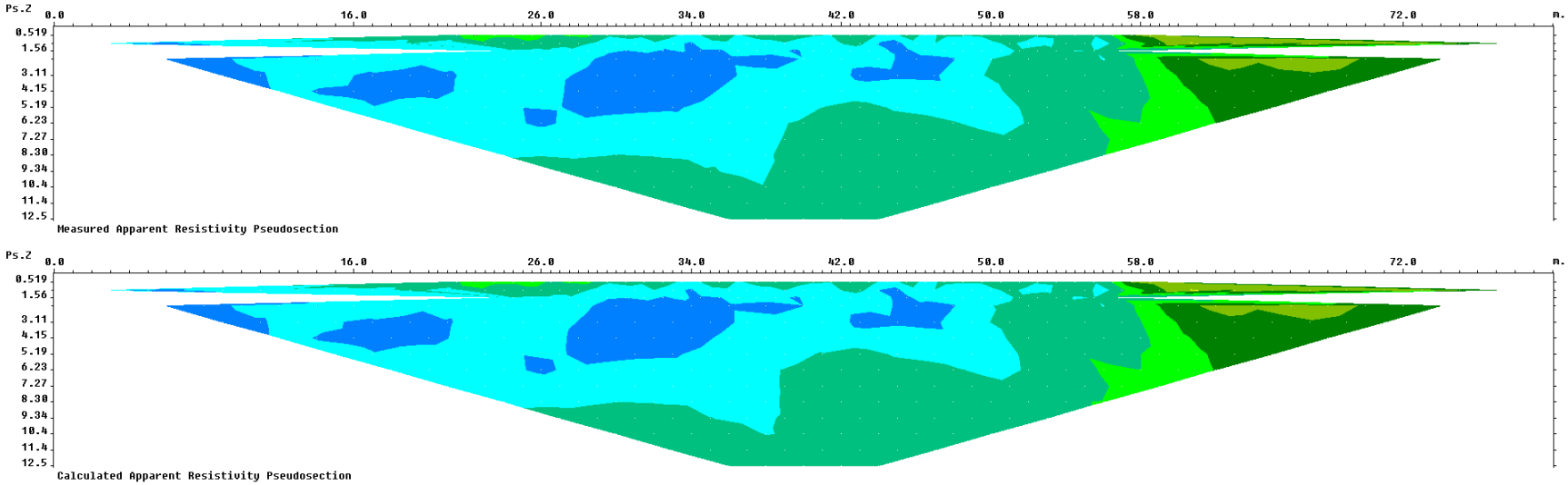

Figure J7 - Measured and calculated apparent resistivity for the June 2011 survey at MP 681.1

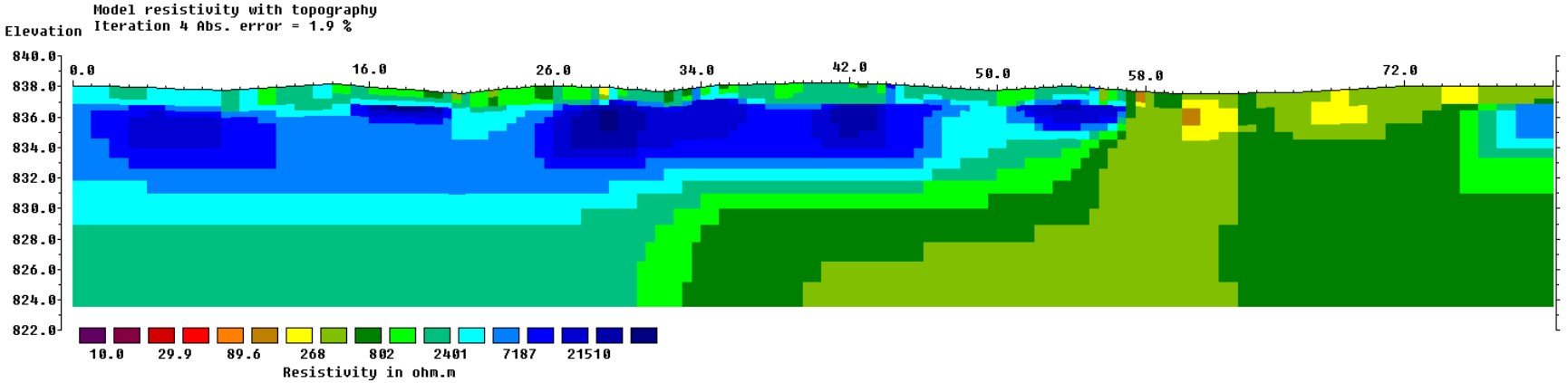

Figure J8 - Model resistivity with topography for the June 2011 survey for MP 681.1

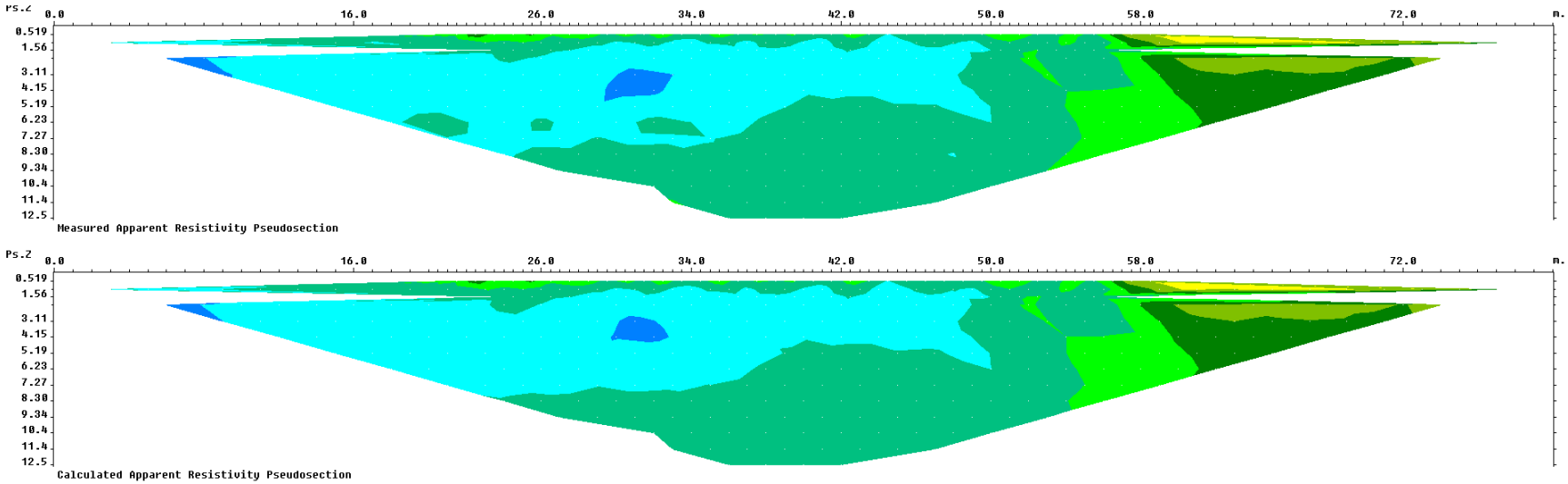

Figure J9 - Measured and calculated apparent resistivity for the July 2011 survey at MP 681.1

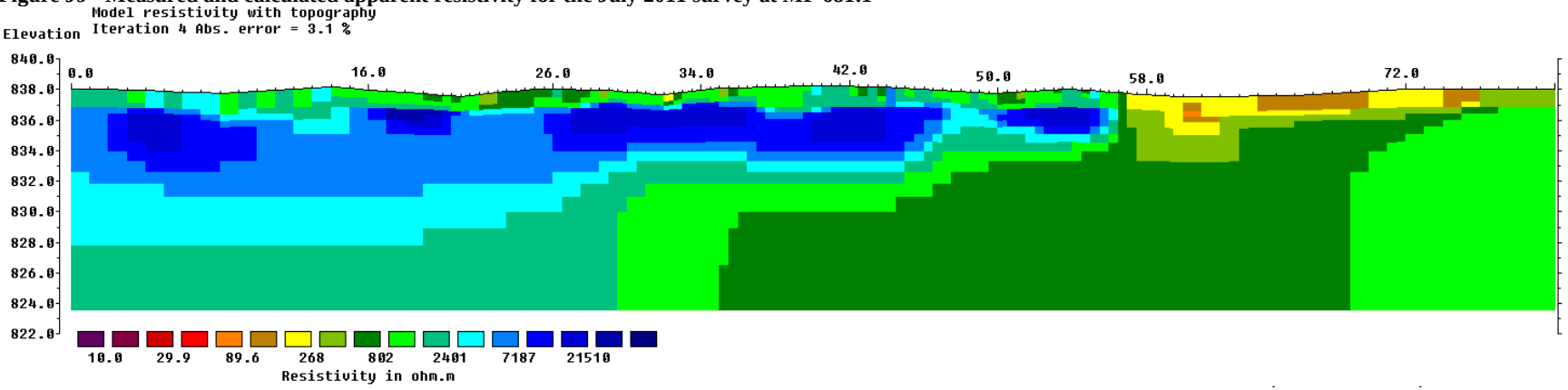

Figure J10 - Model resistivity with topography for the July 2011 survey for MP 681.1

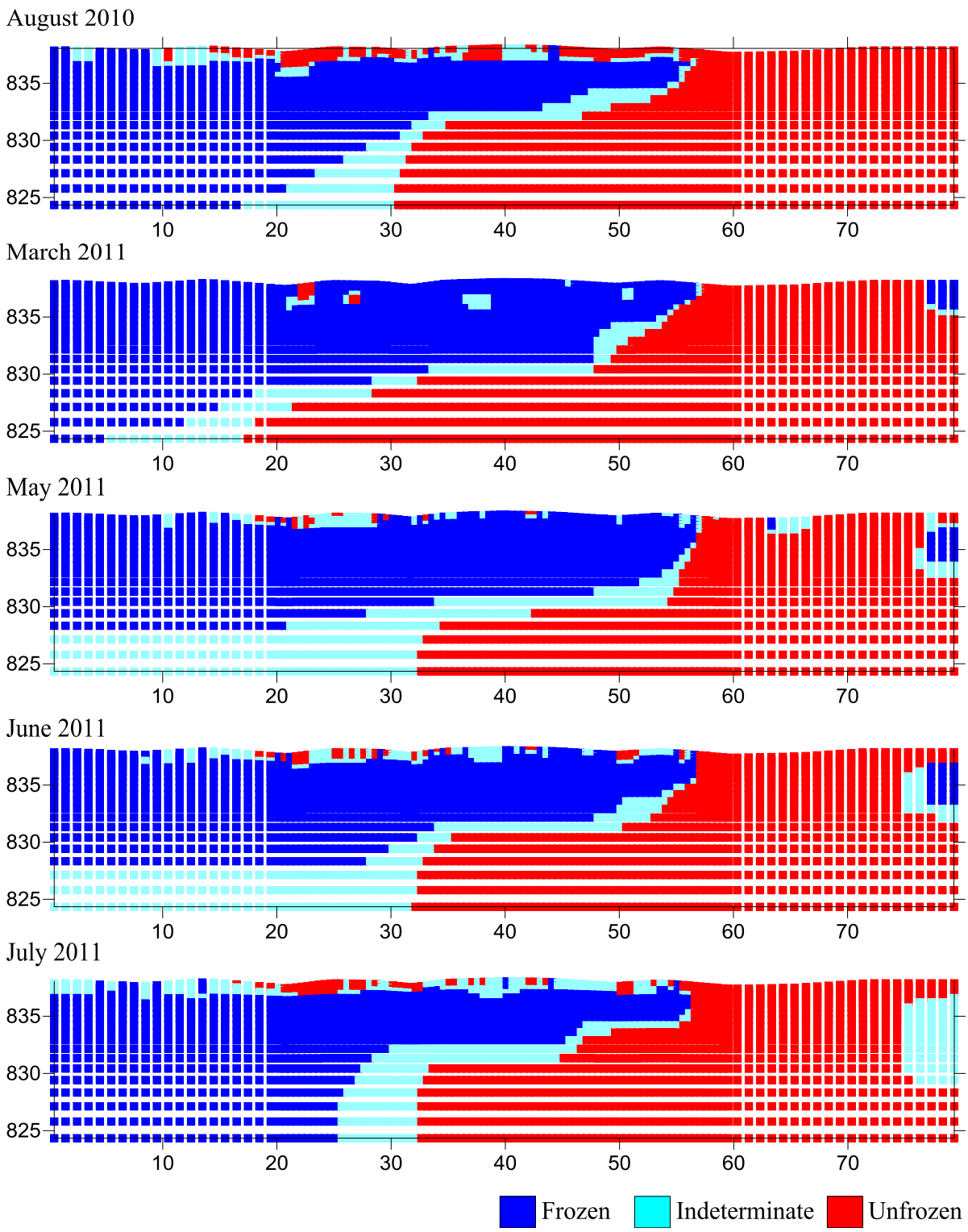

Figure J11 - Permafrost classification images for the surveys conducted at MP 681.1

APPENDIX K

MP 788.5

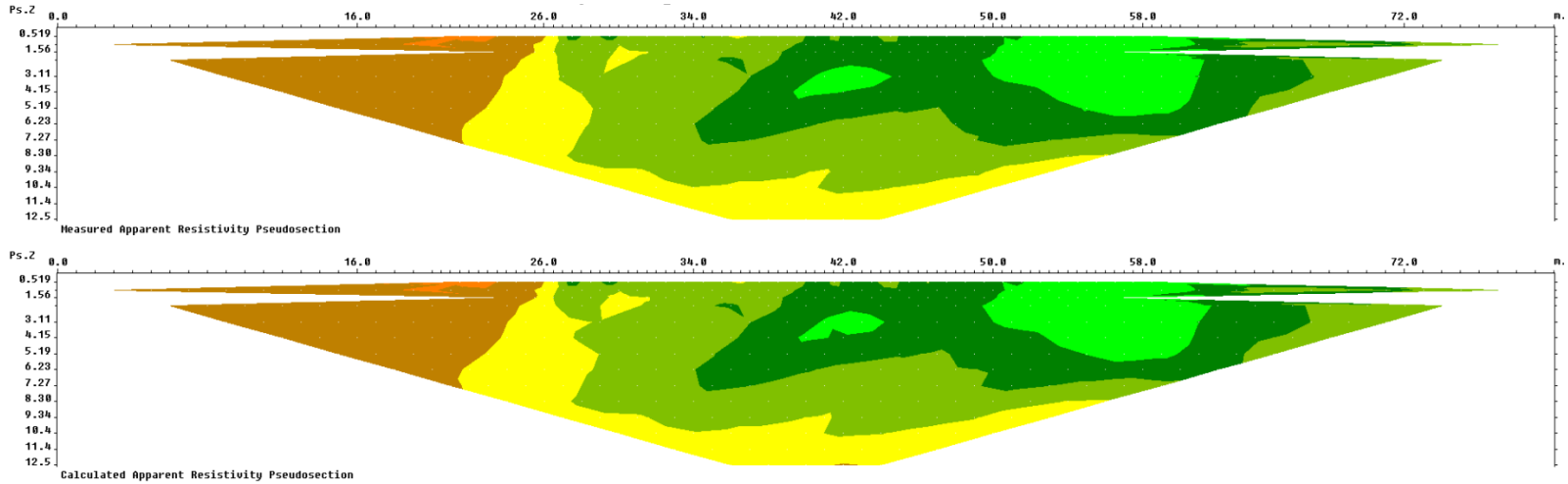

Figure K1 - Measured and calculated apparent resistivity for the August 2010 survey at MP 788.5

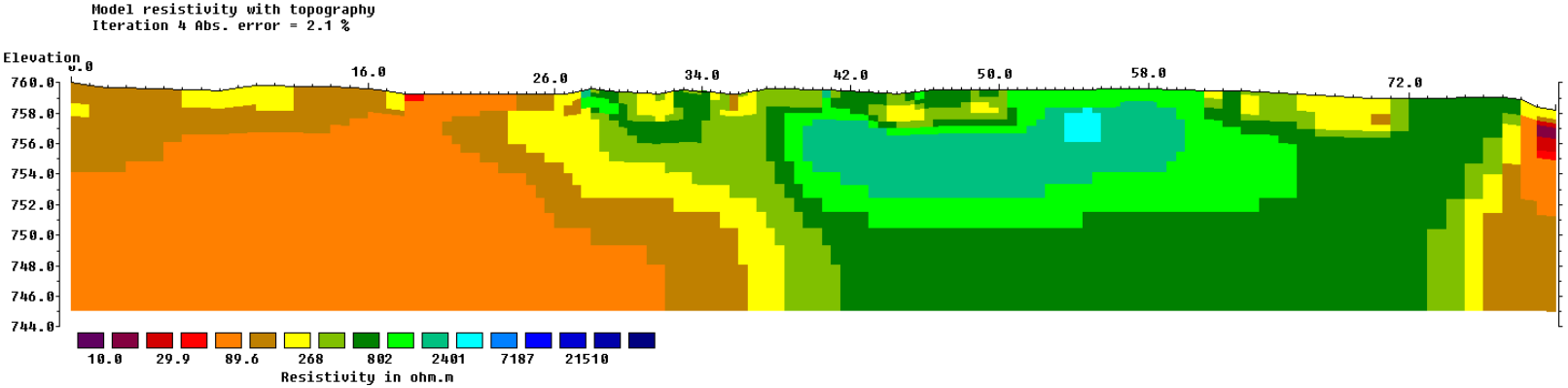

Figure K2 - Model resistivity with topography for the August 2010 survey for MP 788.5

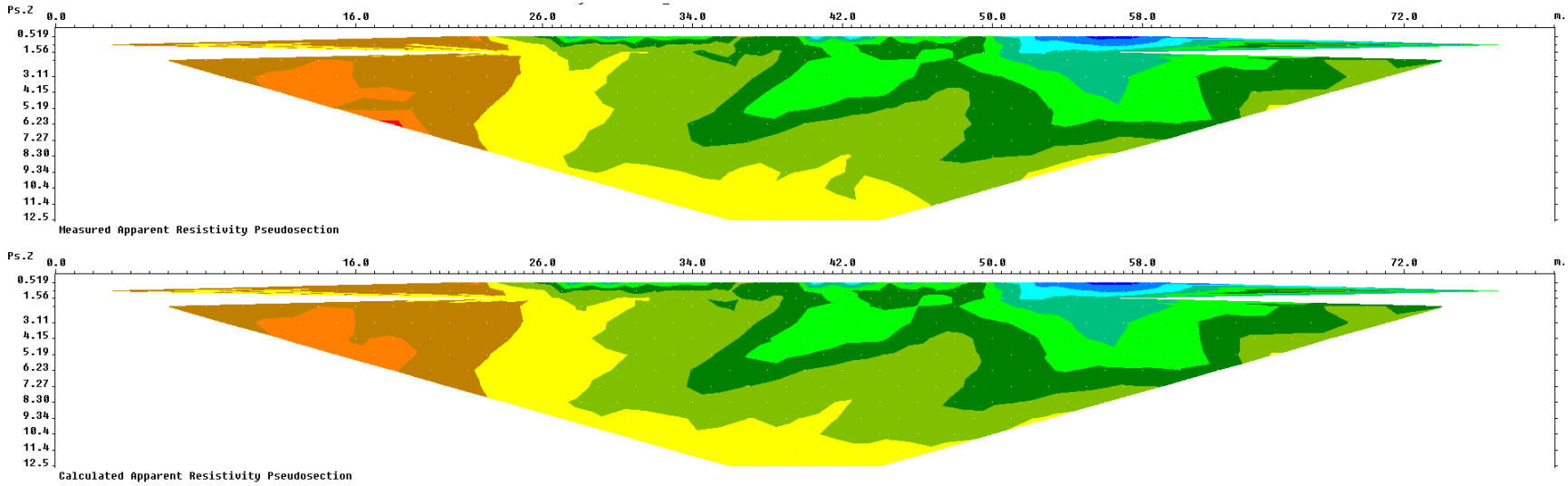

Figure K3 - Measured and calculated apparent resistivity for the March 2011 survey at MP 788.5

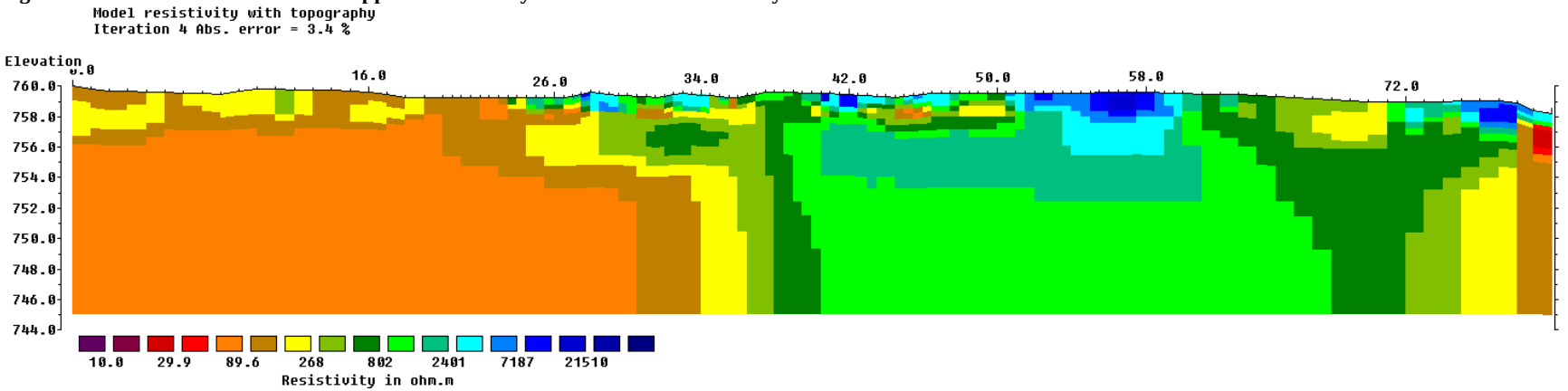

Figure K4 - Model resistivity with topography for the March 2011 survey for MP 788.5

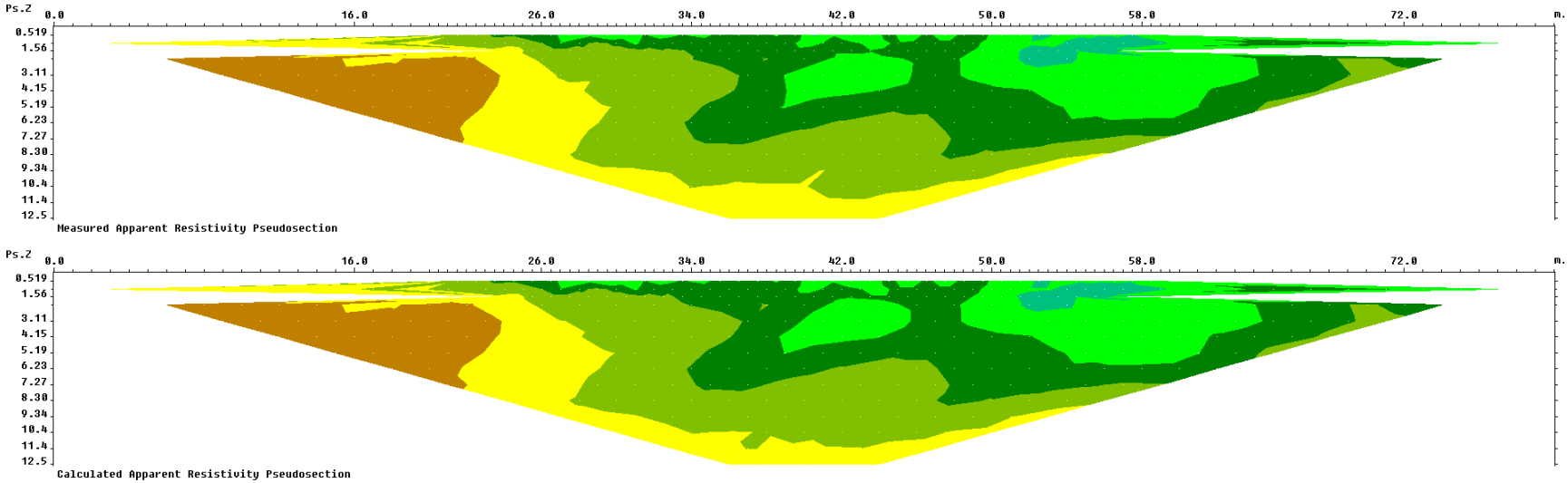

Figure K5 - Measured and calculated apparent resistivity for the May 2011 survey at MP 788.5

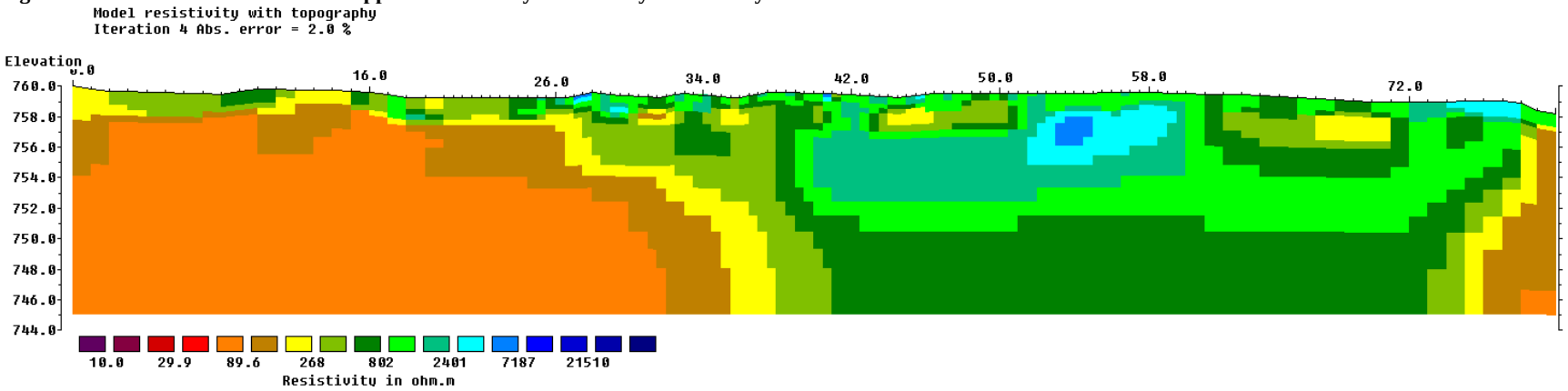

Figure K6 - Model resistivity with topography for the May 2011 survey for MP 788.5

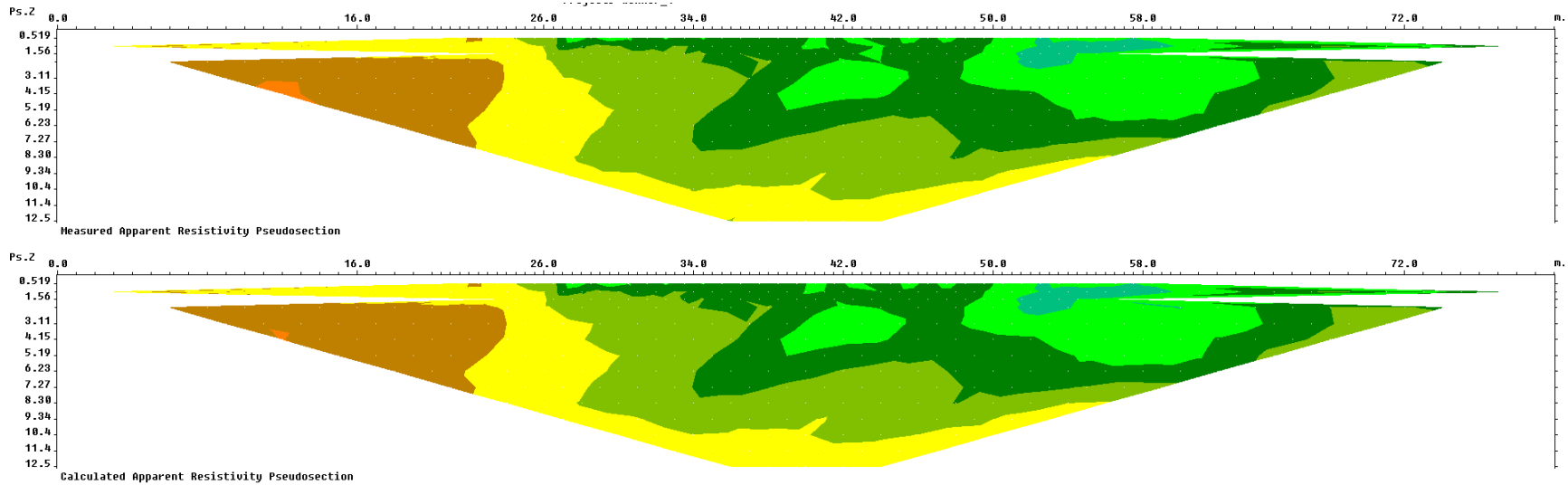

Figure K7 - Measured and calculated apparent resistivity for the June 2011 survey at MP 788.5

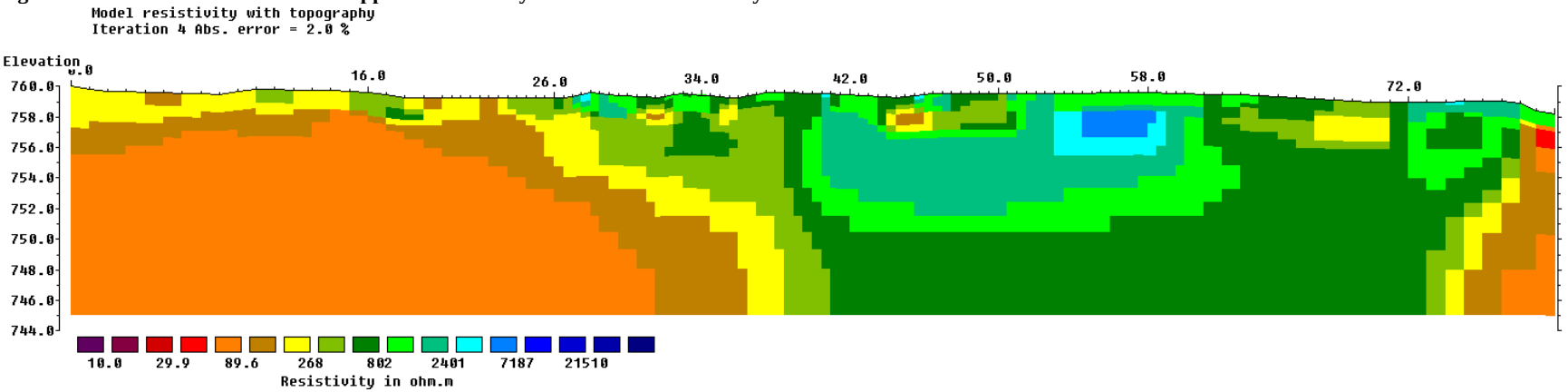

Figure K8 - Model resistivity with topography for the June 2011 survey for MP 788.5

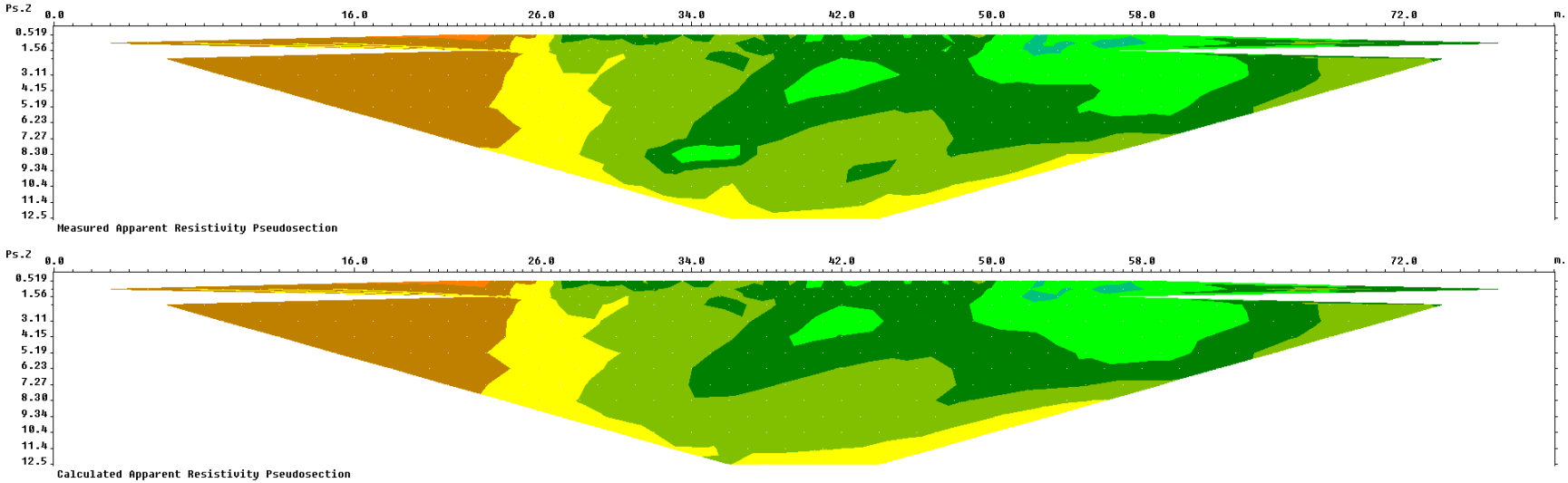

Figure K9 - Measured and calculated apparent resistivity for the July 2011 survey at MP 788.5

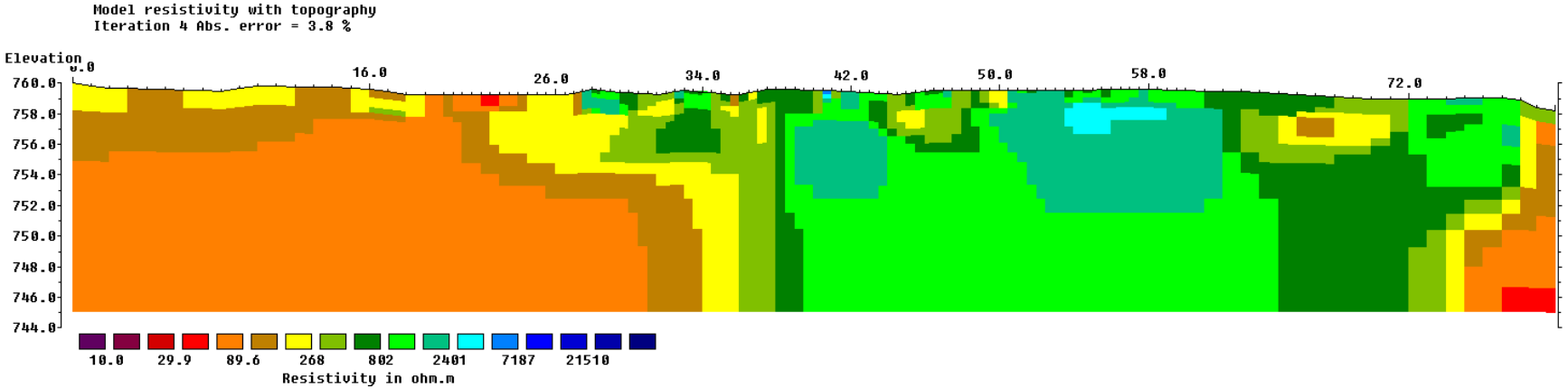

Figure K10 - Model resistivity with topography for the July 2011 survey for MP 788.5

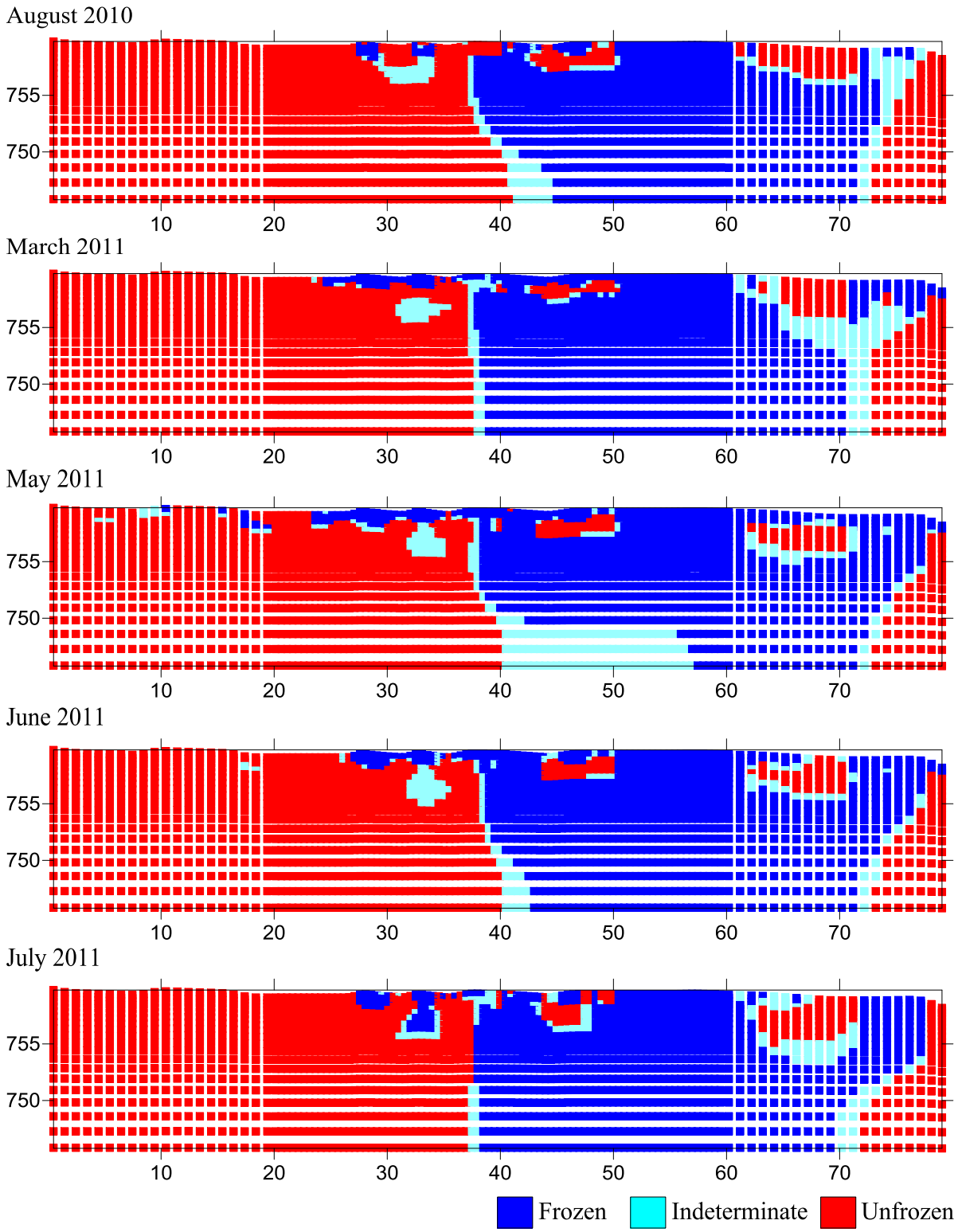

Figure K11 - Permafrost classification images for the surveys conducted at MP 788.5

APPENDIX L

MP 825.2

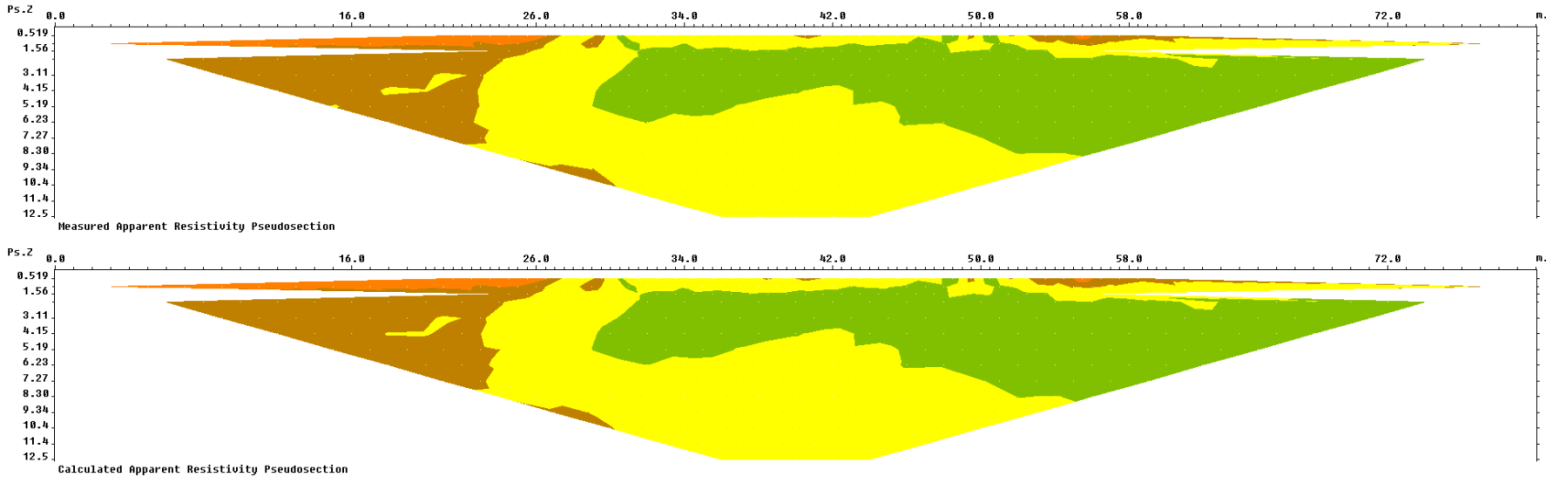

Figure L1 - Measured and calculated apparent resistivity for the August 2010 survey at MP 825.2

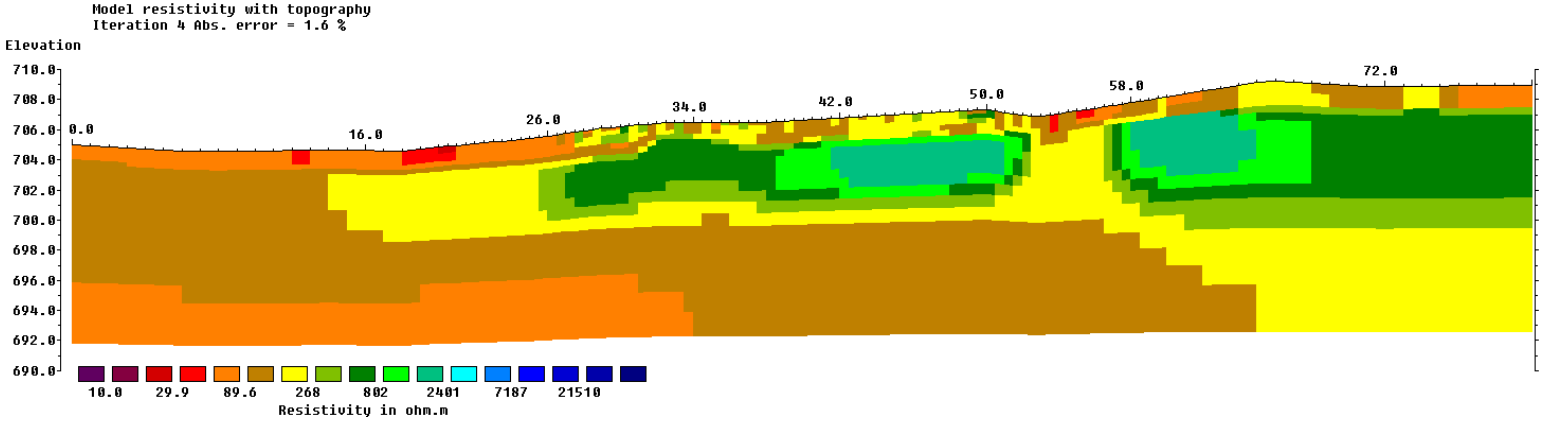

Figure L2 - Model resistivity with topography for the August 2010 survey for MP 825.2

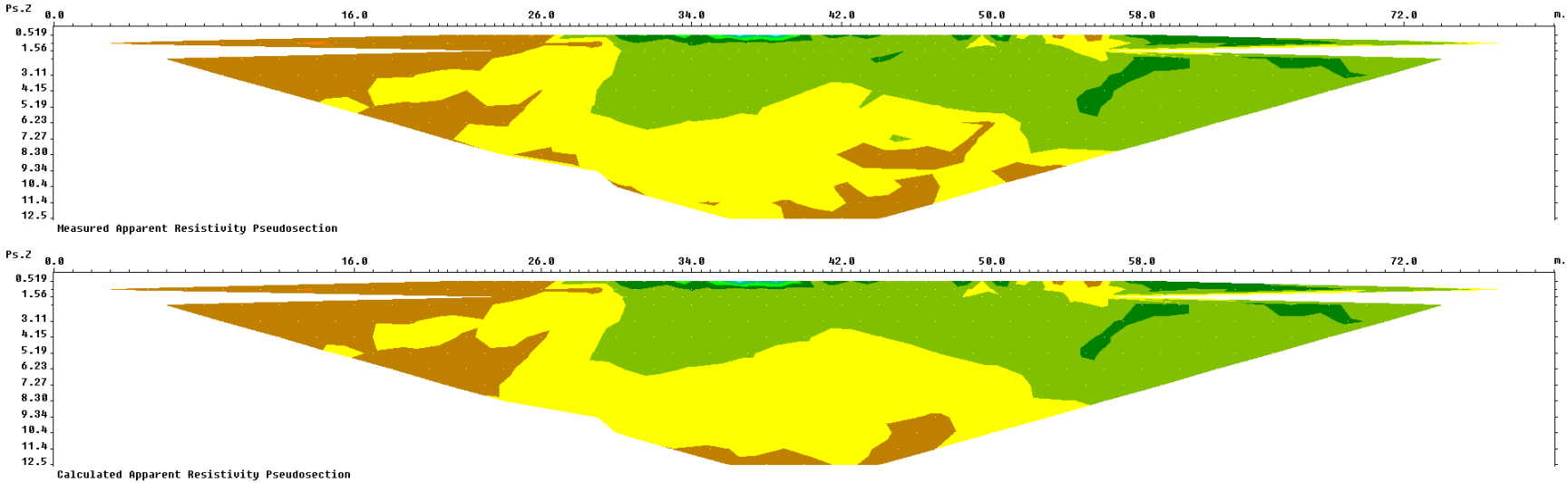

Figure L3 - Measured and calculated apparent resistivity for the March 2011 survey at MP 825.2

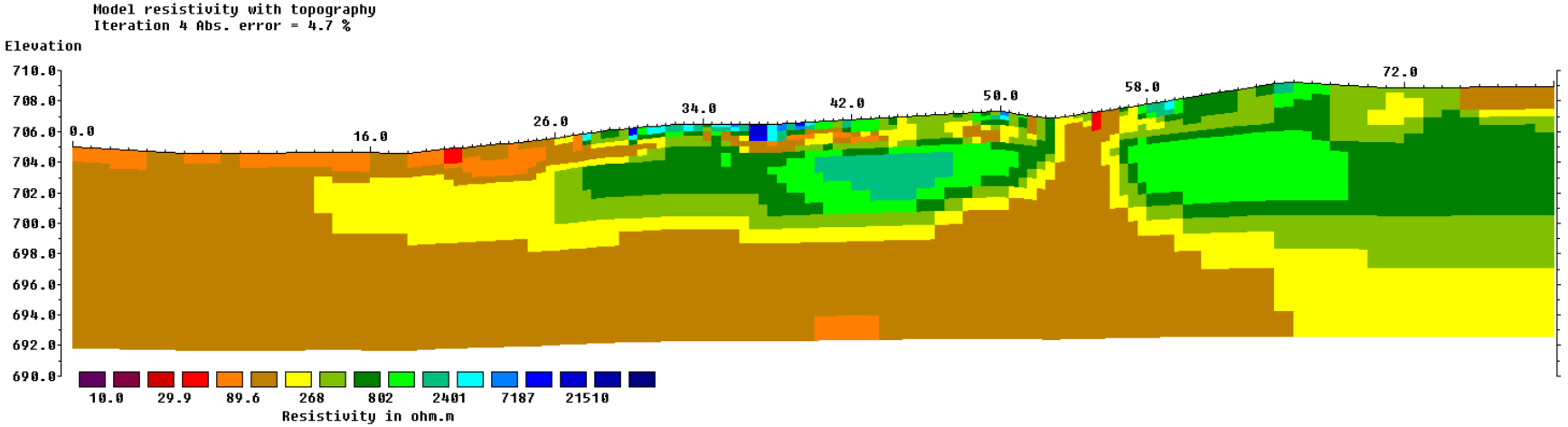

Figure L4 - Model resistivity with topography for the March 2011 survey for MP 825.2

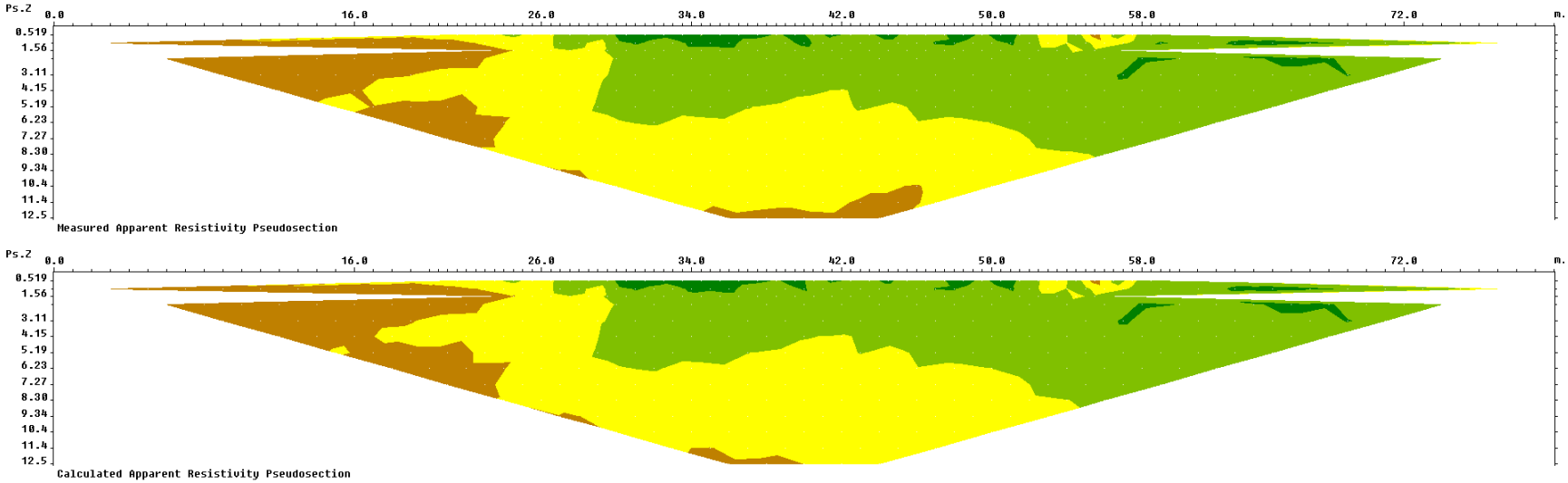

Figure L5 - Measured and calculated apparent resistivity for the May 2011 survey at MP 825.2

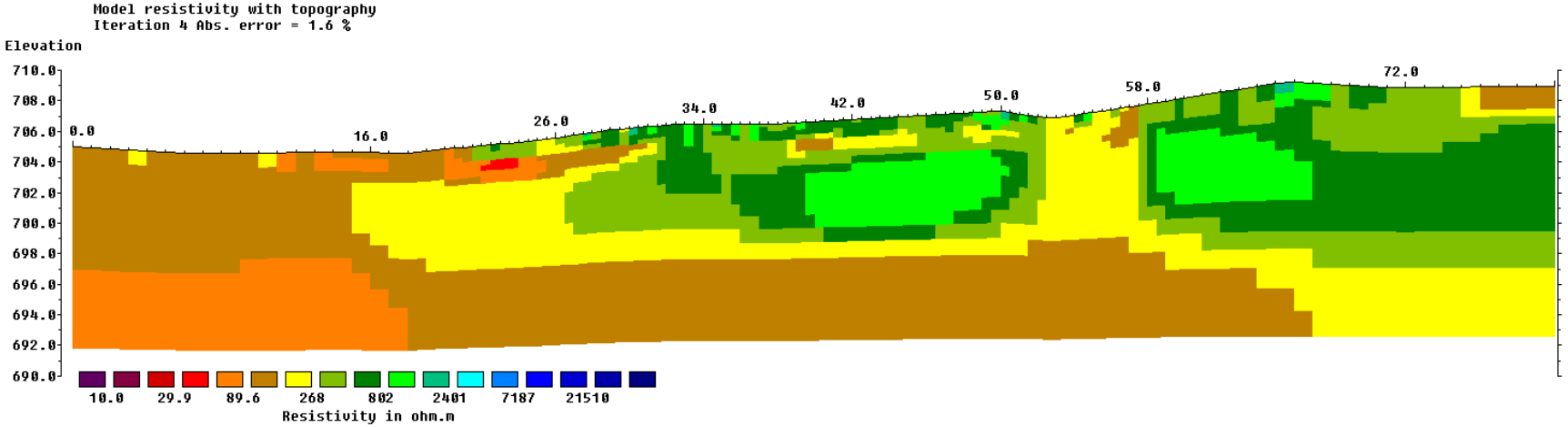

Figure L6 - Model resistivity with topography for the May 2011 survey for MP 825.2

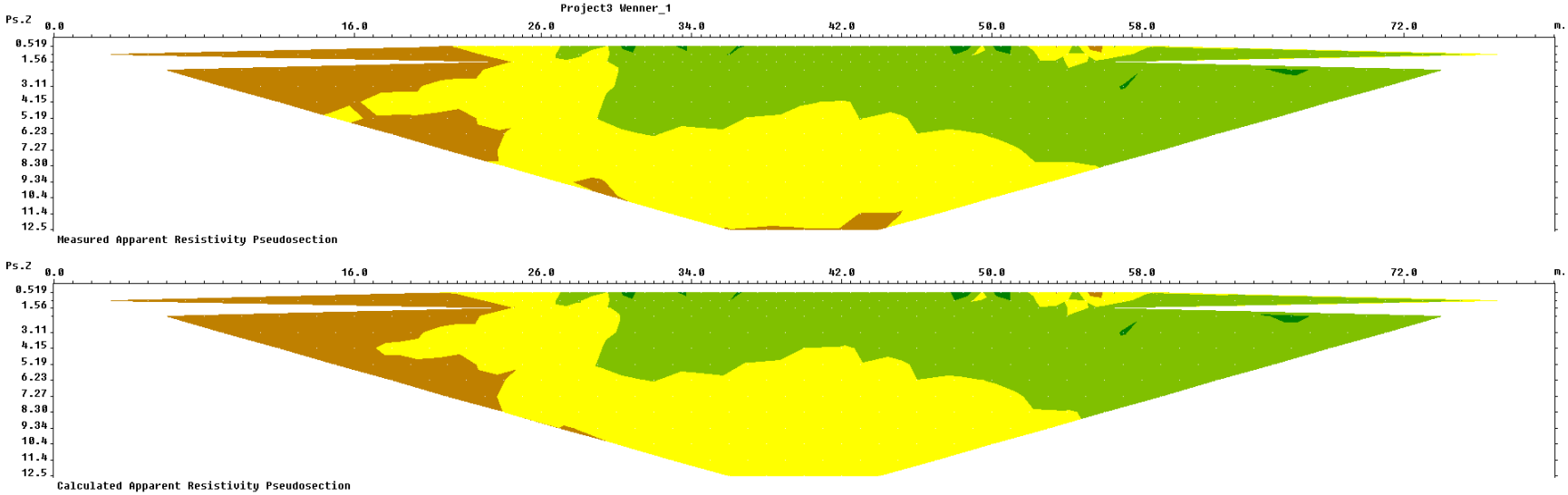

Figure L7 - Measured and calculated apparent resistivity for the June 2011 survey at MP 825.2

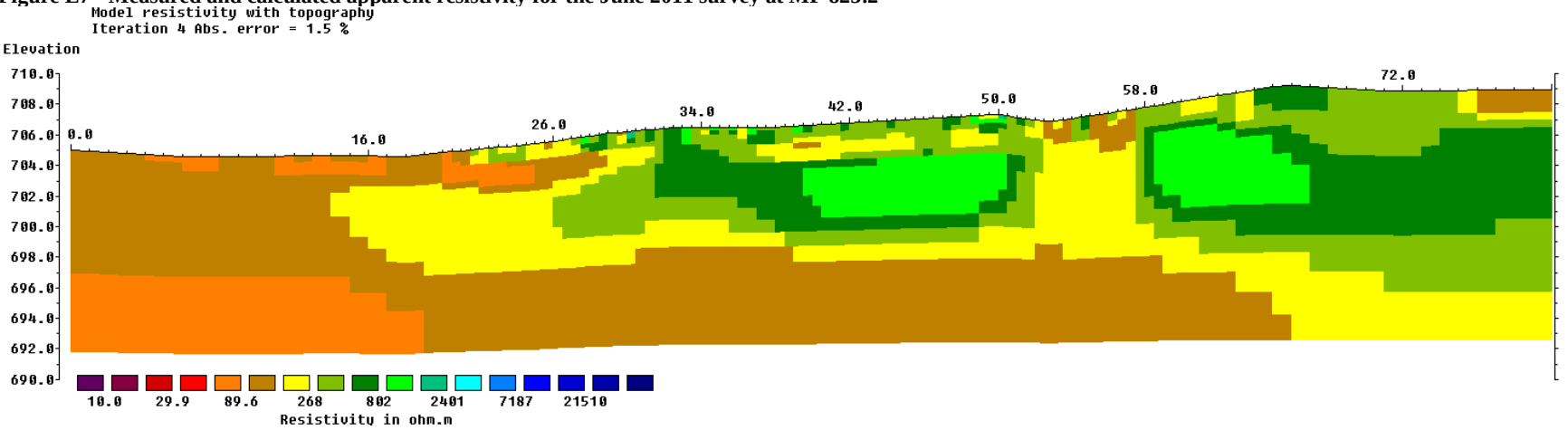

Figure L8 - Model resistivity with topography for the June 2011 survey for MP 825.2

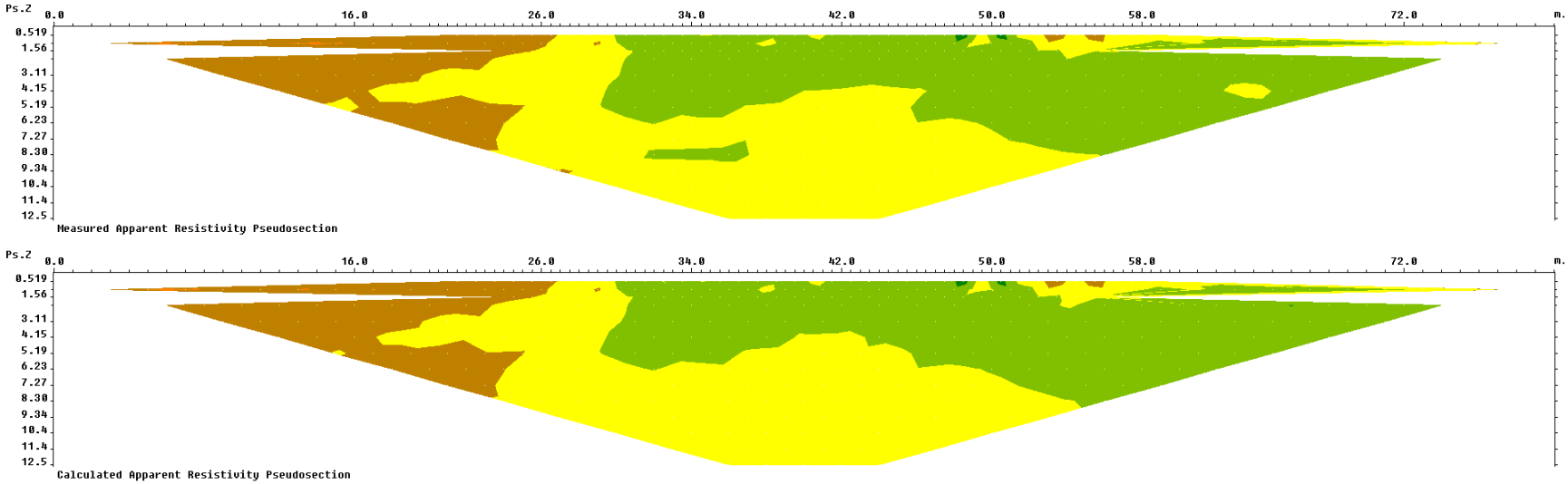

Figure L9 - Measured and calculated apparent resistivity for the July 2011 survey at MP 825.2

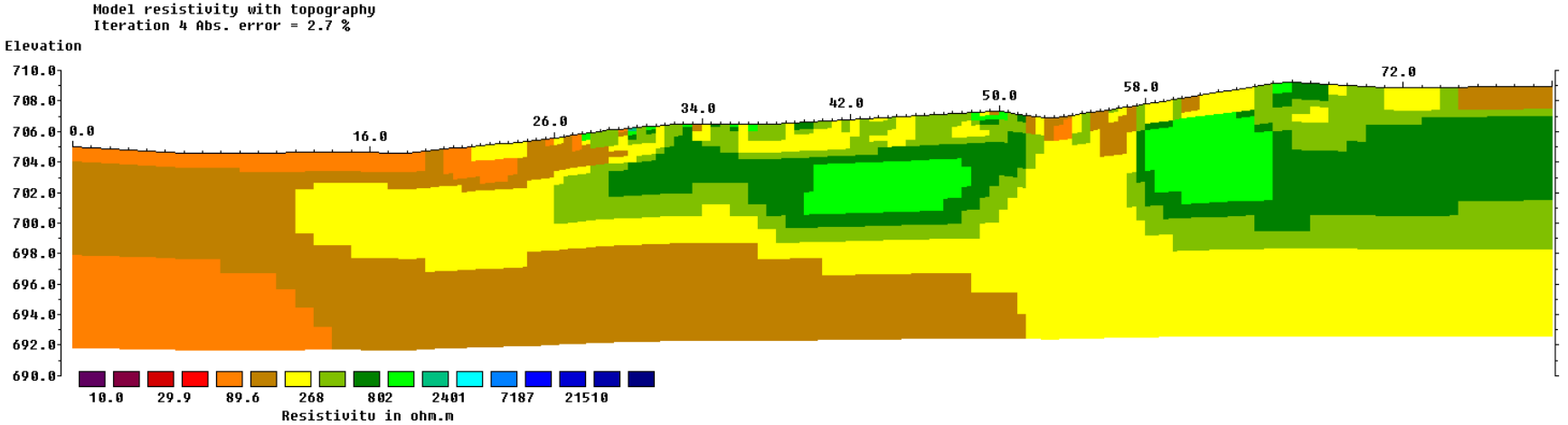

Figure L10 - Model resistivity with topography for the July 2011 survey for MP 825.2

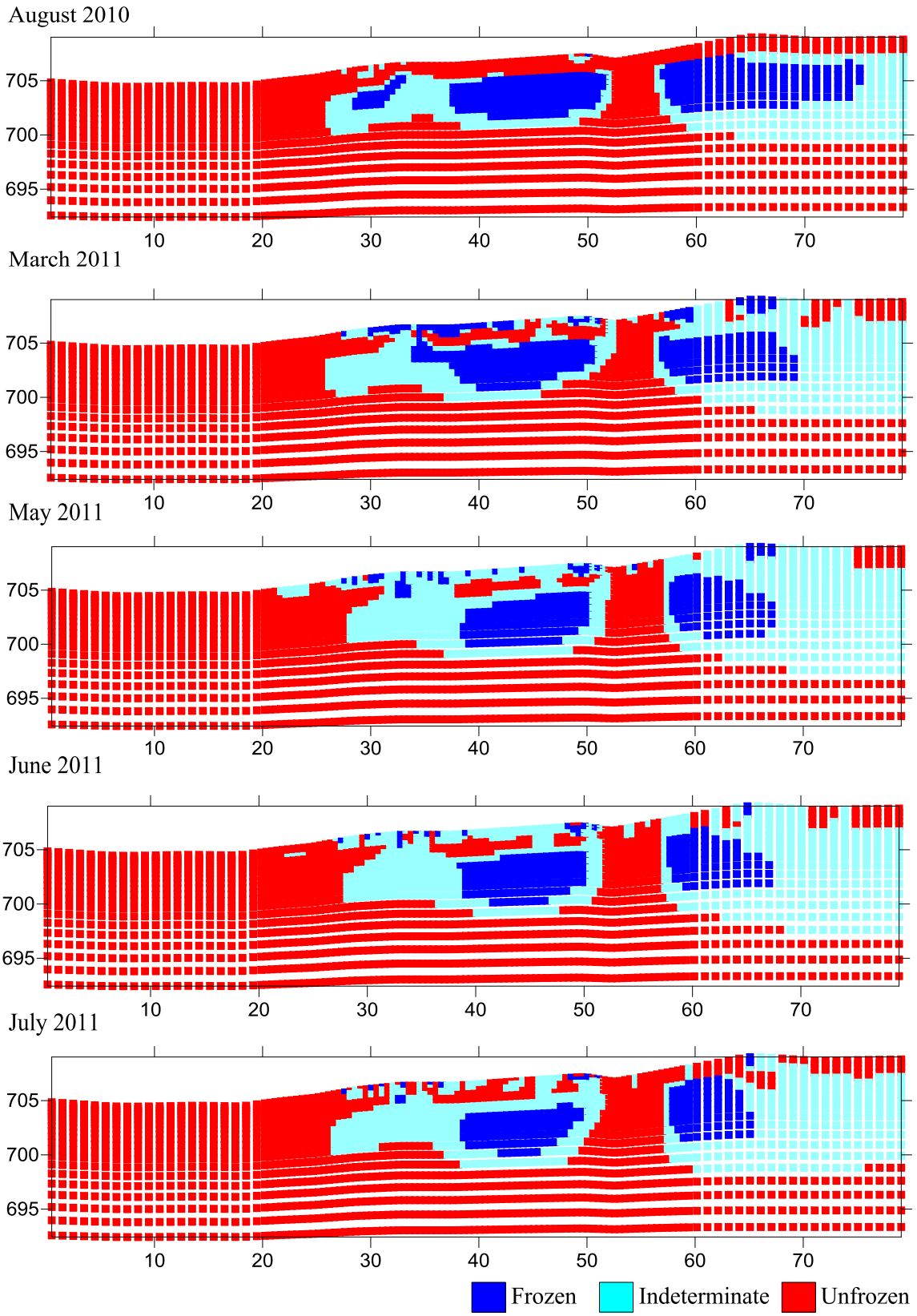

Figure L11 - Permafrost classification images for the surveys conducted at MP 825.2

APPENDIX M

MP 844.1

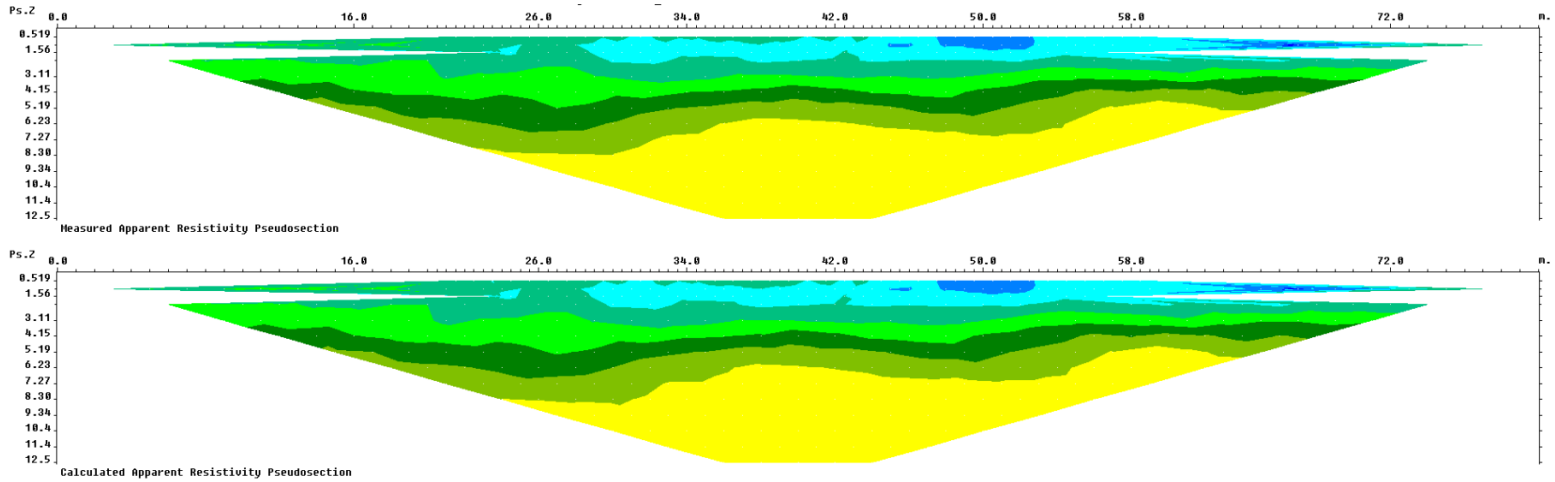

Figure M1 - Measured and calculated apparent resistivity for the August 2010 survey at MP 844.1

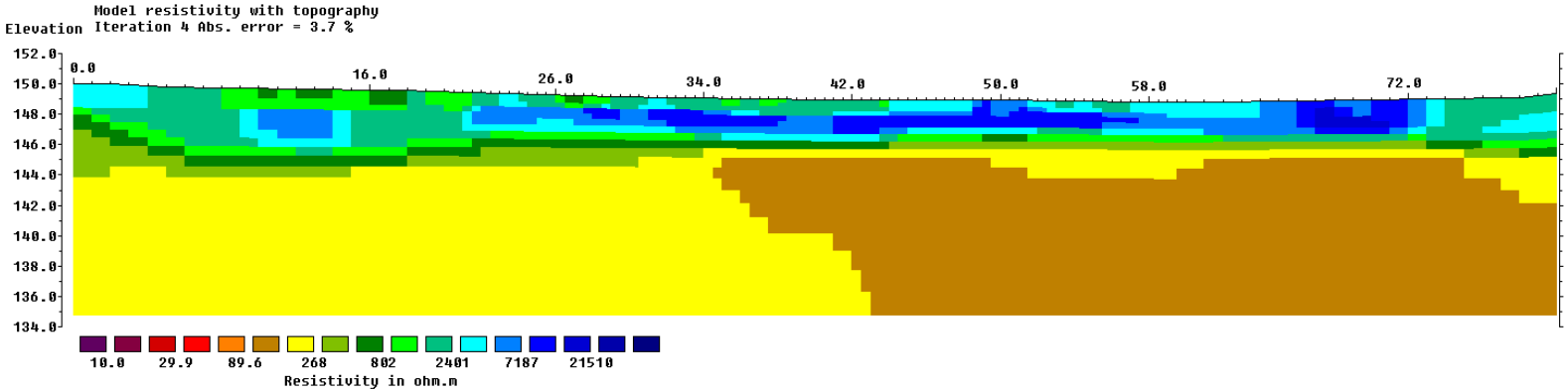

Figure M2 - Model resistivity with topography for the August 2010 survey for MP 844.1

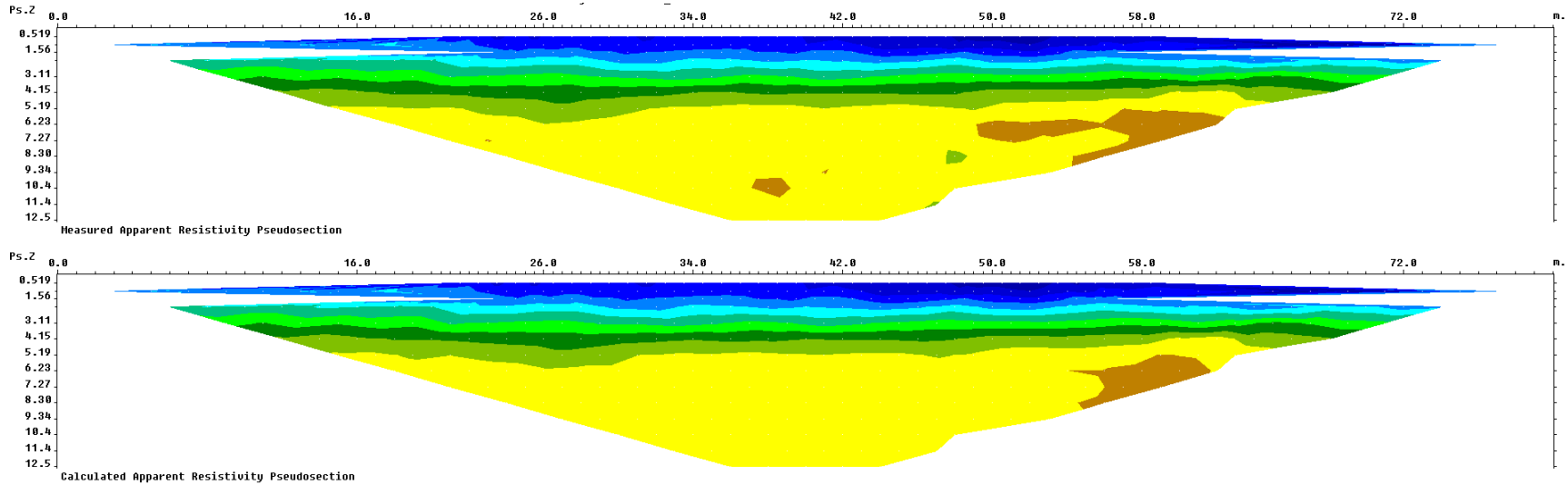

Figure M3 - Measured and calculated apparent resistivity for the March 2011 survey at MP 844.1

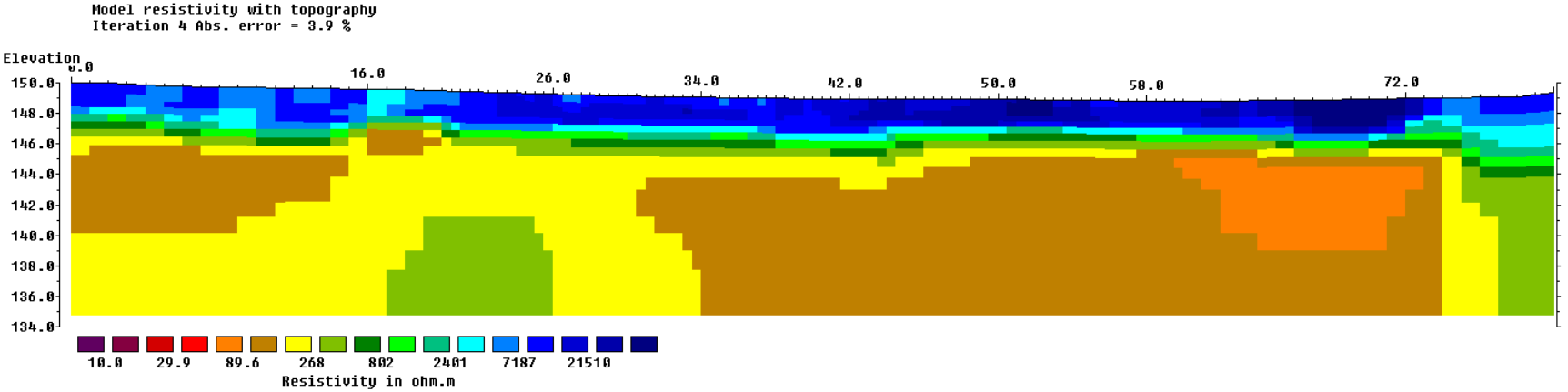

Figure M4 - Model resistivity with topography for the March 2011 survey for MP 844.1

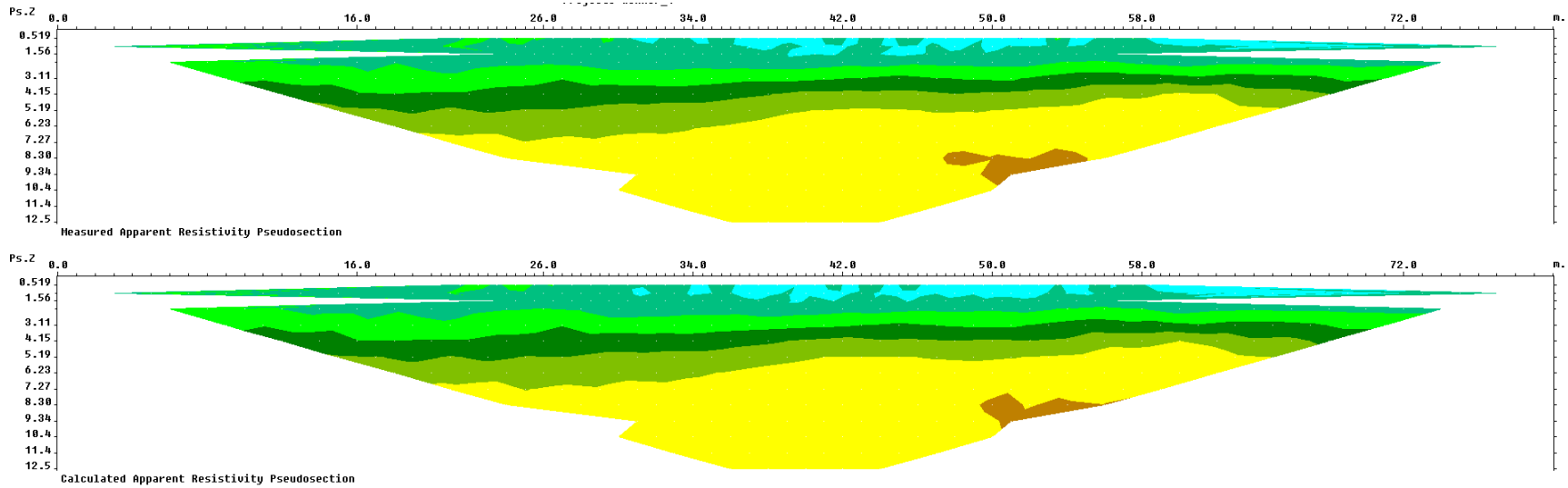

Figure M5 - Measured and calculated apparent resistivity for the May 2011 survey at MP 844.1

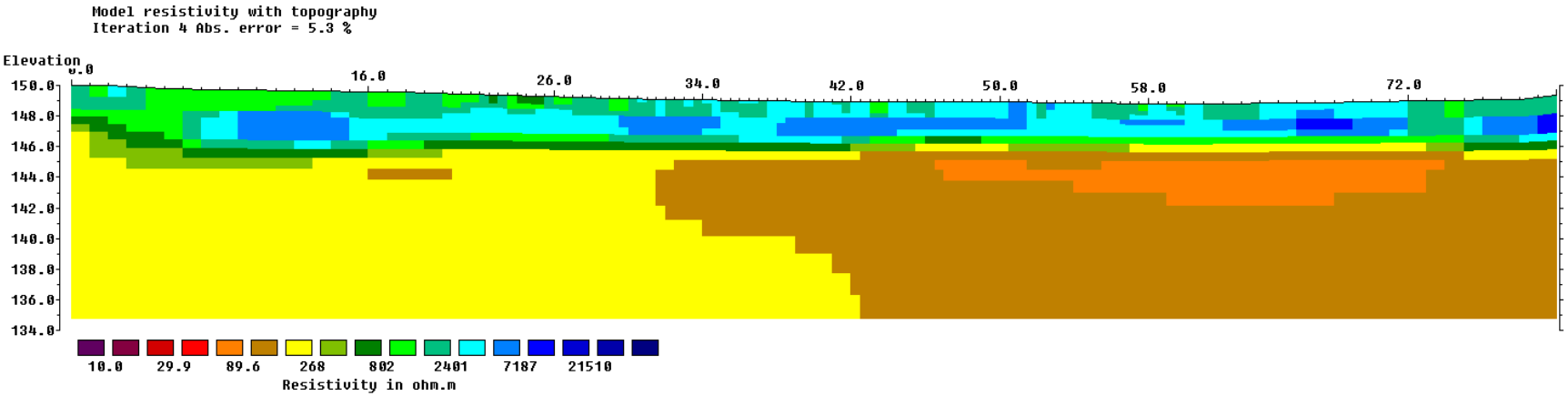

Figure M6 - Model resistivity with topography for the May 2011 survey for MP 844.1

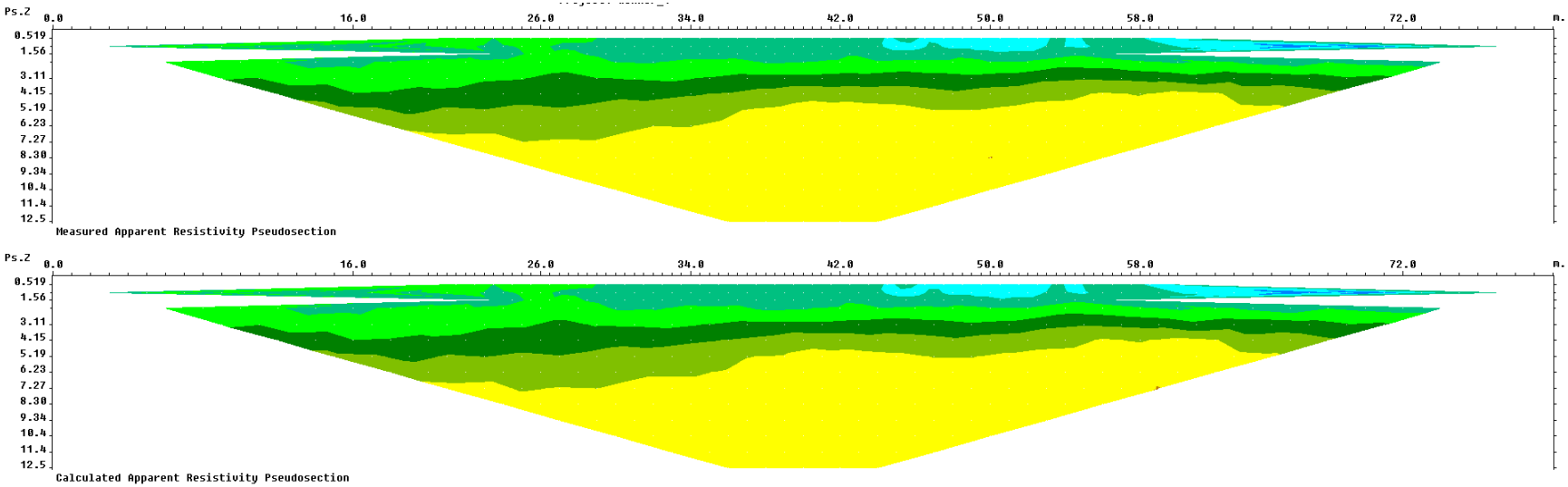

Figure M7 - Measured and calculated apparent resistivity for the June 2011 survey at MP 844.1

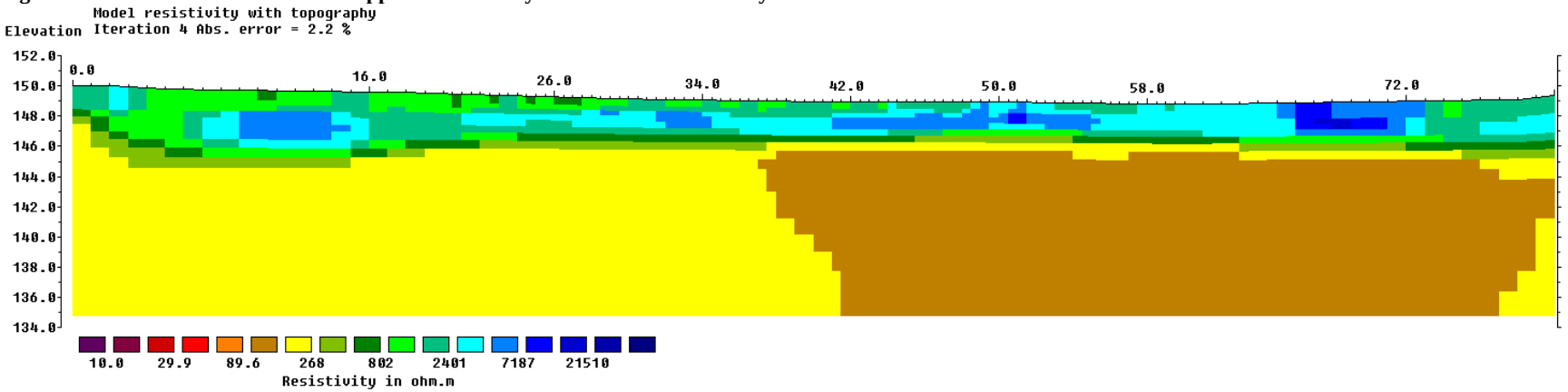

Figure M8 - Model resistivity with topography for the June 2011 survey for MP 844.1

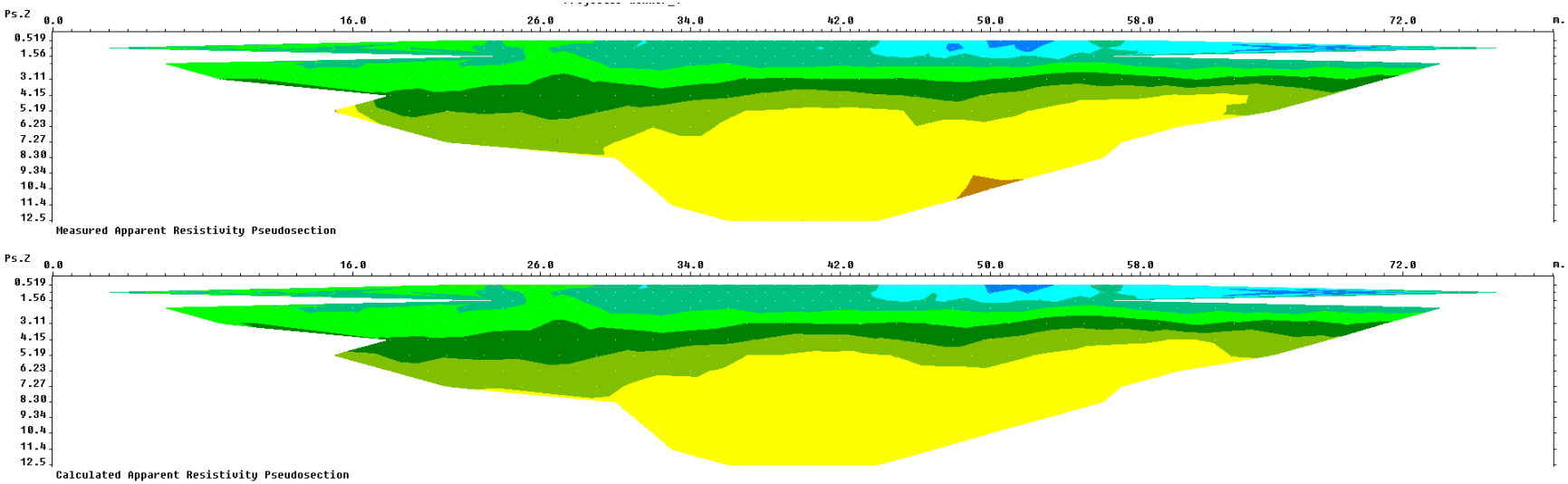

Figure M9 - Measured and calculated apparent resistivity for the July 2011 survey at MP 844.1

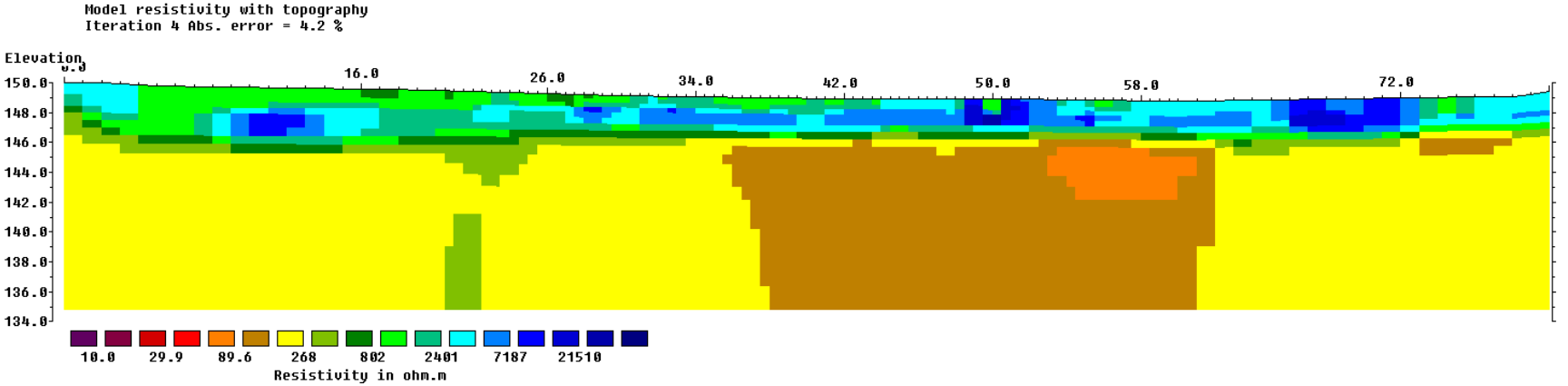

Figure M10 - Model resistivity with topography for the July 2011 survey for MP 844.1

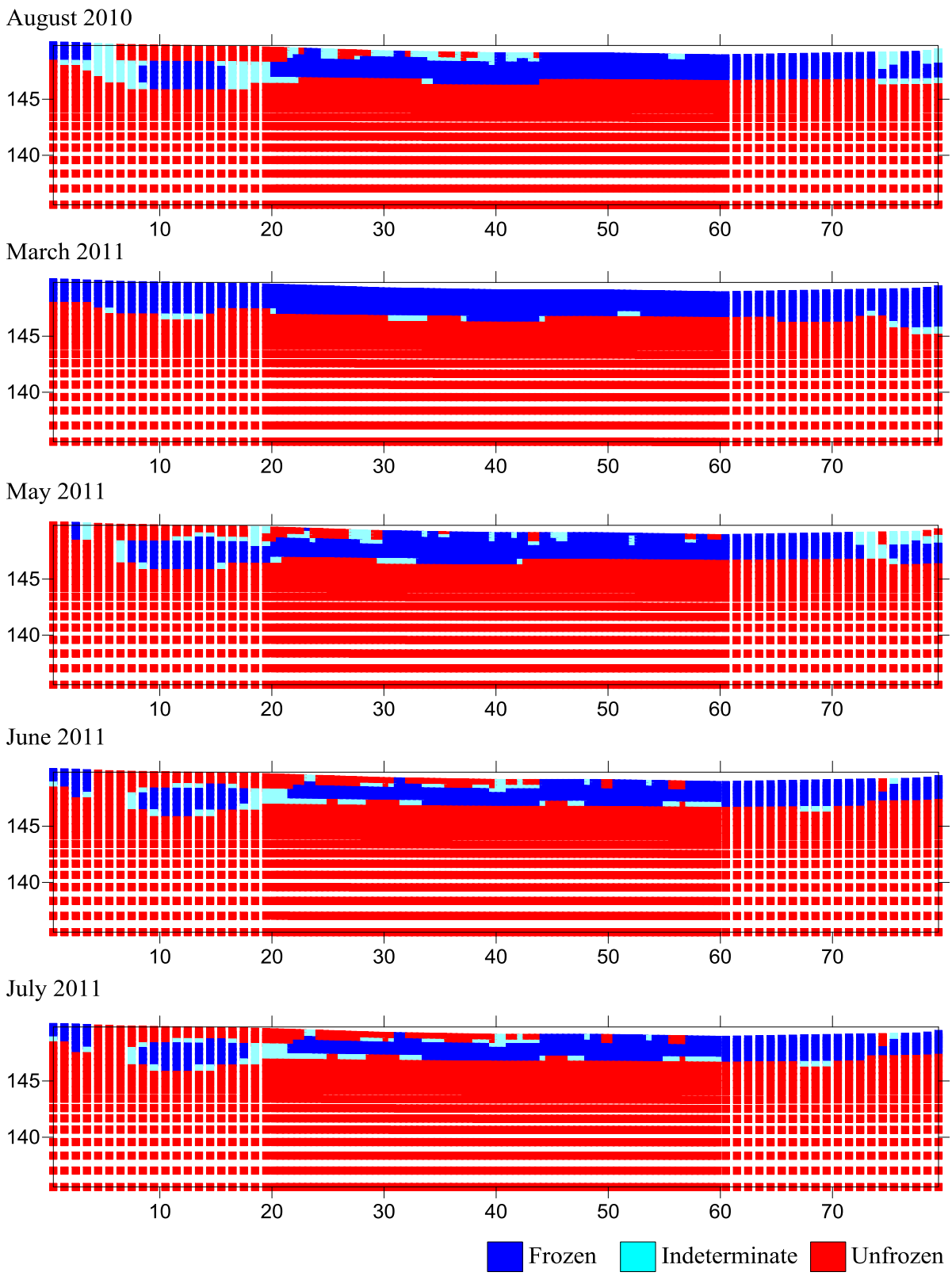

Figure M11 – Permafrost classification images for the surveys conducted at MP 844.1